KERNFORSCHUNGSANLAGE JÜLICH GmbH
Institut für Kernphysik

Microscopic Description of Giant Electric and Magnetic Multipole Resonances in Closed - Shell Nuclei

by

Sanchez - Dehesa, J.

Jül - 1425
Juni 1977

Als Manuskript gedruckt
ISSN 0366-0885

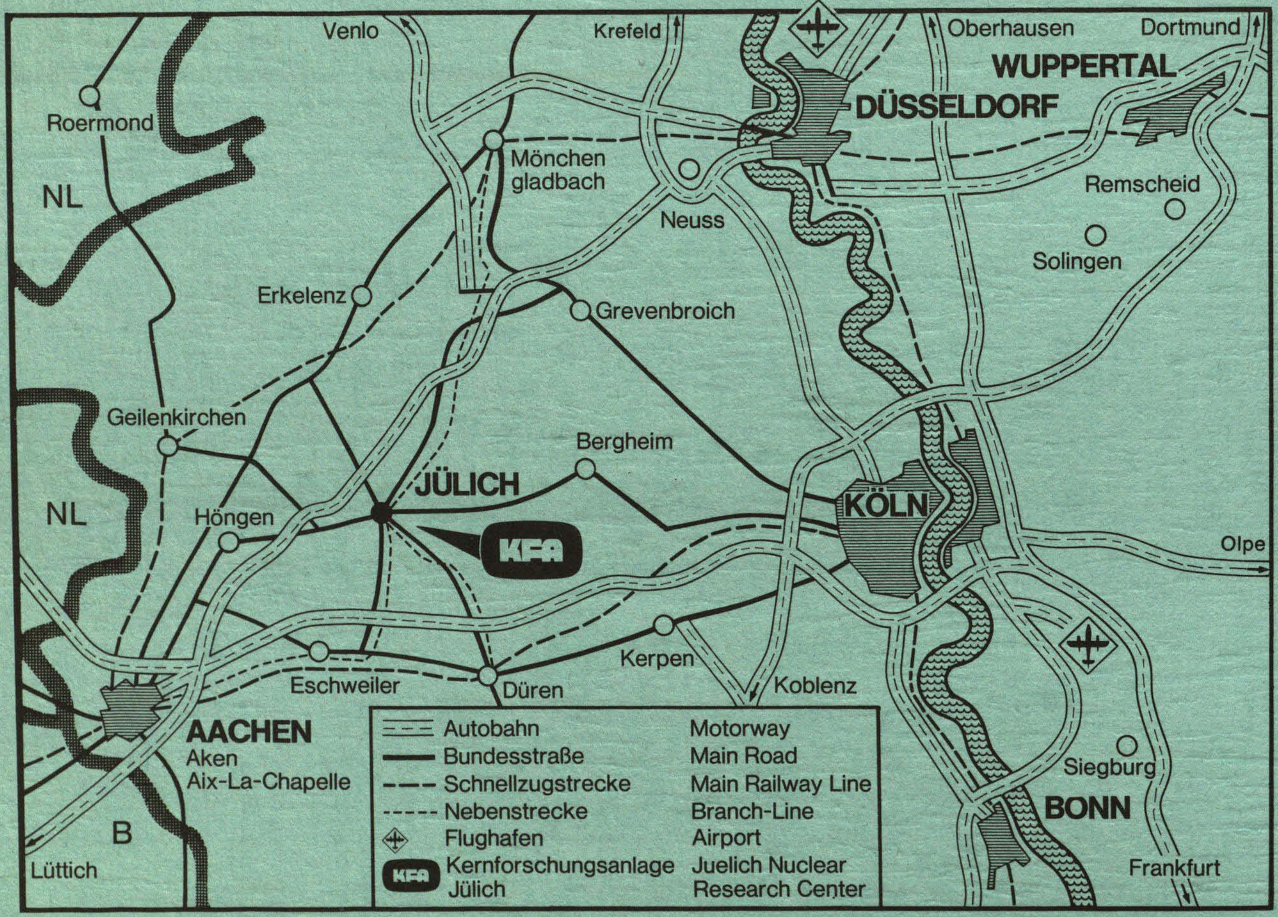

Berichte der Kernforschungsanlage Jülich – Nr. 1425

Institut für Kernphysik Jül - 1425

Im Tausch zu beziehen durch: ZENTRALBIBLIOTHEK der Kernforschungsanlage Jülich GmbH,
Jülich, Bundesrepublik Deutschland

Microscopic Description of Giant Electric and Magnetic Multipole Resonances in Closed - Shell Nuclei

by

Sanchez - Dehesa, J.

D 5 (Diss. Uni. Bonn)

CONTENTS

V o r w o r t

Für die Anregung zum Thema der vorliegenden Arbeit bin ich Herrn Prof. Dr. Amand Fäßler und Herrn Prof. Dr. Josef Speth zu besonderem Dank verplichtet. Ihre wohlwollende Unterstützung sowie ihre wertvollen Anregungen und nützlichen Hinweise waren mir eine große Hilfe. Außerdem möchte ich Herrn Dr. Siegfried Krewald für die fruchtbare Zusammenarbeit, viele hilfreiche Diskussionen und seinen freundschaftlichen Rat Dank sagen.

Sehr wichtig waren mir auch die zahlreichen Hinweise, freundliche Hilfe und Interesse an meiner Arbeit der Herren Dr. E. Hefter, Dr. V. Klemt, Prof. Dr. V. Madsen, Prof. Dr. C. Mayer-Böricke, Dr. M. Ploszajczak und Dipl. Phys. J. Wambach. Ihnen und allen anderen Institutsmitgliedern danke ich für die vielen kritischen Diskussionen.

Die umfangreichen numerischen Rechnungen wurden mir durch die hervorragende Arbeit des Rechenzentrums der Kernforschungsanlage Jülich sowie zahlreiche und hilfreiche programmtechnische Hinweise von Herrn Ewald Brökel ermöglicht. Frau D. Krüger und Fräulein M. Heese gilt mein herzlicher Dank für ihre Geduld und Sorgfalt bei der Zusammenstellung des Manuskripts. Gloria möchte ich an dieser Stelle für ihr Verständnis danken, das sie zeigte, als ich diese Arbeit schrieb.

Nicht zuletzt danke ich dem DAAD und der Kernforschungsanlage Jülich für die finanzielle Unterstützung.

To

my parents

Eugenio and Rosa

I. INTRODUCTION

In the last few years one of the most exciting phenomena in nuclear physics has been the observation of the so-called giant multipole resonances. One can define a Giant Multipole Resonance (GMR) as any nuclear state or group of overlapping states which has the following properties:

i) It exhausts a large fraction of the energy-weighted sum rule (EWSR) strength allowed for that multipole and type (isoscalar or isovector) of excitation

ii) It appears in a systematic way in many nuclei

iii) It is concentrated in a relatively narrow energy region

Contrary to the resolved discrete low-lying ("bound") states (i. e. those characterized by excitation energies of order 1 MeV) which depend on the detailed shell structure of nuclei, the giant resonances, whose characteristic energies are of order 10 MeV, have structure governed by gross or average nuclear properties. These collective multipole states are then caracteristic normal modes of nuclei.

Nowadays apart from the well known electric isovector giant dipole resonance, recent experimental evidence has firmly established the existence of an isoscalar giant quadrupole resonance over the whole periodic table. Moreover there is some evidence for other electric resonances such as the isoscalar monopole and octupole and the isovector quadrupole states as well as for the magnetic dipole excitations. To identify these normal modes and elucidate their properties is a fundamental task for the understanding of nuclei. It is of special interest the identification of the giant magnetic dipole resonance because it can supply a very accurate test of the spin-dependent part of the effective nucleon-nucleon interaction and the giant monopole "breathing" or compressional mode from which one can directly extract the nuclear compressibility which is very difficult to obtain otherwise.

In the present work all of these normal modes in the nuclei ^{12}C, ^{16}O, ^{90}Zr and ^{208}Pb are investigated with the use of the zero-range density-dependent Migdal force in framework of a new method which we have called Core-Coupling Random-Pahse-Approximation (in short, Core-Coupling RPA). This method is developed in section III. It is a special type of two particle - two hole RPA approach which has two important advantages compared to the conventional one: first we get more physical insight into the structure of giant multipole resonances and secondly, we avoid the diagonalization of very large matrices. The latter permit us to treat almost equally easily light, medium and heavy nuclei. In this procedure the GMR's are described by means of quasiparticle-quasihole excitations, i. e. in terms of conventional 1p-1h plus 2p-2h configurations. In order to properly situate our work in this rapidly changing field, a short experimental and theoretical outlook is presented in chapter II. The performance of the numerical calculations in the Core-Coupling RPA theory is explained in detail in the fourth chapter.

In chapter V the (1p-1h + 2p-2h) description of the giant electric and magnetic multipole resonances is explicitly shown. In particular the location and spreading widths of the resonances, their detailed wavefunctions, the electromagnetic transition probabilities to the ground state, ... In chapter VI we sum up the results of our work. The principal conclusion is that we have developed a microscopic theory which, to a very large extent, is able to describe with the same density-dependent nucleon-nucleon interaction, (1) the gross features of the low-lying and the intermediate giant resonance energy region, e. g. the percentages of the EWSR limits depleted by the different types of multipole resonances in the closed-shell nuclei, and (2) the detailed structure of the excited states existing in both regions. Chapter VII and VIII contain appendices and references, respectively.

II. EXPERIMENTAL AND THEORETICAL OUTLOOK

Till this decade the only known GMR was the electric isovector giant dipole resonance (GDR; 1^-, T = 1) whose excitation energy ranges from $\sim$ 63 $A^{-1/3}$ in light nuclei to $\sim$ 80 $A^{-1/3}$ in medium and heavy nuclei. This resonance was predicted theoretically by Migdal[1] and observed in photoabsorption cross-section[2-6] over the whole periodic table. It was found its width to vary between 3 and 6 MeV. Phenomenological descriptions of this resonance were given by Goldhaber & Teller[25] and Steinwendel & Jensen[26] as a collective oscillation of protons against neutrons. Microscopically Wilkinson[7] proposed first a description of the GDR in terms of the shell model; Brown & Bolsterli[8] gave a qualitative description in terms of the schematic model[9] by intoducing a (residual) particle-hole interaction. A realistic description of the odd-parity states in closed-shell nuclei was given by Gillet et al.[10] in the framework of the Random-Phase-Approximation. The decay width of the GDR has been calculated[11-17] by several authors in the continuum shell model[18]. It has been shown that the 1p-1h formalism is unable to reproduce the observed fine structure of the GDR. Qualitative approaches have been suggested by Gillet et al.[14] and by Wang & Shakin[17] in considering the coupling of 1p-1h states with 2p-2h or 3p-3h configurations, respectively.

An isoscalar electric quadrupole (E2) resonance was predicted on quite general arguments by Blatt & Weisskopf[18a] and Bohr & Mottelson[19,20] who placed it at an excitation energy of 58$A^{-1/3}$ MeV. From the experimental side, one could also suspect the possible existence of giant resonances of multipolarity other than E1. Table I shows the results from inelastic proton and alpha measurements[21-24], which excite isoscalar transitions in a very selective way, on the nuclei ^{40}Ca and ^{208}Pb in which the states of the entire "bound" excitation region (i. e. excitation energies up to approximately the neutron separation energy) are examined by means of their depletion of collective multipole sum rule strengths. From this table one naturally infers that a great part of the EWSR limits of different multipoles is to be found at higher excitation energies. Because of approximate selection rules of multipole operators between single-particle harmonic oscillator states one could expect that his missing collective multipole strength is to be concentrated in the giant resonance region, i. e. at excitation energies of the order of 10 MeV.

Many inelastic electron[27-30] and proton measurements as well as inelastic helium-3 [31,32], alpha[35,36] and deuteron[37] scattering and particle capture reaction (x,γ)[38-43] have shown evidence of electric giant resonances other than E1. In particular the existence of a new giant resonance, which is predominantly of T = 0 E2 character, seems now to be firmly established at an excitation energy of about $\sim 63\ A^{-1/3}$ in nuclei with $A > 40$. Its width ranges[24] from ~ 3 to 6 MeV and its excitation strength exhausts[44] a major part (> 50 %) of the isoscalar E2 EWSR. In lighter nuclei the E2 strength seems to be spread over a larger energy region (~ 10 MeV) what causes more difficulties for its identification[35,45-55].

The localization of the multipole collective strength other than E1 and E2 at high excitation energies is still rudimentary. Two different groups in inelastic electron[56,57,58] and deuteron[59] scattering experiments seem to have found evidence of an isoscalar monopole resonance at $\sim 80\ A^{-1/3}$ in ^{40}Ca, ^{90}Zr and ^{208}Pb. At about the same energy, inelastic α-scattering measurements[60] have shown the existence of a new isoscalar resonance in addition to the well-known GQR. The angular distribution of the new resonance is well described by a L = 0 or L = 2 transfer although the L = 4 transfer is also not consistent. Indirect evidence of isoscalar E4 and E0 in the GQR region has been also given by comparing microscopic model calculations[61] with hadron scattering measurements. There is no systematic observation of a giant octupole resonance, although in some (α,α') spectra in nuclei from ^{90}Zr to ^{154}Sm a T = 0 E3 resonance has been detected and seems to deplete 17 - 22 % of the isoscalar E3 EWSR. Finally, two-step methods[52,62-66] have also been used to make resonance predictions; they are based on microscopic analyses of nucleon scattering to low-lying unnatural parity states (e. g. 2^- levels) in which the giant resonances are considered as doorway states.

Experimental evidence concerning magnetic excitations is shown up at backward angles in the electron scattering spectra[67-68]. Especially interesting is the case of ^{208}Pb where photoneutron polarization techniques[69-73] and measurements[74] of directional correlations between particles inelastically scattered and ground state γ-decay have shown evidence that most of the M1 strength is located in two peaks between 7 and 8 MeV. The energy location of these two peaks with respect to the neutron emission threshold ($\sim$7.38 MeV) is a question which is nowadays stirring much controversy. From the theoretical side, Vergados[75] predicted the existence of only one state which would exhaust almost all the M1 strength. In 1973 Ring & Speth[76] were able to predict the existence of two M1 peaks at almost the experimentally observed excitation energies.

The present work[77] presents for the first time a theoretical qualitative and quantitative explanation for the observed fine structure of the low-lying M1 states. On the other hand, Speth et al.[78] have predicted the existence of very collective M1 states at higher excitation energies in ^{208}Pb but so far no experimental evidence has supported them.

There are essentially three groups of microscopic theories which investigate the structure of the giant multipole resonances in spherical nuclei. To the first group belong the generator coordinate methods (GCM)[79,193] the (adiabatic) time-dependent Hartree-Fock[80-82] and the cranking approaches to the collective motion[80-81]. They essentially impose the collective nature of the states from the very beginning; on the other hand the mixing of these states with particle excitations is not treated, hence they say nothing about the width of a collective state. The second class contains the random-phase-approximation (RPA)[76-77,83-99] and other shell model particle-hole calculations[101-104]. Finally there exist the so-called "sum-rule theories"[105-107,82] which are very useful to expose systematic qualitative features of collective excited states in an elegant and simple mathematical way and to establish relations between the first two groups of theories above mentioned. However they present the following deficiency: one has to suppose a resonance line-shape in order to get the spread of the resonance.

The RPA theories appear to be the most complete and detailed method to investigate the collective giant multipole resonances. They have two important merits: (1) the collectivity of excited states emerge from calculations and (2) the spreading of the collective states is treated as arising from interaction with discrete particle, in general multiparticle, excitations (i. e. the so-called spreading width) and with continuum particle excitations (i. e. the decay width). The price one has to pay for that is the performance of at times very large particle-hole calculations what causes serious technical problems.

After the pioneering RPA calculations of Gillet et al.[10,14], many others[76-77,83-104,108] have followed to cover other spherical nuclei. Most of the "bound" 1p-1h RPA calculations are able to explain the position of the giant electric resonances but not the width because either they do not consider continuum single-particle states or, if yes, they discretized them. Among them, those performed in ^{208}Pb by Ring and Speth[76,96] have revealed to be specially successful in predicting the location of giant electric (see also the calculations of Bertsch and Tsai[87])and magnetic resonances; they use the zero-range density-dependent force of Migdal[109] with parameters adjusted[83] to reproduce various known moments and electromagnetic transition probabilities between low-lying levels in the lead region. In these calculations as well as in those performed by Krewald and Speth[84,90] in other spherical nuclei all the single-particle states 2 $\hbar\omega$ above and 2 $\hbar\omega$ below the Fermi surface were for the first time considered.

To get the width of the resonances, two types of extensions of these 1p-1h RPA calculations were undertaken. First the inclusion of the coupling of the particles of the continuum with a proper treatment of this (i. e. no discretization of single-particle continuum states) was performed by Krewald et al.[16,85,90] and by Bertsch et al.[92]. Continuum 1p-1h RPA calculations with the additional improvement of selfconsistency has been done by Krewald et al.[108] and Liu and Giai[93]. These calculations give the decay width of the giant resonances which results to be $\sim$10 % of the total observed width as was previously expected[4,110].

It is then natural to think that the main part of the experimental width of the giant multipole resonances is due to the broadening (spreading width) caused by the coupling of 1p-1h excitations with more complex configurations, e. g. like 2p-2h states. To get the spreading widths of GMR's is then necessary the extension of the bound 1p-1h RPA calculations to include 2p-2h configurations. The first 2p-2h calculations[111-112] were performed in the sixties but their aim was the description of the low-lying states of positive partiy states of ^{16}O. Most recently and simultaneously with the present (1p-1h + 2p-2h) RPA work[77,97-99] more sophisticated shell model calculations with inclusion of 2p-2h states have been done in ^{12}C and ^{16}O by the Erlangen[101,103] group and in ^{16}O and ^{40}Ca by the Tokio[104] group with the purpose of obtaining the spreading widths of GMR's.

III. THEORY

The usual Random-Phase-Approximation or to be more precise the "bound" 1p-1h RPA theory[10,95] permits to calculate excitation energies and ground state transition strengths, and gives a good and consistent description of nuclear spectra in closed shell nuclei. In particular it satisfies sum rules, and one is able at least in principle to separate out spurious excited states; it also allows for the inclusion of correlations in the ground state, i. e. a "diffused" Fermi surface, by the so-called "backward-going" graphs. Different methods have been used to derive the RPA, namely the Green function formalism[96,147], the time-dependent Hartree-Fock theory[148] (TDHF theory), the equations-of-motion method[149] and the so-called quasi-boson approximation or method of linearized equations-of-motion[8]. The final RPA equations are identical in all the four cases.

The Green function formalism gives more insight (see the recent review of Speth et al.[96]) into the validity of the RPA approach. In particular it clearly shows that the RPA amplitudes are the overlap integrals between the excited states and a particle-hole pair $a_1^+ a_2$ acting on the exact or correlated ground state ("physical vacuum"). Therefore the RPA method especially well describes those excited states with a strong transition probability to the ground state. In the usual 1p-1h RPA[8], which is also called "first RPA", the operator which, when acting on the correlated ground state, describes an excited state of a nucleus is written down as follows

$$B_\alpha^+ = \sum_{mi} \left\{ x_{mi}^{(\alpha)} \; a_m^+ \, a_i \; - \; y_{mi}^{(\alpha)} \; a_i^+ \, a_m \right\} \tag{3.1}$$

where a_m^+ creates a particle of angular momentum j_m with projection m_m, and a_i creates a hole of angular momentum j_i and projection $-m_i$. The absence of a particle of projection m_i behaves like a particle with projection $-m_i$. The symbol j stands for a set of all the quantum numbers necessary in specifying the orbit, i. e. (n,l,j). The x's and y's are amplitudes which are determined by requiring the operator to obey the relevant equations of motion.

A step further to the RPA approach is given in the so-called 2p-2h RPA. In this theory the excitation operator, i. e. the operator supposed to describe the excited states of nuclei, includes also mixing of 1p-1h and 2p-2h excitations, i. e.

$$Q^{+} = \sum_{\alpha} \eta_{\alpha} B_{\alpha}^{+} + \sum_{\alpha\lambda} \eta_{\alpha\lambda} B_{\alpha}^{+} B_{\lambda}^{+} \tag{3.2}$$

In this way the dimensions of the corresponding RPA matrix are raised by an order of magnitude due to the inclusion of 2p-2h operators. This obliges to make drastic truncations in the particle-hole space and therefore such calculations[149-151] are hardly realistic.

In this section we develop a formulation of the (2p-2h) RPA which differs much from the originally proposed by Sawicki et al.[150] and used with slight modifications by other authors[151,112]. Although the structure of the final secular matrix is very similar. The purpose of the new formalism, which we have called Core-Coupling Random-Phase-Approximation, is twofold. First we want to have a simple physical picture as in the first RPA. On the other hand we desire to reduce the dimensions of the second RPA secular matrix by working directly with an expansion of the type (3.2) and a limited set of excitation operators of a previous first RPA. To achieve this, one supposes that the excited states of a nucleus are difined by the following operator

$$Q^{+} = \sum_{mi} \left\{ X_{mi}\, \chi_m^{+}\, \chi_i - Y_{mi}\, \chi_i^{+}\, \chi_m \right\} \tag{3.3}$$

when acting on a correlated ground state $|\phi_o\rangle$. The operators χ_m^{+} and χ_i create, when acting on $|\phi_o\rangle$, a "quasiparticle" or "quasihole" state in the Landau-

Migdal sense, i. e. they are defined as

$$\chi_m^+ = C_m\, a_m^+ + \sum_{\alpha\nu} C_{\alpha\nu}^{(m)}\, B_\alpha^+\, a_\nu^+ \tag{3.4}$$

$$\chi_i = C_i\, a_i + \sum_{\alpha\mu} C_{\alpha\mu}^{(i)}\, B_\alpha^+\, a_\mu \tag{3.5}$$

where a_m^+ and a_i are the usual and previously defined creation and annihilation operators. The operator a_2^+ creates a particle state above the Fermi surface ($\nu > F$) and a_μ creates a hole below the Fermi surface ($\mu < F$). The operator B_α^+ is defined by (3.1). Following equation (3.4), a "quasiparticle" is a "dressed" shell model particle, i. e. a single particle of the shell model surrounded by a polarization cloud becuase it polarizes the core via its interactions with the core particles. In other words one can say that a quasiparticle is a single-particle which contains many 2p-1h admixtures. In an analogous way one would define a quasihole as a single-hole in the sense of the shell model but dressed with many 2h-1p admixtures.

From (3.3) one observes that the nucleus may be excited in two different ways which take part simultaneously: by creating quasiparticle-quasihole pairs and by distroying quasiparticle-quasihole pairs already present in the ground state. Then the two-body correlations existing in the ground state imply admixtures of excited 1p-1h and 2p-2h configurations in its wave-functions.

The structure of this chapter is as follows. In section 1 the Hamiltonian, i. e. the assumed residual interactions, is given. In section 2 the way of determining quasiparticle states is shown and its creation operator, i. e. (3.4), (3.5), is derived in extending the theory of finite Fermi systems of Landau-Migdal[1,96]. Section 3 is devoted to derive the equations of motion of the excitation operator Q^+ defined by (3.3). Finally in section 4 the formulae necessary in computing the electromagnetic transition porbabilities are found.

III.1. The Hamiltonian

In the second-quantized form the assumed full nuclear Hamiltonian is:

$$H = H_0 + V = \sum_{\alpha\beta} \varepsilon_{\alpha\beta} \; a_\alpha^+ a_\beta + \frac{1}{2} \sum_{\alpha\beta\gamma\delta} v_{\alpha\beta\gamma\delta} \; a_\alpha^+ a_\beta^+ a_\delta \; a_\gamma \tag{3.6}$$

where a_α^+, a_β are the already defined creation and annihilation operators which obey the usual anticommutation rules

$$\begin{aligned} [a_\alpha, a_{\alpha'}^+] &= a_\alpha \, a_{\alpha'}^+ + a_{\alpha'}^+ \, a_\alpha = \delta_{\alpha\alpha'} \\ [a_\alpha, a_{\alpha'}] &= [a_\alpha^+, \, a_{\alpha'}^+] = 0 \end{aligned} \tag{3.7}$$

The symbol $\varepsilon_{\alpha\beta}$ denotes the sum of contributions from all single-particle operators and the effective single-particle part of the residual interaction V.

Moreover one should understand the antisymmetrized matrix element $v_{\alpha\beta\gamma\delta}$ of the residual interaction V as

$$v_{\alpha\beta\gamma\delta} = \langle\alpha\beta|V|\gamma\delta\rangle$$

On the other hand we shall denote by $|An\rangle$ the exact eigenstates of a nucleus with A nucleons and by E_n^A the corresponding energy eigenvalues, i. e. so that

$$H \; |An\rangle = E_n^A \; |An\rangle \tag{3.8}$$

The states $|An\rangle$ are assumed to be normalized, i. e. $\langle An|An'\rangle = \delta_{nn'}$. In this notation the ground state shall be symbolized by $|A0\rangle$. The particle number A will always refer to a closed shell nucleus; nuclei with a particle more or less than a closed shell nucleus are referred to as A ± 1 nuclei.

III.2. Determination of the Quasiparticle States

One of the fundaments of the Landau-Migdal finite Fermi systems[1,96] (in short FFS theory) is the quasiparticle concept. In the original formulation of this theory the coupling between the particle or hole with the collective excitations of the core is neglected. In this section the FFS theory is extended to include the interaction between the simple quasiparticle states and the core-excitations by the following method developed by Werner et al.[152,153]. This extension of the theory has the additional interest of allowing the calculation of the distribution of single-particle or single-hole strengths, as measured in stripping or pick-up reactions, over single-particle states and states in which single-particle states are coupled to core excitations, i. e. and 2p-1h or 2h-1p states. In this section as in the other ones we only refer to spherical nuclei around closed shells where pairing forces can be neglected.

$$G(1,2) = \frac{1}{i} \langle Ao|T\{a(1)a^+(2)\}|AO\rangle \tag{3.9}$$

where T denotes the time ordering operator and the arguments 1,2 include space, spin and time coordinates. In the spectral representation obtained by taking the Fourier transform of G(1.2), it turns out that

$$G_{\nu_1\nu_2}(\omega) = \sum_{\substack{\alpha \\ \text{Particle states}}} \frac{\sqrt{Z^{(\alpha)}_{\nu_1} Z^{(\alpha)}_{\nu_2}}}{\omega - \omega_\alpha + i\delta} + \sum_{\substack{\mu \\ \text{Hole states}}} \frac{\sqrt{Z^{(\mu)}_{\nu_1} Z^{(\mu)}_{\nu_2}}}{\omega - \omega_\mu - i\delta} \tag{3.10}$$

where the sums run over all states α and μ of the A + 1 nucleus and the A - 1 nucleus respectively. The quantities $Z^{(\alpha)}_\nu$ and $Z^{(\mu)}_\nu$ are defined as follows

$$\begin{aligned} Z^{(\alpha)}_\nu &= |\langle A+1\alpha|a^+_\nu|AO\rangle|^2 \\ Z^{(\mu)}_\nu &= |\langle A-1\mu|a_\nu|AO\rangle|^2 \end{aligned} \tag{3.11}$$

which are usually called single-particle strengths and single-hole strengths of the state ν. Besides the poles of the single-particle propagator locate at the energies

$$\begin{aligned} \omega_\alpha &= E_\alpha^{A+1} - E_o^A \\ \omega_\mu &= E_\mu^{A-1} - E_o^A \end{aligned} \tag{3.12}$$

where E_0^A refers to the ground state energy of the A-particle nucleus.

To calculate the quasiparticle propagator, one has to solve the equation of motion of G or the Dyson equation

$$G_{12}(\omega) = G_{12}^o(\omega) + G_{13}^o(\omega)\ M_{34}(\omega)\ G_{42}(\omega) \tag{3.13}$$

where the $G_{12}^o(\omega)$ represents the unperturbed single-particle propagator and $M_{34}(\omega)$ is the mass operator or proper self-energy[154] (of the quasiparticle) which contains all Feynman graphs which cannot be separated into two pieces by cutting a single-particle or single-hole line. Graphically this equation is shown in figure 1 in which the thick line represents the exact propagator G_{12} and the weak line the unperturbed one.

In the usual cases, G_{12}, G_{12}^o and M_{34} are[154] all diagonal in the matrix indices and the Dyson equation can be written down as:

$$G_\nu(\omega) = G_\nu^o(\omega) + G_\nu^o(\omega)\ M_\nu(\omega)\ G_\nu(\omega) \tag{3.14}$$

G_ν^o is conveniently chosen to be the propagator of a single-particle or single-hole in a shell model potential. The operator $M_\nu(\omega)$ contains only the effect of the residual interactions. One can then write this equation as follows:

$$\left[\omega - T - M(\omega)\right]\ G(\omega) = 1 \tag{3.15}$$

which is equivalent to the following non-local Schrödinger equation

$$- \frac{h^2}{2m} \Delta \phi_\alpha(\vec{r}) + \int dr'^3 \, M(\vec{r},\vec{r}',\omega) \, \phi_\alpha(\vec{r}') = \varepsilon_\alpha(\omega) \, \phi_\alpha(\vec{r}) \tag{3.16}$$

where the single-particle wave function $\phi_\alpha(\vec{r})$ is determined by the requirement

$$\varepsilon_\alpha(\omega) = \omega \tag{3.17}$$

The mass operator can now be splitted into two parts

$$M_\nu(\omega) = M_\nu^{(1)}(\omega) + M_\nu^{(2)}(\omega) = V_0 + M^{(c)}(\omega) \tag{3.18}$$

where the first part is weakly energy dependent and corresponds to a non-local single-particle potential V_0. In actual calculations it is taken into account by a Woods-Saxon potential, the parameters of which are determined by a least square fit of the experimental energies of the single-particle states. The second part is strongly energy dependent and comes from the polarization of the core nucleus due to the motion of the odd particle. Since $M^{(c)}(\omega)$ may also have weakly energy dependent contributions which are already accounted for in V_0, we have to take care of such double counting. It is avoided by changing the potential in such a way that the dominant pole of $G(\omega)$ falls at the experimentally detected energy.

Inserting (3.18) in equation (3.15) one gets:

$$\left[\omega - T - V_0 - M^{(c)}(\omega)\right] G(\omega) = 1 \tag{3.19}$$

whose solutions can be expressed in the form

$$G_\nu(\omega) = \frac{Z_\nu}{\omega - \varepsilon_\nu} + R_\nu(\omega) \tag{3.20}$$

where ε_ν and Z_ν are supposed to be the energy and single-particle strength of the dominant pole. The latter can be obtained as follows:

$$Z_\nu = \left[1 - \left.\frac{dM_\nu^{(c)}(\omega)}{d\omega}\right|_{\omega=\varepsilon_\nu}\right]^{-1} \tag{3.21}$$

The rest $R_\nu(\omega)$ contains all the other poles of $G(\omega)$. In the usual FFS theory only one dominant pole is taken into account; its strength Z_ν and the rest $R_\nu(\omega)$ are considered by a renormalization of the effective interaction. But here the poles other than the dominant one are obtained by solving the following non-linear eigenvalue problem

$$(T+V_0)\ \phi_\alpha(\vec{r}) + \int d\vec{r}\cdot M^{(c)}(\vec{r},\vec{r}\,';\omega)\ \phi_\alpha(\vec{r}\,') = \varepsilon_\alpha(\omega)\ \phi_\alpha(\vec{r}\,') \tag{3.22}$$

which is equivalent to (3.19). The resulting wave functions are single-particle wave functions for the states with small single-particle strength, i. e. for the states corresponding to the "non-dominant" poles.

To go further it is necessary to make an ansatz for the mass operator $M^{(c)}(\omega)$. For that we shall use the core-excitation model, often used in shell model calculations[155)]. In this model the states of a (A+1)-particle nucleus which give rise to large single-particle strengths are states where a single-particle state is coupled to an excited state of the corresponding A nucleus. In our formalism this means that the most important energy-dependent contributions to $M^{(c)}(\omega)$ are those arisen from the coupling between the collective states of the core nucleus and the one-quasiparticle states of neighbouring nuclei. These are graphically shown in Figure 2a. The symbols attached to the lines refer to the quantum numbers of the propagating states. In this graph the straight line represents a single-nucleon propagator and the wriggly line a core excitation, which is also shown on the right hand side of the figure as a string of bubles, i. e. the usual microscopic representation of a core excitation.

The matrix element of the mass operator corresponding to all graphs of the type shown in Fig. 2a is as follows:

$$M^{(c)}_{\nu_1\nu_2}(\omega) = \sum_{\mu m} \frac{(\gamma^{\mu;m}_{\nu_1})^*\ \gamma^{\mu;m}_{\nu_2}}{\omega - \Omega_\mu - \varepsilon_m} \tag{3.23}$$

where the sum runs over all low-lying collective states μ of the core and all quasiparticle states m. Here Ω_μ and ε_m are the energy of the excited core state and the one-quasiparticle energy respectively. The explicit form of the vertex $\gamma_{\nu_1}^{\mu;m}$ which couples the quasiparticle $|m>$ to the core excited configruration $|\mu> \otimes |m>$ can be written down in terms of the particle-hole (ph) interaction F^{ph} and the ph-amplitudes $X^{(\mu)}$ of the core vibration $|\mu>$ as follows:

$$\gamma_\nu^{\mu;m} = \sum_{\varkappa\lambda} F^{ph}_{\nu\varkappa;\mu\lambda} \; X^{(\mu)}_{\varkappa\lambda} \tag{3.24}$$

where $F^{ph}_{\nu\varkappa;\mu\lambda}$ is the renormalized effective ph-interaction, which is parametrized by Migdal et al.[109] by a density dependent contact force with the usual spin and isospin dependence.

It is important to remark that once the ph-interaction has been chosen, no further parameters are necessary in including the mentioned coupling with core vibrations since the ph-amplitudes are obtained by solving the usual RPA equation with the same force. In other words, the vertex γ contains no free parameters. Rigorously speaking one should use solutions of equation (3.22) in the evaluation of γ in order to be selfconsistent but the use of shell model wave functions simplifies very much the whole procedure and is also well justified as is shown in ref.[160].

Although we always refer to quasiparticle states, i. e. states of the A+1 nucleus, the whole treatment is completely analogous for the quasihole states, i. e. states of the A-1 nucleus; in this case the graph corresponding to Fig. 2a is shown in Fig. 2b.

One should emphasize that with the ansatz (3.23) for $M^{(c)}(\omega)$, the Pauli Principle is certainly violated even in this lowest order of particle-core coupling. One reason is because the core excitation is usually calculated independently of the quasiparticle, hence the excited particle of the ph-vibration cannot reach all states since some are already blocked by the additional particle. Another reason is the noninclusion of the exchange graphs of Figure 3 and those graphs which arise because of the pp-ground state correlations as shown in Figure 4. However these graphs contribute to $M^{(c)}(\omega)$ with different signs[156] and we have supposed that they cancelled one to another; actually arguments have been already given[157] in this direction. Other diagrams which are neglected in $M^{(c)}(\omega)$ are all those of higher order in particle-core coupling and which are schematically represented in Fig. 5. In this figure the rectangle symbolizes "any" possible structrue except the free propagation of the particle and core excitation, e. g. the diagrams of Figures 6a and 6b. Here once the propagating particle has excited a core vibration, the quasiparticle-plus-core excitation may polarize yet another core mode. If the original core excitation disappears first, we obtain the diagram of Figure 6a, but if the second excitation deexcites first we get the nested diagram of Fig. 6b.

All these neglected contributions, i. e. diagrams of Fig. 3, 4 and 5, will certainly influence the positions and residua of the secondary poles of the propagators. Therefore we shall not be able to calculate detailed phenomena of the A±1 nuclei such as for example the suptuplet structure observed in ^{209}Bi which arises[158] from the coupling ($1h_{9/2} * 3^-$). However the neglected effects are supposed of little importance in our case since we want to study the average distribution of the poles and their strengths as well as the predominant structure of its corresponding wave functions. Attempts[159] to take into account a number of these neglected diagrams are being done but no definitive conclusion has been achieved.

Taking into account that we work in the diagonal approximation as said before, the mass operator (3.23) adopts the form:

$$M_\nu^{(c)}(\omega) = \sum_{\mu m} \frac{|\gamma_\nu^{\mu;m}|^2}{\omega - \Omega_\mu - \varepsilon_m} \tag{3.25}$$

Then the Dyson equation (3.19) we have to solve is as follows:

$$\left[\omega - \tilde{\varepsilon}_\nu - \sum_{\mu m} \frac{|\gamma_\nu^{\mu;m}|^2}{\omega - \Omega_\mu - \varepsilon_m}\right] G_\nu(\omega) = 1 \tag{3.26}$$

where the symbol $\tilde{\varepsilon}_\nu$ denotes the energy of the quasiparticle state for vanishing quasiparticle-phonon coupling, i. e. when $M^{(c)}(\omega) = 0$. However these energies have no real physical meaning since they are adjusted in such a way that the dominant poles of $G(\omega)$, i. e. the poles with the larger residua, locate at the experimental energies. This is done as follows:

$$\tilde{\varepsilon}_\nu = \varepsilon_{exp} - \sum_{\mu m} \frac{|\gamma_\nu^{\mu;m}|^2}{\varepsilon_{exp} - \Omega_\mu - \varepsilon_m} \tag{3.27}$$

It is then clear that the solution of equation (3.26) is done iteratively. It gives us the energy positions ω of the poles of $G_\nu(\omega)$. Their residua are to be obtained by equation (3.21) from the gradient of $M^{(c)}(\omega)$. Only one pole is obtained by neglecting the mass operator. But when $M^{(c)}(w) \neq 0$, the structure of $G_\nu(w)$ presents further poles due to the supplementary poles from the own structure of the mass operator, what means that higher configurations have been included. If it results that $G_\nu(w)$ has a pole with a single-particle strength (residuum) near to 1 and the other poles have small residua, then we have the quasiparticle interpretation.

In our case we have considered those configurations coming from the graphs of Figure 2, what means 2p-1h and 2h-1p configurations. Following Ring and Werner[153], we solve eq. (3.26) by diagonalizing the matrix

$$\begin{pmatrix} \tilde{\varepsilon}_\nu & \gamma_\nu^{\mu_1;m_2} & \gamma_\nu^{\mu_2;m_2} & . & \cdots & \gamma_\nu^{\mu_r;m_s} \\ \gamma_\nu^{*\mu_1;m_1} & \Omega_{\mu_1}+\varepsilon_{m_1} & 0 & 0 & & 0 \\ \gamma_\nu^{*\mu_2;m_2} & 0 & \Omega_{\mu_2}+\varepsilon_{m_2} & 0 & \cdots & 0 \\ \vdots & 0 & 0 & \ddots & & \\ & \vdots & \vdots & & & \\ \gamma_\nu^{*\mu_r;m_s} & 0 & 0 & \cdots & & \Omega_{\mu_r}+\varepsilon_{m_s} \end{pmatrix} \qquad (3.28)$$

The solutions of the eigenvalue problem of this matrix corresponds to the energies and wavefunctions of the problem of diagonalizing the nuclear Hamiltonian in the space formed by the quasiparticle state $|\nu\rangle$ and the coupled states $|\mu \otimes m\rangle$. To be more precise, the space considered in our calculations is that formed by $|p \equiv$ quasiparticle$\rangle$ + $|2p\text{-}1h\rangle$ configurations if we study the states of the A+1 nucleus, $|h \equiv$ quasihole$\rangle$ + $|2h\text{-}1p\rangle$ configurations if we are considering the states of the A-1 nucleus. One should not forget that the exchange graphs of Fig. 3 are not taken into account.

The poles ω_α of $G_\nu(w)$ are then the eigenvalues of the matrix (3.28) which gives us the quasiparticle energies. The corresponding wavefunctions are easily obtained and turn out to be as follows:

$$\left(1, \frac{\gamma^{*\mu_1;m_1}}{\omega_\alpha - \Omega_{\mu_1} - \varepsilon_{m_1}}, \frac{\gamma^{*\mu_2;m_2}}{\omega_\alpha - \Omega_{\mu_2} - \varepsilon_{m_2}}, \ldots, \frac{\gamma^{*\mu_r;m_s}}{\omega_\alpha - \Omega_{\mu_r} - \varepsilon_{m_s}} \right) \qquad (3.29)$$

The residua or the relative single-particle strengths are according to (3.21) and (3.25):

$$Z_\nu^{(\alpha)} = \left[1 + \sum_{\mu m} \frac{|\gamma_\nu^{\mu;m}|^2}{(\omega_\alpha - \Omega_\mu - \varepsilon_m)^2} \right]^{-1} \qquad (3.30)$$

From (3.29) and after normalization to unity, one easily gets the wave function of the quasiparticle of energy ω_α can be written down as follows:

$$\Psi_\alpha = \sqrt{Z_\nu^{(\alpha)}}\ |\nu> + \sum_{\mu m} \sqrt{Z_{\mu m}^{(\alpha)}}\ |\mu \otimes m> \tag{3.31}$$

were $Z_\nu^{(\alpha)} = |<\nu|\Psi_\alpha>|^2$ is given by (3.30) and $Z_{\mu;m}^{(\alpha)}$ is defined by:

$$Z_{\mu;m}^{(\alpha)} = \frac{\overset{*}{\gamma}{}^{\mu;m}}{\omega_\alpha - \Omega_\mu - \varepsilon_m}\ Z_\nu^{(\alpha)} \tag{3.32}$$

One should note once again that because of the particle-core coupling of Figure 2, the pure state $|\nu>$ distributes its single-particle strength over the mixed configurations $|\Psi_\alpha>$, which have of course the same quantum numbers ν.

III.3. Equations of Motion

In this section the equations of motion of the Core-Coupling RPA will be derived. Given the correlated ground state (physical vacuum) $|\phi_o>$ of the nucleus and the Hamiltonian H one can obtain an excited state $|\Psi>$ of the nucleus of the energy E by:

$$|\Psi> = Q^+ |\phi_o> \tag{3.31}$$

where the operator Q^+ verifies the equation

$$[H,Q^+] = E\ Q^+ \tag{3.32}$$

Choosing the ground state energy $E_0 = 0$, i. e. $H|\phi_o> = E_0 |\phi_o> = 0$, one sees that $|\Psi>$ is an eigenstate of H of the energy E. Since $Q|\phi_o>$ results also to be the eigenstate of H with the energy -E, if we want $|\phi_o>$ to be the ground state it must therefore be the vacuum for the Q-excitations, i. e. there must be no excitations created by Q^+ present in the ground state. In other words it must satisfy

$$Q \; |\phi_o> = 0 \qquad (3.3\text{:}$$

In these cases, to solve exactly equation (3.32) is completely equivalent to solving the Schrödinger equation $H \; |\Psi> = E \; |\Psi>$ for the corresponding states. The complexity of the problem is not altered by the simple replacement of the wave function Ψ by the operator Q^+ which generates Ψ from the ground state. Therefore we are obliged not only to solve (3.32) in an approximate way but also to make an ansatz for the operator Q^+ what implies a precise specification of the excited states of the nucleus to be described. Here we supposed that Q^+ is defined by (3.3), i.e. it has the form

$$Q^+ = \sum_{MI} \left\{ X_{MI} \; \chi^+_M \; \chi_I - Y_{MI} \; \chi^+_I \; \chi_M \right\} \qquad (3.34)$$

where χ^+_M and χ_I are operators which when operating on $|\phi_o>$ create a quasiparticle $|M>$ and a quasihole $|I>$ respectively. These concepts have been discussed in the previous section, e. g. see (3.31). Their expressions are:

$$\chi^+_M = C^{(a)}_m \; a^+_m \; + \sum_{\alpha\nu} C^{(m,a)}_{\alpha\nu} \; B^+_\alpha \; a^+_\nu \qquad (3.35)$$

$$\chi_I = C^{(d)}_i \; a_i \; + \sum_{\alpha\mu} C^{(i,d)}_{\alpha\mu} \; B^+_\alpha \; a_\mu \qquad (3.36)$$

where the operator B^+_α is defined by (3.1) and a^+_m and a_i have been already defined in this chapter. More explicit expressions of χ^+_M and χ_I as well as of their Hermitian conjugates are written down in Appendix VII.A. The subindex $M \equiv (m,a)$ where m symbolizes the quantum numbers $(n_m, \; l_m, \; j_m)$ of a quasiparticle $(\varepsilon_m > \varepsilon_F)$ and $\underline{a}$ specifies the precise piece of such quasiparticle; one should remember at this point that the particle strength of the pure quasiparticle state m is distributed into several states $M \equiv (m,a)$ due to the particle-core coupling. In an analogous way $I \equiv (i,d)$ must be understood.

One can easily note that with the ansatz (3.34) we shall be able to describe only those excited (vibrational) states of the nucleus which can be described by 1p-1h excitations plus 2p-2h exciations.

Inserting the operator Q^+ (3.34) and the Hamiltonian (3.6) in eq. (3.32) we shall obtain on the left hand side terms involving products of two a-operators, of four a-operators, ... up to terms involving products of eight such operators; since the right-hand side of (3.32) includes "only" products of six a's, eq. (3.32) cannot generally be satisfied by a Q^+ of the form (3.34). In fact this was to be expected since a transition from an exact ground state to an exact excited state of a system of n-interacting fermions involves generally all kp-kh excitations with k = 1, 2, 3, ... n. To satisfy (3.32) we invoke here a further approximation, namely to neglect those normal products with eight a's. Furthermore all the terms which give rise to the creation of 3p-3h excitations what is out of the scope of our theory. Therefore in the 2p-2h RPA which we are considering here we neglect all the normal products beyond those with four a-operators.

Taking this into account and operating as Sawicki[150)], the secular equation of our second RPA is now obtained as follows:

$$\begin{pmatrix} A & B \\ B^+ & A^+ \end{pmatrix} \begin{pmatrix} X \\ Y \end{pmatrix} = E \begin{pmatrix} X \\ -Y \end{pmatrix} \tag{3.37}$$

with

$$A_{MI,NH} = (\varepsilon_M - \varepsilon_I)\, C_m^{(a)^2}\, C_i^{(d)^2}\, \delta_{MN}\, \delta_{IH} + \langle HM|\mathcal{H}|\widehat{NI}\rangle \tag{3.38}$$

$$B_{MI,NH} = \langle MN|V|\widehat{IH}\rangle \tag{3.39}$$

Here we have adopted the following convention

$$\langle HM|\mathcal{H}|\widehat{NI}\rangle \equiv \langle HM|\mathcal{H}|NI\rangle - \langle HM|\mathcal{H}|IN\rangle \tag{3.40}$$

$$<MN|V|\hat{IH}> \equiv <MN|V|IH> - <MN|V|HI> \tag{3.41}$$

Note that ${C_m^{(a)}}^2$ and ${C_i^{(d)}}^2$ are the single-particle strengths of the corresponding quasiparticles M and I. Explicitly these matrix elements have the following form:

1) $$<MN|V|IJ> = C_m^{(a)}\ C_n^{(b)}\ C_n^{(c)}\ C_i^{(d)}\ <j_m j_i J|V|j_i^{-1} j_h^{-1} J> \tag{3.42}$$

2) The expression for the matrix elements $<HM|\mathcal{H}|NI>$ is written symbolically as follows:

$$<HM|\mathcal{H}|NI> = T_{11} + T_{12} + T_{22} \tag{3.43}$$

where T_{11}, T_{12} and T_{22} are terms involving matrix elements of the interaction between 1p-1h states, between 1p-1h and 2p-2h states and between 2p-2h configurations respectively. Their corresponding expressions are explicitly as follows:

2.a) $$T_{11} = C_m^{(a)}\ C_n^{(b)}\ C_h^{(c)}\ C_i^{(d)}\ <j_m j_h^{-1};J|V|j_n j_i^{-1};J> \tag{3.44}$$

where J is the total angular momentum of the excited state that we are looking for.

2.b) $$\begin{aligned} T_{12} = {} & C_m^{(a)}C_n^{(b)}C_h^{(c)} \sum_{\alpha\mu_1} C_{\alpha\mu_1}^{(id)} \sum_{m_3 i_3} \eta_{m_3 i_3}^{(\alpha)}\ s(j_n,j_i,J)\ <j_h^{-1} j_m;J|\mathcal{H}|j_{m_3} j_{i_3}^{-1}(J_\alpha) j_{\mu_1}^{-1}(j_{\mu_1}^{-1}(j_i) j_n;J> \\ & + C_m^{(a)}C_h^{(c)}C_i^{(d)} \sum_{\alpha\nu_1} C_{\alpha\nu_2}^{(nb)} \sum_{n_1 i_1} \eta_{n_1 i_1}^{(\alpha)}\ <j_h^{-1} j_m;J|\mathcal{H}|j_{n_1} j_{i_1}^{-1}(J_\alpha) j_{\nu_1}(j_n) j_i^{-1};J> \\ & + C_n^{(b)}C_h^{(c)}C_i^{(d)} \sum_{\alpha\nu_2} C_{\alpha\nu_2}^{(ma)} \sum_{m_1 h_1} \xi_{m_1 h_1}^{(\alpha)} s(j_{\nu_2},J_\alpha,j_m) s(j_h,j_m,J) <j_{m_1} j_{h_1}^{-1}(J_\alpha) j_{\nu 2}(j_m) j_h^{-1} J|\mathcal{H}|j_n j_i^{-1};J> \\ & + C_m^{(a)}C_n^{(b)}C_i^{(d)} \sum_{\alpha\mu_2} C_{\alpha\mu_2}^{(hc)} \sum_{m_4 i_4} \xi_{m_4 i_4}^{(\alpha)} s(j_{\mu_2};J_\alpha,j_h) <j_{m_4} j_{i_4}^{-1}(J_\alpha) j_{\mu_2}^{-1}(j_h) j_m;J|\mathcal{H}|j_n j_i^{-1};J> \end{aligned} \tag{3.45}$$

where

$$\eta_{ab}^{(\alpha)} \equiv X_{ab}^{(\alpha)} - (-1)^{j_a+j_b-J_\alpha} Y_{ab}^{(\alpha)}$$

$$\xi_{ab}^{(\alpha)} = (-1)^{j_a+j_b-J} X_{m_4 i_4}^{(\alpha)} - Y_{m_4 i_4}^{(\alpha)} \tag{3.46}$$

$$s(j_a,j_b,j_c) \equiv (-1)^{j_a+j_b-j_c}$$

2.c) $T_{22} =$

$$C_n^{(b)} C_h^{(c)} \sum_{\alpha\nu_2} C_{\alpha\nu_2}^{(ma)} \sum_{m_1h_1} \xi_{m_1h_1}^{(\alpha)} s(j_{\nu_2},J_\alpha,j_m) s(j_h,j_m,J) \sum_{\alpha\mu_1} C_{\alpha\mu_1}^{(id)} \sum_{m_3i_3} \eta_{m_3i_3}^{(\alpha)} s(j_n,j_i,J) \cdot$$
$$\cdot \langle j_{m_1} j_{h_1}^{-1}(J_\alpha) j_{\nu_2}(j_m) j_h^{-1}; J|\mathcal{H}| j_{m_3} j_{i_3}^{-1}(J_\alpha) j_{\mu_1}^{-1}(j_i) j_n; J\rangle$$

$$+ C_m^{(a)} C_n^{(b)} \sum_{\alpha\mu_2} C_{\alpha\mu_2}^{(hc)} \sum_{m_4i_4} \xi_{m_4i_4}^{(\alpha)} s(j_{\mu_2},J_\alpha,j_h) \sum_{\alpha\mu_1} C_{\alpha\mu_1}^{(id)} \sum_{m_3i_3} \eta_{m_3i_3}^{(\alpha)} s(j_i,j_n,J) \cdot$$
$$\cdot \langle j_{m_4} j_{i_4}^{-1}(J_\alpha) j_{\mu_2}^{-1}(j_h) j_m; J|\mathcal{H}| j_{m_3} j_{i_3}(J_\alpha) j_{\mu_1}^{-1}(j_i) j_n; J\rangle \tag{3.47}$$

$$+ C_h^{(c)} C_i^{(d)} \sum_{\alpha\nu_2} C_{\alpha\nu_2}^{(ma)} \sum_{m_1h_1} \xi_{m_1h_1}^{(\alpha)} s(j_{\nu_2},J_\alpha,j_m) s(j_h,j_m,J) \sum_{\alpha\nu_1} C_{\alpha\nu_1}^{(nb)} \sum_{n_1i_1} \eta_{n_1i_1}^{(\alpha)} \cdot$$
$$\cdot \langle j_{m_1} j_{h_1}^{-1}(J_\alpha) j_{\nu_2}(j_m) j_h^{-1}; J|\mathcal{H}| j_{n_1} j_{i_1}^{-1}(J_\alpha) j_{\nu_1}(j_n) j_i^{-1}; J\rangle$$

$$+ C_m^{(a)} C_i^{(d)} \sum_{\alpha\mu_2} C_{\alpha\mu_2}^{(hc)} \sum_{m_4i_4} \xi_{m_4i_4}^{(\alpha)} s(j_{\mu_2},J_\alpha,j_h) \sum_{\alpha\nu_1} C_{\alpha\nu_1}^{(nb)} \sum_{n_1i_1} \eta_{n_1i_1}^{(\alpha)} \cdot$$
$$\cdot \langle j_{m_4} j_{i_4}^{-1}(J_\alpha) j_{\mu_2}^{-1}(j_h) j_m; J|\mathcal{H}| j_{n_1} j_{i_1}^{-1}(J_\alpha) j_{\nu_1}(j_n) j_i^{-1}; J\rangle$$

To understand the angular momentum coupling involved in these formulae, let us "read" one state, for instance

$$|j_{m_3} j_{i_3}^{-1}(J_\alpha) j_{\mu_1}^{-1}(j_i) j_n; J\rangle$$

It represents a 2p-2h state with a peculiar coupling scheme: the angular momenta j_{m_3} and $j_{i_3}^{-1}$ of a particle and a hole state respectively are coupled to the angular momentum J_α of a core excitation, which is itself coupled with the angular momentum $j_{\mu_1}^{-1}$ of a hole state to form the value j_i. This j_i couples finally with the angular momentum j_n of a particle state producing the total angular momentum of the excited states J in which we are interested.

In Appendix VII.B it is briefly shown tha Racah algebra formulae of the matrix elements involved in expressions (3.44), (3.45) and (3.47).

Let us finally remark that the 2p-2h RPA theory, which at times is referred to as Core-Coupling RPA for being more appropriate and pictorial, here presented has as a particular case the first RPA. One can note that if quasiparticles and quasiholes are pure shell model particles and holes respectively, then

$$M \equiv (m,a) \rightarrow m \qquad H \equiv (h,c) \rightarrow h$$

$$N \equiv (n,b) \rightarrow n \qquad I \equiv (i,d) \rightarrow i$$

Hence in particular $C_m^{(a)^2} = C_i^{(d)^2} = 1$ and the equations (3.37) - (3.39) are those of the usual 1p-1h RPA[8].

III.4. Electromagnetic transition rates

After solving the secular matrix eigenvalue problem of the Core-coupling RPA theory, one can use the eigenvectors thereby obtained to evaluate several observable physical quantities, e. g. the form factors of inelastic electron scattering and transition probabilities of γ-ray emission or absorption. The latter shall be considered in this section. The reduced transition probabilities for emission (or absorption) of a photon of given multipolarity (λ,μ) is given[112] in terms of the matrix element of the multipole operator in the form:

$$B(E\lambda \text{ or } M\lambda; I_i \to I_f) = \frac{1}{2I_i+1} \left| \langle I_f || \hat{\mathcal{M}}_\lambda^{(p)} || I_i \rangle \right|^2 \tag{3.50}$$

with p specifying electric (p = o) or magnetic (p = 1) operator. Here we restrict ourselves to consider transitions to and from the ground state. If we consider transitions from the ground state $|\phi_o\rangle \equiv |o\rangle$ to an excited state $|J\rangle$, a multipole of order $\lambda = J$ will be involved. In this case,

$$B(E\lambda \text{ or } M\lambda)\uparrow \equiv B(E\lambda \text{ or } M\lambda;\ o \to J) = \left| \langle J || \hat{\mathcal{M}}_\lambda^{(p)} || o \rangle \right|^2 \tag{3.51}$$

The final state $|J\rangle$ is a (1p-1h+2p-2h) state of the form (3.31) - (3.34), i. e.

$$|J\rangle = \sum_{MI} \left\{ X_{MI}\ \chi_M^+\ \chi_I - Y_{MI}\ \chi_I^+\ \chi_M \right\} |0\rangle \tag{3.52}$$

with the quasiparticle operators χ_M^+ and χ_I given in (3.35) - (3.36). As already pointed out, since electromagnetic transitions involve one-body operators (we neglect here the two-body parts of the magnetic operator), i. e.

$$\hat{\mathcal{M}}_\lambda^{(p)} = \sum_{\alpha\beta} \langle \alpha | \mathcal{M}_\lambda^{(p)} | \beta \rangle\ a_\alpha^+\ a_\beta \tag{3.53}$$

then only the 1p-1h components of (3.52) will contribute to (3.51). Therefore the value of the $\langle J || \hat{\mathcal{M}}_\lambda^{(p)} || 0 \rangle$ matrix element or transitions amplitude is given by:

$$\langle J || \hat{\mathcal{M}}_\lambda^{(p)} || 0 \rangle = \sum_{\alpha\beta} \langle \alpha | \mathcal{M}_\lambda^{(p)} | \beta \rangle \cdot$$

$$\cdot \langle 0 || \sum_{MI} C_M\ C_I \left\{ X_{MI}\ a_m^+\ a_i - Y_{MI}\ a_i^+\ a_m \right\} a_\alpha^+\ a_\beta || 0 \rangle$$

Operating here and using the commutation relations (3.7) and the condition (3.33), one can readily get (see for instance ref. 161, p. 192) that the transition amplitudes are:

$$\langle J || \hat{\mathcal{M}}_\lambda^{(p)} || 0 \rangle = \sum_{MI} C_M\ C_I \left\{ X_{MI}\ \langle m | \mathcal{M}_\lambda^{(p)} | i \rangle + Y_{MI}\ \langle i | \mathcal{M}_\lambda^{(p)} | m \rangle \right\} \tag{3.54}$$

where as always $M \equiv (m,a)$ and $I \equiv (i,d)$ denote quasiparticle and quasihole respectively. C_M and C_I are the square roots of the single-particle strength and the single-hole strength of the respective quasiparticle M and quasihole I. One should note that apart from C_M and C_I, this is the same expression as in the (1p-1h) RPA.

The electromagnetic multipole moments of a nucleus which we need here have the following forms (see e. g. Bohr & Mottelson[112], p. 382-4):

$$\mathcal{M}_\lambda^{(o)} \equiv \mathcal{M}(E\lambda) = \int \rho(\vec{r})\ r^\lambda\ Y_{\lambda o}(\hat{r})\ d\tau$$
$$\mathcal{M}_\lambda^{(1)} \equiv \mathcal{M}(M\lambda) = \frac{-1}{c(\lambda+1)} \int \vec{j}(\vec{r})(\vec{r}\times\vec{\nabla})\ r^\lambda\ Y_{\lambda o}(\hat{r})\ d\tau \tag{3.55}$$

where $\rho(\vec{r})$ and $\vec{j}(\vec{r})$ are the nuclear and current densities. In the following, $Y_\lambda \equiv Y_{\lambda o}$ will be used.

In the approximation which regards the nucleons of a nucleus as point particles having a charge and a magnetic moment (i. e. by supposing free nucleons in the nucleus), and neglecting relativistic effects, one can easily evaluate the charge and current density and obtain the following simpler forms for the multipole moments of the nucleus:

$$\mathcal{M}(E\lambda) = \frac{e}{2} \sum_i (1 - \tau_3^{(i)})\ r_i^\lambda\ Y_\lambda(\theta_i \varphi_i) \tag{3.56a}$$

$$\mathcal{M}(M\lambda) = \frac{eh}{2m_p c} \sum_i \left\{ \frac{2}{\lambda+1}\ g^{(i)} \left[\nabla(r^\lambda Y_\lambda)\right]\vec{\ell} + \mu^{(i)} \left[\nabla(r^\lambda Y_\lambda)\right]\vec{\sigma} \right\} \tag{3.56b}$$

where the sums extend over all nucleons of the nucleus. Moreover the isospin projection operator τ_3 = -1 for protons and +1 for neutrons[112]. The values of the constants g and μ are

$g = 1$	and	$\mu = \mu_p = 2.793$	for protons
$g = 0$	and	$\mu = \mu_n = -1.913$	for neutrons

The symbol m_p denotes the proton mass, and $\mu_o = e\hbar/2m_p c$ is the nuclear magneton.

However one knows that a nucleus is a system of interacting nucleons. They are able to emit and absorb mesons such as pions, ρ-mesons, etc. In this particle exchange is the origin of nuclear forces. Moreover it is the reason for the existence of currents, usually called "exchange currents"[163], of these particles flowing between nucleons. Since some of the bosons are charged, the exchange currents can interact with an external electromagnetic field. It is then clear that the densities $\rho(\vec{r})$ and $\vec{j}(\vec{r})$ differ from those obtained with the assumption of nucleons to be free and which have been used in going from (3.55) to (3.56). For electric multipole transitions the Siegert theorem holds. This theorem allows the replacement of the nuclear current density by the charge density, and eq. (3.56a) of electric multipole moments can be used. For the magnetic transitions no theorem of the Siegert-type can be applied; then one has to use an effective magnetic operator which corrects for the mesonic exchange currents and the correlations in the nuclear wave-functions. Here we shall use the effective magnetic operator $\mathcal{M}(M\lambda)$ suggested by Bauer et al.[164] which has been proved by Speth et al.[96,164] to be very successful in predicting giant magnetic resonances and other electromagnetic properties in the lead region.

With this effective $\mathcal{M}(M\lambda)$ operator the relative importance of the mesonic exchange currents and the nuclear correlations of the wave function is investigated in sections V.5-V.7 by studying the comparison of the experimentally observe energies and $B(M\lambda)\uparrow$ values of the giant magnetic resonances and those calculated in the framework of the Core-Coupling RPA theory.

IV. NUMERICAL CALCULATION

The arrangement of this chapter is as follows. In the first section we give a specific formulation of the different steps of a Core-Coupling RPA calculation. One observes that for obtaining numerical results in the procedure developed in Chapter III, we have to make three choices, namely the single-particle energies ε_ν, the single-particle wave functions $\varphi_\nu(\vec{r})$ and the residual ph-interaction. Section 2 contains the single-particle basis and the configuration space used in our calculations. In section 3 and 4 the form and parameters of the effective particle-hole interaction and the effective magnetic operator is shown.

IV.1. Specific Formulation

Roughly speaking, a Core-Coupling RPA calculation has two stages: the determination of the quasiparticle and quasihole states, and the solution of the eigenvalue problem of the secular matrix (3.37) - (3.39).

In conventional notation the different steps to be done in our treatment for calculating the quasiparticle energies and wave functions as outlined in section III.2. are as follows:

1. Choice of the single-particle energies and wave functions. They were generated from a Woods-Saxon well adjusted to reproduce correctly the known experimental single-particle energies. Further information is given in the next section.

2. Introduction of an effective interaction (in our case is the zero range density-dependent Migdal force) and solution of the usual 1p-1h RPA equations in order to describe the core excitations as superposition of 1p-1h states.

3. Calculation of the particle-core coupling which is mathematically denoted by the vertex γ. Thus we have to calculate the matrix element

$$\gamma_{\nu}^{\mu;m} = \langle\nu|\gamma|\mu;m\rangle$$

between the single-particle states $|\nu\rangle$ and the mixed $1p+(2p-1h)$ or $1h+(2h-1p)$ configurations $|\mu;m\rangle$. As shown in (3.24), to do that we only need the effective ph-interaction and the 1p-1h wave functions of the core excitations. Here an important choice has to be done, namely the number of core vibrations to be taken into account. A careful study in the closed-shell nuclei ^{12}C, ^{16}O, ^{40}Ca, ^{90}Zr and ^{208}Pb has shown us that as far as the spreading of the giant resonances is concerned, it is sufficient to take into account the low-lying collective (1p-1h) core excitations μ. In table 10 the μ-states considered in our (1p-1h+2p2h) calculations in the different nuclei are shown. The convergence of the method is carefully studied in ^{16}O in investigating the influence of the inclusion of high-lying core states in the structure of the giant E2 resonance. It is shown that the qualitative structure remains but the quantitative distribution of the E2 strength slightly changes.

4. Splitting of quasiparticle states due to core polarization effects. For each quasiparticle of quantum number ν, one has to diagonalize the matrix $H_0+\gamma$ in the space of the functions $|\nu\rangle$ and $|\mu;m\rangle$, i. e. in the space of $|1p\rangle$ and $|2p\text{-}1h\rangle$ states if one deals with a quasiparticle or in the space of $|1h\rangle$ and $|2h\text{-}1p\rangle$ states in the case of a quasihole. H_0 is the shell-model-like Hamiltonian discussed in point 1. In this way one obtains the energies E_α and wave functions Ψ_α, as given by (3.31), of a quasiparticle state as well as the relative single-particle strength of its components. The single-particle energies are taken in this stage in such a way that the 2p-1h (or 2h-1p) state with the largest single-particle strength agrees with the corresponding experimental single-particle energy.

The second stage of a Core-Coupling RPA calculation has the following three steps:

5. Calculation of the matrix elements T_{11}, T_{12} and T_{22}. As already indicated by (3.44), (3.45) and (3.47) respectively, these matrix elements depend on the $<1p\text{-}1h|V|1p\text{-}1h>$ and $<pp|V|pp>$ matrix elements and (see Appendix B) of certain combinations of 6J-symbols. It turns out that all these 6J-symbols belong to one of the following two types:

$$\begin{Bmatrix} j_a & j_c & J_p \\ J_\beta & j_a & J_\alpha \end{Bmatrix} \qquad\qquad \begin{Bmatrix} J & X & Y \\ j_a & J_\beta & j_d \end{Bmatrix} \tag{4.1}$$

1st. type 2nd. type

An estimation on the number of different 6J-symbols of these two types needed in our (1p-1h+2p-2h) RPA calculations (in which all the states $2\hbar\omega$ above and $2\hbar\omega$ below the Fermi surface were taken into account) is given in Table 2 for ^{12}C, ^{16}O, ^{40}Ca, ^{90}Zr and ^{208}Pb. In order to save computing time and money we have calculated all of these 6J-symbols and stored them on a tape or disk data set together with all the ph matrix elements and pp-matrix elements which were previously calculated in step 2 in doing the 1p-1h RPA.

6. The Core-Coupling RPA secular matrix (3.37) is diagonalized and then the eigenvalues E_t (energies of the excited states of the nucleus) and their corresponding wave functions (in the form of quasiparticle-quasihole amplitudes X's and Y's) are obtained. The way to make this diagonalization is identical to that used in the usual (1p-1h) RPA and will not be here described. An idea of the dimensions of the Core-Coupling RPA matrix in our (2p-2h) calculations can be obtained by looking at Table 3 in which the dimensions corresponding to some J^π states of different spherical

nuclei are explicitly given.

7. Finally the amplitudes X's and Y's are used to evaluate electromagnetic transition rates B(EL) or B(ML) defined by (3.54), which are to be directly compared with the corresponding values experimentally observed for instance in photonucleon experiments, in (α, α') scattering experiments, etc.

IV.2. Single-particle energies and wave functions

In our 1p-1h+2p-2h calculations we use a configuration space which includes all the single-particle states within two oscillator major shells above and below the Fermi surface. The inclusion of the second major shell is especially important for the description of positive parity states, see Figure 7. One should remark that with all the states within $2\hbar\omega$ above and below the Fermi surface, all the $E\lambda$ ($\lambda = 0$, 1, 2) strength and all the M1 strength will be included. For higher multipolarities some strength is missing especially in the high-lying region in which states have ph-contributions coming also from single-particle states out of our configuration space i. e. with energies bigger than $2\hbar\omega$. For low-lying nuclear properties one can approximately correct these neglected configurations by renormalizing the ph-interaction. Then the ph-interaction depends on the size of the configuration space which is included in the numerical values of the force parameters (see section IV.3). The single-particle wave functions were generated by solving the Schrödinger equation with a real Woods-Saxon well[165] with parameters adjusted to reproduce correctly those single-particle energies which are known from experiment. In the following, this is explained in a more detailed way.

The Woods-Saxon potential is defined[165,166] by

$$V(r) = \frac{V_o}{1+\exp(\frac{r-R_o}{a_o})} + (\frac{\hbar}{mc})^2 \; V_{LS}(\vec{\ell}\cdot\vec{\sigma}) \; \frac{1}{r}\frac{d}{dr} \frac{1}{1+\exp(\frac{r-R_{LS}}{\alpha_{LS}})} + V_c(r) \qquad (4.2)$$

where V_o, R_o and a_o are the depth ($V_o < 0$) of the central potential, its radius ($R_o = r_o A^{1/3}$; r_o is approximately constant over the whole periodic system) and its diffusivity parameter. V_{LS}, R_{LS} and α_{LS} are the corresponding values for the spin-orbit well. On the other hand $(\hbar/mc)^2 = 2.0$ fm^2 is the reduced Compton wave-length of the nucleon. The operator $\vec{s}$ ($\vec{s} = \hbar\,\vec{\sigma}/2$) and $\vec{\ell}$ are given in units of $\hbar$.

The term $V_c(r)$ is the Coulomb potential of a spherical, uniform charge distribution of the radius $R_c = r_c\, A^{1/3}$ and is given by:

$$V_c(r) = \begin{cases} \dfrac{Ze^2}{r} & \text{if} \quad r \geqslant R_c \\[2ex] \dfrac{Ze^2}{2R_c}\,(3 - \dfrac{r^2}{R_c^2}) & \text{if} \quad r \leqslant R_c \end{cases} \qquad (4.3)$$

The eigenvalues and eigenfunctions of our single-particle potential are obtained by expanding the Woods-Saxon wave functions in an oscillator basis containing up to 8 oscillator states for each set of angular momentum numbers ℓ, j. One can symbolically write

$$|\ell j>_{WS} = \sum_{m=1}^{M} a_r(\ell,j)\; |m\ell j>_{HO} \qquad (4.4)$$

Following Klemt[168)], the Woods-Saxon radial wave functions are expanded as follows

$$R_{\ell j}(r) = \sum_{m=1}^{M} a_r(\ell,j)\; r_{m\ell}(r) \qquad (4.5)$$

where the oscillator wave functions $r_{n\ell}(r)$ are defined by:

$$r_{n\ell}(r) = \sqrt{\frac{2(n-1)!}{\Gamma(n+\ell+\frac{1}{2})b^3}}\; (\frac{r}{b})^{\ell}\; L_{n-1}^{\ell+1/2}(\frac{r^2}{b^2})\; e^{-r^2/2b^2} = \qquad (4.6)$$

$$= \sqrt{\frac{2}{b^3}(n-1)!\,\Gamma(n+\ell+\frac{1}{2})}\; \sum_{\nu=0}^{n-1} \frac{(-1)^{\nu}\,(r/b)^{2\nu+\ell}}{\Gamma(\nu+\ell+\frac{3}{2})\,\nu!\,(n-\nu-1)!}\; e^{-\frac{r^2}{2b^2}} \tag{4.7}$$

Convergence in expansion (4.4) or (4.5) is generally achieved for $M = 5$ or at most $M = 8$. In our calculations we took up to $M = 8$ expansion coefficients. With this method[168] one gets not only the energies and wave functions for the bound ($E < 0$) single-particle states but also bound solutions ε, $\varphi_{\ell j}(\varepsilon,r)$ for states with positive energies.

In this work the single-particle wave functions have also been obtained by an alternative method due to Speth & Froebrich[169] in which the exact scattering wave $\varphi_{\ell j}(\varepsilon,r)$ is first obtained by numerical integration of the Schrödinger equation and then is expanded in harmonic oscillator wave function with energy-dependent expansion coefficients. The discretization is done by averaging over the interval of the resonance, i. e.

$$\bar{\varphi}_{\ell j} = \int_{\varepsilon-\Delta}^{\varepsilon+\Delta} \varphi(\varepsilon,r)d\varepsilon = \sum_{m=1}^{M} \left[\int_{\varepsilon-\Delta}^{\varepsilon+\Delta} a_{m\ell j}(\varepsilon,r)d\varepsilon\right] |m\ell j>_{HO} \tag{4.8}$$

As a last step one has to normalize the resulting continuum single-particle states and ortogonalize together with the bound wave functions. As single-particle energy one takes the resonance energy. Both discretization procedures give almost the same results for the lowest continuum single-particle states. However both are not very much adequate when the partial wave $\varphi_{\ell j}(\varepsilon,r)$ does not show resonance structure, i. e. when its width is very broad such as for example the $g_{9/2}$-wave or $p_{3/2}$ and $p_{1/2}$ waves in ^{16}O.

The parameters of the Woods-Saxon potential were adjusted by fitting experimental single-particle energies of the odd-mass nuclei in the neighbourhood of nuclei we are interested in, i. e. ^{12}C, ^{16}O, ^{40}Ca, ^{90}Zr, ^{208}Pb. The parameters used in our calculations are shown in Table 4. Contrary to the calculations done by other authors, here the same potential is used for all partial waves.

The difference of the particle energies and the hole energies is defined[168] by

$$\varepsilon_m - \varepsilon_i = [E_m(A+1) - E_o(A)] - [E_o(A) - E_i(A-1)] = \omega_m + \omega_i + \Delta\mu \qquad (4.9)$$

where ω_m and ω_i are the single-particle and single-hole energies measured from the ground state of the given nucleus and $\Delta\mu = \mu_+ - \mu_-$ is the difference between the chemical potentials. For ^{208}Pb e. g. one obtains $\Delta\mu_p = 4.232$ MeV for neutrons. The single-particle energies used in our calculations are shown in Tables 5, 6 and 7.

IV.3. Form and Parameters of the effective interaction

In our calculations the Migdal's ansatz[1] for the density-dependent effective interaction is used:

$$F^{ph}(1,2) = C_o\delta(\vec{r}_1-\vec{r}_2)\{f(\rho)+f'(\rho)\vec{\tau}_1\cdot\vec{\tau}_2+g(\rho)\vec{\sigma}_1\cdot\vec{\sigma}_2+g'(\rho)(\vec{\sigma}_1\cdot\vec{\sigma}_2)(\vec{\tau}_1\cdot\vec{\tau}_2)\} \qquad (4.10)$$

where the parameters f, f', g, g' are dimensionless parameters which depend on the center of mass coordinate $\vec{r}$ in the following way

$$F(\rho) \equiv F(\vec{r}) = F^{ex} + (F^{in} - F^{ex})\ \rho(\vec{r}) \qquad (4.11)$$

$\rho(\vec{r})$ being the density distribution of the nucleus, which is here approximated by a Fermi function, i. e.

$$\rho(\vec{r}) = \frac{1}{1+\exp\left(\frac{r-R}{a}\right)} \qquad (4.12)$$

where R and a are approximately equal to the nuclear radius and the diffuseness parameter respectively. F^{ex} and F^{in} denote the parameter sets outside and inside the nucleus respectively. With the assumption (4.11) one interpolates between the interaction inside the nucleus and the interaction outside the nucleus which may be different in principle. For convenience the following combination of parameters will be used.

$$f_{pp} = f_{nn} = f + f' \qquad g_{pp} = g_{nn} = g + g'$$
$$f_{pn} = f_{np} = f - f' \qquad g_{pn} = g_{np} = g - g' \tag{4.13}$$

It turns out[76,83] that only the parameters f and f' are different inside and outside the nucleus whereas g and g' do not show practically any density dependence. The way that parameters influence the properties of the excited states of nuclei depend on the spin and isospin part of the wave function; this is explicitly written down in Table 7.1 of the review of the theory of finite Fermi systems by Speth et al.[96].

The constant C_o is usually taken as follows:

$$C_o = 1/(\frac{dn}{d\varepsilon})_{\varepsilon=\varepsilon_F} \tag{4.14}$$

where the donominator is the density of states at the Fermi surface, i.e. the number of states per unit energy and unit volume, which is related to the effective mass of the nucleons in the following way:

$$(\frac{dn}{d\varepsilon})_{\varepsilon=\varepsilon_F} = \frac{2m^* k_F}{\hbar^2 \pi^2} = \frac{16}{9} \pi \varepsilon_F r_o^2 \tag{4.15}$$

ε_F being the Fermi constant. Because of the different single-particle potentials for protons and neutrons, the density distributions (4.12) of protons and neutrons will have slightly different radii. The parameters of the Migdal interaction have been very carefully adjusted[76,83,171] in the lead region to reproduce correctly electromagnetic properties such as excitation energies and transition probabilities, isotope shifts and moments. Thus this force seems to be appropriate for the calculation of electric and magnetic excitations in the intermediate energy or giant resonance region. The force parameters f's and g's are given in Table 8. The diffuseness parameter has been taken[171] to be the same for protons and neutrons. The interpolation radii R_{pp}, R_{nn} and R_{pn} vary with the nucleus mass A; $R_{pn} = \frac{1}{2}(R_{pp} + R_{nn})$. Together with the strength of the force C_o (in units of fm^3 MeV), they are shown in Table 9. The radii R and the parameter C_o are adjusted in each nucleus to obtain as good as possible the location and the B(EL) value of the low-lying strongest collective excitation, i. e. 3^- in ^{208}Pb.

One should remark that the parameters of the force depend on the configuration space and of the single-particle model used. The latter was already discussed in section IV.2. In all our (1p-1h)- and (2p-2h)-RPA calculations two oscillator shells above and below the Fermi surface have been used.

IV.4. Form and Parameters of the effective magnetic operator

In our (1p-1h)- and (2p-2h)-RPA calculations both the bare (Schmidt) magnetic operators defined by (3.56b) and the following effective magnetic operator have been used:

$$\mathcal{M}^{(eff)}(M\lambda) = \frac{\hbar e}{2m_p c} \sum_i \left\{ \frac{2}{\lambda+1} \tilde{g}^{(i)} \left[\vec{\nabla}(r^\lambda Y_\lambda)\right]\vec{\ell} + \tilde{\mu}^{(i)} \left[\vec{\nabla}(r^\lambda Y_\lambda)\right]\vec{\sigma} + \sqrt{\frac{3}{4\pi}}\, \varkappa r^2 \tau_3 (Y_2 \otimes \vec{\sigma})_1 \delta_{\lambda 1} \right\} \tag{4.16}$$

where τ_3 is the z-component of the isospin vector ($\tau_3 = -1$ for protons). On the other hand the effective values $\tilde{g}$ and $\tilde{\mu}$ are defined by:

$$\begin{aligned} \tilde{g}_p &= 1 - \xi_{\ell_p} & \tilde{\mu}_p &= \mu_p(1 - \xi_{s_p}) + \mu_n \xi_{s_p} \\ \tilde{g}_n &= \xi_{\ell_n} & \tilde{\mu}_n &= \mu_p \xi_{s_n} + \mu_n(1 - \xi_{s_n}) \end{aligned} \tag{4.17}$$

where μ_p and μ_n are given in (3.57).

In our calculations the following set of parameters for (4.16) - (4.17) is used in all the nuclei:

$$\xi_{\ell_p} = -0.119 \qquad \xi_{s_p} = \xi_{s_n} = 0.113$$
$$\xi_{\ell_n} = -0.031 \qquad \varkappa = 0.0723 \text{ fm}^{-2} \tag{4.18}$$

With these values and the expressions (3.57) and (4.17), one gets

$$\tilde{g}_p = 1.119 \qquad \tilde{\mu}_p = 2.26\ \mu_o = 0.8092\ \mu_p^{free}$$
$$\tilde{g}_n = -0.031 \qquad \tilde{\mu}_n = 1.38\ \mu_o = 0.7213\ \mu_n^{free}$$

where μ_o is the nuclear magneton ($\mu_o = \hbar e/2m_pc$).

V. RESULTS AND DISCUSSION

V.1. Giant electric resonances in ^{16}O

a) Quasiparticle states in the oxygen region. As pointed out in chapter III and section IV.1, once the single-particle model (see Table 2 and section IV.2) and the effective interaction (see Table 8 and section IV.3) have been chosen the first thing to do in the Core-Coupling RPA approach is to solve the 2p-1h or 2h-1p problem, i. e. to calculate the distribution of the single-particle strength of the quasiparticle and/or quasihole states according to expressions (3.31) or (3.35)- (3.36). Equation (3.35) shows that the amount of 2p-1h admixtures increases with the number of core states α which are to be coupled with the single-particle degrees of freedom ν. Our calculations in ^{16}O take into account as α core states the strongest collective low-lying 3^- (6.13 MeV) state, the 1^- (13.10 MeV) state and the 2^- (12.53 MeV) state. Further inclusion of other (1p-1h) core excited states is studied later on.

Due to the (3^-, 1^-, 2^-)-core-coupling, the sd-shell quasiparticle states of ^{17}F created by χ_m^+, eq. (3.35), in putting a proton on the said orbits in ^{16}O core, remain almost unsplitted $5/2^+$ at -0.60 MeV with 95 % of the single-particle strength (SPS in short), $3/2^+$ at 4.54 MeV with 92 % of the corresponding SPS and $1/2^+$ at -0.10 MeV with 93 % of SPS. The missing pieces have been pushed up at high energies ($\sim$20 MeV). However the quasiparticle states $7/2^-$ and $5/2^-$ are very much fragmented as shown in Figure 8. In this figure one finds that the unperturbed $f_{7/2}$ single-particle strength (left side) is splitted in several parts from 4.8- to 18.8 MeV with the centroid at 14.4 MeV; the locations, the relative strength and the detailed structure of the calculated $7/2^-$ peaks are given in Table 11. Therein one notices three main $7/2^-$ states at 4.8 MeV (19.8 %), 11.6 MeV (11 %) and 15.5 MeV (53 %).

The $f_{5/2}$ single-particle strength is also fragmented into several states (see Fig. 8 and Table 12) ranging from 5.4- to 19.2 MeV with centroid at 17.347 MeV. There are four main $5/2^-$ peaks at 5.48 MeV (11.8 %), 11.2 MeV (9.4 %), 18.9 MeV (52.4 %) and 19.2 MeV (16.7 %). A similar splitting is shown in Tables 13 and 14 for the corresponding quasiparticle states in ^{17}O. In both nuclei the calculated $7/2^-$ and $5/2^-$ single-particle strength distribution compares nicely with that observed in proton polarized measurements[178] (^{17}F case) and in neutron cross sections[179] (^{17}O case). At times as it occurs for $f_{7/2}$ in ^{17}F, we get almost exactly the location of peaks and percentages of SPS. However our $5/2^-$ centroid is perhaps 2 or 3 MeV too high according to Fowler et al.[179] experiments.

It is interesting to remark that in all the proton and neutron $7/2^-$ and $5/2^-$ resonances with a relatively strong single-particle strength ($\gtrsim$ 7 %), the dominant 2p-1h admixtures are those from $3^- \times 1d_{5/2}$ and $3^- \times 1d_{3/2}$.

b) Giant Quadrupole and Giant Hexadecapole Resonances. The distribution of quadrupole (E2) strength and of hexadecapole (E4) strength obtained in our (1p-1h) RPA and (2p-2h) Core-Coupling RPA calculations are shown in Figure 9. In the upper part the (1p-1h) RPA calculations show a giant T = 0 E2 resonance at 23.1 MeV, whose main ph components are $(f_{7/2} \times p^{-1}_{3/2})$ and $(f_{5/2} \times p^{-1}_{1/2})$, and a giant T = 1 E2 peak at 43.1 MeV in which $(d_{5/2} \times 1s^{-1}_{1/2})$ is the main ph contribution. As we have already seen above, the $(3^-, 2^-, 1^-)$ core coupling causes a strong fragmentation of the single-particle states $7/2^-$ and $5/2^-$ but leaves the $d_{5/2}$ state unaffected. Therefore we expect that the inclusion of the corresponding 2p-2h configurations will produce a strong fragmentation of the isoscalar (1p-1h) giant quadrupole resonance (in short GQR). This is seen in the lower part of the figure and is examined and compared with various recent experiments in Table 17. Nice agreement is found everywhere except with the $^{15}N(p,\gamma_0)$ and the (e,e') experiments. The discrepancy with the former experiment is most likely due to the fact that this reaction does not permit direct excitation in the $f_{7/2}$ channel, owing to the initial $p_{1/2}$ hole in ^{15}N. Therefore what Hanna et al.[40] observe in their (p,γ_0) experiments might be only the $(f_{5/2} \times p_{1/2}^{-1})$ contributions. In this respect the (p,γ_0) experiment gives us the possibility to excite selectively these especial components of the GQR. The too low EWSR fraction reported by (e,e') experiments is probably[44] due to the difficulty in substracting the GQR from the GDR. Finally the difference between the two (α,α') measurements is coming from the fact that Knöpfle et al.[50] assume the whole structure from 15- to -28 MeV as a single E2 bump; the better resolution of Harakeh et al.[50] permits to distinguish multipolarities other than 2^+, hence reducing the fraction of T = 0 E2 EWSR limit (which is 2087.4 e^2 fm^4 MeV according to our calculations) to be exhausted. There is always some ambiguity in extracting the B(E2) values; it comes from (a) the substraction of the background and (b) the collective model analysis in DWBA calculations. Therefore one should make large error bars on the experimental sum rules extracted from (α,α') reactions. On the other hand one should remember that the sum rules are defined for electromagnetic operators.

In the T = 0 GQR region, i. e. between 16 and 28 MeV, one gets theoretically three main E2 peaks which exhaust 55 % of the T = 0 EWSR whose energies and wave functions are explicitly written down in Table 18. One can observe that the two main components of the lower E2 peak wave functions are the proton and neutron $(3^- \times d_{5/2})_{5/2^-} \times p_{1/2}^{-1}$ excitations, and the intermediate peak at 20.66 MeV has a main component of its core coupling RPA wave function the proton and neutron $(3^- \times d_{5/2})_{7/2^-} \times p_{3/2}^{-1}$ excitations. In the case of the third E2 peak at 27.5 MeV there are not dominant (1p-1h+

2p-2h) components in its wave function but many of them of comparable strengths.

The experimentally observed 2^+ levels at 6.92, 11.52 and 13.1 MeV, which carry an appreciable fraction ($\sim$20 %) of the sum rule strength, are not described in our calculation because they have important admixtures of 4p-4h excitations[191]. These higher configurations are presumable also responsible for a larger fragmentation of the isoscalar E2 resonance in the interval between 16 and 28 MeV compared with the present results. This would further improve the agreement with the exprimental data, see Table 17.

The position of the isovector GQR remains unchanged at 43 MeV but its B(E2) value is slightly reduced. We also find that $\sim$8 % of the T = 0 EWSR falls over the 30- to 35- MeV region and 33 % of the T = 0 + T = 1 EWSR is exhausted between 30 and 40 MeV.

On the right hand side of Figure 9 we observe that the giant isoscalar (1p-1h) E4 resonance at 25.5 MeV is very much fragmented, although keeping the main strength at 21.3 MeV. We find that $\sim$30 % of the isoscalar E4 EWSR (this limit is $0.55 * 10^6$ e^2 fm^8 MeV as shown in Table 16).

c) Giant Resonances other than E2 and E4. The (1p-1h+2p-2h) monopole, dipole and quadrupole resonances of the core-coupling RPA theory are compared with those given by the first (1p-1h) approach in Figures 10, 11 and 12 respectively. In Fig. 10 one observes that the inclusion of the 2p-2h configurations produces a fragmentation of the giant isoscalar (1p-1h) E0 resonance (also called breathing mode) at 27.3 MeV into three T = 0 states, keeping the main strength at practically the same location which exhaust 99 % of the $\sum_0^p$ (T = 0) sum rule (see Appendix VII.C and Table 16). Taking into account that the main ph-components of this peak are $p_{3/2} - 1p_{3/2}^{-1}$

and $p_{1/2}$-$1p_{1/2}^{-1}$, one expects that the inclusion of further 2p-2h configurations and especially the inclusion of the continuum will spread out the E0 strength on a large energy interval since the states $p_{3/2}$ and $p_{1/2}$ are[108] pure scattering wave, i.e. they have no resonance character. The other two T=0 E0 peaks are located at 24.8 MeV and 26.7 MeV, depleting 7.4 % and 10.2 % of the $\sum_0^p$ (T = 0) sum rule respectively. Some experimental evidence seems to have been found in (α,α') experiment by Harakeh et al.[49] for the existence of a 0^+ state at 23.85 MeV which exhausts $\sim$4.8 % of the sum rule. The giant T = 1 (1p-1h) E0 resonance at 43.9 MeV is almost unaffected by the inclusion of the 2p-2h configurations; it depletes 78 % of the $\sum_0^p$ (T = 1) sum rule. However if one would include the 2p-2h configurations coming from the coupling of the highlying core excitations with the single-particle degrees of freedom, the isovector E0 resonance completely fragments. This is valid for the resonances of any multipolarity lying at high energies. The energy of the breathing mode has also been calculated in the GCM approach[79,193].

In Figure 11 the (1p-1h) and (2p-2h) E1 resonances are shown. We obtain three main (2p-2h) E1 peaks at $\sim$14 MeV, 21 MeV and 26.6 MeV which deplete 2.9 %, $\sim$84 % and 5.9 % of the classical dipole sum rule respectively. The location of the E1 peaks differs from the experimental 22.3 and 24 MeV; this is an intrinsic fact of the Migdal force as pointed out by Speth et al.[96]. The fact that the (1p-1h) GDR is not affected by the inclusion of 2p-2h configurations seems to indicate that the experimental E1 strength distribution into the said two peaks is due to the coupling of more complex (e.g. 3p-3h) configurations and/or to the consideration of some fundamental part (e.g. the tensor force, ...) in the density-dependent interaction.

The octupole resonances are shown in Figure 12. The main effect of the inclusion of (2p-2h) states is the shifting and fragmentation of T = 0 (1p-1h) E3 peak at 44.9 MeV and the T = 1 (1p-1h) peak at 57.2 MeV peak. Part of the strength of the latter peak has been pushed up by $\sim$5 MeV and half of the strength of the former one has been pushed down at 35.5 MeV. The lowest (1p-1h) T = 0 E3 state at 6.29 MeV reduces slightly its B(E3) value and exhausts $\sim$23 % of the $\sum_3^p$ (T = 0) sum rule. From the inclusion of the continuum (escape width) we expect that the resonance at about 35 MeV is distributed over a wide range of energy. See also ref. 62.

c) Summary and Convergence. In Table 19 there are shown the percentages of various sum rules depleted by the resonances E0, E2, E3 and E4 in the 12-to-30 MeV region according to our core-coupling RPA calculations already mentioned in Figures 9 - 12. The E3 and E4 sum rules are those given in Table 16. The corresponding EWSR limits for E0 and E2 are taken directly from the calculations since in our configuration space ($2\hbar\omega$ above and below Fermi surface) all the possibilities to create such states are included; these values are as follows:

T = 0 + T = 1 E0 EWSR = 4995 e^2 fm^4 MeV

T = 0 E0 EWSR = 2398.5 e^2 fm^4 MeV

T = 0 + T = 1 E2 EWSR = 4501 e^2 fm^4 MeV

T = 0 E2 EWSR = 2087.4 e^2 fm^4 MeV

We find that 4.1 % of the isoscalar + isovector E3 EWSR is exhausted in the 16-to-20 MeV, and 4.7 % of the $\sum_3^p$ (T = 0) is depleted between 22 and 26 MeV. Both facts strongly support some evidence of E3 strength detected by (α,α') scattering measurements of Harakeh et al.[49] in such regions. Furthermore we find that $\sim$55 % of the $\sum_3^p$ (T = 0) sum rule falls between 30 and 55 MeV, what would nicely agree with the recent semidirect reaction analysis of the Jülich-Hamburg-Grenoble collaboration[64] but disagrees with the original predictions of ref. 62. However the inclusion of the continuum would broaden the E3 strength, especially at high energies.

Finally we should remark that for a consistent (2p-2h) RPA approach one cannot describe the low-lying positive parity core-states because these states as said before are built up by higher np-nh ($n > 2$) configurations.

The convergence of our method, i.e. the dependence of the results of the Core-Coupling RPA on the number of core states, is studied in Figure 13b, c where we have considered much larger bases and calculated the distribution of the E2 strength. In part (a) the (2p-2h) E2 states of Fig. 9 are shown again. In part (b) the additional 3^- core state at 13.25 MeV was included. In part (c) the basis was still more enlarged by taking into account two further core states, namely 1^- at 12.44 MeV and 2^- at 12.97 MeV. All of these states are known to be fairly well described by the 1p-1h RPA. Looking at Fig. 13, one observes that the strength distribution in the isoscalar GQR region remains practically unchanged, i. e. there are always three main peaks exhausting the same portion of the T = 0 E2 EWSR strength. The only appreciable change is the fragmentation of the high-lying isovector E2 peak at $\sim$43 MeV into three pieces. The strength remains however in the same energy region.

V.2. Giant electric resonances in ^{12}C

In this nucleus the two strongest core excited states are by far 2^+ at 4.44 MeV and 3^- at 9.64 MeV. The coupling of these two core excitations with single-particle states will produce the quasiparticle states (3.35) and the subsequent 2p-2h configurations included in (3.31; 3.34). In the following we show the spreading width of the giant electric multipole resonances in ^{12}C caused by the influence of such 2p-2h states and compare the results with recently available (α,α') scattering measurements.

a) Giant quadrupole and hexadecapole resonances

The E2 and E4 states in ^{12}C obtained in our calculations are presented in Figure 14. In the upper part the 1p-1h calculations show a strong isoscalar E2 resonance at 25 MeV and an isovector one at 31.4 MeV. Both resonances have as main particle-hole components the pairs $2p_{1/2}$-$1p^{-1}_{1/2}$ and $1f_{7/2}$-$1p^{-1}_{3/2}$. Owing to the (2^+, 3^-) core coupling the unperturbed $f_{7/2}$ state strongly fragments by shifting up more than 50 % of its single-particle strength in an interval of ~15 MeV. Consequently we have to expect that the inclusion of the 2p-2h states will give rise to a large fragmentation of the (1p-1h) GQR. This is seen in the lower part of the figure and is examined in terms of percentages of sum rules in Table 20.

We find that all the E2 states between 15 and 26 MeV, except the narrow one at 15 MeV, are purely isoscalar and deplete 13 % of the T = 0 E2 EWSR limit. We also observe two concentrations of E2 strength in the 30-to-40 MeV region and in the 45-to-55 MeV energy region exhausting 32 % and 25 % of the (T = 0 + T = 1) E2 EWSR strength respectively. In the GQR region two main isoscalar narrow peaks at 24 MeV and at 30.7 MeV jump out. Whereas the first one contains many p-h configurations none of which is dominant, the second peak has a large component of the ($f_{7/2}$-$p^{-1}_{3/2}$) configuration where the quasiparticle $f_{7/2}$ state contains 35 % of the single-particle state. Consequently the second peak at 30.7 MeV depends strongly on the "unperturbed" energy $\varepsilon(f_{7/2})$ which is not known experimentally.

These results are in agreement with the (α,α') scattering measurements at 150 MeV of Knöpfle et al.[46] which have found 12.9 % of T = 0 E2 EWSR between 18.3 MeV and 26.2 MeV; we find 13.2 % in such a region. The indirect analysis of E2 strength from $^{12}C(p,p')$, see ref. 52, and $^{11}B(\vec{p},\gamma)$, see ref. 182, data gave >30 % of the T = 0 E2 EWSR. Our calculations also disagree with the percentage of 30 to 50 % reported by (d,d'), see ref. 54, and (α,α'), see ref. 53, measurements to be localized in a broad peak near 27 MeV. Rather our calculations confirm the observations in ^{12}C (α,α') spectra at 104 MeV[183] and at 96 MeV[53] of a gross structure peak in such a region, of which only a fraction has a E2 character. As seen also in Table 20 and discussed below, that structure would have an important contribution of T = 0 E4 nature which might also be the peak at 29.2 MeV (whose angular distribution has no E2 character) found in (α,α') experiments at 172 MeV by the Jülich group[128].

According to the continuum shell model calculations of Birkholz[16], the inclusion of the continuum in our approach would lead us to a better agreement with Knöpfle et al.[46], e. g. our E2 strength would be slightly more spread so that a small fraction ($\sim$2 %) falls between 15 and 18 MeV.

Concerning the E4 resonances, we observe that the inclusion of 2p-2h configurations produces a strong fragmentation of the two big (1p-1h) T = 0 states and a huge shifting of the (1p-1h) isovector strength from $\sim$40 MeV up to the region around 50 MeV. The distribution of the E4 strength is examined in terms of sum rules in the last column of Table 20. One should remark that the EWSR limits $\sum_4^P$ and $\sum_4^P$ (T = 0) were evaluated (see Appendix VII.C) with the assumption of a uniform ground state distribution of radius R = 1.2 $A^{-1/3}$. As shown in Appendix VII.D, these limits are $\sim$25 % of the real (T = 0 + T = 1) E4 EWSR and T = 0 E4 EWSR respectively. Taken into account this fact we find $\sim$5 % of the isoscalar sum rule in the 26.5-to-30 MeV and $\sim$4 % between 30 and 35 MeV. On the other hand we also observe $\sim$11.5 % of the isoscalar + isovector sum rule strength between 30 and 40 MeV, and $\sim$10 % in the 45-to-50 MeV range.

b) Giant monopole and octupole resonances

The E0 states found in our calculations are shown in Figure 16 and are analysed in terms of sum rules in the first column of Table 20. The inclusion of the 2p-2h states fragments the giant isoscalar (1p-1h) E0 resonance (often called breathing mode) located at 27.6 MeV in two pieces so that $\sim$2 % of the T = 0 E0 EWSR limit (this value, 1556 e^2 fm^4 MeV, emerges directly from the calculations) falls in the GQR region and $\sim$74 % of that strength is depleted between 30 and 35 MeV. Experimentally there is so far no detection of the breathing mode in ^{12}C. Recent GCM calculations[80] with Skyrme forces locate the E0 resonance at $\sim$34.7 MeV although they do not calculate the strength.

The distribution of E3 strength is shown in Figure 15 and is analysed in the third column of Table 20 in terms of sum rules. We should say that the values $\sum_3^p$ and $\sum_3^p$ (T = 0) are $\sim$63 % of the total isoscalar + isovector E3 EWSR and of the isoscalar E3 EWSR strengths respectively. We find that the 2p-2h configurations push an important fraction of the (1p-1h) T = 0 E3 strength located between 12 and 20 MeV up to higher energeis in the 30-to-45 MeV region. However $\sim$2 % of the T = 0 E3 sum rule remains between 15 and 18 MeV. A concentration of $\sim$15 % of isoscalar strength is found to occur between 35 and 45 MeV. The latter corroborates indirect evidence found in analyses of inelastic nucleon scattering[52] to low-lying nuclear states. In inelastic (p,p') and (α,α') measurements[184] E3 states at 18.35 MeV, 20.57 MeV and 21.65 have been proposed. However only the second state which is of isovector character seems to be firmly established.

Finally in Figure 17 the influence of the 2p-2h configurations on the 1p-1h E1 states is shown. The giant (1p-1h) T = 1 E1 resonance is splitted by shifting 50 % of its strength to higher energies. A concentration of isovector dipole strength is found between 25 and 40 MeV. In the 15-to-25 MeV region three main T = 1 E1 peaks show up at 17.5, 20.3 and 24.4 MeV exhausting 7.2, 35 and 8 % of the classical dipole sum rule. The same arguments as in case of dipole states in oxygen can be given to explain the disagreement with the experimental isovector dipole resonances[116,6] at ∿23.5 MeV and 25.5 MeV.

V.3. Giant electric resonances in ^{90}Zr

As said before the configuration space of our 1p-1h and 2p-2h calculations contains all the single-particle states within $2\hbar\omega$ above and below the Fermi surface. The single-particle energies of ^{90}Zr are shown in Table 6. Here we first calculate the distribution of the single-hole strength due to the admixtures of the six low-lying core excited states shown in Table 10, namely the states 2^+ (2.186 MeV), 3^- (2.749 MeV), 4^- (2.736 MeV), 4^+ (3.077 MeV), 5_1^- (2.319 MeV) and 5_2^- (3.975 MeV). In the following we show the fragmentation of the 1p-1h giant resonances induced by the 2p-2h configurations which are yielded by the 2h-1p admixtures according to eq. (3.31; 3.34).

a) Giant monopole and quadrupole resonances

The E0 states obtained in our (1p-1h) RPA and (2p-2h) Core-Coupling RPA calculations are shown in Figure 18 and analysed in terms of sum rules in the first column of Table 21. In the upper part of Figure 18 we find two giant (1p-1h) isoscalar peaks at ∿15 MeV and a stronger T = 0 state at 20.7 MeV. The summed strength at ∿15 MeV is larger than that at 20.7 MeV. A giant 1p-1h T = 1 resonance is located at ∿32 MeV. The (1p-1h) state at 28.5 MeV has a strong mixture of isoscalar and isovector characters. As shown in the lower part of the figure, the inclusion of 2p-2h configurations strongly fragments all the three isoscalar resonances and slightly splits the giant isovector state, whereas the $T = 0 + T = 1$ state at 28.5 MeV remains unchanged.

Below 25 MeV we observe three concentrations of isoscalar E0 strength. The first one is centered around 14.7 MeV with a width of 4 MeV and exhausting 36 % of the $T = 0$ E0 EWSR strength (this sum rule was taken directly from the calculations: it is 33185 e^2 fm^4 MeV). Secondly we find 8.7 % of this sum rule to be depleted between 17.5 and 20 MeV. Finally in the 20-to-22.5 MeV region 42.5 % of this isoscalar E0 sum rule is exhausted; this fraction of E0 strength has its centroid at 21.25 MeV with a width of 2 MeV. Above 25 MeV we find that 8.1 % of the $T = 0$ E0 sum rule is depleted between 25 and 30 MeV. (The strong peak at 28.2 MeV was considered $T \neq 0$ although it has a certain amount of isoscalar character.) From an experimental point of view two groups have proposed the existence of a large amount of monopole strength at ∿17 MeV, i. e. at the energy of the giant dipole resonance. Whereas Marty et al.[120)] observes 13 to 27 % of the monopole sum rule at (17.5 ± 0.5) MeV from inelastic deuteron and α-scattering experiments, the Tohoku group[28,56)] suggests from inelastic (e,e') measurements the existence of an E0 peak with a width of 4 MeV which would deplete 91.1 % of our $T = 0$ E0 EWSR limit (the value they take for this limit is 28000 e^2 fm^4 MeV). This strength value depends very sensitively first upon the way the GDR cross section is substracted (Torizuka et al.[56)] used the Goldhaber and Teller model for the GDR transition density) and secondly upon the way of substracting the background[44)].

A further experimental uncertainty emanates from distinguishing between E0 and E2 character. In our calculations half of the strength of the first $T = 0$ E0 peak falls in the same energy range, i. e. between 12.5 and 15 MeV, than the Giant Quadrupole resonance (see later on). Furthermore 8.7 % of the T = 0 E0 strength lies down between 17.5 and 20 MeV, i. e. in the same place as 22.0 % of the T = 0 E2 EWSR strength is exhausted. It is then natural to infer that the experimental monopole proposal should be regarded as tentative and they need of further corroboration.

From the first column of Table 21, one can also get information about the distribution of the isovector monopole strength. The (T = 0 + T = 1) E0 EWSR given by our calculations turns out to be 64057 e^2 fm^4 MeV. We find that $\sim$10 % of the T = 1 E0 EWSR is exhausted in each of the following energy intervals: 15 MeV - 17.5 MeV, 17.5 - 22.5 and 22.5 - 25 MeV. The other 2/3 of the isovector strength is found to be exhausted by equal amount in the 25-to-30 MeV and in the 30-to-35 MeV regions.

Figure 19 shows the E2 states obtained in our calculations. One can observe that the inclusion of the 2p-2h configurations produces a strong splitting of the giant isoscalar (1p-1h) E2 resonance at 13.3 MeV and the (1p-1h) E2 state at 19.2 MeV. Contrary to this the giant (1p-1h) E2 resonance at $\sim$26 MeV is practically unaffected. Two concentrations of isoscalar E2 strength are found. One has the centroid at 13.6 MeV with a width of $\sim$2.5 MeV, exhausting $\sim$47 % of the T = 0 E2 EWSR limit (the value of this limit is 36472.5 e^2 fm^4 MeV from the calculations). Also 22 % of this sum rule strength appears to be located between 17.5 and 20 MeV.

The first experimental location of E2 strength in ^{90}Zr was done in inelastic (e,e') experiments by the Tohoku group[28] at 14 MeV exhausting (38.3 ± 11.6) % of our T = 0 E2 EWSR strength (This group uses an isoscalar E2 sum rule equal to 24900 e^2 fm^4 MeV; respect to this limit, the 14 MeV E2 peak would exhaust 56 ± 17 %). Later (α,α') scattering measurements done by Youngblood et al.[35] have located the isoscalar GQR at (14.5 ± 0.2) MeV with a width of 4 MeV depleting (54 ± 15) % of the isoscalar sum rule. Recent new inelastic electron scattering experiments of the same group at Tohoku University[56] have shown the appearance of additional (E0 or E2, or E0 + E2) strength between 10 and 20 MeV. If the assumption of this additional strength to be E0 is made, then 91 % of our T = 0 E0 EWSR is exhausted. But if that strength is E2, these authors found 33 % and 43.5 % of our T = 0 EWSR to be depleted in the 10-to-15 MeV and in the 15-to-20 MeV energy regions respectively. If the latter were the case these (e,e') results would be almost reproduced by our calculations what would imply a real splitting of the T = 0 GQR. Most likely the additional strength found by Torizuka et al.[56] has both E0 and E2 character (also suggested by our calculations; see Table 21), what would mean a slight reduction of their estimated E2 strength fractions; this would give rise to closer agreement with our values.

Regarding the T = 1 GQR, the only experimental observation in ^{90}Zr comes from inelastic (e,e') scattering experiments doen by the Tohoku group[56] who finds it at 26 MeV with a width of $\sim$7 MeV exhausting 73 % of the isovector E2 sum rule strength. In our calculations $\sim$26 % of that strength is depeleted between 17.5 and 22.5 MeV, and $\sim$74 % is exhausted in the 22.5-to-35 MeV energy region.

b) Giant dipole resonances

The E1 states obtained in our (1p-1h) RPA and Core-Coupling RPA calculations is shown in Figure 20. The inclusion of the 2p-2h states produces a large fragmentation of the strongest 1p-1h E1 resonance located at 12.66 MeV and a comparatively small reduction of the strength of the (1p-1h) peak at $\sim$16 MeV. One can say that the 2p-2h configurations move the (1p-1h) GDR up to the energy region (16.5 MeV) where it has been experimentally observed.

The distribution of E1 strength is examined in the first column of Table 22 in terms of the classical dipole sum rule $\sum_1^P$ (T = 1) = 14.8 $\cdot \frac{NZ}{A} e^2 fm^2$ MeV $\simeq$ 329 e^2 fm^2 MeV and in terms of the (T = 0 + T = 1) E1 EWSR which emanate from the claculations and whose value is 377.4 e^2 fm^2 MeV. We obtain two main concentrations of E1 strength: between 10 and 15 MeV, and between 15 and 20 MeV. In these energy regions 69.6 % and 52.2 % of the classical di-ple sum rule are exhausted respectively. Besides we find 9.5 % of that strength in the 5-to-10 MeV energy range and around 3 % between 20 and 25 MeV. Altogether we find that the classical dipole sum rule is overexhausted between 5 and 30 MeV. This is also found in another similar (2p-2h) calculation by Soloviev et al.[185] whose percentages of the sum rules exhausted in the different energy subintervals are very similar to ours.

Experimentally it is well known the energy of the GDR peak at $\sim$16.7 MeV from photoneutron reactions[116] and from inelastic electron scattering experiments[56]. The latter have also given estimations (using the Goldhaber & Teller model) of the fractions of the dipole sum rule depleted in the different intervals of the energy spectrum; they find (14.5 ± 9.6) %, (22.5 ± 3.0) %, (49 ± 4) % and (13.7 ± 7.0) % of the classical dipole sum rule $\sum_1^P$ (T = 1) in the following energy regions: (6-10 MeV), (10-15 MeV), (15-20 MeV) and (20-30 MeV) respectively. In their paper Torizuka et al.[56] use the value 264 e^2 fm^2 MeV as the E1 sum rule, hence the percentages exhausted in the different energy intervals are different. Bearing in mind the uncertainties (already said) inherent to the extraction of these numbers from experiments, one observes that one also gets experimentally two concentrations of E1 strength between 10 and 15 MeV, and between 15 and 20 MeV. However the relative percentage of the sum rule in these two intervals is the inverse situation as in the (2p-2h) calculations.

c) Giant Octupole Resonances

The 3^- states calculated in the (1p-1h) RPA and the Core-Coupling RPA approaches are shown in Figure 21 and discussed in terms of sum rules in the second column of Table 22. Let us first describe the gross features of the octupole states in the whole spectrum, i. e. between 0 and 45 MeV, then we shall analyse in detail the low-lying energy region, i. e. between 0 and 9 MeV, from which most recent data are available[142].

In the upper part of Figure 21, the (1p-1h) RPA results show above 5 MeV the existence of two narrow T = 0 E3 peaks at 6.1 MeV and 28.2 MeV respectively, and an isovector resonance peaked at 29.7 MeV. Besides there are essentially three concentrations of E3 strength of T = 0 and T = 1 character between 7 and 14 MeV, between 16 and 19 MeV and in the 32-to-37 MeV energy region. The inclusion of the 2p-2h configurations does not modify very much this landscape; it produces the fragmentation into three pieces of the two narrow isoscalar peaks although their entroids remain at the same energy. On the other hand the well-known and strong low-lying 3^- state (experimentally at $\sim$2.75 MeV) only reduces slightly its strength. The (2p-2h) octupole strength is analysed in terms of sum rules in Table 22. We should remember once again that the sum rules $\sum_3^P$ and $\sum_3^P$ (T = 0) were calculated (see Appendix VII.C) with the assumption of a uniform ground state distribution with radius $R = 1.2\ A^{+1/3}$ fm. These sum rules are, see Appendix VII.D, 75.7 % of the total (T = 0 + T = 1) E3 and T = 0 E3 sum rules respectively; these limits turn out to be $4.6 * 10^6$ and $2.05 * 10^6\ e^2\ fm^4$ MeV again respectively. These values exactly coincide with those estimated by Liu and Brown[89] in using Hartree-Fock ground states; see Table 3 of ref. 89. We find that 21 % of the T = 0 E3 strength is exhausted below 10 MeV. In the 10-to-15 MeV and in the 15-to-20 MeV energy region it is also found ∿6 % and 3 % of that isoscalar limit. At higher energies we find two concentrations of isoscalar strength between 25 and 30 MeV and between 30 and 35 MeV where 32 % and ∿18.5 % of the T = 0 E3 limit are depleted respectively. On the other hand we find that the T = 1 E3 strength is distributed in a very similar way as the isoscalar strength.

To the best of our information the only published experimental results concerning the distribution of E3 strength above 10 MeV of excitation energy are those of Torizuka et al.[56] in inelastic (e,e') scattering experiments. These authors decompose the "background" in the electron spectra into several multipole (L = 1, 2, 3, 4, 5, 6) components. However one should point out that their results must be regarded as tentative due to considerable uncertainties in such analyses. They have found in the 10-to-15 MeV and in the 15-to-20 MeV energy regions ∿20 % and ∿12 % of our T = 0 E3 EWSR strength respectively.

Let us now discuss the low-lying E3 region, i. e. the energy region below 10 MeV. Youngblood et al.[142] have observed what they called a Low-lying Energy Octupole Resonance (LEOR) centered around $\approx 32\ A^{-1/3} = 7.2$ MeV exhausting ∿19 % of the isoscalar E3 sum rule which they estimate to be $S_0 \simeq 1.75 * 10^6\ e^2\ fm^4$ MeV (they assume a ground state distribution of the radius $R \simeq 1.123\ A^{1/3} = 5.033$ fm). In Table 23 a comparison between experimental results[56,142,186], the (1p-1h) RPA and the (2p-2h) Core-Coupling RPA calculations and two different Continuum (1p-1h) RPA calculations is made. For the sake of clarity we have used in this table the sum rule S_0.

We first observe that the lowest 3^- state reduces its strength from 20.5 % of S_0 to 17.8 E of S_0 due to the inclusion of 2p-2h configurations. The latter value is still far from 7.1 % which is observed by Youngblood et al.[142] but practically coincides with the value 17.0 % obtained from electromagnetic measurements[186]. Between this state and 9 MeV we find threee isoscalar E3 states exhausting 6.4 % of S_0 and two isovector states at 8.08 MeV and 8.47 MeV. All of these five states fragment very much with the inclusion of 2p-2h configurations giving rise to six T = 0 E3 states and four T = 1 states of smaller B(E3) value. The six isoscalar states locate practically at the same positions of the six 3^- levels observed by Youngblood et al.[142] in the region between 3 and 9 MeV. Our (1p-1h+2p-2h) calculations also coincide with these authors (a) in locating the main peak at 5.6 MeV and (b) in exhausting approximately the same fraction of S_0 below 9 MeV. Indeed this group of Texas A & M University finds 23 % of S_0 without inclusion of what they called "high energy tail" and 26 % of S_0 if one includes this ambiguous term. In the same energy region we find 24.5 % of S_0 and 26 % of S_0 if we would assume the T = 1 E3 states of that region to have isoscalar character. However our calculations distribute the E3 strength below 9 MeV in a different manner as these authors observe in their measurements: (1) they assign 7.1 % to the lowest 3^- state whereas our calculations find 17.8 % in agreement with electromagnetic measurements[186]. (2) They assign $\sim$19 % to the LEOR whereas our calculations locate $\sim$8.2 %. (3) They locate the controid of LEOR at $\sim 32\ A^{-1/3} = 7.14$ MeV, whereas our calculations find it at 6.55 MeV $\simeq$ $29\ A^{-1/3}$.

The inclusion of the continuum in our (1p-1h+2p-2h) calculations would certainly be very useful to solve this disagreement. However the only two available continuum (1p-1h) RPA calculations[108,87] are very much different in locating the E3 strength below 9 MeV as one can observe in the two last columns of Table 23.

d) Higher multipole resonances

The 4^+ and 5^- resonances calculated in the (1p-1h) RPA and in the Core-Coupling RPA approaches are shown in Figures 22 and 23 respectively and are analysed in terms of sum rules in Table 22. In the upper part of Fig. 22 one observes the existence of a giant (1p-1h) T = 0 hexadecapole resonance at 11.6 MeV which exhausts 32 % of the $\sum_4^P$ (T = 0) sum rule strength or 21 % of the "real" T = 0 E4 EWSR (see Appendix VI.D; therein one can extract that the $\sum_4^P$(T = 0) is ~65.8 % of the total T = 0 E4 EWSR which turns out to be $1.17 * 10^8$ e^2 fm^8 MeV). Besides two narrow (1p-1h) peaks at 17.87 and 18.35 MeV jump out; both are of isovector nature although the second one has some admixtures of T = 0 character. The inclusion of 2p-2h configurations reduce the strength of the (1p-1h) giant E4 resonance by fragmenting it into several pieces; now its strength exhaust 13.5 % of the T = 0 E4 sum rule.

From the third column of Table 22 we also see that ~16.5 % of this strength is depleted between 10 and 12.5 MeV, and 27.7 % falls in the 10-to-15 MeV energy region. Furthermore 4.2 % and ~6 % of such an isoscalar sum rule limit lie down between 15 and 20 MeV, and between 20 and 25 MeV. Looking at Tables 21 and 22 one can remark that much of the isoscalar strength of multipolarity L = 0, 1, 2, 4 (and in a lower amount the L = 3) is exhausted in the 10-to-15 MeV region, and especially between 12.5 MeV and 15 MeV.

The influence of the mixing of 2p-2h states on the (1p-1h) E5 resonances is shown in Figure 23. The main effect is the strongfragmentation undergone by the giant narrow T = 0 peak at 7.3 MeV and by the giant (1p-1h) isovector resonance located at 21.1 MeV. According to the arguments given in Appendix VII.D, only ~57 % of the total T = 0 + T = 1 E5 EWSR strength is exhausted in our E5 spectrum. As discussed previously, this is due to the fact that in our calculations those ph-contributions from states distant from the Fermi surface by more than $2\hbar\omega$, are not taken into account; these contributions are important in the description of resonances of multipolarity $L \geqslant 3$.

V.4. Giant electric resonances in ^{208}Pb

The energies of the single-particle states $2\hbar\omega$ above and below the Fermi surface are shown in Table 7. The core excitations taken into account in our calculations are written down in Table 10; they are practically all the firmly established low-lying states which are well described by the (1p-1h) RPA approach. The coupling of these core excited states with the single-hole states causes a large amount of 2h-1p admixtures which, as seen in equations (3.31) and (3.34), give rise to a huge number of 2p-2h configurations.

In this section we shall show the influence of these 2p-2h states on the well known giant (1p-1h) electric resonances. The latter were first calculated by Ring & Speth[76] and later by Krewald & Speth[84], Bertsch & Tsai[87] and Liu & Brown[89]. The (1p-1h) calculations done in ^{208}Pb have been recently reviewed by Speth et al.[96]; see this review for other references.

a) Giant monopole and quadrupole resonances

The E0 and E2 resonances calculated in the (1p-1h) RPA and in the Core-Coupling RPA theories are shown in Figures 24 and 25 respectively, and are analysed in terms of sum rules in Table 24. In the upper part of Figure 24 one observes a giant (1p-1h) T = 0 E0 peak at 15 MeV exhausting 69.2 % of the T = 0 E0 EWSR (whose value is 86545 e^2 fm^4 MeF from the calculations) and two narrow isovector peaks at 18.2 MeV and 21.8 MeV of comparable strength. The inclusion of the 2p-2h configurations completely fragments the T = 1 peak at 18.2 MeV although its centroid remains practically at the same place. The breathing mode at $\sim$15 MeV splits into several pieces but $\sim$55.4 % of the T = 0 E0 strength remains in the 14-to-16 MeV region. We also find $\sim$8 % of that isoscalar sum rule between 10 and 12 MeV, and $\sim$18.7 % between 12 and 14 MeV. Above the compressional or breathing mode we observe $\sim$18 % of the isoscalar E0 limit in the 16-to-20 MeV interval. Further details about the distribution of E0 strength can be seen in the first column of Table 24. In particular we find 26.8 % of the T = 0 + T = 1 E0 EWSR (whose value is 189130 e^2 fm^4 MeV from the calculations) to be exhausted in the 20-to-22 MeV energy interval. However this strength lies down in fact at the 21.76 MeV peak which is of pure isovector nature.

Regarding the E2 states one can observe from Figure 25 and the second column of Table 24 that the main features which the inclusion of 2p-2h configurations produced in the landscape of (1p-2h) 2^+ resonances are as follows:

1. The giant (1p-1h) T = 0 E2 resonance at $\sim$11.2 MeV strongly fragments giving rise to a redistribution of its strength between 8 and 14 MeV. We find 18.6 % of the T = 0 E2 EWSR (whose value is 76598 e^2 fm^4 MeV from the calculations) in the 8-to-10 MeV, 56.5 % between 10 and 12 MeV and 31 % between 12 and 14 MeV. This structure is discussed more in detail in the paragraph V.4.C in which a comparison with experiments is also done.

2. The giant isovector (1p-1h) E2 resonance at 16.7 MeV is no longer concentrated in a narrow peak but is distributed between 16 and 17 MeV.

In the 16-to-18 MeV region we find 23.8 % of the T = 0 + T = 1 E2 EWSR (whose value 174280 e^2 fm^4 MeV is from the calculations) to be depleted.

3. The low-lying E2 states are almost unaffected. We find that $\sim$22 % of the T = 0 E2 EWSR falls down below 8 MeV. For the sake of comparison with other authors we have written down in the last column of Table 24 the fractions of the $\sum_2^P$ (T = 0) sum rule (calculated according to a radius $R = 1.2\ A^{1/3}$ for the ground state distribution assumed to be uniform) which are exhausted in several energy intervals of the 2^+ spectrum.

b) Higher Multipole Resonances

In this subsection the E3, E4 and E5 resonances obtained in the first RPA and in the Core-Coupling RPA approaches will be presented. The octupole resonances are shown in Figure 26 and analysed in terms of sum rules in Table 26. From the figure we observe that the inclusion of 2p-2h excitations reduces the strength of all the (1p-1h) E3 peaks by giving rise to many states of small B(E3) value. The attention is drawn to the following point: fragmentation undergone by four states localized between 20.1 and 20.6 MeV. They have a mixed isovector-plus-isoscalar character. Their strength is spread out due to the 2p-2h coupling in a range of $\sim$3 MeV although the centroid is located around 20.4 MeV. We find that 24.6 % of the T = 0 + T = 1 E3 EWSR (whose value is $1.57 * 10^7$ e^2 fm^6 MeV; this is the exact isoscalar + isovector sum rule estimated according to Appendix VII.D) is exhausted between 20 and 22 MeV. In this interval we also find that $\sim$25 % of the T = 0 E3 EWSR; the value of this sum rule, which is $0.62 * 10^7$ e^2 fm^6 MeV, has been estimated according to Appendix VII.D.

The E4 states obtained in our 1p-1h and 2p-2h calculations are shown in

Figure 27. Here one observes that all the (1p-1h) E4 states get reduced their strength with the inclusion of the interaction of 2p-2h excitations. The main feature of the 4^+ spectrum is the large fragmentation undergone by the giant isoscalar (1p-1h) E4 resonance at 11.5 MeV. We find that whereas in the (1p-1h) calculation $\sim$27 % of the "exact" T = 0 E4 EWSR (0.452 * 10^9 e^2 fm^8 MeV; Appendix VII.D) is exhaused between 11 and 12 MeV, in the (1p-1h+2p-2h) calculation "only" $\sim$16.8 % remain in that interval. The main part of the missing strength is pushed downwards: 3.5 % and 4.2 % locate in the 9-to-10 MeV and in the 8-to-9 MeV regions respectively as it is shownin the last column of Table 25. On the other hand it is interesting to remark that the lowest 4^+ state at $\sim$4.7 MeV exhausts 6.6 % of the T = 0 E4 EWSR and in the 5-to-8 MeV region $\sim$11 % of that strength is depleted.

The (1p-1h) and (1p-1h+2p-2h) E5 states are shown in Figure 28. We observe that especially all the states in the 10-to-20 MeV are very much fragmented due to the inclusion of 2p-2h configurations. Many states of comparable B(E5) value exist in that interval. A substantial part of E5 strength has also been pushed up at energies above 20 MeV.

c) Fine Structure in the GQR region

Here the GQR region, i. e. between 8 and 15 MeV, is examined in detail by evaluating the percentages of the isoscalar EWSR corresponding to the multipolarities E0, E2 and E4. The results are shown in Table 25. It turns out that the mixing of the 2p-2h configurations is the main responsible for the fine structure recently observed in a variety of experiments[29,120,35,122-124,57]. Indeed we find the follwing features:

1. E0 strength.

About half of the isoscalar E0 sum rule is depleted between 14 and 15 MeV with a centroid at 14.2 MeV. A fraction of 16.8 % falls down in the 13-to-

14 MeV region with a centroid at 13.3 MeV. Between 11 and 12 MeV we find 8.9 % of that isoscalar sum rule centered around 11.8 MeV. Overall speaking, the inclusion of 2p-2h excitations reduces the portion of the isoscalar E0 sum rule to be exhausted in the GQR region from 91.9 % to 78.1 %. Furthermore the (1p-1h) T = 0 E0 centroid is pushed down from 14.4 MeV ($\equiv$ 85.3 $A^{-1/3}$) to 13.7 MeV, i. e. $\sim$81 $A^{-1/3}$ MeV.

2. E2 strength.

Here the fragmentation undergone by the giant (1p-1h) T = 0 E2 resonance is clearly shown. First we find 18.5 % of the isoscalar E2 sum rule to be depleted in the 9-to-10 MeV interval with the centroid at 9.7 MeV (= 57.5 $A^{-1/3}$). In this energy region we observe four relatively important peaks at 9.31, 9.76, 9.84 and 9.97 MeV exhausting 1.3, 3.0, 5.6 and 5.4 % of the sum rule respectively. Secondly 53.5 % of the T = 0 EWSR lies down between 11 and 12 MeV with the centroid at 11.4 MeV ($\simeq$ 67.6 $A^{-1/3}$); the strongest peak of this interval locates at 11.1 MeV ($\simeq$ 66 $A^{-1/3}$) and exhaust 17.3 % of the sum rule. In this energy region there are also five additional narrow peaks located at 10.67, 11.01, 11.28, 11.54 and 11.76 MeV exhausting 1.6, 6.0, 10.2, 8.5 and 5.4 % of the T = 0 EWSR strength respectively. Finally a third important fraction (29.7 %) of the sum rule is found to fall down between 12 and 13 MeV with the centroid at 12.14 MeV ($\simeq$ 72 $A^{-1/3}$). In this interval the strongest peak is at 12.44 MeV ($\simeq$ 73.7 $A^{-1/3}$) and exhaust 14.3 % of the sum rule. There are also three additional peaks in this interval, namely at 12.09, 12.11 and 12.50 MeV depleting 3.1, 2.5 and 7.3 % of the T = 0 E2 EWSR limit.

Overall speaking the inclusion of 2p-2h excitations first reduces the portion of the isoscalar quadrupole sum rule to be exhausted between 8 MeV and 15 MeV from 115.4 % to 96.5 %. On the other hand the centroid comes down from 11.3 MeV ($\simeq$ 67 $A^{-1/3}$) to 10.2 MeV ($\simeq$ 60.4 $A^{-1/3}$).

3. E4 strength.

We observe in this case two main points. First the existence of $\sim$8 % of the isoscalar E4 EWSR between 9 and 10 MeV. Secondly the depletion of 16.8 % of that sum rule in the 11-to-12 MeV interval. In the whole GQR energy region we find that 31.6 % of the isoscalar sum rule is exhausted with the centroid located at 10.3 MeV.

From an experimental point of view, it has been firmly established the existence of a broad isoscalar GQR at $\sim$63 $A^{-1/3}$ MeV in both electron and hadron scattering (see typical spectra in Bertrand[44] and Youngblood et al.[35]) exhausting more than 50 % of the isoscalar E2 sum rule. Its width is not so well established varying from 3 to 6 MeV with different experiments.

A pronounced fine structrue previously believed to have E0 nature was observed at $\sim$8.9 MeV by (e,e') reaction experiments[29]. However very recently it has been proved in inelastic proton scattering[123] the existence of a resonance at $\sim$56 $A^{-1/3}$ MeV ($\simeq$ 9.4 MeV) whose angular distribution is well described for an E2 or E3 excitation, but not for an E0 excitation. Furthermore it was seen[123] that if that resonance is E2, then it exhausts 16 % of the T = 0 E2 sum rule. This is in a fair agreement with our (1p-1h+2p-2h) calculations.

From inelastic electron[57] and deuteron[120] scattering experiments it has been suggested the existence of an isoscalar monopole resonance at $\sim$13.5 MeV. More recently inelastic 120 MeV α-scattering experiments[60] have observed an isoscalar resonance at $\sim$13.9 MeV with a width of $\sim$2.5 MeV; the angular distribution of this resonance seem to be well described by an E0 or an E2 assignment although it is not inconsistent with an E4 character. If would exhaust 100 %, 50 % or 17 % of the corresponding isoscalar

E0, E2 or E4 sum rules respectively.

Finally there is some evidence for an L = 4 resonance in the GQR region which has been provided by comparing microscopic-model[61)] calculations with measurements in ^{208}Pb. In such calculations the (1p-1h) RPA wave functions of Ring & Speth[76)] were used.

V.5. Magnetic dipole states in closed-shell nuclei

In recent years evidence (see Fagg[67)]) has been found for the existence of Giant Magnetic Dipole Resonances throughout the nuclei comparable in universality to the well-known E1 Resonance. They are conspicously absent for a few light doubly closed-shell nuclei such as ^4He, ^{16}O and ^{40}Ca (only a few, very weak M1 bevels are presented here). Since the operator for M1 transitions is mostly isovector and mostly a spin operator, M1 states enjoy a relatively unique position for probing the spin and isospin characteristics of the nucleus. Furthermore from a comparison of the calculated and experimentally observed distributions of the M1 strength one can get accurate information (see Speth[140)]) about the spin-dependent part of the residual interaction, i. e. about the parameters g_0 and g'_0 of eq. (4.10) and (4.13).

The origin of the giant M1 resonances lies in the spin-flip configurations

$$\left[\ell_{j>}^{-1}\ \ell_{j<}\right]_{1^+} \tag{5.1}$$

of the excited states corresponding to an excitation through $0\hbar\omega$. Here we denote $j_< = \ell - 1/2$ and $j_> = \ell + 1/2$. For the p- and sd-shell nuclei, (5.1) involves the configurations

$$\left[p_{3/2}^{-1},\ p_{1/2}\right]_{1^+} \quad \text{and} \quad \left[d_{5/2}^{-1},\ d_{3/2}\right]_{1^+}$$

respectively. In ^{90}Zr in which the 2p-1f shell and the $1g_{9/2}$ neutron are filled, the ground state M1 transition strength will reside exclusively in the neutron axcitation

$$\left[g_{9/2}^{-1}\ g_{7/2}\right]_{1^+}^{(n)}$$

In ^{208}Pb the M1 strength will be concentrated in states built upon the excitations

$$\left[1h_{11/2}^{-1} - 1h_{9/2}\right]_{1^+}^{(p)} \quad \text{and} \quad \left[1i_{13/2}^{-1} - 1i_{11/2}\right]_{1^+}^{(n)}$$

Due to the presence of the residual two-body interaction, these two configurations in ^{208}Pb will mix. Vergados[75] and Ring & Speth[76] have shown in (1p-1h) calculations that most of the M1 strength is depleted between 7 and 8 MeV in only one state (the former author) and in two states (the latter). The inclusion of the 2p-2h states fragments the M1 strength as pointed out by Lee & Pittel[144]. We have done a careful investigation about the fragmentation due to the mixing of 2p-2h configurations of the (1p-1h) M1 strength in ^{208}Pb (subsection V.5.a), in ^{90}Zr (subsection V.5.b) and in light nuclei (see subsection V.5.c) by using the Core Coupong RPA theory.

a) M1 strength in ^{208}Pb and the spin dependent part of the residual interaction

The magnetic properties of nuclei depend only on the spin-dependent part of the particle-hole interaction, i. e.

$$F_{ph}(\sigma\cdot\sigma') \propto g_o\ \bar{\sigma}\cdot\bar{\sigma}' + g_o'\ (\bar{\sigma}\cdot\bar{\sigma}')(\bar{\tau}\cdot\bar{\tau}') \qquad (5.2)$$

Here we shall use the parameters contained in Table 8, i. e.

$$g_o = 0.575 \quad \text{and} \quad g_o' = 0.725 \qquad (5.3)$$

Therefore the spin-dependent proton-proton and proton-neutron interactions (4.13) will have the values

$$g_{pp} = g_o + g_o' = 1.30 \qquad (5.4)$$

$$g_{pn} = g_o - g_o' = -0.15$$

Using these values for the p-h interaction and the expressions (4.16-4.19) for the effective magnetic operator, Ring and Speth[76] in (1p-1h) RPA calculations predicted two states of comparable strength and separated out by 0.8 MeV. Similar calculations done by Vergades[75] (using Kuo-Brown matrix elements) found only one T = 1 M1 resonance at 7.5 MeV which takes the bulk of M1 strength and one isoscalar M1 resonance at 5.5 MeV. This author uses a particle-hole interaction such that the spin-isospin exchange part (g_o') is much larger than the purely spin exchange contribution (g_o), and takes into account the bare magnetic operator. The comparison between the M1 results of both (1p-1h) calculations and experiment[70,74] (although the results of this are still very unclear) is done in Table 27. Therein one can observe that the present available experiment seems to favour approximately equal values for g_o and g_o', i. e. a small difference for g_{pn}.

The (1p-1h) structure of the two M1 states is of the form:

$$|1^+\rangle_{1p-1h} = A_p\ |1\pi h_{9/2} - 1\pi h_{11/2}^{-1}\rangle + A_n\ |1\nu i_{11/2} - 1\nu i_{13/2}^{-1}\rangle \qquad (5.5)$$

The dependence on g^{pn} of the energies, B(M1) values and wave functions of the two (1p-1h) states is given[188] in Table 28. If $g_o' > g_o$, the upper M1 state has a stronger transition probability than the lower one since in that case the proton amplitude A_p and the neutron amplitude A_n add coherently. If $g_o' < g_o$ the situation is inversed.

Our purpose here is to investigate how the distribution of the (1p-1h) M1 strength of Ring and Speth[76] (heretoforth to be referred as RS) is affected with the inclusion of the (2p-2h) configurations. First we shall use the effective magnetic operator of these authors (see section IV.4). The results are shown in Figure 29. Part a contains the (1p-1h) 1^+ states of RS. Part b shows the splitting of these states due to the (2p-2h) configuration which comes from the lowest 3^- core coupling. In part c a much larger amount of 2p-2h states coming from the coupling of the fragmented single-hole states, due to seven low-lying core excitations (see Table 10), with the single-particle degrees of freedom is taken into account.

From figure 29a and b one sees that the strength of the upper (1p-1h) M1 level at 8.31 MeV is reduced by half giving rise to two additional strong 1^+ levels about 1 MeV and 1.8 MeV higher in energy. With the inclusion of many more 2p-2h states, this structure changes qualitatively: the two new M1 levels redistribute their strength among many levels in the 8-to-11 MeV region. The explicit energies and transition probabilities of the (2p-2h) M1 resonances are given in the first column of Table 29. In this table the variation of the (2p-2h) M1 levels with the renormalization constant $\xi_s \equiv \xi_{s_p} = \xi_{s_n}$ of the effective magnetic operator (see section IV.4) is also shown.

From figure 29a and c one observes that the sum of the M1 strength (16.7 μ_o^2) of the two (1p-1h) levels has been redistributed due to the inclusion of 2p-2h states, the main features being as follows: (1) the strongest M1 state reduces its strength by half and its energy is lowered by $\sim$610 keV, (2) the energy difference between the two largest states remains ($\sim$800 keV), and (3) about 50 % of the (1p-1h) M1 strength is distributed among many states of small, comparable strength in the 8-to-11 MeV region.

Let us now perform the same (2p-2h) RPA calculations but with the bare magnetic operator, i. e. with the operator (4.16)-(4.19) in with $\varkappa = \xi_{\ell_p} =$

$\xi_{\ell_n} = \xi_{s_p} = \xi_{s_n} = 0$. The obtained results are shown in Figure 30. For the sake of comparison we have also included in this figure the (1p-1h) RPA calculations of RS with effective M1 operator (part a) and with bare M1 operator (part b). In part c only the lowest 3^- core coupling is taken into account, whereas in part d the whole amount of 2p-2h configurations coming from the coupling of the seven low-lying core excitations of Table 10 has been considered. Since now we are using the bare M1 operator, the two (1p-1h) 1^+ states have stronger B(M1) values: both sum 33 μ_0^2. Roughly speaking the inclusion of 2p-2h configurations produces the fragmentation of this strength in the same way as previously discussed in the calculations with an effective M1 operator. However there are some differences: (1) the upper strong (1p-1h) M1 level at 8.31 MeV strongly reduces its strength, half of which is exhausted by two narrow and very close levels of similar strength at 7.85 MeV and 7.93 MeV; the other half is pushed up to higher energies. (2) about 30 % of the (1p-1h) M1 strength lies down in the 8-to-11 MeV interval.

From figure 30a and 30d, one observes that, if we add up the two states near 8 MeV, the distribution of M1 strength obtained in the (1p-1h) RPA calculations by Ring & Speth in using an effective M1 operator is very similar to that obtained here in our (2p-2h) RPA calculations with the bare M1 operator. This might perhaps be an indication that the main contributions to the effective operator are of 2p-2h character. However one should bear in mind that also the meson-exchange currents might produce an enhancement of the transition probability.

In order to check the stability of the splitting just below 8 MeV, we have performed calculations with different values of g_{pp} and g_{pn}. First we have maintained the value $g_{pp} = 1.30$ and given to the spin-dependent part of the proton-neutron interaction g_{pn} the following small positive values:

+0.02, +0.05 and +0.10. The corresponding results are shown in Figure 31 and in the three last columns of Table 30. A surprising phenomenon is the disappearance of the splitting of the strong state at $\sim$7.9 MeV. This effect can be understood by looking at the wave functions of the two splitted states. For $g_{pn} = 0$ the 7.85 MeV level is predominantly a 1p-1h neutron state $(i_{11/2} - i^{-1}_{13/2})$, whereas the dominant structure of the 7.93 MeV state is of the form $(5^-_1 \otimes \pi 3s^{-1}_{1/2})_{11/2^-} \otimes \pi 1h_{9/2}$ plus a $\pi 1h_{9/2} \times \pi 1h^{-1}_{11/2}$ admixture of 0.2 in amplitude. A finite proton-neutron interaction gives rise to a mixture of the two states. The 1p-1h M1 components of the two states add coherently in the upper state if $g_{pn} < 0$ $(g_0 < g'_0)$ and destructively if $g_{pn} > 0$ $(g_0 > g'_0)$. For small positive g_{pn} they nearly cancel each other. The structure of the 7.10 MeV level is predominantly $\pi 1h_{9/2} \otimes \pi 1h^{-1}_{11/2}$ whereas the levels between 8 and 11 MeV are of 2p-2h character with small 1p-1h admixtures. The higher states in Figures 30 and 31 are due to $2\hbar\omega$ excitations; the collectivity of these M1 levels has been recently studied by Speth et al.[78].

In Table 30 the comparison with experiment is also made. With the most recent available measurements, our (2p-2h) calculations are in qualitative agreement. Below 8 MeV both experiment and calculations find the M1 strength mainly concentrated in two peaks at $\sim$7 MeV and $\sim$8 MeV, i. e. one peak below the neutron emission threshold (7.38 MeV) and the other above it. Above 8 MeV both experiment and theory locate about 30 to 40 % (of the strength below 8 MeV) distributed in many levels in the 8-to-11 MeV interval. From table 30 one would say that the present experimental data seem to favour a small positive g_{pn} value $(g'_0 < g_0)$. However one should bear in mind that (1) the experimental results are still unclear and (2) we are using in our calculations a zero-range force. The finite-range character of the residual interaction (which is mainly due to one-π exchange) reduces[189] the g_0' parameter, hence it might bring g_{pn} to change the sign.

Secondly let us now keep fixed g_{pn} = -0.15 and vary the parameter g_{pp}. From second and third column of Table 31 one observes that changing g_{pp} from 1.30 to 1.10, the splitting of the (2p-2h) M1 state at around 7.9 MeV disappears, what proves that peak to be unstable and "artificious". In all the (2p-2h) calculations of Table 31 the bare M1 operator has been used. The present experimental results were included for comparison.

b) <u>M1 resonances in ^{90}Zr</u>

Here we present the M1 states found in the (2p-2h) RPA calculations. We shall use the value g_{pn} = +0.10 as one could infer from the comparison between experimental and theoretical results in the previous section. All the hole states $2\hbar\omega$ below the Fermi surface are in a first step splitted due to the coupling of six low-lying core excitations (see Table 10). The (1p-1h) RPA and (2p-2h) RPA results are shown in Figure 31 and Table 33. We observe only one (1p-1h) 1^+ level at $\sim$9.8 MeV with B(M1)$\uparrow$ value of 5.44 μ_0^2 (if we use the effective magnetic operator, see section IV.4) or 11.11 μ_0^2 if we use the bare magnetic operator. Its structure is exclusively built up by the particle-hole ($g_{9/2}^{-1}$ - $g_{7/2}$) excitation.

Due to the coupling of core excitations the single-hole state $g_{9/2}$ splits weakly as shown in Table 32, the main strength (90.75 %) remain at the experimental energy -11.75 MeV. There are other three relatively important pieces at -14.66 MeV (with 3.17 % of the single-hole strength), at -19.81 MeV (2.94 %). Many other fragmented $g_{9/2}$ pieces (those beyond 20 MeV are not written down) with very small strengths also appear.

As a consequence of the splitting of this hole state one also expects fragmentation of the (1p-1h) M1 resonance due to the inclusion of the (2p-2h) configurations. The bare M1 operator has been used. This is seen in the lower part of Figure 32 where we mainly notice four narrow peaks of relatively important B(M1) value, and many other 1^+ states with very small strengths. The energies of all these states and the wave functions of the four strongest ones are shown in Table 33. One observes that the (1p-1h) M1 strength ($\sim$11.1 μ_0^2) is now distributed between 9 and 16 MeV. Although its centroid is 10.4 MeV, the strongest M1 level is at 9.47 MeV ($\sim$42.4 $A^{-1/3}$), i. e. 330 keV below its initial (1p-1h) position. It is also interesting to remark from Tables 32 and 33 that the reduction of the strength undergone by the (1p-1h) M1 resonance and the structure of the two other strongest M1 states at 10.5 and 11.1 MeV are mainly due to the following admixtures

$$1g_{7/2} \times (2^+ \times 1g_{9/2}) \qquad \text{and} \qquad 1g_{7/2} \times (4^+ \times 1g_{9/2})$$

From an experimental point of view the situation of the M1 strength is unclear. There are indications (see Fagg[67)]) of a certain amount of M1 strength between 7.5 MeV and 10.5 MeV peaked at about 9 MeV. On the other hand recent inelastic electron scattering of Torizuka[68)] have also shown the existence of a large bump at $\sim$9 MeV in which several isovector magnetic multipole resonances are superposed.

c) M1 resonances in ^{12}C

In Figure 33 the (1p-1h) and (2p-2h) RPA calculations of M1 states in ^{12}C are shown. In all of these calculations the parameter g_{pp} = 1.30 has been used. As suggested by the study of M1 states in ^{208}Pb, we have used the value g_{pn} = -0.15 in those calculations with the effective magnetic operator, and g_{pn} = +0.10 in those with the bare M1 operator. From this figure we observe that (1) the amount of M1 strength is increased by using the bare M1 operator, what has already been seen in lead and zirconium. (2)

the (2p-2h) states pushes down the strongest M1 level to the experimentally observed energy ($\sim$15.1 MeV) and fragments it by creating a narrow state at $\sim$23.7 MeV and locating a portion of its strength in the 45-to-55 MeV region; no experimental information about magnetic resonances above 16 MeV is apparently available. Below 16 MeV the calculations are in qualitative agreement with experiment[67)] in which two M1 peaks are known. They are located at 12.7 MeV and 15.1 MeV with B(M1) values of 0.0444 μ_0^2 and 2.79 μ_0^2 respectively.

In Figure 34 both 2p-2h RPA calculations with g_{pn} = -0.15 and effective M1 operator (picture upstairs), and with g_{pn} = +0.10 and bare M1 ooperator (picture downstairs) are compared. The overall structure of M1 strength is the same in both pictures, the only difference being the smaller amount of strength upstairs due to the distinct magnetic operator. As a conclusion we would say that the coupling of low-lying core excitations other than 2^+ (4.44 MeV) and 3^- (9.61 MeV) might have to be included in order to get a closer comparison with experiment.

V.6. Magnetic quadrupole states in closed-shell nuclei

The existence of giant M2 resonances is experimentally not well established. The (1p-1h) RPA calculations of Ring & Speth[76)] predicted a giant M2 resonance at $\sim$7.5 MeV in ^{208}Pb. This has been corroborated to a large extent by Lindgren et al.[146)] using 180^0 inelastic electron scattering. Other indications of giant M2 states have been given by Torizuka[68)] in ^{90}Zr. In paragraph a we observe the influence of 2p-2h configurations on the (1p-1h) M2 results of RS[76)]. Furthermore we present here (1p-1h) and (2p-2h) RPA calculations of M2 states in ^{90}Zr (paragraph b), in ^{16}O (paragraph c) and in ^{12}C (paragraph d).

a) Giant M2 resonances in ^{208}Pb

In figure 35 the effect of including the 2p-2h states on the (1p-1h) M2 resonances of Ring & Speth[76] is shown. We observe that the M2 resonance at 7.2 MeV reduces its strength ($B(M2) \simeq 38\ B_W(M2)$; see Table 15 to know the Weisskopf units) by fragmenting it in several peaks in the 7-to-9 MeV region. The strongest peak remains however at the same energy with $B(M2) \simeq 26.8\ B_W(M2)$. The influence of the 2p-2h configurations on the whole (1p-1h) M2 spectrum is shown in Table 34. A reduction of the strength in the 7-to-8 MeV interval and an enhancement in the 8-to-9 MeV and in the 10-to-11 MeV regions are found.

If one uses the parameter $g_{pn} = +0.10$ and the bare magnetic operator, the qualitative distribution of the (2p-2h) M2 strength does not change. Then three main peaks appear. The strongest one is at 7.5 MeV with $B(M2) = 30\ B_W(M2)$. The other two are located at 8.65 MeV with $B(M2) = 7.45\ B_W(M2)$, and at 9.19 MeV with $B(M2) = 3.5\ B_W(M2)$.

b) Giant M2 resonances in ^{90}Zr

In figure 36 the M2 resonances obtained in the (1p-1h) RPA and in the (2p-2h) RPA calculations are shown. Comparing the picture at the top with that at the bottom one observes that the qualitative structure is very similar. Two strongest M2 states jump out at 13.1 MeV and 14.3 MeV (see bottom picture), having together $B(M2) = 13.5\ B_W(M2)$. Essentially three concentrations of the strength are shown: between 8 and 11 MeV, between 11 and 15 MeV and in the 15-to-20 MeV region.

c) Giant M2 resonances in light nuclei

Let us first discuss the M2 states in ^{16}O. The (1p-1h) RPA and (2p-2h) RPA results are shown in figures 37 and 38. A qualitative change in the distribution of the (1p-1h) M2 strength is found. The energies and strengths of those M2 resonances with a transition probability larger than one Weisskopf unit are shown in Table 35.

The calculated M2 states in ^{12}C in the (1p-1h) RPA and (2p-2h) RPA approaches are shown in figures 39 and 40. Again the qualitative distribution of M2 strength is changed. Around half of the strength is pushed up to higher energies (mainly between 35 and 55 MeV) due to the inclusion of 2p-2h configurations. In figure 40 the comparison between two different 2p-2h calculations is made; in the picture at the top the effective M2 operator and $g_{pn} = -0.15$ have been used. In both calculations three main peaks appear between 13 and 18 MeV.

V.7. Higher magnetic multipole resonances in closed-shell nuclei

First the calculated M3 and M4 resonances shall be discussed. These states of ^{90}Zr are calculated in the (1p-1h) RPA and (2p-2h) RPA approaches and shown in Figures 41 and 42 respectively. Using the bare magnetic operator and the parameter $g_{pn} = 0.10$, the (2p-2h) calculations show that the bulk of the M3 strength lies down in the 15-to-30 MeV interval. Below 15 MeV only two M3 states with a reliable transition probability are found: one is located at $\sim$8 MeV and 13.6 MeV with B(M3) values of 6.57 B_W(M3) and 4.60 B_W(M3) respectively (see Table 15 for the Weisskopf units).

The (2p-2h) M4 calculations at bottom of figure 42 shows that the M4 strength is distributed almost uniformly in the whole spectrum except a huge concentration in the 30-to-35 MeV region. Below 15 MeV we find a total $B(M4) = 1.89 * 10^7 \ \mu_o^2 \ fm^6$, which is distributed as follows: 20.2 B_W(M4) is depleted by two narrow peaks below 5 MeV, 54.7 B_W(M4) lies down between 5 and 10 MeV, and the rest, i. e. 73.7 $B_W(M4)$, is comparted by many states of comparable strength in the 10-to-15 MeV interval.

In Figures 43 and 44 the M3 resonances in ^{16}O calculated in the (1p-1h) RPA and (2p-2h) RPA theories are shown. In the former approach the total strength is located in the 30-to-45 MeV region. With the inclusion of (2p-2h) configurations, although the bulk of the strength remains between 35 and 45 MeV, there is a substantial portion which is pushed up in an interval of 20 MeV. On the other hand we also find two relatively important peaks slightly above 15 MeV of excitation energy. The M4 resonances in ^{16}O of the (1p-1h) and (2p-2h) calculations are shown in Figures 45 and 46. The (1p-1h) M4 strength is concentrated in two energy regions, namely between 20 and 25 MeV and between 40 and 60 MeV. Therefore there exists an empty gap of $\sim$20 MeV. This gap is to a large extent filled up with the inclusion of 2p-2h configurations. In figure 46 two different 2p-2h calculations are shown; in the picture upstairs the effective magnetic operator (see section IV.4) and the parameter $g_{pn} = -0.15$ have been used. In the picture downstairs the bare M4 operator and $g_{pn} = +0.10$ were taken into account. The qualitative structure in both pictures is the same but the states upstairs have a small B(M4) value due to the effectiveness of the magnetic operatur.

The M3 states in ^{12}C are shown in Figures 47 and 48. Here the large shift up to higher energies (also observed in ^{16}O) undergone by the (1p-1h) magnetic octupole resonances due to the inclusion of (2p-2h) configurations is more pronounced. In both 2p-2h calculations with effective magnetic operator and $g_{pn} = -0.15$ (top of figure 48) and with bare M3 operator and $g_{pn} = +0.10$ (bottom of figure 48), we find the strength located at $\sim$30 MeV and at $\sim$50 MeV. In between these two energies we find many other M3 states of comparable, small transition probability. The M4 resonances in ^{12}C are presented in Figures 49 and 50. Here the gap ($\sim$30 MeV) existing between the two locations of (1p-1h) M4 strength is bigger and sharper than in ^{16}O. As in this case the (2p-2h) configurations produce a fragmentation of the two narrow (1p-1h) resonances by filling that gap and locating a large portion of strength at higher energies, mainly between 65 and 75 MeV.

Important experimental evidence on the higher giant magnetic multipoles is being obtained by radiative pion capture[190)] and inelastic electron scattering at backward angles[68)]. However the evidence on M2 resonances is not extensive enough throughout the periodic table to provide for a systematic description of its location and strength. The evidence on higher magnetic multipoles is even less developed.

VI. SUMMARY AND CONCLUSION

Here we have developed the Core-Coupling Random-Phase-Approximation. In this theory one solves the secular eigenvalue problem obtained from the closed system of linearized equations of motion for the 1p-1h operators and 2p-2h operators. The spectra of the closed-shell nuclei ^{12}C, ^{16}O, ^{90}Zr and ^{208}Pb are investigated in the framework of the new theory by using the density-dependent, zero-range Migdal interaction. The low-lying collective states and the giant resonances are microscopically described in a simple and pictorial way, namely by means of quasiparticle-quasihole excitations (e. g. in terms of the conventional 1p-1h plus 2p-2h excitations).

Although the single-particle configuration space of our calculations contains two major oscillator shells above and below the Fermi surface, our method is able to deal almost equally easily with light, medium and heavy nuclei.
Main points of our work are as follows:

i) The broadening of the Giant Quadrupole Resonance in ^{12}C and ^{16}O, and very probably in all the light nuclei ($A \leq 30$), is due to the fragmentation of the $f_{7/2}$ resonance since the narrow part of the GQR is mainly built up by the $f_{7/2} \times p_{3/2}^{-1}$ configuration. The other possible configurations contribute only to a broad background, since the (theoretical) widths of the $f_{5/2}$, $p_{3/2}$ and $p_{1/2}$ single-particle resonances are very large.

   In heavier nuclei ($A > 30$) this situation changes because other channels than the $f_{7/2}$ show also a narrow width. In that case one obtains the normal situation of a coherent superposition of many 1p-1h configurations.

ii) A natural explanation of the different experimental results in ^{16}O obtained with (p,γ_0), $(^3He,^3He')$ and (α,α') reactions is given. In the first experiment the (narrow) $f_{7/2} \times p_{3/2}^{-1}$ configuration cannot be excited via the $p_{1/2}$ hole. On the other hand, in the (^3He,$^3He'$) and (α,α') experiments also the (narrow) $f_{7/2} \times p^{-1}_{3/2}$ component is excited.

iii) The fine structure of the giant quadrupole resonance (GQR) can be roughly explained within our approach. Qualitative agreement with the present available experiments is obtained. In light nuclei an appreciable fraction of the E4 sum rule strength is here found to be concentrated in the same region as the GQR. In ^{208}Pb several narrow peaks of E0, E2 and E4 multipolarities are found to be superimposed on the broad GQR peak. This one should bear in mind if one tries to deduce quantitatively B(E2) strength from inelastic hadron scattering experiments and in comparing the sum rule fraction of the GQR obtained by different experimental methods.

iv) The fragmentation of the M1 resoannces due to the admixtures of (2p-2h) configurations have been calculated. The qualitative structure of the 1p-1h calculation of Ring & Speth[76)] remains but about 30 % of the M1 strength is shifted to higher energies and is distributed over many levels between 8 and 11 MeV. In addition we have shown that the M1 strength distribution of the main peaks depends very sensitively on the spin-dependent proton-neutron interaction. The comparison of our results with the present experimental data seems to favor a small positive g^{pn} value ($g'_0 < g_0$). To this point we should point out that a zero-range force has been used in our calculations. One can not exclude a slight influence[189)] of the finite-range character of nuclear forces on the parameter g_{pn}.

v) Predictions about the splitting of the low-lying giant M1 resonance in ^{90}Zr and about the strength distribution of higher magnetic multipole resonances in this and other closed-shell nuclei are made.

In summary we have investigated the giant electric and magnetic multipole resonances achieving a qualitative and in some cases nearly quantitative agreement with recent experiments. We have shown the spreading width of the giant multipole resonances to be mainly produced by the 2p-2h configurations which comes from the coupling of the low-lying core excitations with the single-particle degrees of freedom. Our approach is also able to give the percentages of the sum rule strength of the different types of multipole resonances depleted in the giant resonance region, and the microscopic structure of the excited states existing in that region.

VII. APPENDICES

VII.A. Explicit form of quasiparticle and quasihole operators

The quasiparticle operators are:

$$x_M^+ = C_m^{(a)} a_m^+ + \sum_{\alpha\nu_2} C_{\alpha\nu_2}^{(ma)} \sum_{m_1h_1} \left\{\left[X_{m_1h_1}^{(\alpha)} (a_{m_1}^+ a_{h_1})_{J_\alpha} - Y_{m_1h_1}^{(\alpha)} (a_{h_1}^+ a_{m_1})_{J_\alpha}\right] \otimes a_{\nu_2}^+\right\}_m$$

$$x_N^+ = C_n^{(b)} a_n^+ + \sum_{\alpha\nu_1} C_{\alpha\nu_1}^{(nb)} \sum_{n_1i_1} \left\{\left[X_{n_1i_1}^{(\alpha)} (a_{n_1}^+ a_{i_1})_{J_\alpha} - Y_{n_1i_1}^{(\alpha)} (a_{i_1}^+ a_{n_1})_{J_\alpha}\right] \otimes a_{\nu_1}^+\right\}_n$$

The quasihole operators are:

$$x_I = C_i^{(d)} a_i + \sum_{\alpha\mu_1} C_{\alpha\mu_1}^{(id)} \sum_{m_3i_3} \left\{\left[X_{m_3i_3}^{(\alpha)} (a_{m_3}^+ a_{i_3})_{J_\alpha} - Y_{m_3i_3}^{(\alpha)} (a_{i_3}^+ a_{m_3})_{J_\alpha}\right] \otimes a_{\mu_1}\right\}_i$$

$$x_H = C_h^{(c)} a_h + \sum_{\alpha\mu_2} C_{\alpha\mu_2}^{(hc)} \sum_{m_4i_4} \left\{\left[X_{m_4i_4}^{(\alpha)} (a_{m_4}^+ a_{i_4})_{J_\alpha} - Y_{m_4i_4}^{(\alpha)} (a_{i_4}^+ a_{m_4})_{J_\alpha}\right] \otimes a_{\mu_2}\right\}_h$$

Here $M \equiv (m,a)$, $N \equiv (n,b)$, $H \equiv (h,c)$ and $I \equiv (i,d)$. Moreover the subscripts m, n, m_1, m_2, m_3, m_4, ν_2, ν_1 are reserved for particle states, i. e. single-particle states above the Fermi energy, and i, h, h_1, i_1, i_3, i_4, μ_1, μ_2 are reserved for hole states, i. e. single-particle states below the Fermi energy. The term "Fermi energy" is used rather loosely here. It is to be understood as that energy such that, if all particles occupied the lowest-possible single-particle states, all states below the Fermi energy would be occupied and all states above it would be empty.

VII.B. Formulae of Racah Algebra

We define[112,8,192] the antisymmetric 1p-1h and 2p-2h states in second quantization as follows:

$$|j_1 j_2^{-1};JM\rangle = \sum_{m_1 m_2} \langle j_1 m_1 j_2 -m_2|JM\rangle\, (-)^{j_2-m_2}\, a^+_{j_1 m_1}\, a_{j_2 m_2}|\phi_o\rangle \tag{B.1}$$

$$\begin{aligned}|j_1^{-1} j_2^{-1}(J_h) j_3 j_4 (J_p);JM\rangle &= \sigma_{12}\sigma_{34} \sum_{m_1 m_2 m_3 m_4 M_h M_p} \langle j_1 -m_1 j_2 -m_2|J_h M_h\rangle \cdot \langle j_3 m_3 j_4 m_4|J_p M_p\rangle \cdot \\ &\cdot \langle J_h M_h J_p M_p|JM\rangle (-1)^{j_1-m_1}\, (-1)^{j_2-m_2}\, a^+_{j_4 m_4} a^+_{j_3 m_3} a_{j_2 m_2} a_{j_1 m_1}|\phi_o\rangle\end{aligned} \tag{B.2}$$

where

$\sigma_{12} = (1+\delta_{j_1 j_2})^{-1/2}$ and $\delta_{j_1 j_2}$ is zero unless state j_1, which is defined by $(n_1 \ell_1 j_1)$, is equal to state j_2.

In order to put our peculiar coupling scheme in the form (B.2) one should use the following recoupling formula:

$$\begin{aligned}|j_a j_b^{-1}(J_\alpha) j_c (J_\beta) j_d^{-1};J\rangle &= \sum_{J_h J_p} (-)^{J_\alpha + J_p - j_b - j_c}\, \hat{J}_\alpha \hat{J}_\beta \hat{J}_h \hat{J}_p \cdot \\ &\cdot \begin{Bmatrix} j_b & J_p & J_\beta \\ j_c & J_\alpha & j_a \end{Bmatrix} \begin{Bmatrix} j_b & J_p & J_\beta \\ J & j_d & J_h \end{Bmatrix} |j_d^{-1} j_b^{-1}(J_h) j_a j_c (J_p);J\rangle\end{aligned}$$

where $\hat{J}$ is defined by $\hat{J} = \sqrt{2J+1}$

In the following we show the 1p-1h matrix elements, the (1p-1h)-(2p-2h) matrix elements and the 2p-2h matrix elements used in our calculations.

1. One particle-One hole matrix elements

$$\begin{aligned}\langle j_a j_b^{-1};J|\mathscr{H}|j_c j_d^{-1};J\rangle &= (\varepsilon_{j_a} - \varepsilon_{j_b})\, \delta_{j_a j_c}\, \delta_{j_b j_d} - \\ &- \sum_{J'} (2J'+1) \begin{Bmatrix} j_b & j_a & J \\ j_d & j_c & J' \end{Bmatrix} (-1)^{j_a+j_b+j_c+j_d} \langle j_a j_d;J'|V|j_c j_b;J'\rangle\end{aligned}$$

The first term on the right-hand side is the (diagonal) single-particle contribution and the second the pure particle-hole interaction, i. e. $\langle j_a j_b^{-1};J|V|j_c j_d^{-1};J\rangle$

2. (One particle-One hole)-(Two particle-Two hole) matrix elements

$$<j_a j_b^{-1}(J_\alpha) j_c (J_\beta) j_d^{-1}; JM|\mathcal{H}| j_b^{'-1} j_a^{'}; JM> = C_1 + C_2 + C_3 + C_4$$

where C_1, C_2, C_3 and C_4 are given as follows:

$$C_1 = (-1)^{j_c+j_d+j_b^{'}+J_\beta} \sigma_{ac} \hat{J}_\alpha \hat{J}_\beta \begin{Bmatrix} J_\alpha & j_d & j_b^{'} \\ J & j_c & J_\beta \end{Bmatrix} \cdot$$

$$\cdot \sum_{J_h} (2J_h+1) \begin{Bmatrix} j_b & j_d & J_h \\ j_b^{'} & j_a & J_\alpha \end{Bmatrix} <j_d j_b J_h |V| j_a j_b^{'} J_h> \delta_{j_a^{'} j_c}$$

$$C_2 = (-1)^{J_\alpha+J-j_b+j_c+1} \sigma_{ac} \hat{J}_\alpha \hat{J}_\beta \sum_{J_h J_p} \hat{J}_h^2 \hat{J}_p^2 (-1)^{J_h} \begin{Bmatrix} j_b & J_\beta & J_p \\ j_c & j_a & J_\alpha \end{Bmatrix} \cdot$$

$$\cdot \begin{Bmatrix} j_b & j_d & J_h \\ J & J_p & J_\beta \end{Bmatrix} \cdot \begin{Bmatrix} j_b^{'} & j_c & J_h \\ J_p & J & j_a \end{Bmatrix} <j_d j_b; J_h |V| j_c j_b^{'}; J_h> \delta_{j_a^{'} j_a}$$

$$C_3 = (-1)^{J_\alpha+J+j_d-j_c+2j_b+1} \sigma_{ab} \hat{J}_\alpha \hat{J}_\beta^{-1} \sum_{J_p} \hat{J}_p^2 \cdot \begin{Bmatrix} j_b & j_a^{'} & J_p \\ j_c & j_a & J_\alpha \end{Bmatrix} \cdot$$

$$\cdot <j_a^{'} j_b; J_p |V| j_a j_c; J_p> \delta_{j_d j_b^{'}} \delta_{J_\beta j_a^{'}}$$

$$C_4 = (-1)^{J_\alpha+J+j_b-j_c-j_a^{'}-J_\beta} \sigma_{db} \hat{J}_\alpha \hat{J}_\beta \sum_{J_p} \begin{Bmatrix} j_b & J_\beta & J_p \\ j_c & j_a & J_\alpha \end{Bmatrix} \cdot \begin{Bmatrix} j_a^{'} & j_d & J_p \\ J_\beta & j_b & J \end{Bmatrix} \cdot \hat{J}_p^2$$

$$\cdot <j_a^{'} j_d; J_p |V| j_a j_c; J_p> \delta_{j_b j_b^{'}}$$

3. (Two particle-Two hole)-(Two particle-Two hole) matrix elements

$$<j_a j_b^{-1}(J_\alpha) j_c (J_\beta) j_d^{-1}; JM|\mathcal{H}| j_a^{'} j_b^{'-1} (J_\alpha^{'}) j_c^{'} (J_\beta^{'}) j_d^{'-1}; JM> =$$

$$= (\varepsilon_{j_a} + \varepsilon_{j_c} - \varepsilon_{j_d} - \varepsilon_{j_b}) \sigma_{db} \sigma_{ac} \sigma_{d'b'} \sigma_{a'c'} \delta_{j_d j_d^{'}} \delta_{j_b j_b^{'}} \delta_{j_a j_a^{'}} \delta_{j_c j_c^{'}} \delta_{J_\alpha J_\alpha^{'}} \delta_{J_\beta J_\beta^{'}}$$

$$+ D_1 + D_2 + \sum_{i=1}^{16} E_i$$

The terms D_1, D_2 and $\{E_i,\ i=1, \ldots , 16\}$ are given as follows:

$$D_1 = (-1)^{J_\alpha+J'_\alpha-j_b-j'_b+2j_a}\ \hat{J}_\alpha\hat{J}_\beta\hat{J}'_\alpha\hat{J}'_\beta\sigma_{ac}\sigma_{a'c'}\delta_{j_aj'_a}\delta_{j_cj'_c}\ \cdot$$

$$\cdot \sum_{J_p} \hat{j}_p^2 \begin{Bmatrix} j_b & J_\beta & J_p \\ j_c & j_a & J_\alpha \end{Bmatrix} \begin{Bmatrix} j_c & j_a & J_p \\ j'_b & J'_\beta & J'_\alpha \end{Bmatrix} \cdot \sum_{J_h} \hat{J}_h^2 \begin{Bmatrix} j'_b & j'_d & J_h \\ J & J_p & J'_\beta \end{Bmatrix} \begin{Bmatrix} J & J_p & J_h \\ j_b & j_d & J_\beta \end{Bmatrix} \cdot$$

$$\cdot \ \langle j_dj_b;J_h|V|j'_dj'_bJ_h\rangle$$

$$D_2 = (-1)^{J_\alpha+J'_\alpha-j_c-j'_c+2j_b}\ \hat{J}_\alpha\hat{J}'_\alpha\sigma_{db}\sigma_{d'b'}\delta_{j_dj'_d}\delta_{j_bj'_b}\delta_{J_\beta J'_\beta}\ \cdot$$

$$\cdot \sum_{J_p} (-)^{2J_p}\ \hat{j}_p^2 \begin{Bmatrix} j_b & J_\beta & J_p \\ j_c & j_a & J_\alpha \end{Bmatrix} \begin{Bmatrix} j'_c & j'_a & J_p \\ j_a & J_\beta & J'_\alpha \end{Bmatrix} \langle j_aj_cJ_p|V|j'_aj'_cJ_p\rangle$$

$$E_1 = \sigma_{db}\sigma_{ac}\sigma_{d'b'}\sigma_{a'c'}\ \hat{J}_\alpha\hat{J}'_\alpha\hat{J}_\beta\hat{J}'_\beta\ \delta_{j_bj'_b}\delta_{j_cj'_c}\ \cdot \sum_X \hat{X}^2\ \langle j_d^{-1}j_a;X|V|j_d'^{-1}j'_a;X\rangle\ \cdot$$

$$\cdot \sum_Y (-)^{2Y}\ \hat{Y}^2 \begin{Bmatrix} X & J & Y \\ J_\beta & j_a & j_d \end{Bmatrix} \begin{Bmatrix} X & J & Y \\ J'_\beta & j'_a & j'_d \end{Bmatrix} \begin{Bmatrix} j_b & j_c & Y \\ J_\beta & j_a & J_\alpha \end{Bmatrix} \begin{Bmatrix} j_b & j_c & Y \\ J'_\beta & j'_a & J'_\alpha \end{Bmatrix}$$

$$E_2 = (-1)^{j_c+j_a+j_b+j_d+J}\ \sigma_{db}\sigma_{ac}\sigma_{d'b'}\sigma_{a'c'}\ \hat{J}_\alpha\hat{J}_\beta\hat{J}'_\alpha\hat{J}'_\beta\ \delta_{j_dj'_b}\delta_{j_cj'_c}\ \cdot$$

$$\cdot \ \langle j_b^{-1}j_a;J_\alpha|V|j_d'^{-1}j'_a;J_\alpha\rangle \cdot \sum_Y \hat{Y}^2 \begin{Bmatrix} j'_a & J'_\beta & Y \\ j_c & j_d & J'_\alpha \end{Bmatrix} \begin{Bmatrix} J_\alpha & J & Y \\ j_d & j_c & J_\beta \end{Bmatrix} \begin{Bmatrix} J_\alpha & J & Y \\ J'_\beta & j'_a & j'_d \end{Bmatrix}$$

$$E_3 = -(-1)^{2(j_b+j'_a-j_c)}\ \sigma_{db}\sigma_{ac}\sigma_{d'b'}\sigma_{a'c'}\ \hat{J}_\alpha\hat{J}'_\alpha\hat{J}_\beta\hat{J}'_\beta\ \delta_{j_bj'_b}\ \delta_{j_aj'_c}\ \cdot$$

$$\cdot \begin{Bmatrix} j_b & j'_a & J'_\alpha \\ J'_\beta & j_a & J_\alpha \end{Bmatrix} \cdot \sum_X \hat{X}^2 \begin{Bmatrix} J & J_\alpha & X \\ j_c & j_d & J_\beta \end{Bmatrix} \begin{Bmatrix} J & J_\alpha & X \\ j'_a & j'_d & J'_\beta \end{Bmatrix} \langle j_d^{-1}j_c;X|V|j_d'^{-1}j'_a;X\rangle$$

$$E_4 = (-1)^{j_b+j_d+j_c+j_a+J}\ \sigma_{db}\sigma_{ac}\sigma_{d'b'}\sigma_{a'c'}\ \hat{J}_\alpha\hat{J}_\beta\hat{J}'_\alpha\hat{J}'_\beta\ \delta_{j_dj'_b}\ \delta_{j_aj'_c}\ \cdot$$

$$\sum_X \hat{X}^2 \begin{Bmatrix} j_b & j_c & X \\ J_\beta & j_a & J_\alpha \end{Bmatrix} \langle j_b^{-1} j_c ; X | V | j_d'^{-1} j_a' ; X \rangle \sum_Y \hat{Y}^2 \begin{Bmatrix} j_a & j_d & Y \\ j_a' & J_\beta' & J_\alpha' \end{Bmatrix} \begin{Bmatrix} j_d & j_a & Y \\ X & J & J_\beta \end{Bmatrix} \begin{Bmatrix} X & J & Y \\ J_\beta' & j_a' & j_d' \end{Bmatrix}$$

$$E_5 = -(-)^{j_a+j_b'+j_a'-j_c+J} \sigma_{db}\sigma_{ac}\sigma_{d'b'}\sigma_{a'c'} \hat{J}_\alpha \hat{J}_\beta \hat{J}_\alpha' \hat{J}_\beta' \delta_{j_b j_d'} \delta_{j_c j_c'} \langle j_d^{-1} j_a ; J_\alpha' | V | j_b'^{-1} j_a' ; J_\alpha' \rangle$$

$$\sum_Y \hat{Y}^2 \begin{Bmatrix} j_c & j_b & Y \\ j_a & J_\beta & J_\alpha \end{Bmatrix} \begin{Bmatrix} J_\alpha' & J & Y \\ J_\beta & j_a & j_d \end{Bmatrix} \begin{Bmatrix} J_\alpha' & J & Y \\ j_b & j_c & J_\beta' \end{Bmatrix}$$

$$E_6 = -(-1)^{j_a+j_b+j_c+j_d+J} \sigma_{db}\sigma_{ac}\sigma_{d'b'}\sigma_{a'c'} \hat{J}_\alpha \hat{J}_\beta \hat{J}_\alpha' \hat{J}_\beta' \cdot \delta_{j_d j_b'} \delta_{j_c j_a'} \cdot$$

$$\cdot \begin{Bmatrix} J_\alpha & J_\alpha' & J \\ j_d & J_\beta & j_c \end{Bmatrix} \begin{Bmatrix} J_\alpha & J_\alpha' & J \\ J_\beta' & j_d' & j_c' \end{Bmatrix} \langle j_b^{-1} j_a ; J_\alpha | V | j_d'^{-1} j_c' ; J_\alpha \rangle$$

$$E_7 = -(-1)^{j_a+j_b+j_a'+j_b'} \sigma_{db}\sigma_{ac}\sigma_{d'b'}\sigma_{a'c'} \hat{J}_\alpha \hat{J}_\beta \hat{J}_\alpha' \hat{J}_\beta' \delta_{j_b j_d'} \delta_{j_a j_c'} \cdot$$

$$\cdot \begin{Bmatrix} J_\alpha' & J_\alpha & J \\ J_\beta & j_d & j_c \end{Bmatrix} \begin{Bmatrix} J_\alpha' & J_\alpha & J \\ j_b & J_\beta' & j_a \end{Bmatrix} \langle j_d^{-1} j_c ; J_\alpha' | V | j_b'^{-1} j_a' \; J_\alpha' \rangle$$

$$E_8 = (-1)^{j_a+j_b+j_c+j_d+J+2j_c} \sigma_{db}\sigma_{ac}\sigma_{d'b'}\sigma_{a'c'} \hat{J}_\alpha \hat{J}_\beta \hat{J}_\alpha' \hat{J}_\beta' \delta_{j_d j_b'} \delta_{j_a j_a'} \cdot$$

$$\cdot \sum_X \hat{X}^2 \begin{Bmatrix} j_b & j_c & X \\ J_\beta & j_a & J_\alpha \end{Bmatrix} \begin{Bmatrix} J & J_\alpha' & X \\ j_a & J_\beta & j_d \end{Bmatrix} \begin{Bmatrix} J & J_\alpha' & X \\ j_c' & j_d' & J_\beta' \end{Bmatrix} \langle j_b^{-1} j_c ; X | V | j_d' j_c' ; X \rangle$$

$$E_9 = -(-1)^{2(j_b+j_a-j_c')} \sigma_{db}\sigma_{ac}\sigma_{d'b'}\sigma_{a'c'} \hat{J}_\alpha \hat{J}_\alpha' \hat{J}_\beta \hat{J}_\beta' \delta_{j_b j_b'} \delta_{j_c j_a'} \cdot$$

$$\cdot \begin{Bmatrix} j_c & J_\beta & J_\alpha \\ j_a & j_b & J_\alpha' \end{Bmatrix} \sum_X \hat{X}^2 \begin{Bmatrix} J & J_\alpha' & X \\ j_a & j_d & J_\beta \end{Bmatrix} \begin{Bmatrix} J & J_\alpha' & X \\ j_c' & j_d' & J_\beta' \end{Bmatrix} \langle j_d^{-1} j_a ; X | V | j_d'^{-1} j_c' ; X \rangle$$

$$E_{10} = -(-1)^{j_a+j_b+j_a'+j_b'} \sigma_{db}\sigma_{ac}\sigma_{d'b'}\sigma_{a'c'} \delta_{j_d j_d'} \delta_{j_c j_c'} \delta_{J_\alpha J_\alpha'} \delta_{J_\beta J_\beta'} \cdot$$

$$\cdot \langle j_b^{-1} j_a ; J_\alpha | V | j_b'^{-1} j_a' ; J_\alpha \rangle$$

$$E_{11} = -\hat{J}_\beta \hat{J}_\beta' \sigma_{db}\sigma_{ac}\sigma_{d'b'}\sigma_{a'c'} \delta_{j_b j_b'} \delta_{j_a j_a'} \delta_{J_\alpha J_\alpha'} \cdot$$

$$\cdot \sum_X \hat{X}^2 \begin{Bmatrix} J & J_\alpha & X \\ j_c & j_d & J_\beta \end{Bmatrix} \begin{Bmatrix} J & J_\alpha & X \\ j_c' & j_d' & J_\beta' \end{Bmatrix} \langle j_d^{-1} j_c ; X | V | j_d'^{-1} j_c' ; X \rangle$$

$$E_{12} = -(-1)^{2j_a}\, \sigma_{db}\sigma_{ac}\sigma_{d'b'}\sigma_{a'c'}\; \hat{J}_\alpha \hat{J}_{\alpha'}\; \delta_{j_d j'_d}\delta_{j_c j'_a}\; \delta_{J_\beta J'_\beta}\, \cdot$$

$$\cdot \begin{Bmatrix} j'_b & j_c & J'_\alpha \\ J'_\beta & j'_c & J_\alpha \end{Bmatrix} \langle j_b^{-1} j_a; J_\alpha | V | j_b'^{-1} j'_c J_\alpha \rangle$$

$$E_{13} = (-1)^{j_c+j'_b+j'_c+j_b+J}\, \sigma_{db}\sigma_{ac}\sigma_{d'b'}\sigma_{a'c'}\; \hat{J}_\alpha \hat{J}_\beta \hat{J}'_\alpha \hat{J}'_\beta\;\; \delta_{j_b j'_d}\; \delta_{j_c j'_a}\, \cdot$$

$$\cdot \sum_X \hat{X}^2 \begin{Bmatrix} J'_\beta & j_c & X \\ j'_b & j'_c & J'_\alpha \end{Bmatrix} \langle j_d^{-1} j_a; X | V | j_b'^{-1} j'_c; X \rangle \,\cdot$$

$$\cdot \sum_Y \hat{Y}^2 \begin{Bmatrix} j_c & j_b & Y \\ j_a & J_\beta & J_\alpha \end{Bmatrix} \begin{Bmatrix} j_b & j_c & Y \\ X & J & J'_\beta \end{Bmatrix} \begin{Bmatrix} X & J & Y \\ J_\beta & j_a & j_d \end{Bmatrix}$$

$$E_{14} = -(-1)^{2j'_a}\, (-1)^{j_b+j_c+j'_a+j'_b}\, \sigma_{db}\sigma_{ac}\sigma_{d'b'}\sigma_{a'c'}\; \hat{J}_\alpha \hat{J}_{\alpha'}\; \delta_{j_d j'_d}\delta_{j_a j'_c}\delta_{J_\beta J'_\beta}\, \cdot$$

$$\cdot \begin{Bmatrix} j_b & j_a & J_\alpha \\ J_\beta & j_c & J'_\alpha \end{Bmatrix} \cdot \langle j_b^{-1} j_c; J'_\alpha | V | j_b'^{-1} j'_a J'_\alpha \rangle$$

$$E_{15} = (-1)^{2j_c}\, (-1)^{j_a+j_b+j'_b+j'_c+J}\, \sigma_{db}\sigma_{ac}\sigma_{d'b'}\sigma_{a'c'}\; \hat{J}_\alpha \hat{J}_\beta \hat{J}'_\alpha \hat{J}'_\beta\; \delta_{j_b j'_d}\sigma_{j_a j'_a}\, \cdot$$

$$\cdot \sum_X \hat{X}^2 \begin{Bmatrix} j'_b & j'_c & X \\ J'_\beta & j_a & J'_\alpha \end{Bmatrix} \begin{Bmatrix} j_a & J'_\beta & X \\ J & J_\alpha & j_b \end{Bmatrix} \begin{Bmatrix} J & J_\alpha & X \\ j_c & j_d & J_\beta \end{Bmatrix} \langle j_d^{-1} j_c; X | V | j_b'^{-1} j'_c; X \rangle$$

$$E_{16} = -(-1)^{j_d+j_c+j'_b+j'_c}\, \sigma_{db}\sigma_{ac}\sigma_{d'b'}\sigma_{a'c'}\; \hat{J}_\alpha \hat{J}'_\alpha\; \delta_{j_d j'_d}\delta_{j_a j'_a}\delta_{J_\beta J'_\beta}\, \cdot$$

$$\cdot \sum_X \hat{X}^2 \begin{Bmatrix} j_c & j_b & X \\ j_a & J_\beta & J_\alpha \end{Bmatrix} \begin{Bmatrix} j'_c & j'_b & X \\ j_a & J_\beta & J'_\alpha \end{Bmatrix}$$

In actual calculations some of these sixteen E components vanish due to the delta functions and others are equal among themselves. In reality there are only four independent terms which correspond to some configuration-diagonal matrix element where neither the holes nor the particles are in equivalent orbits.

VII.C. Single-Particle Estimates and Sum Rules

Two measures can be used for characterizing an excitation as a collective excitation: either by comparison of its transition strength, i. e. its B(EL) or B(ML) value, with the single particle (also called Weisskopf) estimate or by expressing its transition strength in terms of a theoretical limit for the strength, a so-called sum rule.

Let us first consider the first measure. The single-particle estimate[112], or Weisskopf unit for electromagnetic transition strengths, provided by the interaction operator $r^L\ Y_{LM}$ for an excitation of a spin-zero nucleus to a state with spin L is given by the reduced transition probabilities

$$B_W(EL)\uparrow \equiv B_W(EL;0\to L) = \left(\frac{2L+1}{4\pi}\right)\left(\frac{3}{L+3}\right)^2 (1.2\ A^{1/3})^{2L}\ e^2\ fm^{2L} \tag{C.1}$$

$$B_W(ML)\uparrow \equiv B_W(ML;0\to L) = \frac{10}{\pi}\ (2L+1)\left(\frac{3}{L+3}\right)^2 (1.2\ A^{1/3})^{2L-2}\ \mu_o^2\ fm^{2L-2}$$

for electric and magnetic excitations respectively. Here R is the nuclear radius and $\mu_o = e\hbar/2m_pc$ is the nuclear magneton; it turns out that $\mu_o^2 =$ 0.01589 MeV fm^3.

An excitation is generally considered collective if its transition strength verifies that

$$\frac{B(EL)\uparrow}{B_W(EL)\uparrow} > 10 \tag{C.2}$$

Weisskopf B_W values for various excitations of closed shell nuclei are given in Table 15.

Le us now deal with the second way of identifying a collective excitation, namely by looking at the sum rules. One can speak about a Giant Resonance when a fair fraction of the sum rule strength is localized at a certain excitation energy or in a narrow excitation energy interval. Particularly useful, because they are almost model-independent, is a linearly energy-weighted sum-rule (EWSR) for the electric multipole operator (3.56a) for a nucleus of A nucleons, i. e.

$$Q_{p\ell M} \equiv \mathcal{M}(E\lambda) = \frac{e}{2} \sum_{i=1}^{A} (1-\tau_3^{(i)})\, r_i^L\, Y_{LM}(\theta_i,\varphi_i) \tag{C.3}$$

As already pointed out, τ_3 = -1 for protons and +1 for neutrons. For electric transitions the sum rules are usually defined as

$$\sum{}_L^P = \sum_k E_k\, B_k\, (EL)\uparrow \tag{C.4}$$

where the summation runs over all excited states k of the same multipolarity, and $B_k(EL)\uparrow$ is the usual reduced transition probability, i. e.

$$B_k(EL)\uparrow = B_k(EL;0\rightarrow L) = \sum_M |\langle k,LM|Q_{pLM}|0;00\rangle|^2 \tag{C.5}$$

Here it is assumed the ground state to have spin zero and located at E_0 = 0. Some authors define the $B_k(EL)$ value with respect to the operator $Q_{p\ell o}$ by

$$B_k^*(EL)\uparrow = |\langle k,LM|Q_{pLo}|0;00\rangle|^2 \tag{C.6}$$

Due to the fact that in spherical nuclei (see Table 1 as an example) the percentage of EWSR limits exhausted by the 2^L-pole excitation of bound states is in general less than 20 %, except L = 3 in some nuclei where such percentage is between 30 and 40 %, some authors[180] argued that T → T transitions are mostly dominated by collective motions in which the neutron and proton matter move together. Hence the proton operator Q_{pLM} is effectively separated out into two parts as follows:

$$Q_{pLM} = Q_{pLM}^{(0)} + Q_{pLM}^{(1)} \tag{C.7}$$

with

$$Q^{(0)}_{pLM} = \frac{e}{2} \sum_i (1 - <\tau_3^{(i)}>) \; r_i^L \; Y_{LM}(\theta_i \varphi_i) \qquad (C.8a)$$

$$Q^{(1)}_{pLM} = - \frac{e}{2} \sum_i (\tau_3^{(i)} - <\tau_3^{(i)}>) \; r_i^L \; Y_{LM}(\theta_i \varphi_i) \qquad (C.8b)$$

where the average $<\tau_3^{(i)}>$ is taken to be (N-Z)/A. Here $Q^{(o)}_{pLM}$ is assumed to act on isoscalar, i. e. $\Delta T = 0$, transitions and $Q^{(1)}_{pLM}$ on isovector, i.e. $|\Delta T| = 1$, transitions.

According to (C.4) and (C.5), the corresponding isoscalar and isovector EWSR limits for L > 1 are respectively as follows:

$$\sum_L^P (T = 0) \equiv \sum_k B_k^{(IS)}(EL)\uparrow = \frac{\hbar^2 e^2}{8\pi m} L \; (2L+1)^2 \; \frac{Z^2}{A} \; \overline{<r^{2L-2}>} \qquad (C.9a)$$

$$\sum_L^P (T = 1) \equiv \sum_k E_k \; B_k^{(IV)}(EL)\uparrow = \frac{\hbar^2 e^2}{8\pi m} L \; (2L+1)^2 \; \frac{NZ}{A} \; \overline{<r^{2L-2}>} \qquad (C.9b)$$

where m is the nucleon mass ($1 m_p c^2$ = 938.256 MeV; $1\hbar c$ = 197.32 MeV fm) and the average of r^{2L-2} is taken over the ground state ground proton distribution.

$$\overline{<r^{2L-2}>} = \frac{\int \rho(r) \; r^{2L-2} \; d^3r}{\int \rho(r) \; d^3r}$$

The total sum rule for isoscalar and isovector excitations shall be then the sum of these two parts, i. e.

$$\sum_L^P \equiv \sum_L^P (T = 0 + T = 1) = \frac{\hbar^2 e^2}{8\pi m} L \; (2L+1)^2 \; Z \quad \overline{<r^{2L-2}>} \qquad (C.10)$$

One can notice that

$$\sum_L^P = \frac{A}{Z} \sum_L^P (T = 0) = \frac{A}{N} \sum_L^P (T = 1) \qquad (C.11)$$

Therefore for N = Z nuclei we have

$$\sum_L^P (T = 0) = \sum_L^P (T = 1) = \frac{1}{2} \sum_L^P \qquad \text{(C.11b)}$$

Assuming an uniform ground state distribution of radius R, one gets

$$\overline{\langle r^{2L-2} \rangle} = \frac{3}{2L+1} \; R^{2L-2} \qquad \text{(C.12)}$$

(One can always define an equivalent uniform radius R which gives the same value of $\langle r^{2L-2} \rangle$ as the true density; this R will depend on L). With (C.11), equations (C.9) and (C.10) adopt the form:

$$\sum_L^P (T = 0) = \frac{3\hbar^2 e^2}{8\pi m} \, L \, (2L+1) \, \frac{Z^2}{A} \; R^{2L-2} \qquad \text{(C.13a)}$$

$$\sum_L^P (T = 1) = \frac{3\hbar^2 e^2}{8\pi m} \, L \, (2L+1) \, \frac{NZ}{A} \; R^{2L-2} \qquad \text{(C.13b)}$$

$$\sum_L^P \equiv \sum_L^P (T = 0 + T = 1) = \frac{3\hbar^2 e^2}{8\pi m} \, L \, (2L+1) \, Z \, R^{2L-2} \qquad \text{(C.13c)}$$

Here $3\hbar^2/8\pi m = 4.9534 \text{ MeV} \cdot \text{fm}^2$.

At this point one should remark that by using the definition $B^*(EL)$ (C.6) instead of B(EL) in (C.5), one gets the following sum rules:

$$S_L^P \, (T = 0) = \frac{1}{2L+1} \sum_L^P (T = 0) \qquad \text{(C.14a)}$$

$$S_L^P \, (T = 1) = \frac{1}{2L+1} \sum_L^P (T = 0) \qquad \text{(C.14b)}$$

$$S_L^P \equiv S_L^P \, (T = 0 + T = 1) = \frac{1}{2L+1} \sum_L^P (T = 0 + T = 1) \qquad \text{(C.14c)}$$

For the sake of comparison with experimental data, we shall take in our calculations the sum rules $\sum_L^P$ with $R = 1.2\ A^{1/3}$ fm, unless we say the opposite. Such values are explicitly shown in Table 16. However one should here mention that the sum rules calculated with uniform mass distribution are only between $\sim$20 % and $\sim$93 % of those calculated with Hartree-Fock ground states for multipoles $L < 1$, as shown by Liu and Brown[89].

For the monopole excitations we shall use the operator

$$Q_{p00} = \frac{e}{2} \sum_i (1 - \tau_3^{(i)})\ r_i^2 \tag{C.15}$$

and one gets[19] the corresponding isoscalar (IS), isovector (IV) and IS + IV EWSR limits as follows:

$$\sum_0^P (T = 0) = \frac{2\hbar^2 e^2}{m}\ \frac{Z^2}{A} \overline{\langle r^2 \rangle} \tag{C.16a}$$

$$\sum_0^P (T = 1) = \frac{2\hbar^2 e^2}{m}\ \frac{NZ}{A}\ \overline{\langle r^2 \rangle} \tag{C.16b}$$

$$\sum_0^P \equiv \sum_0^P (T = 0 + T = 1) = \frac{2\hbar^2 e^2}{m}\ Z\ \overline{\langle r^2 \rangle} \tag{C.16c}$$

Conventionally the electric dipole sum rule is expressed in terms of the classical sum rule. Taken into account the center of mass, the electric dipole operator[19] is

$$\begin{aligned} Q_{p1M} &= \frac{e}{2} \sum_i (1 - \tau_3^{(i)})\ r_i\ Y_{1M} - \frac{Ze}{A} \sum_i r_i\ Y_{1M} \\ &= e\,\frac{N}{A} \sum_p r_p\ Y_{1M}\ (\hat{r}_p) - e\,\frac{Z}{A} \sum_n r_n\ Y_{1M}\ (\hat{r}_n) \end{aligned} \tag{C.17}$$

and the dipole sum rule results to be as follows:

$$\sum_1^P (T = 1) = \sum_k E_k \, B_k(E1)\uparrow = \frac{9\hbar^2 e^2}{8\pi m} \, \frac{NZ}{A} = 14.8 \, \frac{NZ}{A} \, e^2 \, fm^2 \, MeV \qquad (C.18)$$

In Table 16 we also show the values of monopole sum rules by assuming an uniform ground state distribution ($\overline{<r^2>} = \frac{3}{5} R^2$; $R = 1.2 \, A^{1/3}$ fm) and the classical sum rule (C.18).

For the sake of completeness and also to facilitate discussion of Chapter V, in the following we mention similar sum rules used by other people (see recent review of Satchler[24]). They define the isoscalar (T = 0) and isovector (T = 1) operators by

$$Q_{0LM} = \sum_i r_i^L \, Y_{LM}(\theta_i \varphi_i) \qquad \text{and} \qquad Q_{1LM} = \sum_i \tau_3^{(i)} \, r_i^L \, Y_{LM}(\theta_i \varphi_i) \qquad (C.19)$$

There is a simple relation between these operators and the proton operator (C.3) and the neutron operator Q_{nLM}, namely:

$$Q_{pLM} = \frac{1}{2} \, (Q_{0LM} - Q_{1LM}); \qquad Q_{nLM} = \frac{1}{2} \sum \, (Q_{0LM} + Q_{1LM}) \qquad (C.20)$$

By using the operators (C.19), the definition (C.5) for the reduced transition probability and a similar relation (C.4), one can get the following sum rules for $L > 1$

$$\sum_L^{(0)} = \sum_L^{(1)} = \frac{\hbar^2 e^2}{8\pi m} \, L \, (2L+1)^2 \, A \, \overline{<r^{2L-2}>}$$

$$\sum_L = \sum_L^{(0)} + \sum_L^{(1)} = \frac{\hbar^2 e^2}{4\pi m} \, L(2L+1)^2 \, A \, \overline{<r^{2L-2}>} \qquad (C.21)$$

and for $L = 0$

$$\sum_0^{(0)} = \sum_0^{(1)} = \frac{2\hbar^2 e^2}{m} \, A \, \overline{<r^2>}$$

For the sake of comparison with experimental data, we shall take in our calculations the sum rules $\sum_L^P$ with $R = 1.2\ A^{1/3}$ fm, unless we say the opposite. Such values are explicitly shown in Table 16. However one should here mention that the sum rules calculated with uniform mass distribution are only between $\sim$20 % and $\sim$93 % of those calculated with Hartree-Fock ground states for multipoles $L < 1$, as shown by Liu and Brown[89].

For the monopole excitations we shall use the operator

$$Q_{p00} = \frac{e}{2} \sum_i (1 - \tau_3^{(i)})\ r_i^2 \tag{C.15}$$

and one gets[19] the corresponding isoscalar (IS), isovector (IV) and IS + IV EWSR limits as follows:

$$\sum_0^P (T = 0) = \frac{2\hbar^2 e^2}{m} \frac{Z^2}{A} \overline{\langle r^2 \rangle} \tag{C.16a}$$

$$\sum_0^P (T = 1) = \frac{2\hbar^2 e^2}{m} \frac{NZ}{A} \overline{\langle r^2 \rangle} \tag{C.16b}$$

$$\sum_0^P \equiv \sum_0^P (T = 0 + T = 1) = \frac{2\hbar^2 e^2}{m} Z \overline{\langle r^2 \rangle} \tag{C.16c}$$

Conventionally the electric dipole sum rule is expressed in terms of the classical sum rule. Taken into account the center of mass, the electric dipole operator[19] is

$$\begin{aligned} Q_{p1M} &= \frac{e}{2} \sum_i (1 - \tau_3^{(i)})\ r_i\ Y_{1M} - \frac{Ze}{A} \sum_i r_i\ Y_{1M} \\ &= e\,\frac{N}{A} \sum_p r_p\ Y_{1M}\ (\hat{r}_p) - e\,\frac{Z}{A} \sum_n r_n\ Y_{1M}\ (\hat{r}_n) \end{aligned} \tag{C.17}$$

and the dipole sum rule results to be as follows:

$$\sum_1^P (T = 1) = \sum_k E_k \; B_k(E1)\uparrow = \frac{9\hbar^2 e^2}{8\pi m} \; \frac{NZ}{A} = 14.8 \, \frac{NZ}{A} \, e^2 \, fm^2 \, MeV \tag{C.18}$$

In Table 16 we also show the values of monopole sum rules by assuming an uniform ground state distribution ($\overline{<r^2>} = \frac{3}{5} R^2$; $R = 1.2 \; A^{1/3}$ fm) and the classical sum rule (C.18).

For the sake of completeness and also to facilitate discussion of Chapter V, in the following we mention similar sum rules used by other people (see recent review of Satchler[24]). They define the isoscalar (T = 0) and isovector (T = 1) operators by

$$Q_{0LM} = \sum_i r_i^L \; Y_{LM}(\theta_i \varphi_i) \qquad \text{and} \qquad Q_{1LM} = \sum_i \tau_3^{(i)} \; r_i^L \; Y_{LM}(\theta_i \varphi_i) \tag{C.19}$$

There is a simple relation between these operators and the proton operator (C.3) and the neutron operator Q_{nLM}, namely:

$$Q_{pLM} = \frac{1}{2} \, (Q_{0LM} - Q_{1LM}); \qquad Q_{nLM} = \frac{1}{2} \sum \, (Q_{0LM} + Q_{1LM}) \tag{C.20}$$

By using the operators (C.19), the definition (C.5) for the reduced transition probability and a similar relation (C.4), one can get the following sum rules for L > 1

$$\begin{aligned} \sum_L^{(0)} &= \sum_L^{(1)} = \frac{\hbar^2 e^2}{8\pi m} \, L \, (2L+1)^2 \, A \, \overline{<r^{2L-2}>} \\ \sum_L &= \sum_L^{(0)} + \sum_L^{(1)} = \frac{\hbar^2 e^2}{4\pi m} \, L(2L+1)^2 \, A \, \overline{<r^{2L-2}>} \end{aligned} \tag{C.21}$$

and for L = 0

$$\sum_0^{(0)} = \sum_0^{(1)} = \frac{2\hbar^2 e^2}{m} \, A \, \overline{<r^2>}$$

$$\sum_0 = \sum_0^{(0)} + \sum_0^{(1)} = \frac{4\hbar^2 e^2}{m} A \langle\overline{r^2}\rangle \tag{C.22}$$

The comparison of (C.21) and (C.22) with (C.13) and (C.16) gives rise to the following relations valid for $L \geqslant 0$:

$$\sum_L^{(0)} = \left(\frac{A}{Z}\right)^2 \sum_L^P \; (T = 0) \tag{C.23a}$$

$$\sum_L^{(1)} = \frac{A^2}{NZ} \sum_L^P \; (T = 1) \tag{C.23b}$$

$$\sum_L = \frac{2A}{Z} \sum_L^P \tag{C.23c}$$

Further explanations and references about sum rules can be found in Satchler[24], O'Connell[181], Halbert et al.[61] and Bohr & Mottelson[19].

VII.D. Total Energy-Weighted-Sum-Rules of EL, L > 2, resonances

The configuration space in our calculations takes into account all the single-particle states within $2\hbar\omega$ above and below Fermi surface. Therefore the total EWSR limits for the 0^+, 1^- and 2^+ states emerge directly from the calculations since practically all the possible particle-hole excitations which contribute to those states are within such a configuration space. However this is not the case for the E3, E4 and E5 resonances which we are interested in. For the sake of a proper comparison with experimental measurements it is important to have a "realistic estimate" of the total EWSR strength of these resonances.

To get such an estimate we first take the total (T = 0 + T = 1) E2 EWSR, to be denoted by S_2, and evaluate an equivalent radius R for the uniform ground state distribution by using equation (C.13a). It turns out that

$$R = \left(\frac{S_2}{49.534\ Z}\right)^{1/2}\ \text{fm}$$

where S_2 is given in units of $e^2\ \text{fm}^4$ MeV.

With this radius and using again for $L \geqslant 3$ the equation (C.13a), one has that the total ($T = 0 + T = 1$) EL sum rule is given in terms of S_2 as follows:

$$S_L = 4.9534\ L\ (2L+1)\ Z\ \left(\frac{S_2}{49.534\ Z}\right)^{L-1}\ e^2\ \text{fm}^{2L}\ \text{MeV}$$

The total isoscalar and isovector EL sum rules would then have the following expressions

$$S_L\ (T = 0) = 4.9534\ L\ (2L+1)\ \frac{Z^2}{A}\ \left(\frac{S_2}{49.534\ Z}\right)^{L-1}\ e^2\ \text{fm}^{2L}\ \text{MeV}$$

$$S_L\ (T = 1) = 4.9534\ L\ (2L+1)\ \frac{NZ}{A}\ \left(\frac{S_2}{49.534\ Z}\right)^{L-1}\ e^2\ \text{fm}^{2L}\ \text{MeV}$$

Finally let's write down what fraction of these sum rules is taken in the EWSR $\sum_L^P$; $L = 3, 4, 5$, evaluated with $R = 1.2\ A^{1/3}$ and given in Table 16. One can readily obtain

$$\frac{\sum_L^P}{S_L} = \left(\frac{71.329}{S_2}\ Z\ A^{2/3}\right)^{L-1}\ ; \qquad L \geqslant 3$$

The same relation maintains for isoscalar and isovector EL EWSR strengths. For instance in ^{12}C for which $S_2 = 3565\ e^2\ \text{fm}^4$ MeV, the value $\sum_4^P$ is only $\sim$25 % of the total ($T = 0 + T = 1$) E4 EWSR strength S_4.

VIII. REFERENCES

1) A.B. Migdal, J. Phys. USSR 8 (1944) 331;
A.B. Migdal, Zh. Eksp. Teor. Fiz. 15 (1945) 81.

2) G.C. Baldwin and G.S. Klaiber, Phys. Rev. 71 (1947) 3 and Phys. Rev. 73 (1948) 1156.

3) A. Degre, Thêse d'Etat, University of Strasbourg, 1975.

4) F.T. Kuchnir, P. Axel, L. Criegee, D. Drake, A.O. Hanson and D. Sulton, Phys. Rev. 161 (1967) 1236.

5) E. Hayward in: Nuclear Structure and Electromagnetic Interactions, p. 141, edit. N. MacDonald, Oliver and Boyd, Edinburgh, 1965.

6) J. Ahrens, H. Borchert, K.H. Crock, H.B. Eppler, H. Gim, H. Gundrum, M. Kröning, P. Riehn, G. Sita Ram, A. Ziegler and B. Ziegler, Nucl. Phys. A 251 (1975) 479.

7) D.H. Wilkinson, Physica 23 (1956) 1039;
D.H. Wilkinson, Phys. Rev. Letters 3 (1959) 388.

8) G.E. Brown and M. Bolsterli, Phys. Rev. Lett. 3 (1959) 472;

9) G.E. Brown, Unified Theory of Nuclear Models and Forces, North-Holland, Amsterdam, 1971.

10) V. Gillet and N. Vinh Mau, Nucl. Phys. 54 (1964) 321;
V. Gillet and E.A. Sanderson, Nucl. Phys. 54 (1964) 472;
V. Gillet and M.A. Melkanoff, Phys. Rev. 133 (1964) 1190;
V. Gillet, A.M. Green and E.A. Sanderson, Nucl. Phys. 88 (1966) 321.

11) B. Buck and A.D. Hill, Nucl. Phys. A 95 (1967) 271;
J. Raynal, M.A. Melkanoff and T. Sawada, Nucl. Phys. A 101 (1967) 369.

12) M. Marangoni and A.M. Saruis, Phys. Lett. 24 B (1967) 218;
M. Marangoni and A.M. Saruis, Nucl. Phys. A 132 (1969) 433.

13) Q. Ho-Kim, Phys. Rev. C 8 (1973) 1574.

14) V. Gillet, M.A. Melkanoff and J. Raynal, Nucl. Phys. A 97 (1967) 631.

15) G. Baur, Helv. Phys. Acta 44 (1971) 49.

16) J. Birkholz, Phys. Lett. 34 B (1971) 1;
J. Birkholz, Nucl. Phys. A 184 (1972) 385.

17) C.M. Shakin and W.L. Wang, Phys. Rev. Lett. 26 (1971) 902;
C.M. Shakin and W.L. Wang, Phys. Rev. C 5 (1972) 1898;
W.L. Wang and C.M. Shakin, Phys. Rev. Lett. 30 (1973) 301.

18) C. Bloch, Proceedings XXXVI Intern. School of Physics, Enrico Fermi Course (Academic Press, New York, 1966);
C. Mahaux and H.A. Weidenmüller, Shell-Model Approach to Nuclear Reactions (North-Holland, Amsterdam 1969);

18a) J.M. Blatt and V.F.Weiskopf, Theoretical Nuclar Physics. Wiley & Sons, New York, 1962, p. 508.

19) A. Bohr and B. Mottelson, Nuclear Structure, Vol. 2 (Benjamin, New York, 1976).

20) B.R. Mottelson, Proceedings XV Solvay Conf. Physics, Brussels, edit. I. Prigogine, New York, Gordon and Breach, 1970.

21) C.R. Gruhn, T.Y.T. Kuo, C.J. Maggiore, H. McManus, F. Petrovich and B.M. Preedom, Phys. Rev. C 6 (1972) 915.

22) M.B. Lewis, F.E. Bertrand and C.B. Fulmer, Phys. Rev. C 7 (1973) 1966.

23) W.T. Wagner, G.W. Crawley, G.R. Hammerstein and H. McManns, Phys. Rev. C 12 (1975) 757.

24) G.R. Satchler, Lectures delivered at Internat. School of Physics "Enrico Fermi", Varenna, Italy, 1976.

25) M. Goldhaber and E. Teller, Phys. Rev. 74 (1948) 1046.

26) H. Steinwedel and J.H.D. Jensen, Z. Naturforschung 5 a (1950) 413.

27) R. Pitthan and Th Walcher, Phys. Letters 36 B (1971) 563.

28) S. Fukuda and Y. Torizuka, Phys. Rev. Letters 29 (1972) 1109.

29) R. Pitthan and Th. Walcher, Z. Naturforschung 27 a (1972) 1683;
F.R. Buskirk, H.D. Gräf, R. Pitthan, H. Theissen, O. Titze and Th. Walcher, Phys. Letters 42 B (1972) 194;
M. Nagao and Y. Torizuka, Phys. Rev. Letters 30 (1973) 1068.

30) Y. Torizuka, Y. Kohima, T. Saito, K. Itoh, A. Nakada, S. Mitsonobu, N. Nagao, K. Hosoyama and S. Fukuda, Proceedings Intern. Conf. Nuclear Structure Studies using electron scattering and Photoreaction, Sendai, 1972, edit. by K. Shoda and H.Ui, pp. 171-182. Suppl. Rep. Lab. Nucl. Sci., Tohoku University, vol. 15.

31) A. Moalem, W. Benenson and G.W. Crawley, Phys. Rev. Letters 31 (1973) 482.

32) J. Arvieux, M. Buenerd, A.J. Cole, P. de Saintignon, G. Perrin and D.J. Horen, Nucl. Phys. A 247 (1975) 238.

34) D.J. Horen, J. Arvieux, M. Buenerd, A.J. Cole, G. Perrin and P. de Saintignon. Phys. Rev. C 11 (1975) 1247.

35) J.M. Moss, C.M. Rozsa, J.D. Bronson, D.H. Youngblood, Phys. Lett. 53 B (1974) 51;
D.H. Youngblood, J.M. Moss, C.M. Rozsa, J.D. Bronson, A.D. Bacher and D.R. Brown, Phys. Rev. C 13 (1976) 994;
J.M. Moss, C.M. Rozsa, D.H. Youngblood, J.D. Bronson and A.D. Bacher, Phys. Rev. Lett. 34 (1975) 748.

36) C.C. Chang, F.E. Bertrand and D.C. Kocher, Phys. Rev. Letters 34 (1975) 221.

37) R. Pitthan, F.R. Buskirk, E.B. Dally, J.N. Dyer and X.K. Maruyama, Phys. Rev. Letters 33 (1974) 849; ibid (erratum) 34 (1975) 848.

38) R.G. Allas, S.S. Hanna, L. Meyer-Schützmeister and R.E. Segel, Nucl. Phys. 58 (1964) 122.

39) D.E. Frederick, R.J.J. Stewart and R.C. Morrison, Phys. Rev. 186 (1969) 992.

40) S.S. Hanna, H.F. Glavish, R. Avida, J.R. Calarco, E. Kuhlman and R. LaCanna, Phys. Rev. Lett. 32 (1974) 114.

41) E. Kuhlman, E. Ventura, J.R. Calarco, D.G. Mavis and S.S. Hanna, Phys. Rev. C 11 (1975) 1525.

42) K.A. Snover, E.G. Adelberger and D.R. Brown, Phys. Rev. Lett. 32 (1974) 1061.

43) L. Meyer-Schützmeister, W. Wharton, P. Debevec, R.E. Segel and K. Raghunathan, Bull. Am. Phys. Soc. 20 (1975) 565.

44) F.E. Bertrand, Ann. Rev. of Nucl. Science 26 (1976) 427.

45) A. Kiss, C. Mayer-Böricke, M. Rogge, P. Turek and S. Wiktor, Phys. Rev. Lett. 37 (1976) 1188.

46) K.T. Knöpfle, G.J. Wagner, A. Kiss, M. Rogge, C. Mayer-Böricke and Th. Bauer, Phys. Lett. 64 B (1976) 263.

47) A. Hotta, K. Itto and T. Saito, Phys. Lett. 33 (1974) 790.

48) A. Moalem, W. Benenson and G.M. Grawley, Nucl. Phys. A 236 (1974) 307.

49) M.N. Harakeh, A.R. Arends, M.J.A. de Voigt, A.G. Prentje, S.Y. van der Werf and A. van der Woude, Nucl. Phys. A 265 (1976) 189.

50) K.T. Knöpfle, G.J. Wagner, H. Breuer, M. Rogge and C. Mayer-Böricke, Phys. Rev. Lett. 35 (1975) 779.

51) K.A. Snover, K. Ebisawa, D.R. Brown and P. Paul, Phys. Rev. Lett. 32 (1974) 317.

52) H.V. Geramb, K. Amos, R. Sprickmann, K.T. Knöpfle, M. Rogge, D. Ingham and C. Mayer-Böricke, Phys. Rev. C 12 (1975) 1697.

53) D.H. Youngblood in Proceedings Intern. Symposium on Highly Excited States in Nuclei, edit. by A. Faessler, C. Mayer-Böricke and P. Turek (Kernforschungsanlage Jülich, 1975), vol. 2, pp. 50.

54) C.C. Chang, J.P. Didelez, K. Kwiatkowski and J. Wu in: Proceedings Int. Symposium of Jülich (see ref. 53), vol. 1, pp. 1.

55) K.W. Schmid and G. Do Dang, Phys. Lett. 66 B (1976) 5; Phys. Rev. C 15 (1977) 1515.

56) S. Fukuda and Y. Torizuka, Phys. Lett. 62 B (1976) 146.

57) M. Sasao and Y. Torizuka, Phys. Rev. C 15 (1977) 217.

58) M. Nagao and Y. Torizuka, Phys. Rev. Lett. 30 (1973) 1068.

59) N. Marty, M. Morlet, A. Willis, V. Comparat and R. Frascaria in: Proc. Int. Symposium of Jülich (see ref. 53) and preprint.

60) M.N. Harakeh, K. van der Borg, T. Ishimatsu, H.P. Morsch, A. van der Woude and F.E. Bertrand, to appear in Phys. Rev. Lett. (1977).

61) E.C. Halbert, J.B. McGrory, G.R. Satchler and J. Speth, Nucl. Phys. A 245 (1975) 189.

62) H.V. Geramb, R. Sprickmann and G.L. Strobel, Nucl. Phys. A 199 (1973) 545.

63) D. Lebrun, G. Perrin, P. Martin, P. de Saintignon, J. Arvieux, M. Buenerd, H.V. Geramb and K.A. Amos, Nucl. Phys. A 265 (1976) 291; D. Lebrun, Thèse de 3ème Cycle. Université de Grenoble, 1975.

64) G. Perrin, D. Lebrun, J. Chauvin, P. Martin, P. de Saintignon, H.V. Geramb, D. Eppel, H.L. Yadav and V.A. Madsen, to appear in Phys. Lett. (1977).

65) H.L. Yadav and H.V. Geramb, Phys. Rev. C 14 (1976) 1369.

66) H.V. Geramb and K. Amos, Lett. Nuovo Cimento 14 (1975) 526.

67) L.W. Fagg, Rev. Mod. Phys. 47 (1975) 683.

68) Y. Torizuka in Colloque Franco-Japonais sur spectroscopie nucleaire et react. nucl., Dogashima, Japan, September 1976.

69) L.C. Haacke and K.G. McNeill, Canad. J. Phys. 53 (1975) 1422.

70) R.J. Holt and H.E. Jackson, Phys. Rev. Lett. 36 (1976) 244.

71) R.E. Toohey and H.E. Jackson, Phys. Rev. C 6 (1972) 1440.

72) R.J. Holt, R.M. Laszewski and H.E. Jackson, Phys. Rev. C 15 (1977) 827.

73) R.M. Laszewski, R.J. Holt and H.E. Jackson, Phys. Rev. Lett. (1977), in press.

74) S.J. Freedman, C.A. Gagliardi, G.T. Garvey, M.A. Oothoudt and B. Svetitsky, Phys. Rev. Lett. 37 (1976) 1606.

75) J.D. Vergados, Phys. Lett. 36 B (1971) 12.

76) P. Ring and J. Speth, Nucl. Phys. A 235 (1974) 315;
P. Ring and J. Speth, Phys. Lett. 44 B (1973) 447.

77) J.S. Dehesa, J. Speth and A. Faessler, Phys. Rev. Lett. 38 (1977) 208.

78) J. Speth, J. Wambach, V. Klemt and S. Krewald, Phys. Lett. 63 B (1976) 257.

79) S. Krewald, J.E. Galonska and A. Faessler, Phys. Lett. 55 B (1975) 267.

80) E. Caurier and B. Grammaticos in: Proceedings of the XV Int. Winter Meeting of Bormio, Italy, 1976 and to be published;
D. Vautherin, Phys. Letters 57 B (1975) 425.

81) L. Zamick, Phys. Letters 47 B (1973) 119;
L. Zamick and M. Golin, Nucl. Phys. A 249 (1975) 320.

82) K. Goeke, Nucl. Phys. A 265 (1976) 301;
K. Goeke, Habilitationsschrift, University of Bonn, 1977;
K. Goeke, Phys. Rev. Lett. 38 (1977) 212.

83) P. Ring, R. Bauer and J. Speth, Nucl. Phys. A 206 (1973) 97.

84) S. Krewald and J. Speth, Phys. Lett 52 B (1974) 295.

85) S. Krewald, J. Birkholz, A. Faessler and J. Speth, Phys. Rev. Lett. 33 (1974) 1386.

86) G. Saunier, J. LeTourneux, R. Rouben and R. Padjen, Canad. J. Phys. 51 (1973) 629.

87) G.F. Bertsch and S.F. Tsai, Phys. Rep. C 18 (1975) 125.

88) J.P. Blaizot, Phys. Lett. 60 B (1976) 435.

89) K.F. Liu and G.E. Brown, Nucl. Phys. A 265 (1976) 385.

90) S. Krewald, Ph. D. Thesis, University of Bonn, 1976.

91) J.P. Blaizot, D. Gogny, B. Grammaticos, Nucl. Phys. A (1977).

92) G.F. Bertsch, Phys. Rev. Lett. 31 (1973) 121;
S. Schlomo and G. Bertsch, Nucl. Phys. A 243 (1975) 507.

93) K.F. Liu and N. van Giai, Phys. Lett. 65 B (1976) 23.

94) H. Müther, Y.R. Waghmare and A. Faessler, Phys. Lett. 64 B (1977) 125.

95) D. Zawischa and J. Speth, Phys. Rev. Lett. 36 (1976) 846.

96) J. Speth, E. Werner and W. Wild, Phys. Reports C (in press).

97) J.S. Dehesa, S. Krewald, J. Speth and A. Faessler, Phys. Rev. C (1977) in press.

98) J.S. Dehesa, J. Speth and A. Faessler, Preprint 1977.

99) J.S. Dehesa, J. Speth and A. Faessler, to be published.

100) J. Blomquist and T.T.S. Kuo, Phys. Lett. 29 B (1969) 544;
S.M. Pêrez, Nucl. Phys. A 136 (1969) 599.

101) E. Grecksch, W. Knüpfer and M.G. Huber, Lett. Nuovo Cimento 14 (1975) 505.

102) W. Knüpfer and M.G. Huber, Z. Physik A 276 (1976) 99.

103) W. Knüpfer and M.G. Huber, Z. Physik A 276 (1976) 99;
W. Knüpfer and M.G. Huber, Phys. Rev. C 14 (1976) 2254.

104) T. Hoshino and A. Arima, Phys. Rev. Lett. 37 (1976) 266.

105) J. Martorell, O. Bohigas, S. Fallieros and A.M. Lane, Phys. Lett. 60 B (1976) 313;
O. Bohigas, J. Martorell and A.M. Lane, Phys. Lett. 64 B (1976) 1.

106) A.M. Lane in: Proceedings of Int. Symposium on Highly Excited States, Jülich, December 1975, Jül-Conf 16 (vol. 2).

107) M.W. Kirson, Nucl. Phys. A 257 (1976) 58;
E. Lipparini, G. Orlandini and R. Leonardi, Phys. Rev. Lett. 36 (1976) 66.

108) S. Krewald, Ph. D. Thesis, University of Bonn. 1976;
S. Krewald, V. Klemt, J. Speth and A. Faessler, Nucl. Phys. A (1977) in press.

109) A.B. Migdal, Theory of Finite Fermi Systems. Interscience Publ., N.Y., 1967.

110) E.D. Mshelia, K. Roos and W. Greiner, Nucl. Phys. A 212 (1973) 157.

111) J.M. Eisenberg, B.M. Spicer and M.E. Rose, Nucl. Phys. 71 (1965) 273;
J.B. Seaborn and J.M. Eisenberg, Nucl. Phys. 82 (1966) 308.

112) A. Bohr and B. Mottelson, Nuclear Structure, vol. 1, Benjamin, N.Y., 1969.

113) E. Evans, Photonuclear Reactions, N.S.B. Monograph 1971.

114) B.M. Spicer, Advances in Nucl. Physics 2 (1971) 1.

115) B.L. Berman and S.C. Fultz, Rev. Mod. Phys. 47 (1975) 713.

116) B.L. Berman, edit.: Proc. Intern. Conf. on Photonuclear Reactions. (Asilomar, California) (Livermore Laboratory Report CONF-730301, 1973).

117) G.E. Brown, Many-body problems. North-Holland, Amsterdam, 1972.

118) H. Tyren and Th. A.J. Maris, Nucl. Phys. 4 (1957) 637; Nucl. Phys. 4 (1957) 662; Nucl. Phys. 6 (1958) 446; Nucl. Phys. 7 (1958) 24;
D.H. Wilkinson, Proc. Intern. Conf. on Nucl. Structure, Kingston, ed. by A.D. Bromley and E. Vogt (Toronto, 1960).

119) F.E. Bertrand and R.W. Peelle, Phys. Rev. C 8 (1973) 1045;
M.B. Lewis and F.E. Bertrand, Nucl. Phys. A 196 (1972) 337;
M.B. Lewis, F.E. Bertrand and D.J. Horen, Phys. Rev. C 8 (1973) 398.

120) M. Marty, M. Morlet, A. Willis, V. Comparat and R. Frascaria, Nucl. Phys. A 238 (1975) 93.

121) A. Schwierczinski, R. Frey, A. Richter, E. Spamer, H. Theissen, O. Titze, Th. Walcher, S. Krewald and R. Rosenfelder, Phys. Rev. Letters 35 (1975) 1244.

122) N.K. Sherman, H.M. Ferdinande, K.H. Lokan and C.K. Ross, Phys. Rev. Letters 35 (1975) 1215.

123) F.E. Bertrand and D.C. Kocher, Phys. Rev. C 13 (1976) 2241.

124) H.P. Morsch, P. Decowski and W. Benenson, Phys. Rev. Lett. 37 (1976) 263.

125) L. Meyer-Schützmeister, Z. Vager, R.E. Segel and P.P. Singh, Nucl. Phys. A 108 (1968) 180.

126) D. Brandford, Particles and Nuclei 6 (1973) 127;
R.B. Watson, D. Brandford, J.L. Blanck and W.J. Caelli, Nucl. Phys. A 203 (1973) 209;
G.S. Foote et al., Nucl. Phys. A 263 (1976) 349.

127) K.T. Knöpfle, G.J. Wagner, A. Kiss, M. Rogge, C. Mayer-Böricke and Th. Bauer, Phys. Lett. 64 B (1976) 263.

128) C. Mayer-Böricke and P. Turek (private communication).

129) E. Hayward, Photonuclear Reactions, NBS Monograph 118 (1970).

130) I. Hamamoto, Physica Scripta 6 (1972) 266.

131) A. Schwierczienski, R. Frey, E. Spamer, H. Theissen and Th. Walcher, Phys. Lett. 55 B (1975) 171.

132) Y. Torizuka, Y. Kojima, T. Saito, K. Itoh, A. Nakada, S. Mitsonobu, N. Nagao, K. Hosoyama, S. Fukuda and H. Miura, Proceed. Int. Conf. Nuclear Reactions and Applications, Asilomar, ed. B.L. Berman, 1 (1973) 675-683. CONF-730301 U.S. AEC Office of Informat. Services, Oak Ridge.

133) P. Paul in: Proc. Int. Symposium on Highly Excited States in Nuclei, edit. by A. Faessler, C. Mayer-Böricke and P. Turek. Jülich 1975, vol. 2, pp. 71.

134) J. Noê, P. Paul, K.A. Snover, M. Suffert and M.K. Warburton in the: Symposium on Nucl. Structure, Balatonfüred, September 1975.

135) H.W. Baer, J.A. Bistirlich, N. de Bottin, S. Cooper, K.N. Crowe, P. Truol and D. Vergados, Phys. Rev. C 10 (1974) 267.

136) K. Hosoyama and Y. Torizuka. Phys. Rev. Lett. 35 (1975) 199.

137) Y. Torizuka, K. Itoh, Y.M. Shin, Y. Kawazoe, H. Matsuzaki and G. Takeda, Phys. Rev. C 11 (1975) 1174.

138) A. Faessler in: Proceedings Int. Conf. on Selected Topics in Nuclear Structure, Dubna, U.S.S.R., 1976.

139) A.M. Lane in: Proceedings Int. Symp. on Highly Excited States in Nuclei, Jülich, December 1975, Jül-Conf-16 (vol. 2).

140) J. Speth, Invited talk to XV Int. Winter Meeting on Nuclear Physics, Bormio, Italy, 1976.

141) Y.M. Engel, D.M. Brink, K. Goeke, S.J. Krieger and D. Vautherin, Nucl. Phys. A 249 (1975) 215.

142) J.M. Moss, D.H. Youngblood, C.M. Rozsa, D.R. Brown and J. D. Bronson, Phys. Rev. Lett. 37 (1976) 816.

143) E. Grecksch, W. Knüpfer and M.G. Huber, Phys. Rev. C 15 (1977) 837.

144) T.S.H. Lee and S. Pittel, Phys. Rev. C 11 (1975) 607.

145) C.D. Bowman, R.J. Baglan, B.L. Berman and T.W. Phillips, Phys. Rev. Lett. 18 (1970) 1302.

146) R.A. Lindgren, W.L. Beudel, L.W. Fagg and E.C. Jones Jr., Phys. Rev. Lett. 35 (1975) 1423.

147) D.J. Thouless, Nucl. Phys. 22 (1961) 78.

148) M. Baranger, Cargèse Lectures in Theoretical Physics, 1962 (W.A. Benjamin, N.Y. 1963).

149) D.J. Rowe, Nuclear Collective Motion, Methuen, London 1970.

150) J. Sawicki, Phys. Rev. 126 (1962) 2231;
G. Fano and J. Sawicki, Nuovo Cimento 25 (1962) 586.

151) T. Tamura and T. Udagawa, Nucl. Phys. 53 (1964) 33.

152) E. Werner, Z. Physik 191 (1966) 381.

153) P. Ring and E. Werner, Nucl. Phys. A 211 (1973) 198.

154) A.L. Fetter and J.D. Walecka, Quantum Theory of Many-Particle Systems. McGraw-Hill. N.Y. 1971.

155) See for instance L.S. Kisslinger and R.A. Sorensen, Rev. Mod. Phys. 35 (1963) 853.

156) S. Reich, H.M. Sofia and D.R. Bês, Nucl. Phys. A 233 (1974) 105.

157) I. Hamamoto, Preprint, Nordita 75/13.

158) K. Arita and H. Horie, Nucl. Phys. A 173 (1971) 97;
P.F. Bortignon, R.A. Broglia, D.R. Bês, R. Liotta and V. Paar, Phys. Lett. 64 B (1976) 24;
D. Zawischa, Z. Physik 266 (1974) 117;
D. Zawischa, Fizika 7, Suppl. 2 (1975) 105.

159) J.D. Immele and G.L. Struble, Phys. Rev. C 9 (1974);
E. Werner and K. Emrich, Z. Physik 236 (1970) 464;
P. Ring and P. Schuck, Z. Physik 269 (1974) 323.

160) K.G. Bernhardt, W.R. Hering, P. Ring and E. Werner, Nucl. Phys. A 249 (1975).

161) J.M. Eisenberg and W. Greiner, Nuclear Theory, vol. 3, North-Holland, Amsterdam, 1972.

162) A. Siegert, Phys. Rev. 52 (1937) 787;
N. Austern and R.G. Sachs, Phys. Rev. 81 (1951) 710.

163) For a recent discussion, see L. Heller in: Proceedings Gull Lake Symposium on the Two-Body Forces in Nuclei (1971).

164) R. Bauer, J. Speth, V. Klemt, P. Ring, E. Werner and T. Yamazaki, Nucl. Phys. A 209 (1973) 535.

165) J. Blomquist and S. Wahlborn, Arkiv f. Physik 16 (1960) 545.

166) C.M. Perey and F.G. Perey, Atomic Data and Nuclear Data Tables 13 (1974) 293.

167) M.R. Schmorak and R.L. Anble, Nucl. Data B 5 (1971).

168) V. Klemt, Ph. D. Thesis, Universität München, 1970 (unpublished).

169) P. Fröbrich and J. Speth, Proc. Intern. Symp. on Nucl. Physics, Balatonfüred, Hungary, 1975, edit. I. Fodor-Lovas and G. Pälla, vol. 2, p. 571.

170) J. Mattauch et al., Nucl. Phys. 67 (1965) 1.

171) J. Speth, L. Zamick and P. Ring, Nucl. Phys. A 232 (1974) 1.

172) H. Nopre and E. Werner, Z. Physik 254 (1972) 345;
H. Nopre and E. Werner, Z. Physik 257 (1972) 410.

173) S. Wahlborn and J. Blomquist, Nucl. Phys. A 133 (1969) 50.

174) J. Speth in: Proc. Intern. Symp. on Nucl. Physics, Balatonfüred, Hungary 1975, vol. 1, p. 125.

175) D.H. Gloeckner and R.D. Lawson, Phys. Lett. 53 B (1974) 313.

176) J.B. McGrory and B.H. Wildenthal, Phys. Lett. 60 B (1975) 5.

177) H. Miska, H.D. Gräf, A. Richter, R. Schneider, D. Schüll, E. Spamer, O. Titze and Th. Walcher, Phys. Lett. 58 B (1975) 155.

178) H.R. Hiddleston, J.A. Aymar and S.E. Darden, Nucl. Phys. A 242 (1975) 323.

179) J.L. Fowler, C.H. Johnson and R.M. Feezel, Phys. Rev. C 8 (1973) 545.

180) D. Nathan and S.G. Nilsson: Alpha, Beta and Gamma Ray Spectroscopy, ed. by K. Siegbahn (Amsterdam, 1966) p. 640;
E.K. Warburton and J. Weneser, Isospin in Nucl. Phys., ed. by D.H. Wilkinson (Amsterdam 1966).

181) J.S. O'Connell, Electromagentic sum rules, in: Proceedings of Int. Conf. on Photonuclear Reactions, ed. by B.L. Berman, Asilomar, California, 1973.

182) D.G. Mavis et al., Bull. Am. Soc. 21 (1976) 518.

183) T. Bauer et al., to be published.

184) M. Buenerd, Thêse d'Etat, Universitê de Grenoble, France.

185) V.G. Soloviev, Ch. Stoyanov and A.I. Vdovin. Dubna preprint 1977. E4-10397, submitted to Nucl. Phys. A.

186) J. Bellicard et al., Nucl. Phys. A 143 (1970) 213.

187) M. Nagao and Y. Torizuka, Phys. Lett 37 B (1971) 383;
J.F. Ziegler and G.A. Paterson, Phys. Rev. 165 (1968) 1337.

188) J.S. Dehesa, J. Speth, Annual Report 1976, KFA-IKP 10/77.

189) G.E. Brown, S.-O. Bäckman, E. Oset and W. Weise, Preprint 1977.

190) H.W. Baer, K.M. Crowe and P. Truöl. Advances in Nucl. Phys. 9 (1977).

191) G.E. Brown and A.M. Green, Nucl. Phys. 75 (1966) 401.

192) R.J. Philpott and P.R. Szydlik, Phys. Rev. 153 (1967) 1039.

193) H. Flocard and D. Vautherin, Phys. Lett. 55 B (1975) 259;
S. Krewald, R. Rosenfelder, J.E. Galonska and A. Faessler, Nucl. Phys. A 269 (1976) 112.

TABLE CAPTIONS

Table 1: Percentages of isoscalar EWSR multipole strength depleted by exciting "bound" states of ^{40}Ca and ^{208}Pb.

Table 2: Number of different 6J-symbols needed in our (2p-2h) calculations in the nuclei ^{12}C, ^{16}O, ^{90}Zr and ^{208}Pb. The angular momenta of all the states within $2\hbar\omega$ above and below Fermi surface are included. In case of ^{208}Pb, two possibilities are shown which correspond to the inclusion or not of the neutron particle state $1k_{17/2}$.

Table 3: Typical dimensions of the core-coupling RPA matrix corresponding to different spherical nuclei.

Table 4: Parameters of the Woods-Saxon potential, defined by (4.2-4.3), of the nuclei ^{16}O, ^{40}Ca, ^{90}Zr and ^{208}Pb. It is used $r_o = r_{LS}$ and the reduced Coulomb radius r_c = 1.25 fm. The parameters were adjusted by fitting correctly the experimental single-particle energies near the Fermi surface.

Table 5: Single-particle energies used in our (1p-1h) and (2p-2h) RPA calculations in the nuclei ^{12}C, ^{16}O. As far as possible they were taken from experiment. The rest of them was determined from the Woods-Saxon well of Table 4.

Table 6: Single-particle energies in our (1p-1h) and (2p-2h) RPA calculations in the nucleus ^{90}Zr. Those not taken from experiment were calculated by using the Woods-Saxon potential of Table 4.

Table 7: Single-particle energies in our (1p-1h) and (2p-2h) RPA calculations in ^{208}Pb. The states of first shell above and below the Fermi energy are from experiment. The rest of them was calculated by using the Woods-Saxon potential of Table 4.

Table 8: Parameters of the Migdal effective interaction used in our (1p-1h) and (2p-2h) RPA calculations.

Table 9: Strength of the Migdal force and interpolation radii R_{nn} and R_{pp} used in our (1p-1h) and (2p-2h) RPA calculations. The radius $R_{pn} = (R_{pp}+R_{nn})/2$.

Table 10: Low-lying (1p-1h) core excitations (which cause the splitting of quasiparticle and quasihole states) taken into account in our (2p-2h) calculations in the nuclei ^{12}C, ^{16}O, ^{90}Zr and ^{208}Pb.

Table 11: Calculated quasiparticle $7/2^-$ states of ^{17}F. Only those states with single-particle strength (SPS) ≥ 1 % are shown. In the wave functions we have only written down the 2p-1h components whose contribution is in absolute values bigger than 0.050. To interpret the table one should remember eq. (3.31), e.g. the first state would be as follows:

$$|f^{(1)}_{7/2};E=4.83\text{ MeV}\rangle = \sqrt{0.1983}\,|f_{7/2}\rangle - 0.824|3^- x d_{5/2}\rangle -$$

$$- 0.324|3^- x s_{1/2}\rangle - 0.093|3^- x d_{3/2}\rangle -$$

$$- 0.067|3^- x g_{9/2}\rangle$$

Table 12: Calculated quasiparticle states $5/2^-$ of ^{17}F. See comments in the description of Table 11.

Table 13: Calculated quasiparticle states $7/2^-$ of ^{17}O. See comments in the description of Table 11.

Table 14: Calculated quasiparticle states $5/2^-$ of ^{17}O. See comments in the description of Table 11.

Table 15: Electric and magnetic Weisskopf units for electromagnetic transition probabilities of various excitations ($L \leq 5$) in the closed-shell nuclei ^{12}C, ^{16}O, ^{40}Ca, ^{90}Zr and ^{208}Pb. See Appendix VII.C for definitions. The B(EL) values are given in e^2fm^{2L} and the B(ML) values in $\mu_0^2 fm^{2L-2}$.

Table 16: Monopole sum rules (in units e^2fm^4 MeV), classical dipole sum rule and higher ($L = 2,3,4,5$) electric energy-weighted sum rules (in units e^2fm^{2L} MeV) of the closed-shell nuclei ^{12}C, ^{16}O, ^{40}Ca, ^{90}Zr and ^{208}Pb. Equations (C.13), (C.16) and (C.18) were used. The groundstate was assumed to have a uniform distribution with radius $R = 1.2\ A^{1/3}$.

Table 17: Comparison of E2 strength in percentages of the T=0 E2 EWSR with various recent experiments in ^{16}O. The sum rule is $S_{th} \equiv \sum_k E_k B_k(E,L)\uparrow = 2087.4\ e^2fm^4$ MeV. This value emerges directly from the calculations and is to a very good approximation the total T=0 E2 EWSR limit.

Table 18: Main isoscalar E2 resonances in the region from 16-28 MeV in ^{16}O. The main quasiparticle components of their corresponding core-coupling (2p-2h) RPA wave functions are shown. Specially in the state at 27.508 MeV there are several other components of comparable contribution. For instance in the notation $(f^{(3)}_{5/2} \times p^{-1}_{1/2})_p$, the single-particle state $f^{(3)}_{5/2}$ refers to the state $5/2^-$ of number 3 in Table 12.

Table 19: Percentages of various sum rules exhausted by resonances E0, E2, E3 and E4 in ^{16}O. The E3 and E4 EWSR limits are taken from Table 16. The E0 and E2 EWSR values are taken from the calculation since in our configuration space ($2\hbar\omega$ above and below Fermi surface) are included all the possibilities to create such states; the values are

(T=0+T=1)E0 EWSR = 4995 e^2fm^4 MeV; T=0 E0 EWSR = 2398.5 e^2fm^4 MeV
(T=0+T=1)E2 EWSR = 4501 e^2fm^4 MeV; T=0 E2 EWSR = 2087.4 e^2fm^4 MeV.

Table 20: Same as in Table 19 but in ^{12}C. The values for E0 and E2 EWSR are as follows:

T=0+T=1 E0 EWSR = 2952 e^2fm^4 MeV; T=0 E0 EWSR = 1556 e^2fm^4 MeV
T=0+T=1 E2 EWSR = 3565 e^2fm^4 MeV; T=0 E2 EWSR = 1728 e^2fm^4 MeV

On the other hand one should bear in mind that the sum rules $\sum^{o}_{3}$, $\sum^{p}_{3}(T=0)$, $\sum^{p}_{4}$ and $\sum^{p}_{4}(T=0)$ were evaluated with $R = 1.2\ A^{1/3}$; they are in fact lower bounds of the corresponding total sum rules. See Appendix VII.D and further explanations in text (section V.2).

Table 21: Monopole and quadrupole resonances (obtained in our 1p-1h+2p-2h calculations) in ^{90}Zr in terms of sum rules. The E0 and E2 EWSR strengths are as follows:

T=0+T=1 E0 EWSR = 64057 e^2fm^4 MeV; T=0 E0 EWSR = 33185 e^2fm^4 MeV

T=0+T=1 E2 EWSR = 65863 e^2fm^4 MeV; T=0 E2 EWSR = 36472.5 e^2fm^4 MeV

Table 22: Distribution of $E\lambda$, λ = 1,3,4 strength in ^{90}Zr examined in percentages of the $E\lambda$ sum rules listed in Table 16.

Table 23: Low-lying octupole resonances (obtained in our 1p-1h+2p-2h calculations) in ^{90}Zr. For the sake of clarity in comparing with experimental results, the following value of the T=0 E2 sum rule is used: $S_0 = 1.75 \times 10^6$ e^2fm^4 MeV, which corresponds to a ground state with uniform charge distribution of radius $R = 1.123\ A^{1/3}$ fm.

Table 24: Monopole and quadrupole resonances (obtained in our 1p-1h+2p-2h calculations) in ^{208}Pb in terms of sum rules. The E0 and E2 EWSR limits are taken directly from the calculations. Their values are:

T=0+T=1 E0 EWSR = 189130 e^2fm^4 MeV; T=0 E0 EWSR = 86545 e^2fm^4 MeV

T=0+T=1 E2 EWSR = 174280 e^2fm^4 MeV; T=0 E2 EWSR = 76598 e^2fm^4 MeV.

Table 25: Distribution of the isoscalar $E\lambda$ (λ = 0,2,4) strength in the GQR region, i.e. between 8 and 15 MeV, obtained in the (1p-1h) RPA and (1p-1h+2p-2h) RPA calculations in ^{208}Pb. The exact values (which emerge directly from the calculations; see caption of Figure 24) of the T=0 E0 EWSR and T=0 E2 EWSR have been used. For the T=0 E4 EWSR we have used the value 4.52×10^8 e^2fm^8 MeV; this value is a good estimation (see Appendix VII.D) of the exact isoscalar E4 EWSR and it is $\sim$ 60.5 % of the $\sum_4^p(T=0)$ limit.

Table 26: Distribution of E3 strength in ^{208}Pb in terms of sum rules. The values of these are, according to Appendix VII.D, as follows:

$$T{=}0{+}T{=}1 \text{ E3 EWSR} = 1.57 \times 10^7 \; e^2fm^6 \text{ MeV}$$

$$T{=}0 \text{ E3 EWSR} = 0.62 \times 10^7 \; e^2fm^6 \text{ MeV}$$

Table 27: Experimental results and theoretical (1p-1h) predictions for the M1 states in ^{208}Pb.

Table 28: Variation of the energies, B(M1) values and the amplitudes A_p and A_n of the wave functions (see eq. (5.5)) of the two (1p-1h) M1 states in ^{208}Pb with the spin-dependent part g^{pn} of the proton-neutron interaction. The parameter g^{pp} = 1.30. The effective M1 operator discussed in section IV.4 was used here.

Table 29: Variation of the M1 levels calculated in the core-coupling RPA theory with the renormalization constant ξ_s of the effective magnetic operator (see section IV.4). The parameters g_{pp} = 1.30 and g_{pn} = -0.15 are used.

Table 30: Experimental results and (2p-2h) RPA calculations of M1 levels in ^{208}Pb. The parameter g_{pp} = 1.30. Bare (Schmidt) magnetic operator has been used. The coupling of seven low-lying core excitations (see Table 10) was taken into account.

Table 31: Experimental results and (2p-2h) RPA calculations of M1 resonances in ^{208}Pb. Several pairs of (g_{pp}, g_{pn}) parameters have been used. Bare M1 operator is used. The coupling of seven low-lying core excitations (see Table 10) was taken into account.

Table 32: Fragmentation of the strength of the single-hole state $1g_{9/2}$ in ^{90}Zr due to the coupling of six low-lying core excitations (see Table 10).

Table 33: Calculated M1 states in 2p-2h RPA calculations in ^{90}Zr. Bare M1 operator was used. The parameters g_{pp} = 1.30 and g_{pn} = +0.10. The coupling of six low-lying core excitations (see Table 10) has been taken into account.

Table 34: Comparison between the (1p-1h) RPA results of Ring & Speth with our (2p-2h) RPA calculations of M2 resonances in ^{208}Pb. In both cases g_{pp} = 1.30 and g_{pn} = -0.15 and the effective M2 operator have been used.

Table 35: Magnetic quadrupole resonances in ^{16}O with transition probability bigger than one Weisskopf unit calculated in the (1p-1h) RPA and (2p-2h) RPA approaches. The parameter g_{pp} = 1.30.

Table 1

Nucleus	Multipole								
	0	1	2	3	4	5	6	7	8
^{40}Ca	~ 0	~ 0	14	38	7	11	1	0.2	~ 0
^{208}Pb	~ 0	~ 0	20	47	14	3	3	2	1

Table 2

Nucleus	6J-Symbols of 1st type	6J-Symbols of 2nd type
^{12}C	600	500
^{16}O	1220	710
^{90}Zr	5985	7976
^{208}Pb (up to j=15/2)	10524	17148
^{208}Pb (up to j=17/2)	17027	25706

Table 3

Nucleus	J^{π} state	Core-Coupling RPA dimension
^{16}O	2^+	85
^{16}O	4^+	56
^{90}Zr	1^+	179
^{90}Zr	2^+	176
^{90}Zr	4^+	176
^{208}Pb	1^+	169
^{208}Pb	2^+	182
^{208}Pb	4^+	191

Table 4 Parameters of Woods-Saxon Well

Nucleus	Charge	V_o [MeV]	r [fm]	a_o [fm]	V_{LS} [MeV]	r_{LS} [fm]	a_{LS} [fm]	b [fm]
^{16}O	p	-52.88	3.0828	0.53	5.533	3.0828	0.53	1.639
	n	-53.14	3.0828	0.53	5.186	3.0828	0.53	1.639
^{40}Ca	p	-55.81	4.10	0.53	6.675	4.10	0.53	1.80
	n	-55.50	4.10	0.53	7.154	4.10	0.53	1.80
^{90}Zr	p	-57.29	5.736	0.802	7.211	5.736	1.00	2.05
	n	-48.84	5.647	0.765	11.909	5.697	1.00	2.05
^{208}Pb	p	-60.40	7.46	0.790	7.446	7.2	0.59	2.44
	n	-47.58	7.20	0.660	5.640	6.96	0.64	2.44

Table 5: Single-Particle Energies (MeV) in ^{12}C and ^{16}O

	^{12}C		^{16}O	
Orbit	Proton	Neutron	Proton	Neutron
$1s_{1/2}$	-34.80	-38.80	-40.00	-42.00
$1p_{3/2}$	-14.80	-17.00	-18.43	-21.80
$1p_{1/2}$	-1.94	-4.95	-12.10	-15.70
$1d_{5/2}$	1.60	-0.88	-0.60	-4.15
$2s_{1/2}$	1.15	-1.55	-0.10	-3.27
$1d_{3/2}$	5.84	3.00	4.54	1.57
$1f_{7/2}$	15.00	11.00	15.50	12.50
$1f_{5/2}$	21.50	19.60	18.90	15.50
$2p_{3/2}$	19.20	17.00	16.00	14.50
$2p_{1/2}$	20.50	18.80	19.50	16.20
$1g_{9/2}$			27.60	27.00

Table 6: Single-Particle Energies (MeV) in ^{90}Zr

	^{90}Zr	
Orbit	Proton	Neutron
$1d_{5/2}$	-30.21	-37.46
$1d_{3/2}$	-27.19	-34.67
$2s_{1/2}$	-23.69	-31.98
$1f_{7/2}$	-17.57	-24.32
$1f_{5/2}$	-12.61	-19.42
$2p_{3/2}$	-9.47	-17.62
$2p_{1/2}$	-7.91	-15.89
$1g_{9/2}$	-4.91	-11.53
$2d_{5/2}$	-1.54	-7.20
$1g_{7/2}$	-0.48	-4.44
$3s_{1/2}$	-0.01	-5.77
$2d_{3/2}$	0.18	-4.59
$1h_{11/2}$	2.76	-3.31
$2f_{7/2}$	5.40	-0.26
$3p_{3/2}$	5.70	0.40
$3p_{1/2}$	6.60	0.89
$2f_{5/2}$	8.70	4.67
$1h_{9/2}$	9.91	8.13
$1i_{13/2}$	11.40	3.96

Table 7: Single-Particle Energies (MeV) in ^{208}Pb

Orbit	^{208}Pb Protons	^{208}Pb Neutrons
$1f_{7/2}$	-20.802	
$1f_{5/2}$	-18.866	
$2p_{3/2}$	-16.669	
$2p_{1/2}$	-15.851	
$1g_{9/2}$	-15.281	
$1g_{7/2}$	-11.508	-20.750
$2d_{5/2}$	-9.708	-19.190
$1h_{11/2}$	-9.375	-16.552
$2d_{3/2}$	-8.385	-17.393
$3s_{1/2}$	-8.034	-17.187
$1h_{9/2}$	-3.802	-10.786
$2f_{7/2}$	-2.902	-9.717
$1i_{13/2}$	-2.193	-9.010
$2f_{5/2}$	-0.980	-7.947
$3p_{3/2}$	-0.686	-8.275
$3p_{1/2}$	-0.162	-7.377
$2g_{9/2}$	3.547	-3.943
$1i_{11/2}$	3.930	-3.165
$1j_{15/2}$	4.666	-2.521
$3d_{5/2}$	6.212	-2.377
$2g_{7/2}$	6.741	-1.450
$3d_{3/2}$	7.513	-1.404
$2h_{11/2}$	10.271	3.672
$4s_{1/2}$		-1.911
$4p_{3/2}$		2.939
$4p_{1/2}$		3.046
$3f_{7/2}$		3.813
$3f_{5/2}$		4.068

Table 8

f_{pp}^{in}	f_{pn}^{in}	f_{pp}^{ex}	f_{pn}^{ex}	$g_{pp}^{in} = g_{pp}^{ex}$	$g_{pn}^{in} = g_{pn}^{ex}$
0.400	-0.264	-1.700	-2.640	1.300	-0.15

Table 9

Nucleus	RPA calculation	ε_F (MeV)	R_{nn} (fm)	r_o (fm)	R_{pp}	r_o	a
^{12}C	1p-1h	42.50	2.47	1.08	2.47	1.08	0.53
	1p-1h+2p-2h	45.50	"	"	"	"	"
^{16}O	1p-1h	43.00	2.80	1.11	2.80	1.11	0.53
	1p-1h+2p-2h	40.00	"	"	"	"	"
^{90}Zr	1p - 1h	39.00	5.360	1.19	5.160	1.15	0.60
	1p-1h+2p-2h	"	"	"	"	"	"
^{208}Pb	1p-1h	39.37	7.04	1.18	6.80	1.15	0.60
	1p-1h+2p-2h	"	"	"	"	"	"

Table 10

Nucleus	J^{π}	(1p-1h) RPA Theory		Experiment	
		Energy (MeV)	B(Eλ or Mλ)↑ ($e^2fm^{2\lambda}$ or $\mu_o^2 fm^{2\lambda-2}$)	Energy	B(Eλ or Mλ)↑
^{12}C	2^+	4.49	115.84	4.44	
	3^-	12.00	475.36	9.64	
^{16}O	3^-	6.292	1593.71	6.13	1490±70 (1)
	2^-	13.373	1.15	12.53	
	1^-	13.225	0.02	13.10	
^{90}Zr	2^+	3.977	209	2.186	
	5^-	2.894	0.37×10^8	2.319	
	4^-	3.319	0.41×10^6	2.736	
	3^-	3.041	0.12×10^6	2.749	
	4^+	4.139	0.16×10^6	3.077	
	5^-	4.405	0.16×10^8	3.975	
^{208}Pb	3^-	2.622	544×10^6	2.614	$(540\pm30)\times10^3$
	5^-	3.359	319×10^6	3.190	$(462\pm55)\times10^6$
	4^-	3.611	0.97×10^6	3.470	
	5^-	3.827	277×10^6	3.710	330×10^6
	4^-	4.208	0.17×10^6	3.960	
	2^+	4.459	3199	4.080	2920 (2)
	4^+	4.674	785×10^4	4.320	1287×10^4

(1) See inelastic electron scattering experiments of ref. 177

(2) See ref. 187

Table 11: Calculated Quasiparticle $7/2^-$ States of ^{17}F

No.	Energy (MeV)	SPS (%)	Wave Function						
			$3^-xd_{5/2}$	$3^-xs_{1/2}$	$3^-xd_{3/2}$	$1^-xd_{5/2}$	$2^-xd_{5/2}$	$2^-xd_{3/2}$	$3^-xg_{9/2}$
1	4.83	19.83	-0.824	-0.324	-0.093	~ 0	~ 0	~ 0	-0.067
2	7.49	1.05	0.417	-0.902	-0.034	~ 0	~ 0	~ 0	~ 0
3	11.59	11.05	0.228	0.182	-0.868	-0.126	-0.167	-0.053	-0.065
4	12.94	2.13	-0.079	-0.059	-0.295	0.164	0.924	~ 0	~ 0
5	13.50	2.42	-0.077	-0.057	-0.181	0.929	-0.260	~ 0	~ 0
6	15.50	52.97	-0.278	-0.198	-0.337	-0.300	-0.219	0.266	0.173
7	18.87	6.02	-0.068	~ 0	-0.056	~ 0	~ 0	-0.960	0.071

Table 12: Calculated Quasiparticle $5/2^-$ States of ^{17}F

No.	Energy (MeV)	SPS (%)	Wave Function						
			$3^- x d_{5/2}$	$3^- x s_{1/2}$	$3^- x d_{3/2}$	$1^- x d_{3/2}$	$2^- x d_{5/2}$	$2^- x d_{3/2}$	$3^- x g_{9/2}$
1	5.47	11.84	0.851	0.362	0.150	∿0	∿0	∿0	∿0
2	7.42	1.32	-0.437	0.888	0.071	∿0	∿0	∿0	∿0
3	11.17	9.44	-0.198	-0.211	0.897	∿0	0.110	∿0	∿0
4	18.55	5.70	0.058	0.052	0.110	-0.065	∿0	-0.957	∿0
5	18.90	52.37	-0.173	-0.153	-0.316	0.471	-0.084	-0.276	0.114
6	19.22	16.71	-0.095	-0.084	-0.170	-0.879	∿0	-0.076	0.066

Table 13: Calculated Quasiparticle $7/2^-$ States of ^{17}O

No.	Energy (MeV)	SPS (%)	Wave Function						
			$3^- x d_{5/2}$	$3^- x s_{1/2}$	$3^- x d_{3/2}$	$1^- x d_{5/2}$	$2^- x d_{5/2}$	$2^- x d_{3/2}$	$3^- x g_{9/2}$
1	1.28	20.54	0.836	0.289	0.083	0	0	0	0.053
2	4.64	2.24	-0.400	0.902	0	0	0	0	0
3	8.59	6.99	0.181	0.177	-0.922	-0.074	-0.091	0	0
4	10.19	0.99	-0.052	0	-0.120	0.982	-0.070	0	0
5	12.50	64.62	-0.318	-0.258	-0.328	-0.162	-0.104	0.133	0.149
6	15.46	1.47	0	0	0	0	0	0.991	0

Table 14: Calculated Quasiparticle $5/2^-$ States of ^{17}O

No.	Energy (MeV)	SPS (%)	Wave Function				
			$3^- x d_{5/2}$	$3^- x s_{1/2}$	$3^- x d_{3/2}$	$1^- x d_{3/2}$	$2^- x d_{3/2}$
1	1.77	14.53	0.851	0.323	0.152	~ 0	~ 0
2	4.52	2.59	0.427	-0.884	-0.103	~ 0	~ 0
3	8.11	7.81	0.193	0.252	-0.903	~ 0	-0.067
4	15.39	6.04	0.067	0.065	0.111	-0.109	-0.951
5	15.50	54.75	-0.202	-0.196	-0.329	0.399	-0.050
6	16.08	12.94	-0.094	-0.090	-0.147	-0.910	~ 0

Table 15: Weisskopf Units for B(EL or ML) Values

Nucleus / B_W(EL or ML)↑	^{12}C	^{16}O	^{40}Ca	^{90}Zr	^{208}Pb
$B_W(E1)\uparrow$	1.0137	1.2279	2.2617	3.8835	6.7884
$B_W(E2)\uparrow$	8.16	11.97	40.63	119.79	366.05
$B_W(E3)\uparrow$	59.88	106.45	665.32	3368.00	17990.38
$B_W(E4)\uparrow$	426.87	919.44	10584.90	92011.14	8.59×10^5
$B_W(E5)\uparrow$	3015.10	7866.90	1.67×10^5	2.49×10^6	4.06×10^7
$B_W(M1)\uparrow$	5.37	5.37	5.37	5.37	5.37
$B_W(M2)\uparrow$	43.25	52.39	96.50	165.70	289.64
$B_W(M3)\uparrow$	317.34	465.71	1580.17	4658.89	14222.22
$B_W(M4)\uparrow$	2262.44	4022.22	25138.88	1.27×10^5	6.80×10^5
$B_W(M5)\uparrow$	15979.76	34414.40	3.96×10^5	3.44×10^6	3.22×10^7

Table 16: Sum Rules

EWSR \ Nucleus	^{12}C	^{16}O	^{40}Ca	^{90}Zr	^{208}Pb
Σ_o^p	2255.2	3642.5	16774.5	57606.0	2.06×10^5
$\Sigma_o^p(T=0)$	1127.6	1821.3	8387.2	25602.6	0.81×10^5
$\Sigma_o^p(T=1)$	1127.6	1821.3	8387.2	32003.3	1.25×10^5
$\Sigma_1^p(T=1)$	44.4	57.6	148.0	328.9	735.2
Σ_2^p	2243.2	3623.0	16685.3	57300.0	2.05×10^5
$\Sigma_2^p(T=0)$	1121.6	1811.5	8342.6	25466.7	0.81×10^5
$\Sigma_2^p(T=1)$	1121.6	1811.5	8342.6	31833.3	1.24×10^5
Σ_3^p	35555.1	69570.0	5.90×10^5	3.48×10^6	2.18×10^7
$\Sigma_3^p(T=0)$	17777.5	34785.0	2.95×10^5	1.55×10^6	0.86×10^7
$\Sigma_3^p(T=1)$	17777.5	34785.0	2.95×10^5	1.93×10^6	1.32×10^7
Σ_4^p	4.6×10^5	1.1×10^6	1.70×10^7	1.72×10^8	1.89×10^9
$\Sigma_4^p(T=0)$	2.3×10^5	0.55×10^6	0.85×10^7	0.77×10^8	0.74×10^9
$\Sigma_4^p(T=1)$	2.3×10^5	0.55×10^6	0.85×10^7	0.96×10^8	1.14×10^9
Σ_5^p	5.30×10^6	1.52×10^7	4.38×10^8	7.62×10^9	1.46×10^{11}
$\Sigma_5^p(T=0)$	2.65×10^6	0.76×10^7	2.19×10^8	3.39×10^9	0.57×10^{11}
$\Sigma_5^p(T=1)$	2.65×10^6	0.76×10^7	2.19×10^8	4.23×10^9	0.88×10^{11}

Table 17: Distribution of E2 Strength in ^{16}O

E_1-E_2 (MeV)	S_{exp} (%)	Reaction	S_{th} (%)
16-26	40^{+20}_{-10}	(α,α')[a]	55
17-28	75	$(^3He,^3He')$[b]	63
15-28	67±25	(α,α')[c]	83
20-30	$\left\{\begin{matrix}30\\21\end{matrix}\right.$	(p,γ_0)[d] (e,e')[e]	62

a) Hanna et al. See ref. 40

b) Moalem et al. See ref. 48

c) Knöpfle et al. See ref. 50

d) Harakeh et al. See ref. 49

e) Hotta et al. See ref. 47

Table 18: Main T=0 E2 Peaks in the Giant Resonance Region in ^{16}O

Energy (MeV)	Quasiparticle-quasihole components of the core-coupling RPA wave function							
	$(f^{(1)}_{7/2} x p^{-1}_{3/2})_p$	$(f^{(1)}_{5/2} x p^{-1}_{1/2})_p$	$(f^{(5)}_{5/2} x p^{-1}_{1/2})_p$	$(f^{(3)}_{5/2} x p^{-1}_{1/2})_p$	$(f^{(1)}_{7/2} x p^{-1}_{3/2})_n$	$(f^{(3)}_{7/2} x p^{-1}_{3/2})_n$	$(f^{(1)}_{5/2} x p^{-1}_{1/2})_n$	$(f^{(5)}_{5/2} x p^{-1}_{1/2})_n$
16.152	-0.2103	-0.6497	∿0.	∿0.	0.1833	∿0.	-0.6322	-0.1024
20.664	0.5708	∿0.	0.1185	0.2126	-0.4188	0.1444	-0.2886	0.1586
27.508	-0.2620	∿0.	0.2661	∿0.	0.2360	0.3503	∿0.	0.3204

Table 19: Distribution of the Eλ (λ=0,2,3,4) Strength in ^{16}O

Energy Interval (MeV) \ Eλ	E0		E2		E3		E4	
	% T=0+T=1 EWSR	% T=0 EWSR	% (T=0+T=1)EWSR	% T=0 EWSR	% Σ_3^p	% $\Sigma_3^p(T=0)$	% Σ_4^p	% $\Sigma_4^p(T=0)$
12-16	-	-			3.2	3.4	-	-
16-20	-	-	10.4	21.9	4.1	-	3.6	7.2
20-22	-	-	14.8	31.9	-	-	8.0	16.0
22-26	2.9	5.6	2.7	∿1.0	4.7	5.9	5.2	6.8
26-28	36.0	75.0	13.4	28.5	-	-	6.9	13.3
28-30	-	-	2.8	1.3	-	-	1.8	0.
30-35	10.5	20.7	13.0	7.8	1.4	2.8	4.7	7.9
35-40	14.4	15.0	20.0	-	13.3	∿26.6	27.1	$\gtrsim$4.8
40-45	28.5	-	14.6	2.9	2.2	2.5	-	
45-55	∿1.1	-	6.5	∿1.0	25.2	23.0	5.8	
55-75	∿1.3	-	-	-	19.0	-	∿0.5	

Table 20: Distribution of Eλ (λ=0,2,3,4) Strength in ^{12}C

Eλ / Energy Interval (MeV)	E0 % T=0+T=1 EWSR	E0 % T=0 EWSR	E2 % T=0+T=1 EWSR	E2 % T=0 EWSR	E3 % Σ_3^p	E3 % $\Sigma_3^p(T=0)$	E4 % Σ_4^p	E4 % $\Sigma_4^p(T=0)$
11-15	-	-	-	-	1.5	-	-	-
15-18	-	-	3.4	0	1.4	2.9	-	-
18-26.5	0.9	1.8	9.8	13.2	3.1	-	3.6	-
26.5-30	-	-	1.3	2.7	0.5	1.0	10.3	21.0
30-35	39.7	74.4	23.8	16.6	1.9	1.6	21.7	15.0
35-40	8.4	-	8.3	7.1	7.3	11.5	24.6	11.4
40-45	0.6	-	0.9	0.8	6.1	12.3	1.4	-
45-50	34.3	18.9	16.2	10.6	3.6	6.5	38.0	6.5
50-55	-	-	8.9	3.3	4.4	2.7	10.0	-
55-65	8.9	5.4	9.7	10.1	3.9	2.1		
65-75	4.1	-	2.7	0.9	8.6	∿9.7		

Table 21: Distribution of E0 and E2 Strength in ^{90}Zr

Eλ / Energy Interval (MeV)	E0 % (T=0+T=1) EWSR	E0 % T=0 EWSR	E2 % (T=0+T=1) EWSR	E2 % T=0 EWSR
0- 5	-	-	1	1.8
5-10	-	-	0.5	0.8
10-12.5	-	-	0.3	0.6
12.5-15	10.2	19.7	26.4	47.7
15-17.5	13.5	16.3	3.6	0.8
17.5-20	7.1	8.7	20.2	22.0
20-22.5	25.4	42.5	3.9	-
22.5-25	6.7	2.6	4.0	-
25-30	20.1	8.1	24.6	0.5
30-35	15.5	-	4.7	-

Table 22: Distribution of Eλ, λ=1,3,4,5 Strength in ^{90}Zr

Energy Interval (MeV) \ Eλ	E1		E3		E4	
	% (T=0+T=1) EWSR	% Σ_1^p(T=1)	% Σ_3^p	% Σ_3^p(T=0)	% Σ_4^p	% Σ_4^p(T=0)
0-5	-	-	9.0	20.2	0.3	0.8
5-10	8.2	9.5	4.7	7.8	1.1	2.5
10-15	60.6	69.6	8.4	7.6	19.2	42.1
15-20	45.4	52.2	5.1	3.9	16.6	6.4
20-25	2.6	3.0	0.8	1.3	13.0	8.9
25-30	-	0.2	19.3	42.3	7.0	2.7
30-35	-	-	16.8	24.6	4.0	0.9
35-40	-	-	10.1	0.8	-	-
40-45	-	-	0.8	1.2		

Table 23: Low-Lying Octupole Resonances in ^{90}Zr

Present work						Youngblood group[142]			Krewald et al.[108]			Bertsch & Tsai[87]		
(1p-1h) RPA			(1p-1h+2p-2h) RPA			Inelastic (α,α') exp			Continuum (1p-1h) RPA					
E (MeV)	B(E3)↑ $(e^2 fm^6)$	% S_o	E	B(E3)↑	%	E	B(E3)↑	%	E	B(E3)↑	%	E	B(E3)↑	%
2.85	1.26×10^5	20.5	3.28	0.95×10^5	17.8	2.75	0.45×10^5	7.1	3.0	1.2×10^5	20.6	2.6	0.94×10^5	14.0
			5.44	0.33×10^4	1.0									
			5.59	0.69×10^4	2.2	5.60	0.12×10^5	3.8						
6.14	0.17×10^5	6.0	6.24	0.13×10^4	0.5	6.36	0.71×10^4	2,5	6,2	$2,0 \times 10^4$	7.1			
			6.47	0.47×10^4	1.7	6.70	0.84×10^4	3.2						
			$6.98^{(T=1)}$	0.10×10^4	0.4									
7.06	0.06×10^4	0.2	7.06	0.19×10^4	0.8							~7	$1,21 \times 10^5$	48.5
			7.37	0.03×10^4	0.1	7.39	0.77×10^4	3.3						
7.83	0.04×10^4	0.2	7.87	0.08×10^4	0.4	8.19	$0,64 \times 10^4$	3.0						
$8.08^{(T=1)}$	0.03×10^4	0.1	$8.35^{(T=1)}$	0.04×10^4	0.2									
$8.47^{(T=1)}$	0.29×10^4	1.4	$8.84^{(T=1)}$	0.01×10^4	0.1									
			$8.85^{(T=1)}$	0.15×10^4	0.8									
0-9	1.47×10^5	28.4	0-9	1.10×10^5	26.0	0-9	0.87×10^5	23.0	0-9	1.4×10^5	~27.7	0-9	2.15×10^5	~62.5

Table 24: Distribution of E0 and E2 Strength in ^{208}Pb

Energy Interval (MeV)	E0		E2		
	% T=0+T=1 EWSR	% T=0 EWSR	% T=0+T=1 EWSR	% T=0 EWSR	% $\Sigma_2^p(T=0)$
0- 5	-	-	7.4	16.9	16.0
5- 8	-	-	4.7	5.6	5.3
8-10	0.1	0.1	8.1	18.6	17.6
10-12	3.2	7.8	24.7	56.5	53.5
12-14	9.3	18.7	15.2	31.0	29.3
14-16	25.6	55.4	5.1	0.4	0.4
16-18	12.4	12.2	23.8	-	-
18-20	16.4	5.7	2.4	0.4	0.4
20-22	26.8	0.2		-	-
22-32	4.0	-		-	-

Table 25: Distribution of T=0 Eλ, λ=0,2,4 Strength in the GQR Region, i.e. between 8 and 15 MeV, in ^{208}Pb

%	% of T=0 E0 EWSR		% of T=0 E2 EWSR		% of T=0 E4 EWSR	
Energy (MeV)	1p-1h	1p-1h+2p-2h	1p-1h	1p-1h+2p-2h	1p-1h	1p-1h+2p-2h
8- 9	-	-	-	0.1	0.6	4.2
9-10	-	0.1	-	18.5	1.2	3.5
10-11	0.2	0.8	1.7	3.1	-	0.1
11-12	6.1	8.9	111.2	53.5	27.2	16.8
12-13	-	1.7	0.6	29.7	5.3	1.6
13-14	16.4	16.8	1.5	1.3	3.3	5.4
14-15	69.2	50.8	0.4	0.3	0.4	-
8-15	91.9 %	78.1 %	115.4 %	96.5 %	38 %	31.6 %
Centroid	14.4 MeV	13.7 MeV	11.3 MeV	10.2 MeV	11.6 MeV	10.3 MeV

Table 26: Distribution of E3 Strength in ^{208}Pb

Energy Interval (MeV)	% T=0+T=1 E3 EWSR	% T=0 E3 EWSR
0- 5	8.3	20.7
5- 8	3.7	2.4
8-10	4.3	0.1
10-12	2.2	0.2
12-14	3.7	5.4
14-16	2.4	0.3
16-18	2.6	0.1
18-20	6.4	-
20-22	24.6	25.3
22-25	0.4	0.5
25-30	2.1	0.5

Table 27: M1 Resonances in ^{208}Pb. Comparison between (1p-1h) Theories and Experiment

	Energy (MeV)	$B(M1)\uparrow(\mu_o^2)$
Vergados[75)]	5.45 7.52	1.2 48.07
Ring & Speth[76)]	7.50 8.31	5.68 11.00
Experiment[70,74)]	7.06 7.99	16.8 10.0

Table 28: Variation of (1p-1h) M1 States with g^{pn}

g^{pn}	Lower 1^+				Upper 1^+			
	E (MeV)	$B(M1)\uparrow(\mu_o^2)$	A_p	A_n	E (MeV)	$B(M1)\uparrow(\mu_o^2)$	A_p	A_n
-0.90	6.46	0.83	0.80	-0.61	9.04	13.89	0.62	0.80
-0.50	7.10	1.74	0.86	-0.52	8.63	13.96	0.53	0.86
-0.15	7.50	5.68	0.97	-0.26	8.31	11.00	0.26	0.97
-0.10	7.53	6.99	0.99	-0.18	8.29	9.84	0.19	0.99
-0.05	7.55	8.86	1.00	-0.08	8.27	8.15	0.08	1.00
0.00	7.56	10.23	1.00	0	8.26	6.92	0	1.00
0.20	7.46	15.60	0.95	0.32	8.35	2.24	-0.33	0.96
0.30	7.35	17.00	0.92	0.42	8.43	1.22	-0.42	0.91
0.40	7.23	17.93	0.88	0.48	8.52	0.69	-0.48	0.89
0.50	7.10	18.66	0.86	0.52	8.63	0.40	-0.53	0.86
0.90	6.46	21.10	0.80	0.61	9.04	0.04	-0.62	0.80

Table 29: Variation of M1 Resonances with $\xi_s \equiv \xi_{s_p} = \xi_{s_n}$ in the (2p-2h) RPA calculations. The parameters g_{pp} = 1.30 and g_{pn} = -0.15 are used.

Energy (MeV)	$B(M1)\uparrow(\mu_o^2)$						
	ξ_s = 0.113	0.090	0.050	0.000	-0.010	-0.020	-0.030
6.90	3.74	4.21	5.11	6.34	6.61	6.88	7.15
7.51	0.11	0.12	0.14	0.16	0.17	0.17	0.18
7.70	4.94	5.76	7.33	9.57	10.05	10.54	11.05
7.99	0.35	0.40	0.50	0.81	0.66	0.68	0.71
8.38	0.41	0.48	0.62	1.86	0.86	0.90	0.94
8.93	1.07	1.21	1.48	1.44	1.94	2.02	2.10
9.21	0.83	0.94	1.14	1.60	1.50	1.56	1.63
9.55	0.82	0.95	1.22	0.42	1.68	1.76	1.85
9.65	0.23	0.27	0.33	0.71	0.43	0.45	0.47
9.82	0.36	0.42	0.54	0.24	0.74	0.78	0.82
9.97	0.14	0.16	0.19	0.33	0.25	0.27	0.28
10.10	0.17	0.20	0.25	0.25	0.35	0.37	0.38
10.24	0.14	0.16	0.19	0.17	0.26	0.27	0.28
10.40	0.32	0.36	0.13	0.56	0.59	0.61	0.63
10.54	0.21	0.25	0.45	0.42	0.44	0.46	0.48
10.65	0.82	0.93	0.32	1.43	1.48	1.55	1.61
10.84	1.35	1.57	1.14	2.61	2.74	2.87	3.01

Table 30: Comparison between experimental results and (2p-2h) RPA calculations of 1^+ states in ^{208}Pb. Bare M1 operator is used. The parameter $g_{pp} = 1.30$.

Experiment		Theory I $g^{pn} = -0.15$		Theory II $g^{pn} = +0.02$		Theory III $g^{pn} = +0.05$		Theory IV $g^{pn} = +0.10$	
E (MeV)	$B(M1)\uparrow$ (μ_o^2)	E	$B(M1)\uparrow$	E	$B(M1)\uparrow$	E	$B(M1)\uparrow$	E	$B(M1)\uparrow$
7.06[a]	16.8	7.107	6.33	7.131	9.58	7.129	10.42	7.121	12.05
		7.250	0.75	7.256	2.18	7.255	2.29	7.253	2.29
		7.475	0.04	7.475	0.17	7.475	0.19	7.475	0.21
		7.853	5.08	7.863	9.10	7.862	9.03	7.858	8.19
		7.909	0.01	7.909	0.34	7.909	0.09	7.909	0.02
		7.927	0.45	7.910	0.17	7.912	0.03	7.920	0.08
7.99[b]	10.0	7.933	5.47	7.927	0.02	7.927	0.02	7.928	0.04
		7.940	0.03	8.102	0.60	8.102	0.50	8.103	0.37
		8.106	1.49	8.303	0.45	8.303	0.43	8.303	0.42
8.228[b]	1.21±0.03	8.303	0.54	8.402	0.49	8.402	0.45	8.403	0.38
8.367[b]	0.93±0.04	8.404	0.80	8.601	0.27	8.601	0.26	8.601	0.24
8.604[b]	1.35±0.04	8.601	0.33	8.771	0.21	8.770	0.20	8.771	0.18
8.694[b]	1.23±0.08	8.771	0.26	8.835	0.19	8.835	0.18	8.835	0.16
9.008[b]	1.56±0.07	8.835	0.21	8.841	0.43	8.841	0.42	8.841	0.41
9.142[b]	1.39±0.31	8.841	0.55	9.281	0.29	9.281	0.29	9.282	0.29
9.299[b]	0.84±0.16	9.281	0.30	9.651	1.38	9.651	1.36	9.651	1.32
		9.652	1.51	9.983	0.22	9.983	0.22	9.983	0.22
		10.197	0.41	10.197	0.42	10.197	0.42	10.197	0.42
		10.302	0.44	10.302	0.42	10.302	0.41	10.302	0.40
		10.481	0.17	10.481	0.17	10.481	0.18	10.481	0.18
		10.496	0.11	10.496	0.14	10.496	0.15	10.496	0.15
		10.593	1.00	10.593	1.03	10.593	1.04	10.593	1.04
		10.768	0.33	10.770	0.71	10.769	0.78	10.769	0.87
		10.858	2.89	10.853	1.99	10.853	1.81	10.855	1.54

a) Ref. 74) b) Ref. 73)

Table 31: Experimental results and several (2p-2h) RPA calculations of M1 resonances in ^{208}Pb. Bare M1 operator has been used.

Experiment		Theory							
E (MeV)	B(M1)↑(μ_o^2)	g^{pp}=1.30; g^{pn}=-0.15		g^{pp}=1.10; g^{pn}=-0.15		g^{pp}=1.10; g^{pn}=-0.20		g^{pp}=1.10; g^{pn}=+0.10	
		E	B(M1)↑	E	B(M1)↑	E	B(M1)↑	E	B(M1)↑
7.06[a]	16.8	7.107	6.33	6.939	7.90	6.909	4.90	6.962	18.09
		7.250	0.75	7.237	0.08	6.912	1.65	7.238	0.50
		7.475	0.04			7.236	0.03	7.473	0.14
7.99[b]	10.0	7.853	5.08	7.666	13.77	7.680	13.73	7.654	8.68
		7.909	0.01	7.903	1.84	7.907	1.90	7.900	0.36
		7.927	0.45	7.909	0.03	7.909	0.49		
		7.933	5.47						
		7.940	0.03						
		8.106	1.49	8.095	0.89	8.097	1.07	8.094	0.38
8.2-9.5[b]	8.5±0.5	8.2-9.5	3.00	8.2-9.5	2.29	8.2-9.5	2.45	8.2-9.5	1.67
		9.5-11.0	7.00	9.5-11.0	7.05	9.5-11.0	7.27	9.5-11.0	6.03

a) Ref. 74) b) Ref. 73

Table 32: Strength distribution and wave function of the single-hole state $1g_{9/2}$ in ^{90}Zr.

Notation	Energy (MeV)	Single-particle strength (%)	Wave function
$g_{9/2}^{(1)}$	-11.75	90.75	$-0.9526\|1g_{9/2}\rangle-0.1641\|3^{-}\times 2p_{3/2}\rangle-0.1938\|2^{+}\times 1g_{9/2}\rangle$
$g_{9/2}^{(2)}$	-14.66	3.17	$0.1779\|1g_{9/2}\rangle-0.9791\|2^{+}\times 1g_{9/2}\rangle$
$g_{9/2}^{(3)}$	-15.48	0.83	$0.0913\|1g_{9/2}\rangle-0.9934\|4^{+}\times 1g_{9/2}\rangle$
$g_{9/2}^{(4)}$	-18.08	0.43	$0.0656\|1g_{9/2}\rangle-0.9954\|5^{-}\times 2p_{1/2}\rangle$
$g_{9/2}^{(5)}$	-19.13	0.11	$0.0337\|1g_{9/2}\rangle-0.9932\|5^{-}\times 2p_{3/2}\rangle$
$g_{9/2}^{(6)}$	-19.68	0.27	$0.0515\|1g_{9/2}\rangle-0.4845\|3^{-}\times 2p_{3/2}\rangle+0.8721\|5^{-}\times 2p_{1/2}\rangle$
$g_{9/2}^{(7)}$	-19.81	2.94	$0.1714\|1g_{9/2}\rangle-0.8464\|3^{-}\times 2p_{3/2}\rangle-0.4869\|5^{-}\times 2p_{1/2}\rangle$

Table 33: Energies and wave functions of the calculated (2p-2h) M1 states in ^{90}Zr

Energy (MeV)	$B(M1)\uparrow(\mu_o^2)$	Wave function
9.467	5.81	$-0.8790[1g_{7/2}\times 1g_{9/2}^{(1)}]-0.4683[1g_{7/2}\times 1g_{9/2}^{(2)}]-0.1155[1g_{7/2}\times 1g_{9/2}^{(3)}]$
10.521	3.11	$+0.4310[1g_{7/2}\times 1g_{9/2}^{(1)}]-0.8653[1g_{7/2}\times 1g_{9/2}^{(2)}]+0.2560[1g_{7/2}\times 1g_{9/2}^{(3)}]$
11.123	1.15	$-0.2201[1g_{7/2}\times 1g_{9/2}^{(1)}]+0.1739[1g_{7/2}\times 1g_{9/2}^{(2)}]+0.9591[1g_{7/2}\times 1g_{9/2}^{(3)}]$
13.659	0.13	$-0.9983[1g_{7/2}\times(5^-\times 2p_{1/2})_{9/2^+}]$
14.689	0.02	
15.250	0.02	
15.504	0.82	$+0.9772\|1g_{7/2}\times 1g_{9/2}^{(7)}\|+0.1474\|1g_{7/2}\times 1g_{9/2}^{(6)}\|$
16.341	0.03	
17.366	0.04	
17.811	0.07	
19.973	0.02	
20.486	0.01	
26.113	0.02	
28.170	0.02	

Table 34: Distribution of M2 strength in ^{208}Pb

Energy Interval (MeV)	(1p-1h) RPA		(2p-2h) RPA	
	$B(M2)\uparrow(\mu_0^2 fm^2)$	$B(M2)/B_W(M2)$	$B(M2)\uparrow(\mu_0^2 fm^2)$	$B(M2)/B_W(M2)$
0- 7	413	1.43	408	1.41
7- 8	11618	40.11	9115	31.47
8- 9	1084	3.74	1980	6.84
9-10	1565	5.40	1261	4.35
10-11	1385	4.78	2218	7.66
11-12	219	0.76	1174	4.05
12-13	90	0.31	368	1.27
13-15	1933	6.67	1851	6.39
15-18	2005	6.92	1763	6.09
18-30	90	0.31	140	0.48

Table 35: Strongest M2 peaks in ^{16}O

Effective M2 operator; $g_{pn} = -0.15$				Bare M2 operator; $g_{pn} = +0.10$	
(1p-1h) RPA		(2p-2h) RPA		(2p-2h) RPA	
E (MeV)	$B(M2)/B_W(M2)$	E (MeV)	$B(M2)/B_W(M2)$	E (MeV)	$B(M2)/B_W(M2)$
				13.48	1.38
		17.92	2.29	17.86	3.58
		21.07	1.43	20.90	10.31
22.83	6.42	21.45	5.28	24.72	2.18
25.35	3.45	25.04	1.27		
				40.27	1.29

FIGURE CAPTIONS

Fig. 1: Dyson equation for a single-nucleon Green function. The thick line represents the exact propagator, the thin line the unperturbed propagator and M the mass operator.

Fig. 2: The quasiparticle-core excitation coupling which approximates the mass operator $M^c(w)$ in our calculations. On the left hand side the straight line represents a single-nucleon Green function and the wriggly line a core excitation. On the right hand side the string of bubbles shows the usual microscopic RPA description of the core-excitation. In part b the quasihole-core excitation taken into account in our calculations is shown.

Fig. 3: Exchange graphs corresponding to Figures 2.a and 2.b respectively.

Fig. 4: Selfenergy graphs which contribute to $M^c(\omega)$ if pp-ground state correlations were properly considered. They are neglected in our calculations.

Fig. 5: Higher order self-energy graphs neglected in our approach. The rectangle symbolizes any possible structure except the free propagation of the particle and of the core-excitation.

Fig. 6: Higher order corrections to $M^c(\omega)$ as defined in (3.23). There are two diagrams of the type shown in Figure 5. Once the propagating particle has excited a core vibration, the quasiparticle-plus-core excitation may virtually excite yet another core mode. If the original core excitation disappears first we obtain the diagram

(a). But if the second excitation deexcites first, we get the nested diagram (b).

Fig. 7: Particle-hole contribution of the two shells above and below the Fermi energy. Here the term "Fermi energy" is used rather loosely. It is to be understood as that energy such that, if all particles occupied the lowest possible single-particle states, all states below the Fermi energy would be occupied and all states above it would be empty.

Fig. 8: The left side of the Figure shows the unperturbed single-particle position of the last proton in ^{17}F. The right-hand side gives the splitting of the $f_{7/2}$ and $f_{5/2}$ strength due to the coupling of the collective 3^- (6.13 MeV) and the 2^- (12.53 MeV) and 1^- (13.10 MeV) states of the core nucleus ^{16}O with the single-particle degrees of freedom.

Fig. 9: Quadrupole and hexadecapole resonances calculated in the (1p-1h) RPA and in the (2p-2h) core-coupling RPA theory. In this calculation the core excitations 3^-, 1^- and 2^- were considered.

Fig. 10: Monopole resonances in ^{16}O calculated in the (1p-1h) RPA and in the (2p-2h) core-coupling RPA theory. In this calculation the core excitations 3^-, 1^-, 2^- were taken into account.

Fig. 11: Dipole resonances in ^{16}O calculated in the (1p-1h) RPA and in the (2p-2h) core-coupling RPA theory. In this calculation the core excitations 3^-, 1^- and 2^- were taken into account.

Fig. 12: Octupole resonances in ^{16}O calculated in the (1p-1h) RPA and in the (2p-2h) core-coupling RPA theory. In this calculation the core excitations 3^-, 1^- and 2^- were taken into account.

Fig. 13: Distribution of the E2 strength in ^{16}O obtained in the core-coupling RPA approach by using: (a) the (3_1^-, 2_1^-, 1_1^-) core excitations, (b) the (3_1^- 2_1^- 1_1^- 3_2^-) core excitations, (c) the (3_1^- 2_1^- 1_1^- 3_2^- 2_2^- 1_2^-) core excited states. Further explanation is given in the text (section V.1).

Fig. 14: Quadrupole and hexadecapole resonances in ^{12}C calculated in the (1p-1h) RPA and in the core-coupling RPA theories. The low-lying strongly collective 2^+ (4.44 MeV) and 3^- (9.64 MeV) core excitations were taken into account in our (1p-1h+2p-2h) calculations.

Fig. 15: Octupole resonances in ^{12}C. See caption of Figure 14 for further information.

Fig. 16: Monopole resonances in ^{12}C. See caption of Figure 14 for further information.

Fig. 17: Dipole resonances in ^{12}C. See caption of Figure 14 for further information.

Fig. 18: Monopole resonances in ^{90}Zr calculated in the (1p-1h) RPA and in the core-coupling RPA theories. Six low-lying core excitations (see Table 10) were taken into account in our (1p-1h+2p-2h) calculations.

Fig. 19: Quadrupole resonances in ^{90}Zr. See caption of Figure 18 for further details.

Fig. 20: Dipole resonances in ^{90}Zr. See caption of Figure 18 for further details.

Fig. 21: Octupole resonances in ^{90}Zr. See caption of Figure 18 for further details.

Fig. 22: Hexadecapole resonances in ^{90}Zr. See caption of Figure 18 for further details.

Fig. 23: Distribution of the 2^5-pole strength in ^{90}Zr. See caption of Figure 18 for further details.

Fig. 24: Monopole resonances in ^{208}Pb. Seven low-lying core excitations (see Table 10) were taken into account in our calculations.

Fig. 25: Quadrupole resonances in ^{208}Pb. See caption of Figure 24.

Fig. 26: Octupole resonances in ^{208}Pb. See caption of Figure 24.

Fig. 27: Hexadecapole resonances in ^{208}Pb. See caption of Figure 24.

Fig. 28: E5 resonances in ^{208}Pb. See caption of Figure 24.

Fig. 29: Magnetic dipole states in ^{208}Pb calculated in the (1p-1h) RPA and in the (2p-2h) RPA theories. In part b only the lowest 3^- core coupling was considered. In part c seven low-lying core excitations (see Table 10) were taken into account in our calculations.

Fig. 30: In parts a and b the (1p-1h) RPA 1^+ states in ^{208}Pb with effective and bare M1 operator are respectively shown. Pictures c and d correspond to (2p-2h) RPA calculations with the bare M1 operator. In part c only the lowest 3^- core-coupling is considered. In part d the coupling of seven core excitations (see Table 10) is taken into account. In all these calculations $g_{pp} = 1.30$ and $g_{pn} = -0.15$.

Fig. 31: Two particle-two hole RPA calculations in ^{208}Pb with different small positive g_{pn}. The bare magnetic operator and the parameter $g_{pp} = 1.30$ have been used. Here the coupling of seven core excitations (see Table 10) has been taken into account.

Fig. 32: One particle-one hole RPA and (2p-2h) RPA calculations of M1 states in ^{90}Zr. In all the calculations $g_{pp} = 1.30$. In the 2p-2h calculations the coupling of six low-lying core excitations (see Table 10) was taken into account.

Fig. 33: One particle-one hole and 2p-2h RPA calculations of M1 states in ^{12}C. The parameter $g_{pp} = 1.30$. In the 2p-2h calculations the coupling of the collective 2^+ (4.44 MeV) and 3^- (9.61 MeV) core excitations has been taken into account.

Fig. 34: Two particle-two hole RPA calculations of M1 states in ^{12}C. In picture at the top the effective M1 operator and $g_{pn} = -0.15$ are used. In picture at the bottom the bare magnetic operator and $g_{pn} = +0.10$ have been used. In both cases $g_{pp} = 1.30$.

Fig. 35: Magnetic quadrupole states in ^{208}Pb calculated in the (1p-1h) RPA and in the (2p-2h) RPA. In the latter seven low-lying core excitations (see Table 10) were taken into account. Effective magnetic operator and the parameters $g_{pp} = 1.30$ and $g_{pn} = -0.15$ have been used.

Fig. 36: Magnetic quadrupole resonances in ^{90}Zr calculated in the (1p-1h) RPA and in the (2p-2h) RPA. In the latter the coupling of six low-lying core excitations (see Table 10) was taken into account. The parameter $g_{pp} = 1.30$.

Fig. 37: Magnetic quadrupole resonances in ^{16}O calculated in the (1p-1h) RPA and in the (2p-2h) RPA. The latter takes into account the (3^-, 1^-, 2^-) core coupling. The parameter $g_{pp} = 1.30$.

Fig. 38: Two different (2p-2h) RPA calculations of the M2 states in ^{16}O. In both $g_{pp} = 1.30$. For the picture at the top the effective magnetic operator and $g_{pn} = -0.15$ were used. In both calculations the coupling of the (3^-, 1^-, 2^-) core excitations was taken into account.

Fig. 39: Magnetic quadrupole resonances in ^{12}C calculated in the (1p-1h) RPA and in the (2p-2h) RPA. In the latter the coupling of the low-lying collective (3^-, 2^+) core excitations was taken into account. The parameter $g_{pp} = 1.30$.

Fig. 40: Two different 2p-2h RPA calculations of M2 states in ^{12}C. In both the (3^-, 2^+) core coupling was used, and the parameter $g_{pp} = 1.30$. The picture at the top was calculated with the effective magnetic operator and with $g_{pn} = -0.15$.

Fig. 41: M3 resonances in ^{90}Zr calculated in the (1p-1h) RPA and in the (2p-2h) RPA. In the latter the coupling of six low-lying core excitations (see Table 10) was taken into account. Always g_{pp} = 1.30.

Fig. 42: The same as in caption of Figure 41 but for M4 resonances.

Fig. 43: M3 resonances in ^{16}O calculated in the (1p-1h) RPA and in the (2p-2h) RPA. In the latter the (3^-, 1^-, 2^-) core coupling was considered. Always g_{pp} = 1.30.

Fig. 44: (2p-2h) M3 resonances in ^{16}O. The (3^-, 1^-, 2^-) core coupling was taken into account in both (2p-2h) RPA calculations. Always g_{pp} = 1.30. In the picture at the top the effective M3 operator and the parameter g_{pn} = -0.15 were used.

Fig. 45: The same as in caption of Figure 43 but for M4 resonances.

Fig. 46: The same as in caption of Figure 44 but for M4 resonances.

Fig. 47: M3 resonances in ^{12}C calculated in the (1p-1h) RPA and in the (2p-2h) RPA. In the latter the coupling of the low-lying collective (2^+, 3^-) core excitations was taken into account. Always g_{pp} = 1.30.

Fig. 48: (2p-2h) M3 resonances in ^{12}C. The coupling of (2^+, 3^-) core excitations was considered. Always g_{pp} = 1.30. In picture at the top the effective M3 operator was taken into account and the paramter g_{pn} = -0.15.

Fig. 49: The same as in caption of Figure 47 but for M4 resonances.

Fig. 50: The same as in caption of Figure 48 but for M4 resonances.

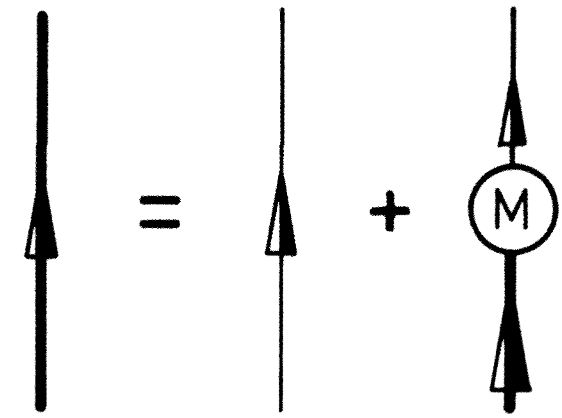

Figure 1

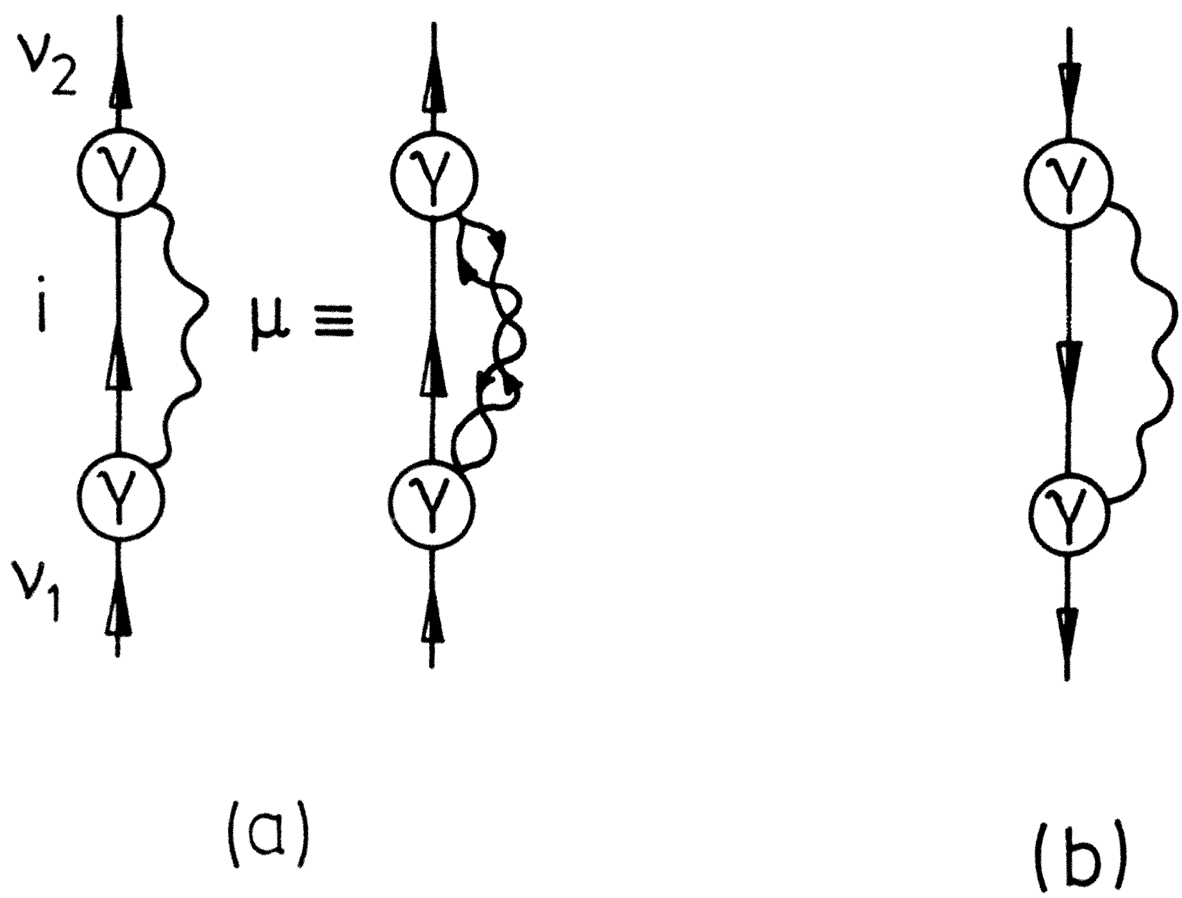

Figure 2

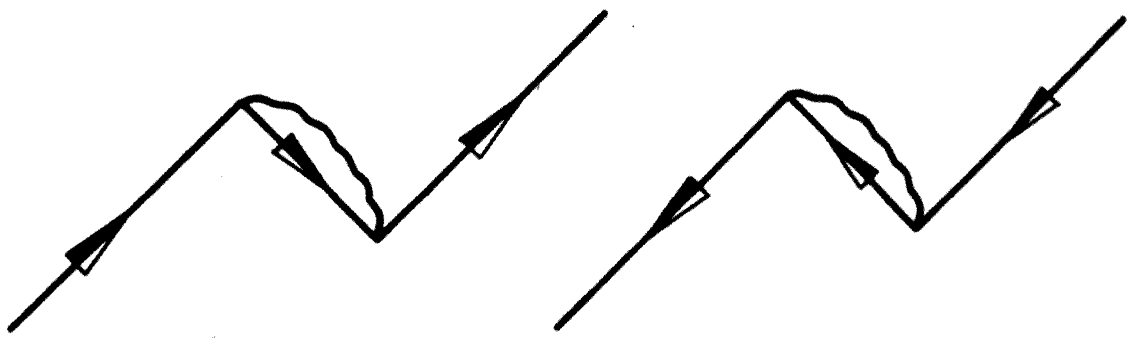

Figure 3

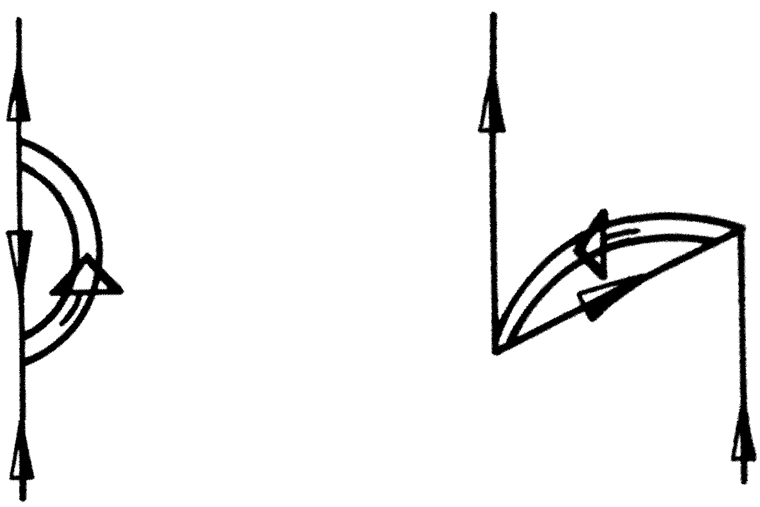

Figure 4

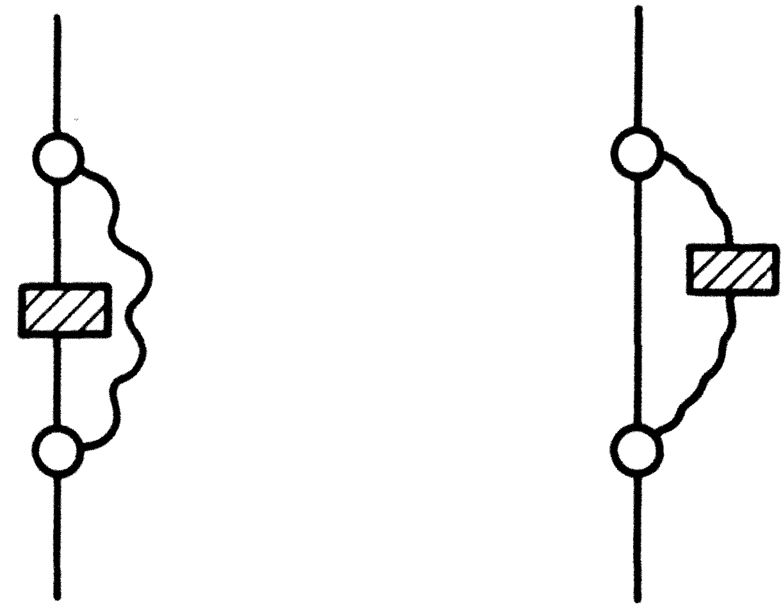

Figure 5

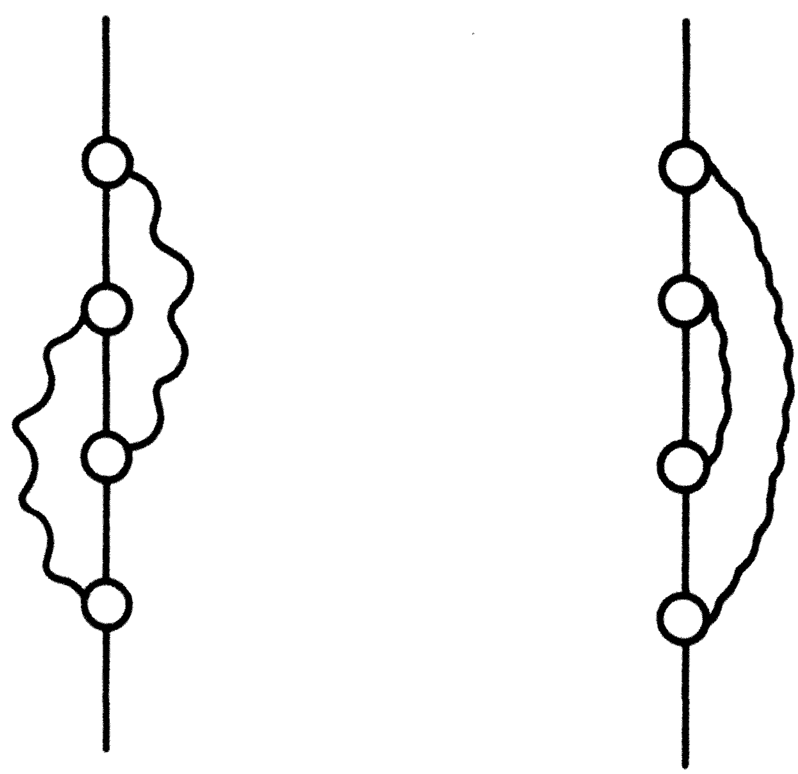

Figure 6

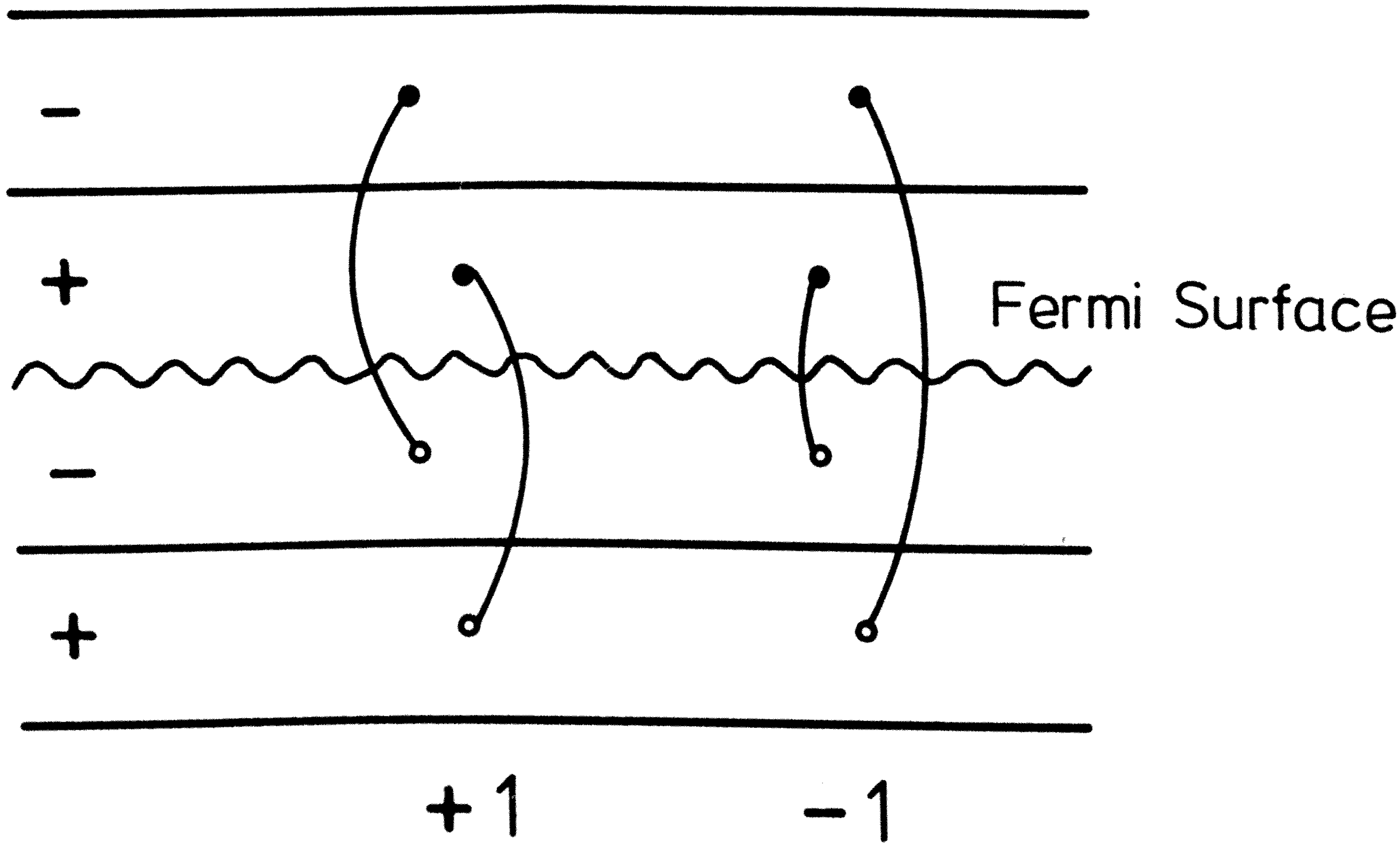

Parity of the shell. Parity of the core-excited state

Figure 7

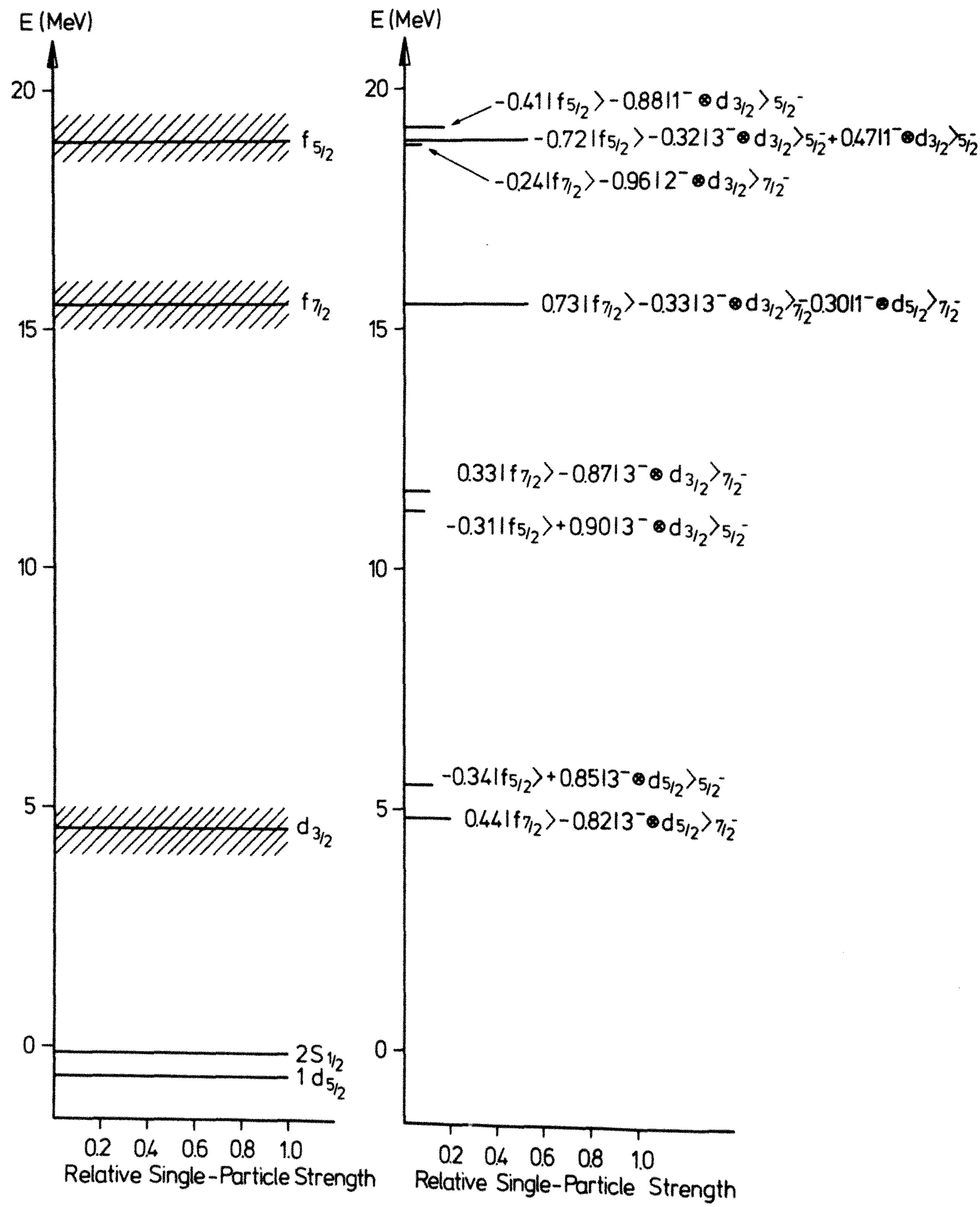

E (MeV)
20
15
10
5
0
$f_{5/2}$
$f_{7/2}$
$d_{3/2}$
$2S_{1/2}$
$1d_{5/2}$
0.2 0.4 0.6 0.8 1.0
Relative Single-Particle Strength
E (MeV)
$-0.41|f_{5/2}\rangle - 0.88|1^- \otimes d_{3/2}\rangle_{5/2^-}$
$-0.72|f_{5/2}\rangle - 0.32|3^- \otimes d_{3/2}\rangle_{5/2^-} + 0.47|1^- \otimes d_{3/2}\rangle_{5/2^-}$
$-0.24|f_{7/2}\rangle - 0.96|2^- \otimes d_{3/2}\rangle_{7/2^-}$
$0.73|f_{7/2}\rangle - 0.33|3^- \otimes d_{3/2}\rangle_{7/2^-} 0.30|1^- \otimes d_{5/2}\rangle_{7/2^-}$
$0.33|f_{7/2}\rangle - 0.87|3^- \otimes d_{3/2}\rangle_{7/2^-}$
$-0.31|f_{5/2}\rangle + 0.90|3^- \otimes d_{3/2}\rangle_{5/2^-}$
$-0.34|f_{5/2}\rangle + 0.85|3^- \otimes d_{5/2}\rangle_{5/2^-}$
$0.44|f_{7/2}\rangle - 0.82|3^- \otimes d_{5/2}\rangle_{7/2^-}$
0.2 0.4 0.6 0.8 1.0
Relative Single-Particle Strength

Figure 8

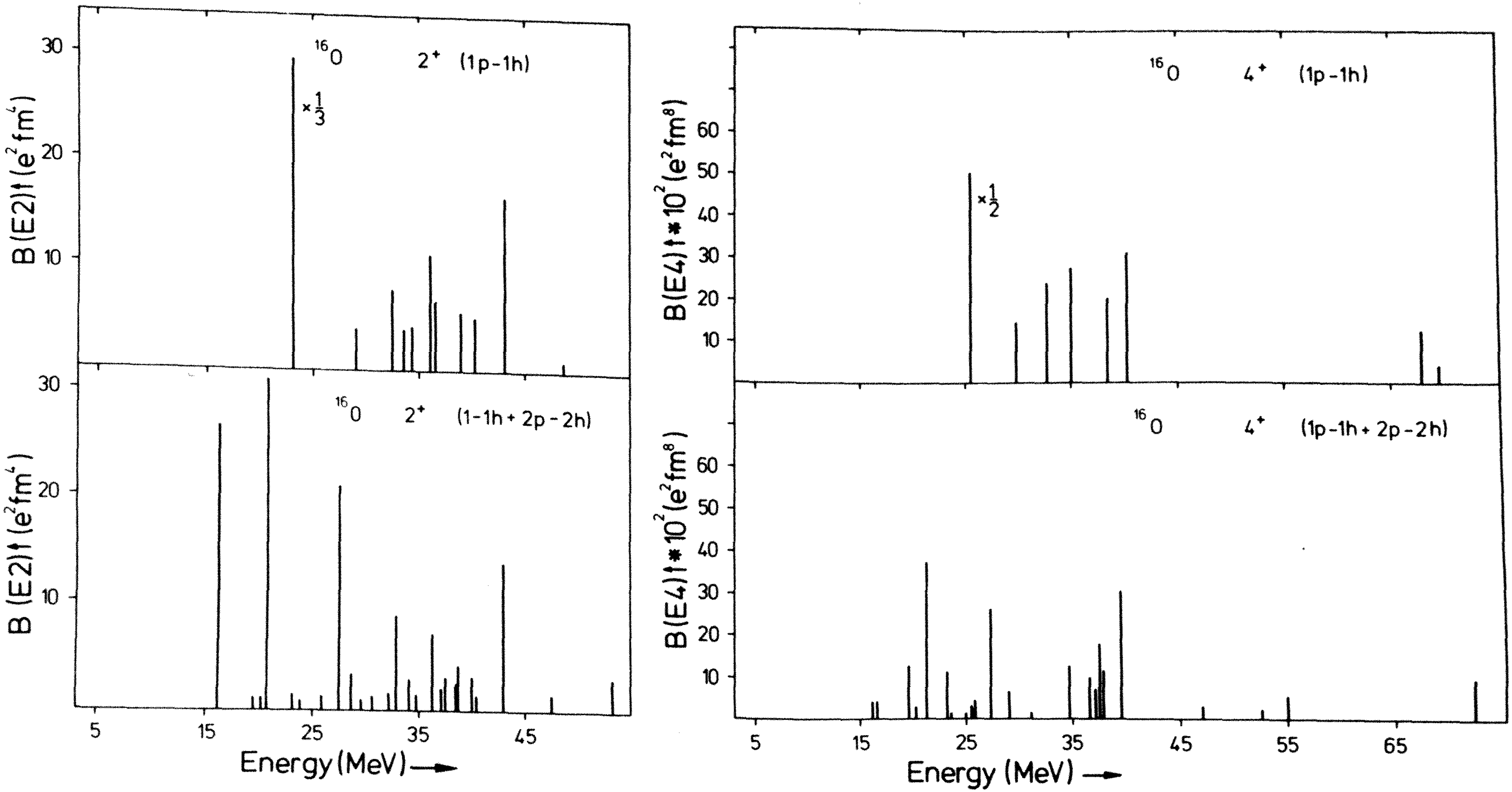

^{16}O 2^+ (1p-1h)
×1/3
B(E2)↑(e²fm⁴)
^{16}O 2^+ (1-1h + 2p-2h)
B(E2)↑(e²fm⁴)
Energy (MeV) →
^{16}O 4^+ (1p-1h)
×1/2
B(E4)↑*10²(e²fm⁸)
^{16}O 4^+ (1p-1h + 2p-2h)
B(E4)↑*10²(e²fm⁸)
Energy (MeV) →

Figure 9

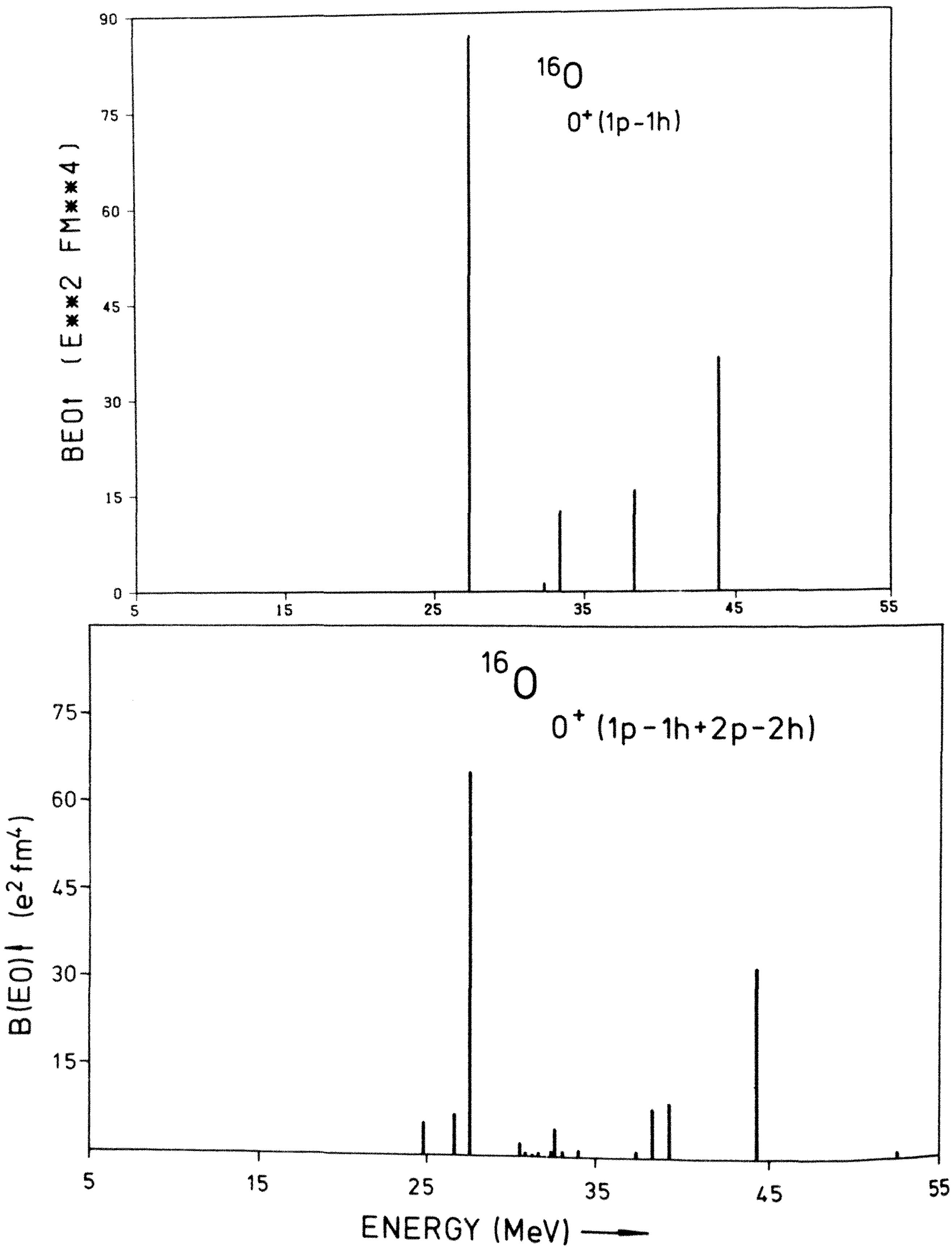

90
75
60
45
30
15
0
BEO↑ (E**2 FM**4)
^{16}O
0$^+$(1p-1h)
5
15
25
35
45
55
75
60
45
30
15
B(EO)↑ (e^2 fm^4)
^{16}O
0$^+$ (1p-1h+2p-2h)
5
15
25
35
45
55
ENERGY (MeV) ⟶

Figure 10

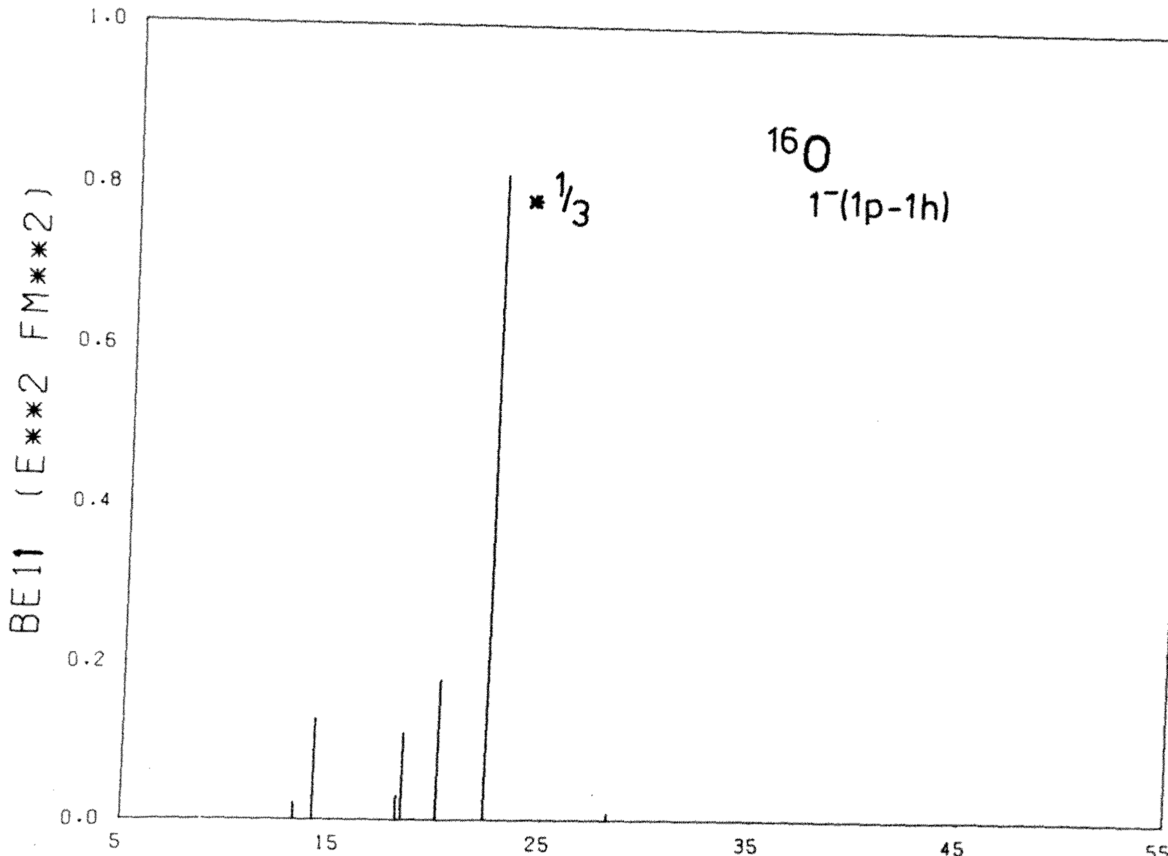

1.0
0.8
0.6
0.4
0.2
0.0
BE1↑ (E**2 FM**2)
^{16}O
1⁻(1p-1h)
*1/3
5
15
25
35
45
55

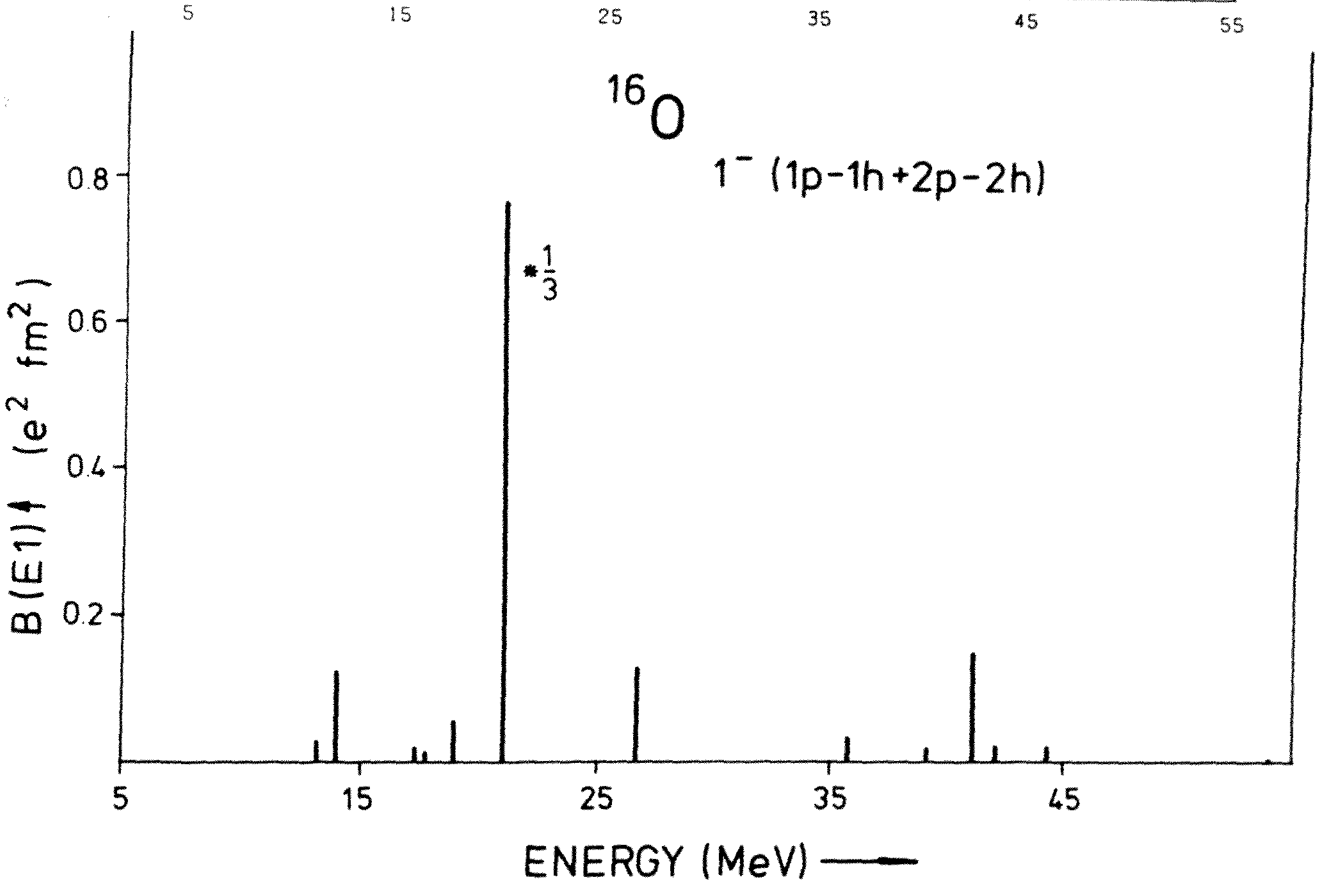

^{16}O
1⁻ (1p-1h+2p-2h)
*1/3
0.8
0.6
0.4
0.2
B(E1)↑ (e^2 fm^2)
5
15
25
35
45
ENERGY (MeV) ⟶

Figure 11

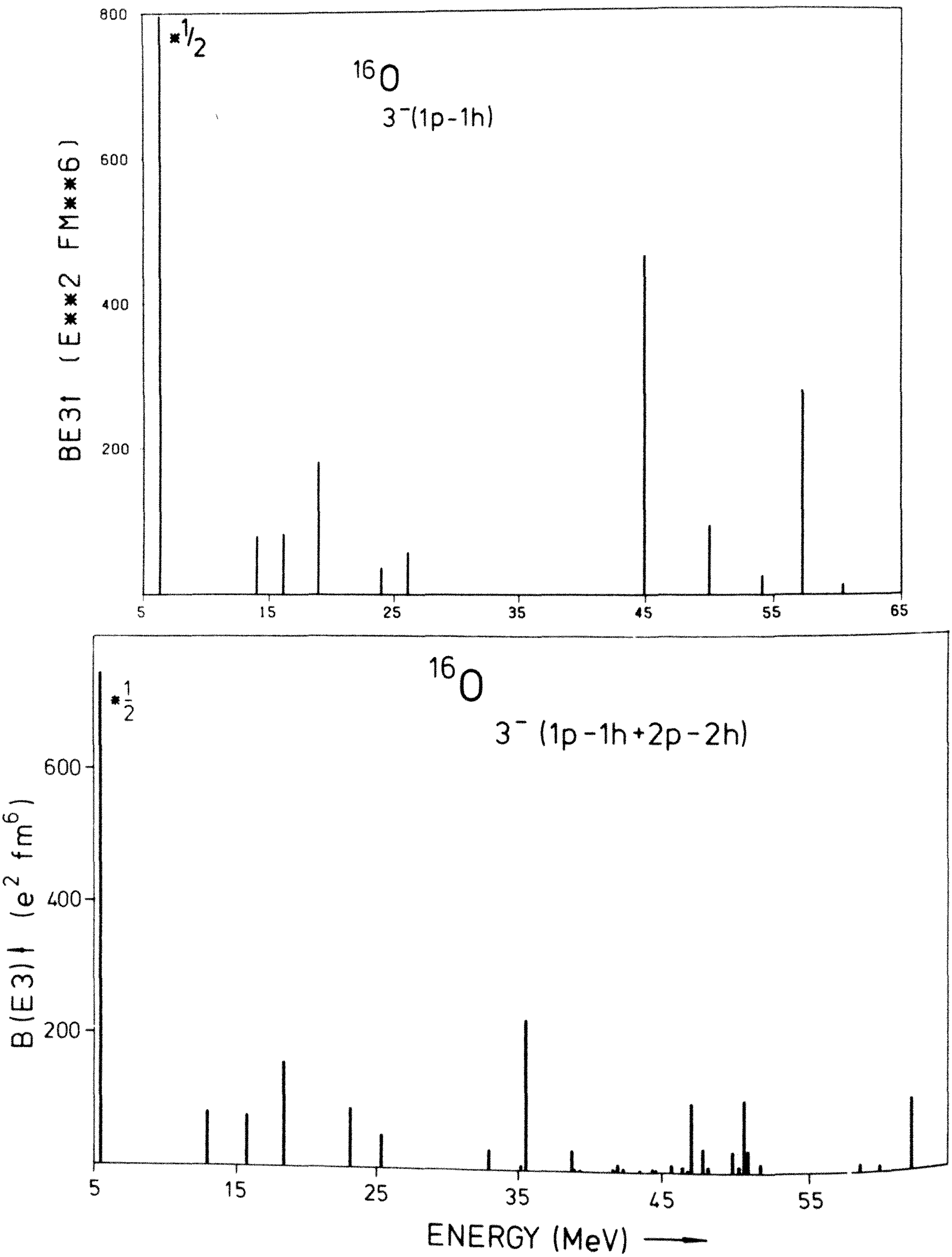

800
600
400
200
BE3↑ (E**2 FM**6)
*1/2
16O
3⁻(1p-1h)
5
15
25
35
45
55
65
16O
3⁻ (1p-1h+2p-2h)
*1/2
600
400
200
B(E3)↑ (e2 fm6)
5
15
25
35
45
55
ENERGY (MeV)

Figure 12

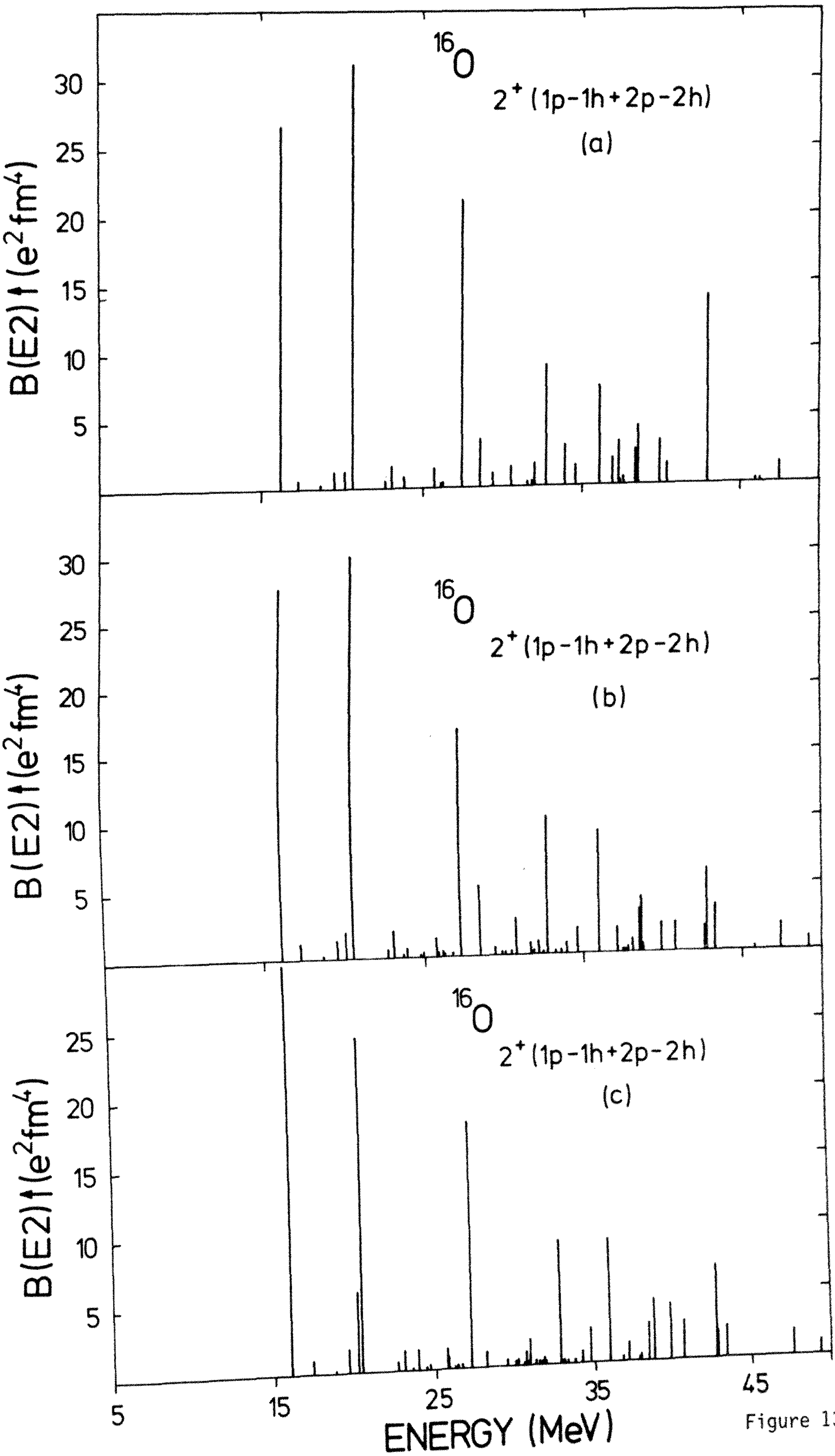

Figure 13

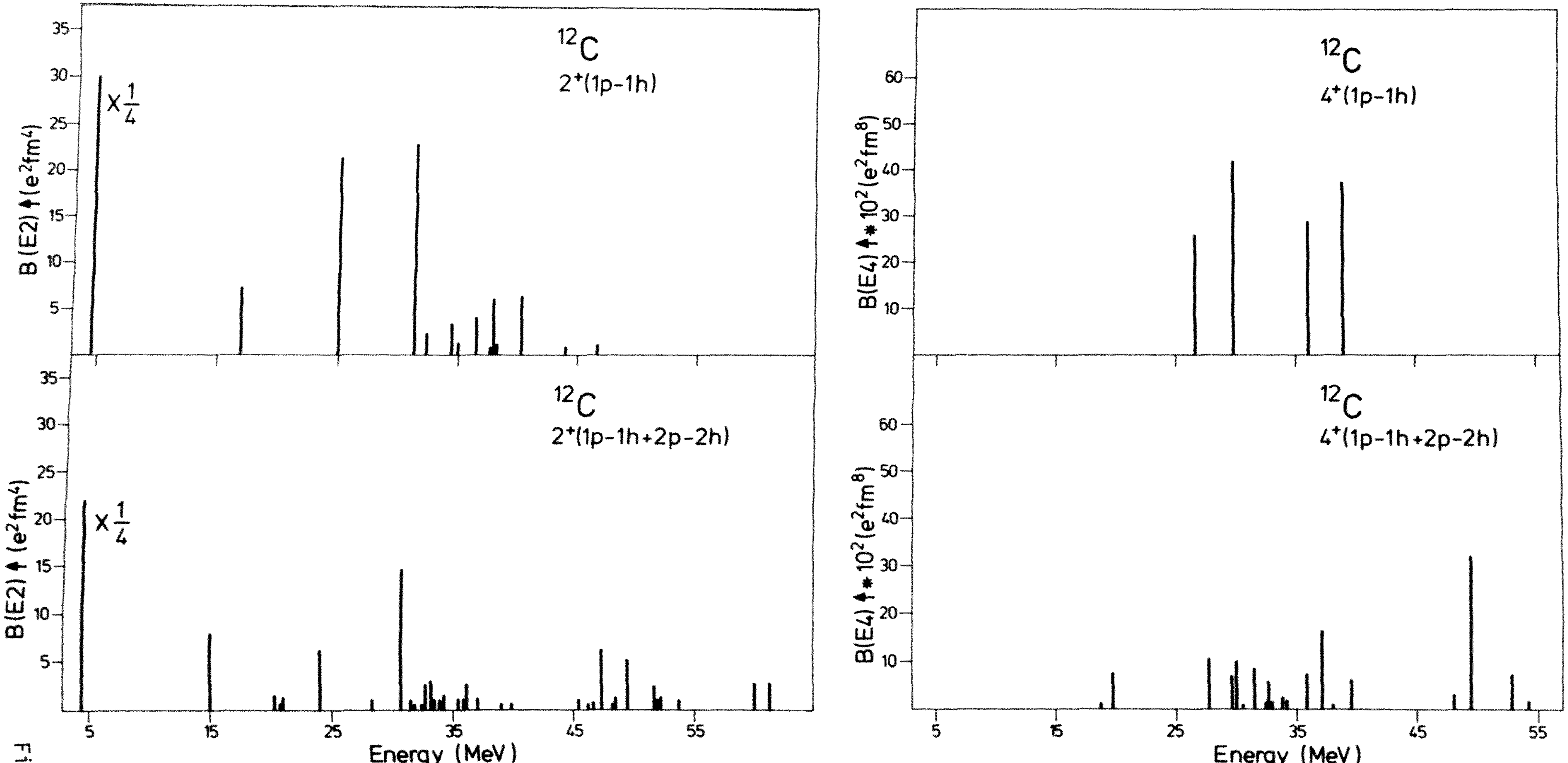

^{12}C
2^+(1p-1h)
X $\frac{1}{4}$
B(E2)↑(e^{2}fm^4)
^{12}C
2^+(1p-1h+2p-2h)
X $\frac{1}{4}$
B(E2)↑(e^{2}fm^4)
Energy (MeV)
^{12}C
4^+(1p-1h)
B(E4)↑*10^2(e^{2}fm^8)
^{12}C
4^+(1p-1h+2p-2h)
B(E4)↑*10^2(e^{2}fm^8)
Energy (MeV)

Figure 14

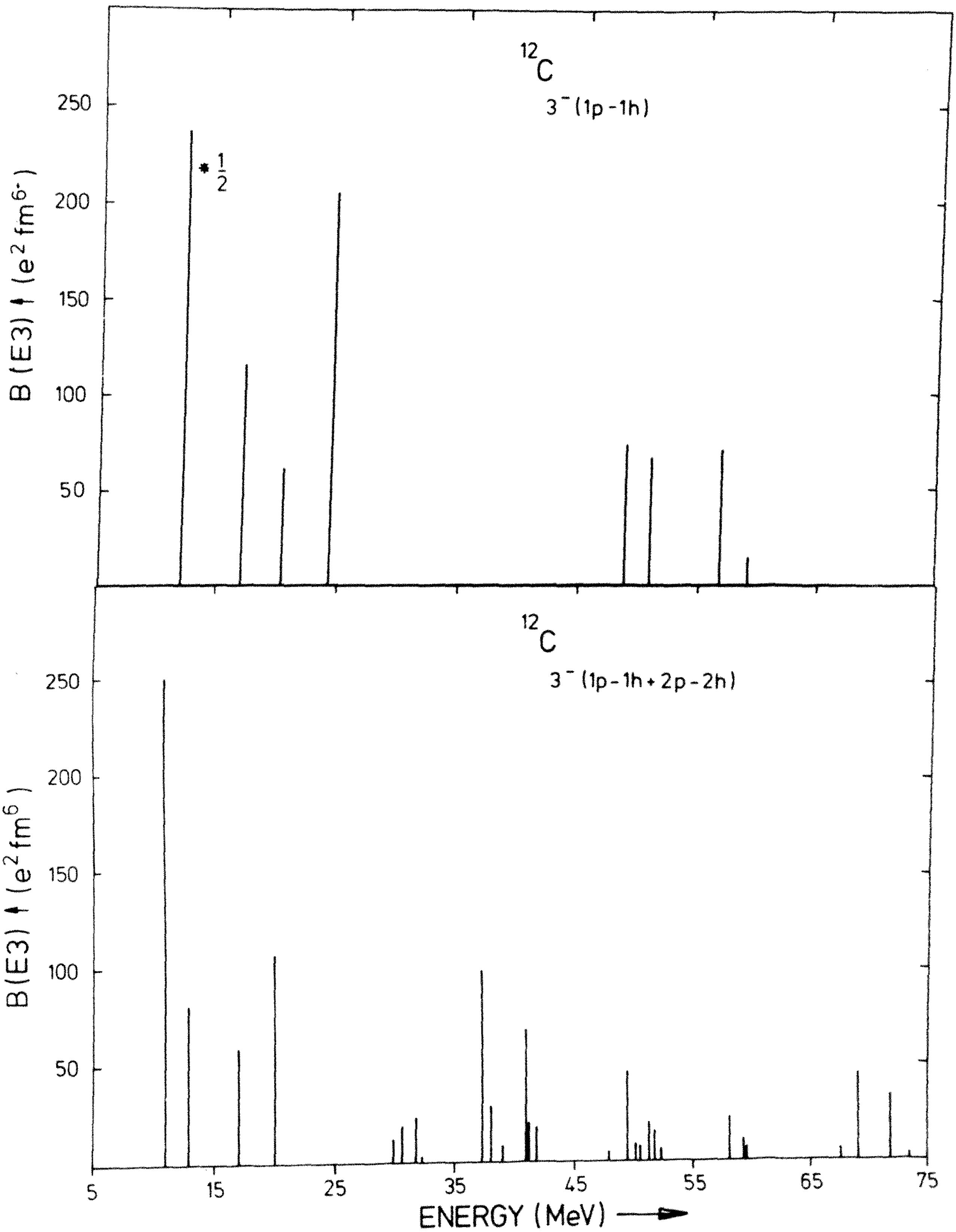

^{12}C
3^-(1p-1h)
$*\frac{1}{2}$
B (E3) ↑ ($e^2 fm^6$)
250
200
150
100
50
^{12}C
3^-(1p-1h+2p-2h)
B(E3) ↑ ($e^2 fm^6$)
250
200
150
100
50
5
15
25
35
45
55
65
75
ENERGY (MeV)

Figure 15

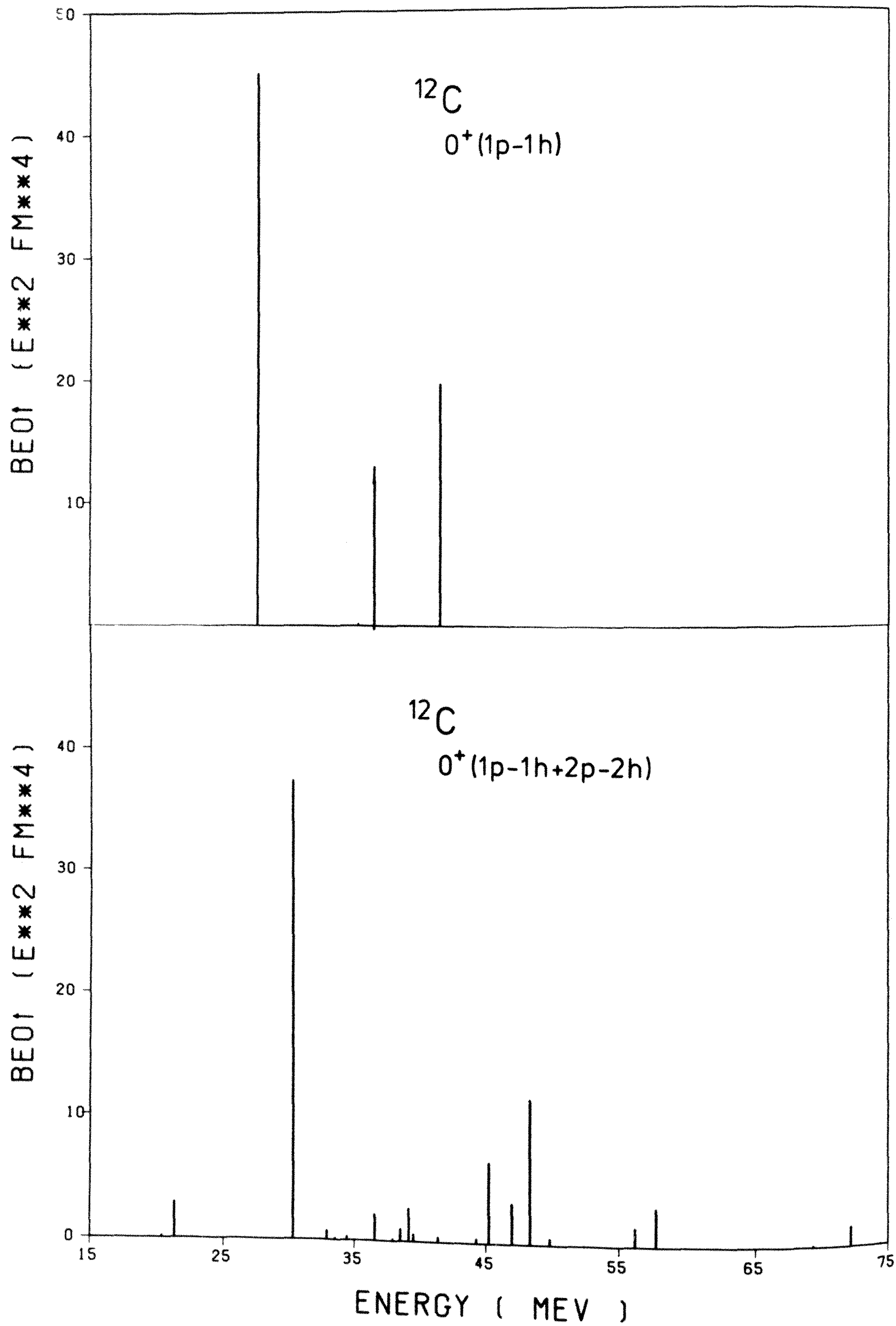

50
40
30
20
10
BE0↑ (E**2 FM**4)
^{12}C
0^{+}(1p-1h)
40
30
20
10
0
BE0↑ (E**2 FM**4)
^{12}C
0^{+}(1p-1h+2p-2h)
15
25
35
45
55
65
75
ENERGY (MEV)

Figure 16

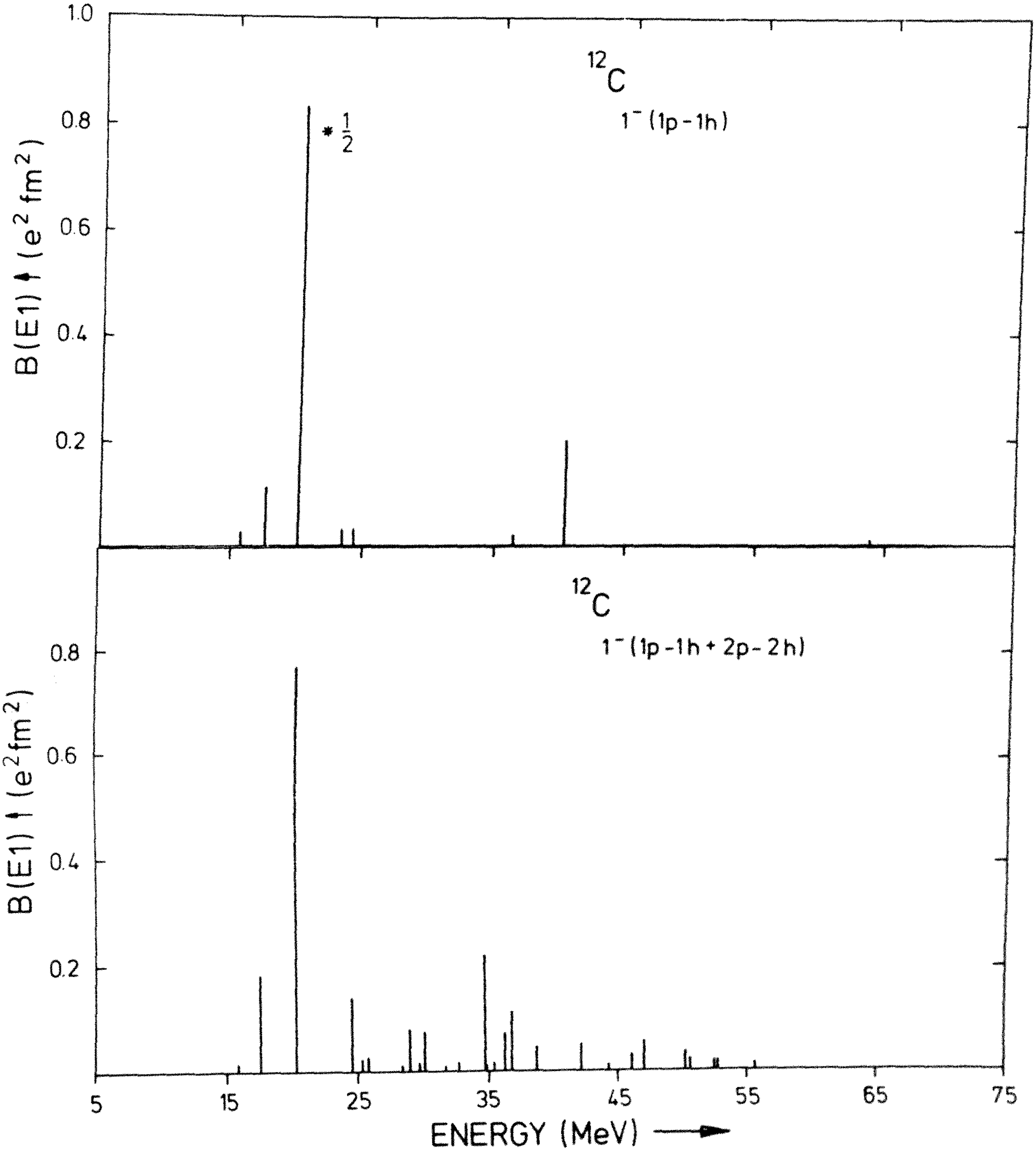
1.0
0.8
0.6
0.4
0.2
B(E1) ↑ (e² fm²)
¹²C
1⁻ (1p-1h)
* 1/2
¹²C
1⁻ (1p-1h + 2p-2h)
5
15
25
35
45
55
65
75
ENERGY (MeV)

Figure 17

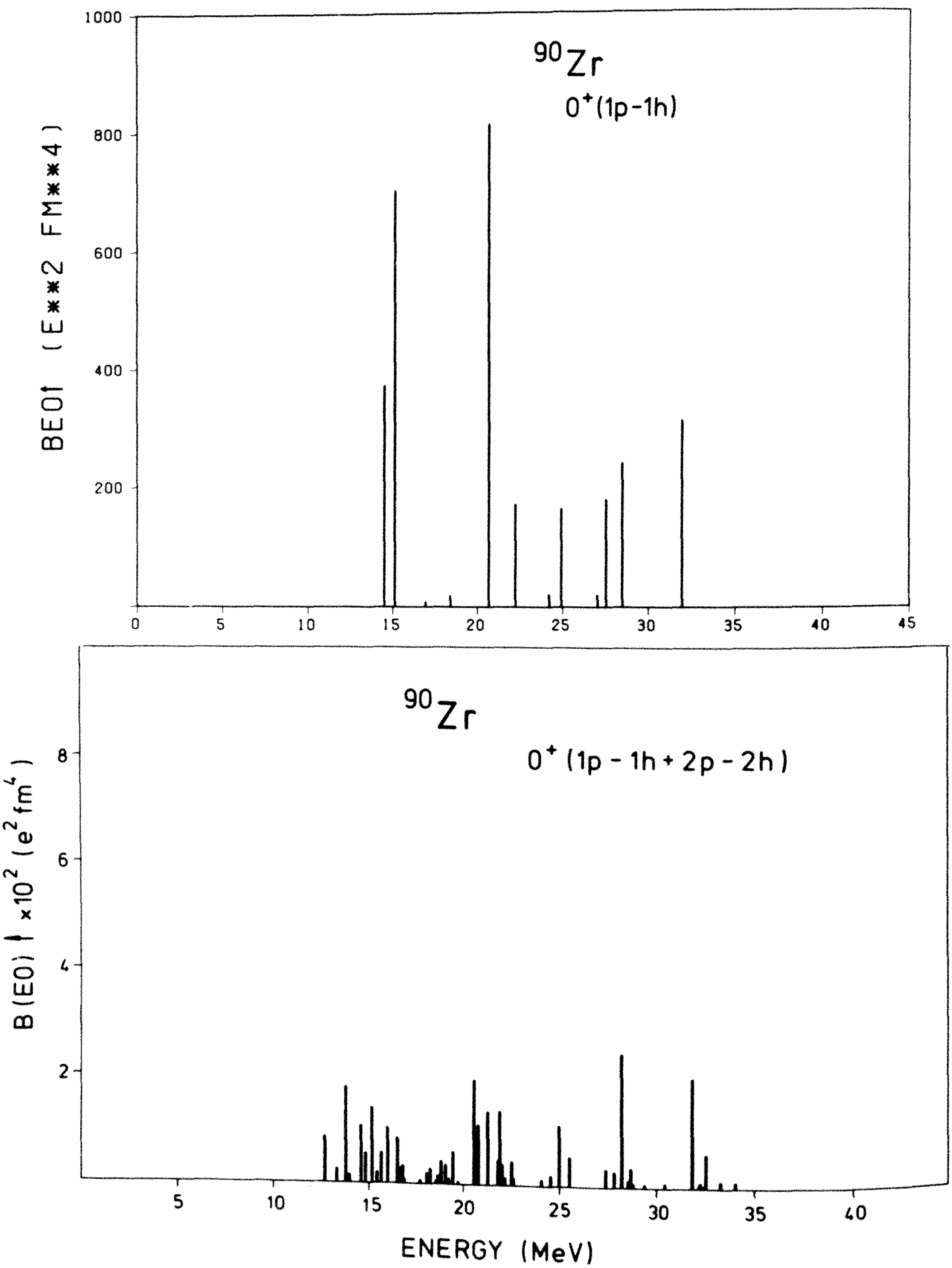

^{90}Zr
0^+(1p-1h)
BE0↑ (E**2 FM**4)
1000
800
600
400
200
0
5
10
15
20
25
30
35
40
45
^{90}Zr
0^+ (1p - 1h + 2p - 2h)
B(E0)↑ ×10^2 (e^{2}fm^4)
8
6
4
2
5
10
15
20
25
30
35
40
ENERGY (MeV)

Figure 18

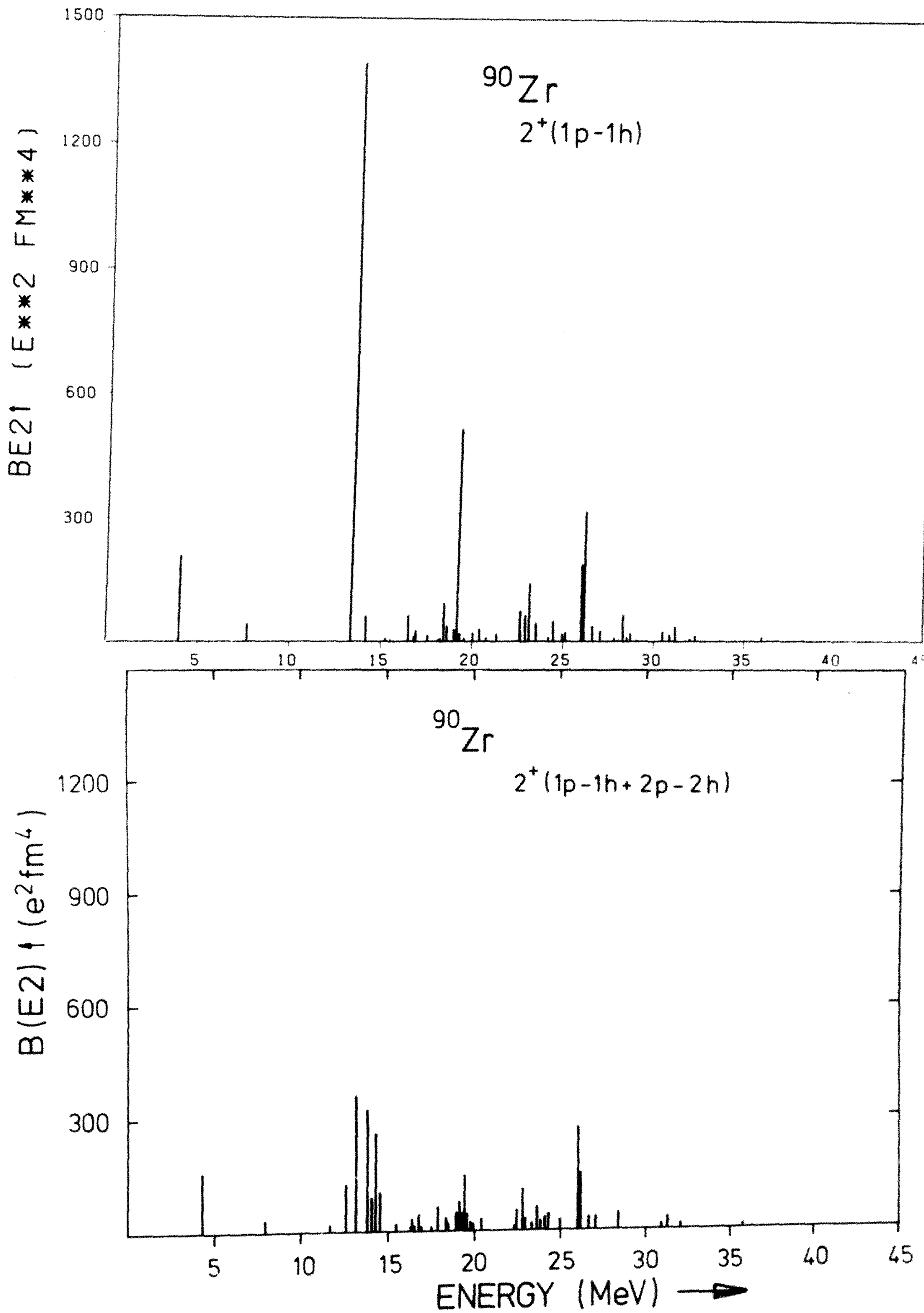

^{90}Zr
$2^+(1p-1h)$
BE2↑ (E**2 FM**4)
1500
1200
900
600
300
5
10
15
20
25
30
35
40
^{90}Zr
$2^+(1p-1h+2p-2h)$
B(E2)↑ (e^2fm^4)
1200
900
600
300
5
10
15
20
25
30
35
40
45
ENERGY (MeV)

Figure 19

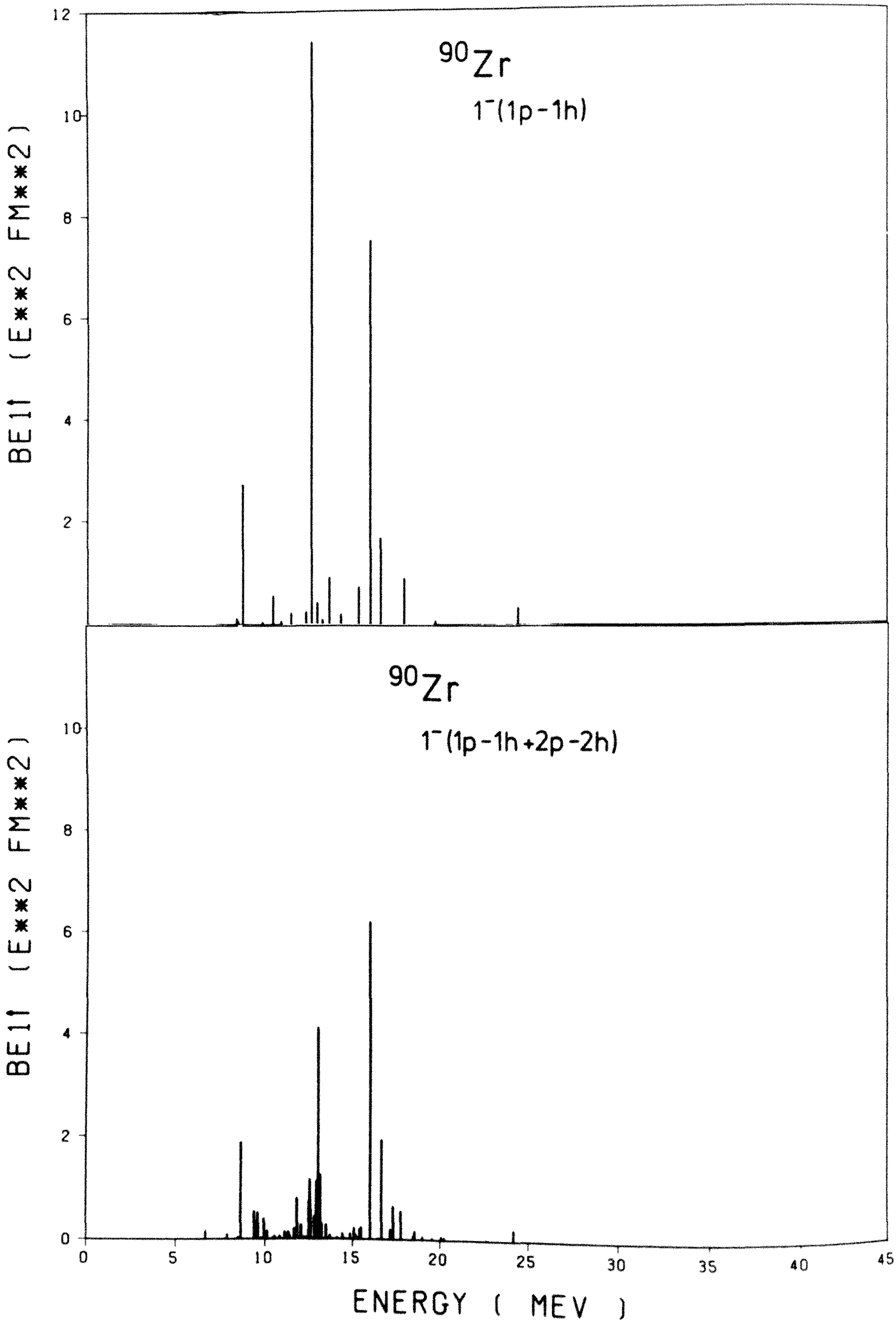

12
10
8
6
4
2
0
BE1↑ (E**2 FM**2)
^{90}Zr
1$^-$(1p-1h)
^{90}Zr
1$^-$(1p-1h+2p-2h)
0
5
10
15
20
25
30
35
40
45
ENERGY (MEV)

Figure 20

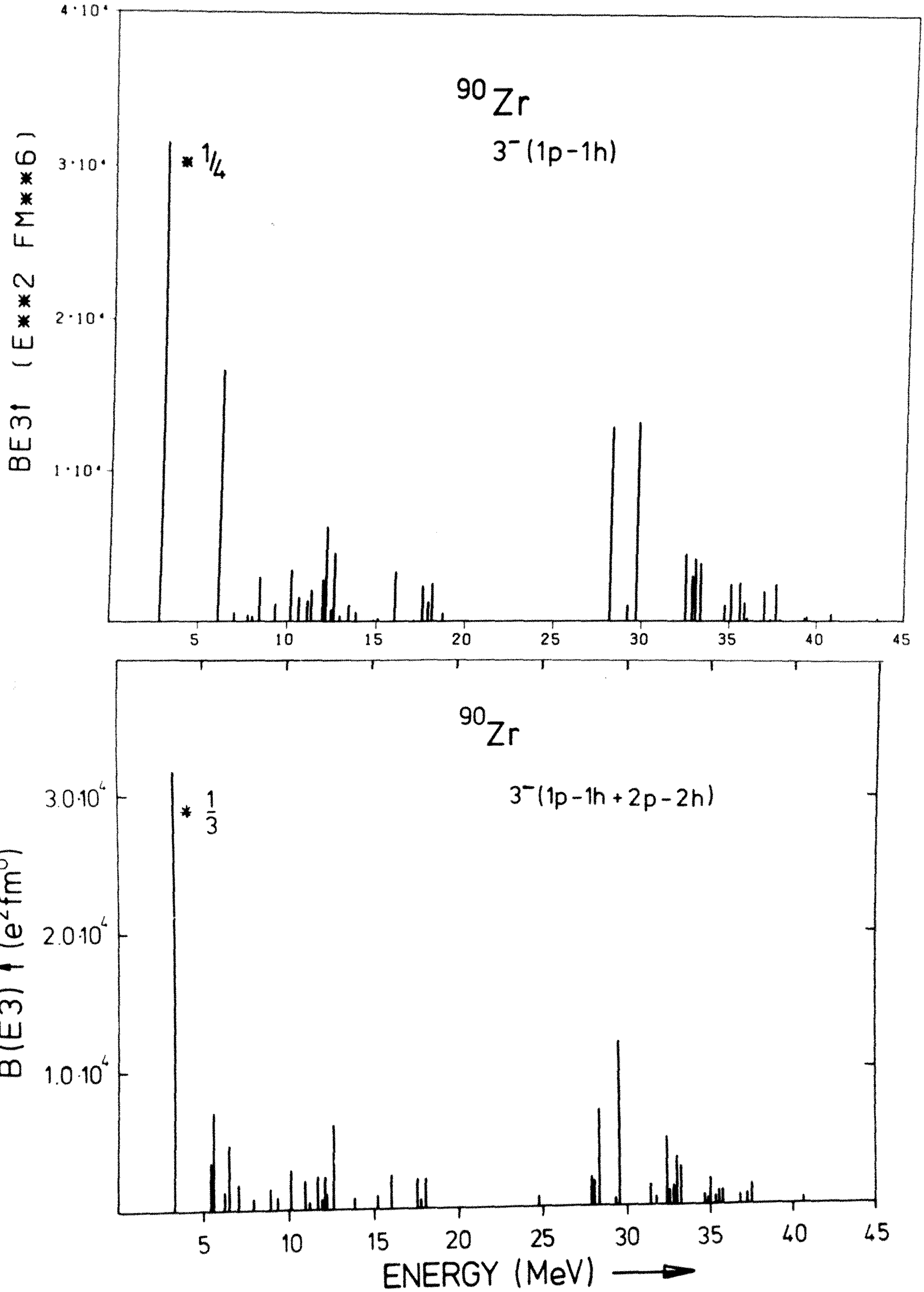

^{90}Zr
3⁻(1p-1h)
* 1/4
BE3↑ (E**2 FM**6)
4·10⁴
3·10⁴
2·10⁴
1·10⁴
5 10 15 20 25 30 35 40 45
^{90}Zr
3⁻(1p-1h+2p-2h)
* 1/3
B(E3)↑ (e²fm⁶)
3.0·10⁴
2.0·10⁴
1.0·10⁴
5 10 15 20 25 30 35 40 45
ENERGY (MeV)

Figure 21

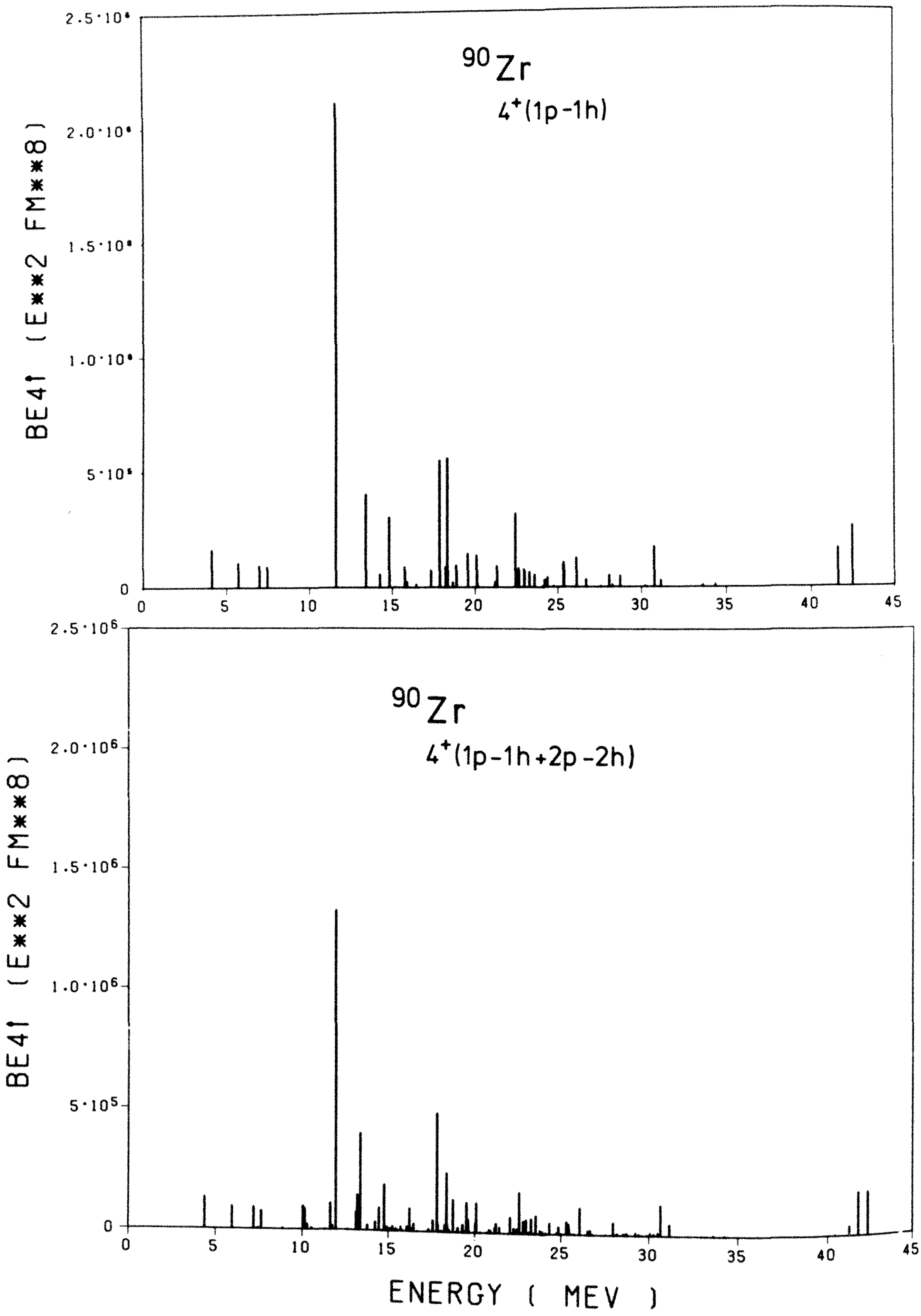

^{90}Zr
4^+(1p-1h)
^{90}Zr
4^+(1p-1h+2p-2h)
BE4↑ (E**2 FM**8)
2.5·10⁶
2.0·10⁶
1.5·10⁶
1.0·10⁶
5·10⁵
0
0 5 10 15 20 25 30 35 40 45
ENERGY (MEV)

Figure 22

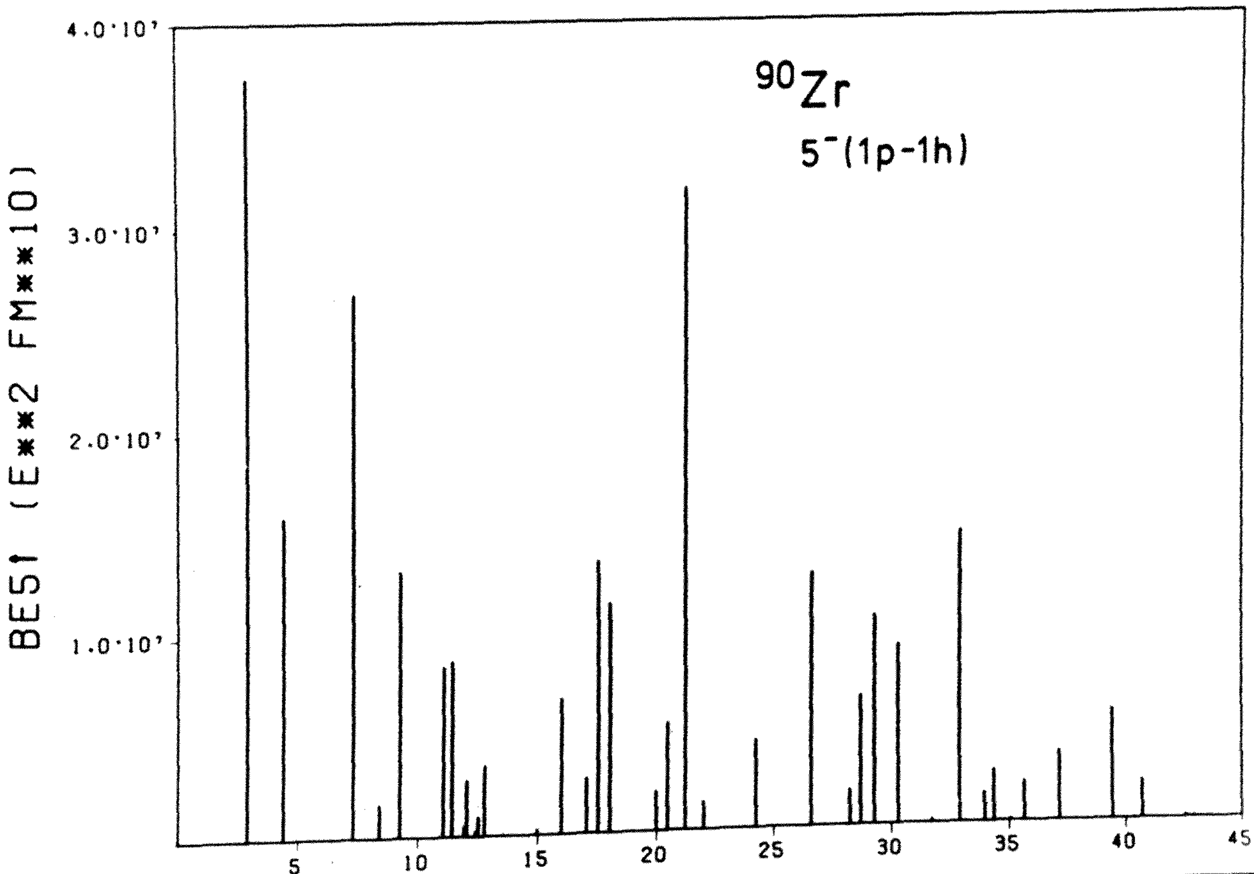

4.0·10⁷
3.0·10⁷
2.0·10⁷
1.0·10⁷
BE5↑ (E**2 FM**10)
^{90}Zr
5⁻(1p-1h)
5
10
15
20
25
30
35
40
45

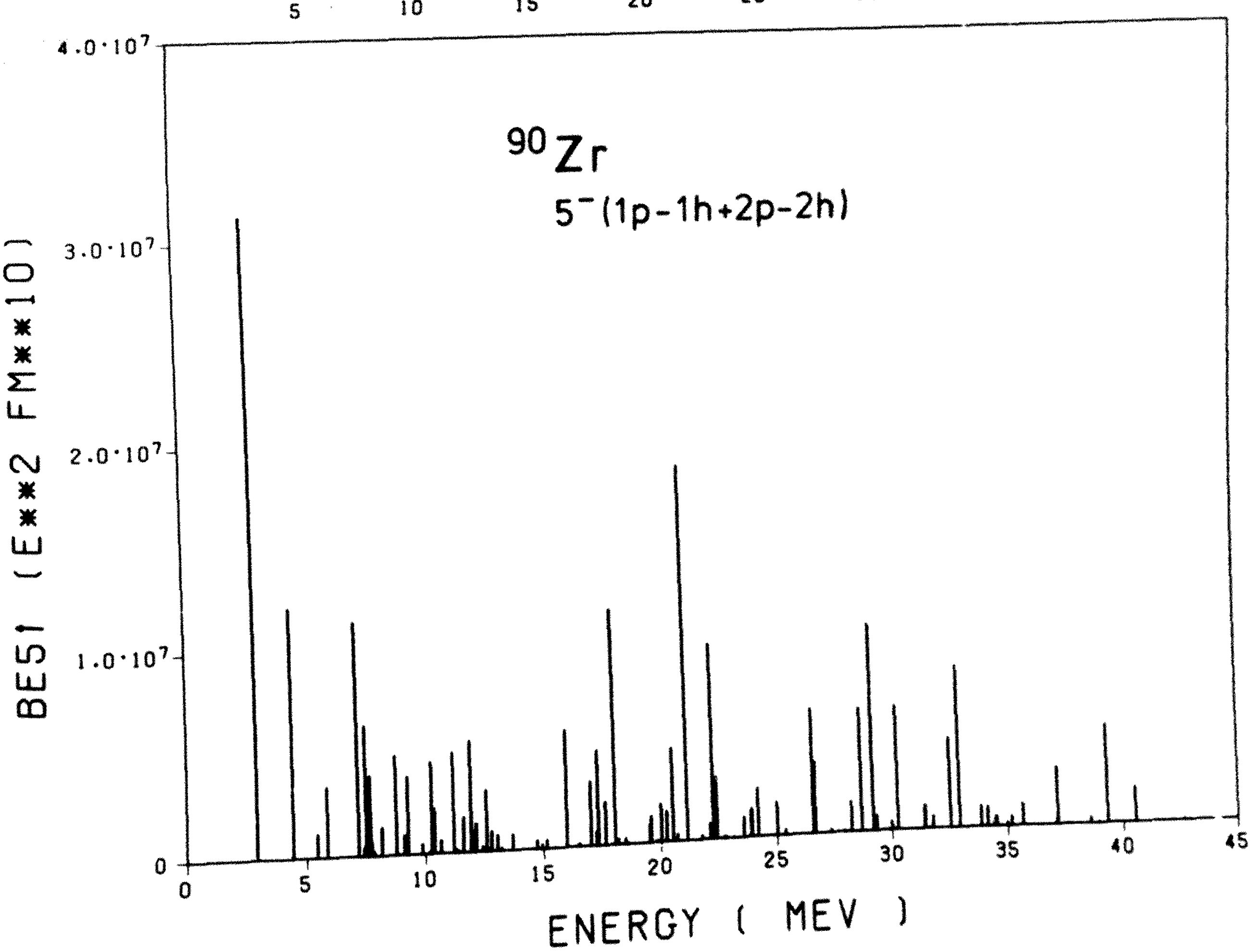

4.0·10⁷
3.0·10⁷
2.0·10⁷
1.0·10⁷
0
BE5↑ (E**2 FM**10)
^{90}Zr
5⁻(1p-1h+2p-2h)
0
5
10
15
20
25
30
35
40
45
ENERGY (MEV)

Figure 23

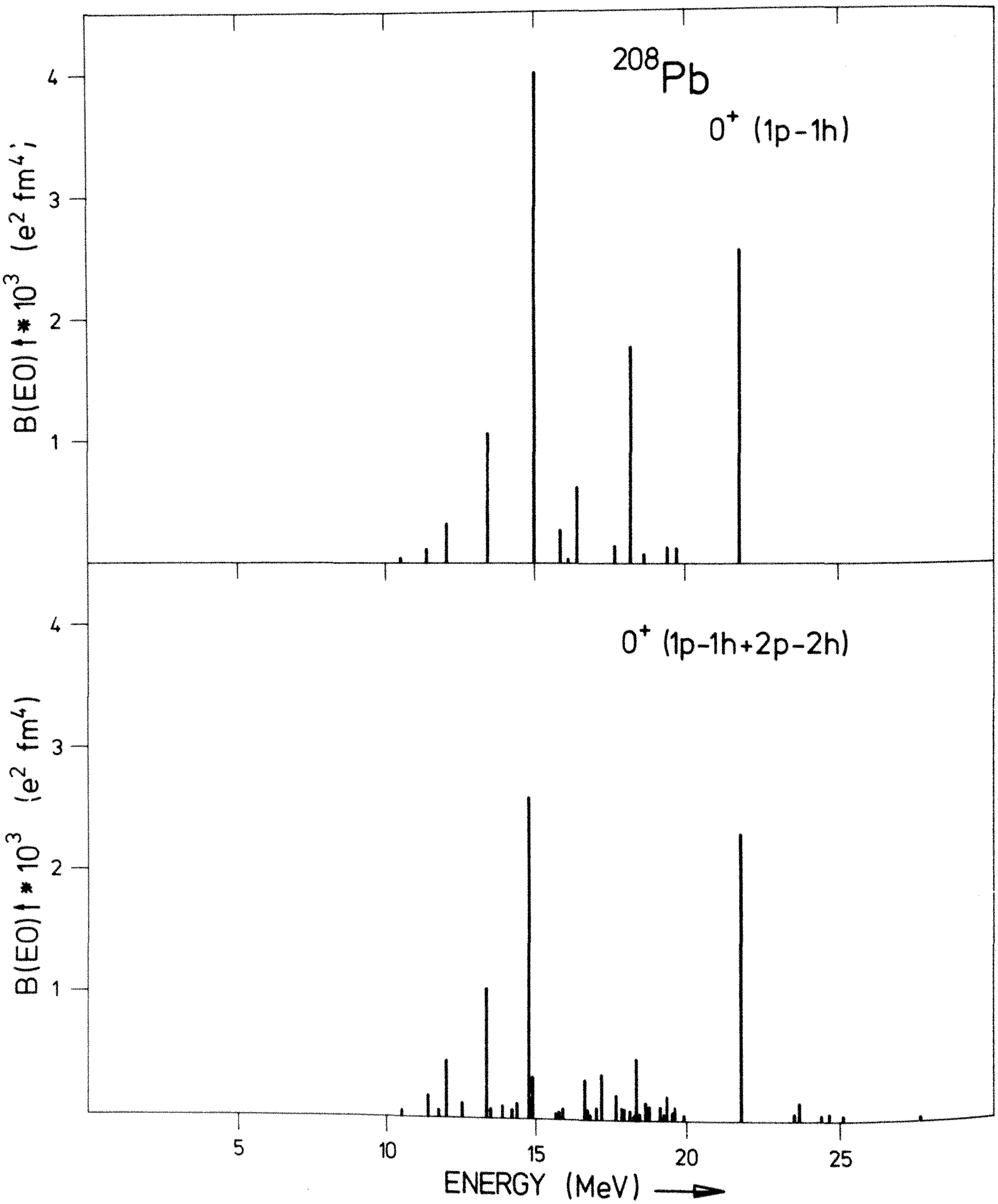

^{208}Pb
0^+ (1p-1h)
0^+ (1p-1h+2p-2h)
B(E0)↑ * 10^3 (e^2 fm^4)
B(E0)↑ * 10^3 (e^2 fm^4)
1
2
3
4
1
2
3
4
5
10
15
20
25
ENERGY (MeV)

Figure 24

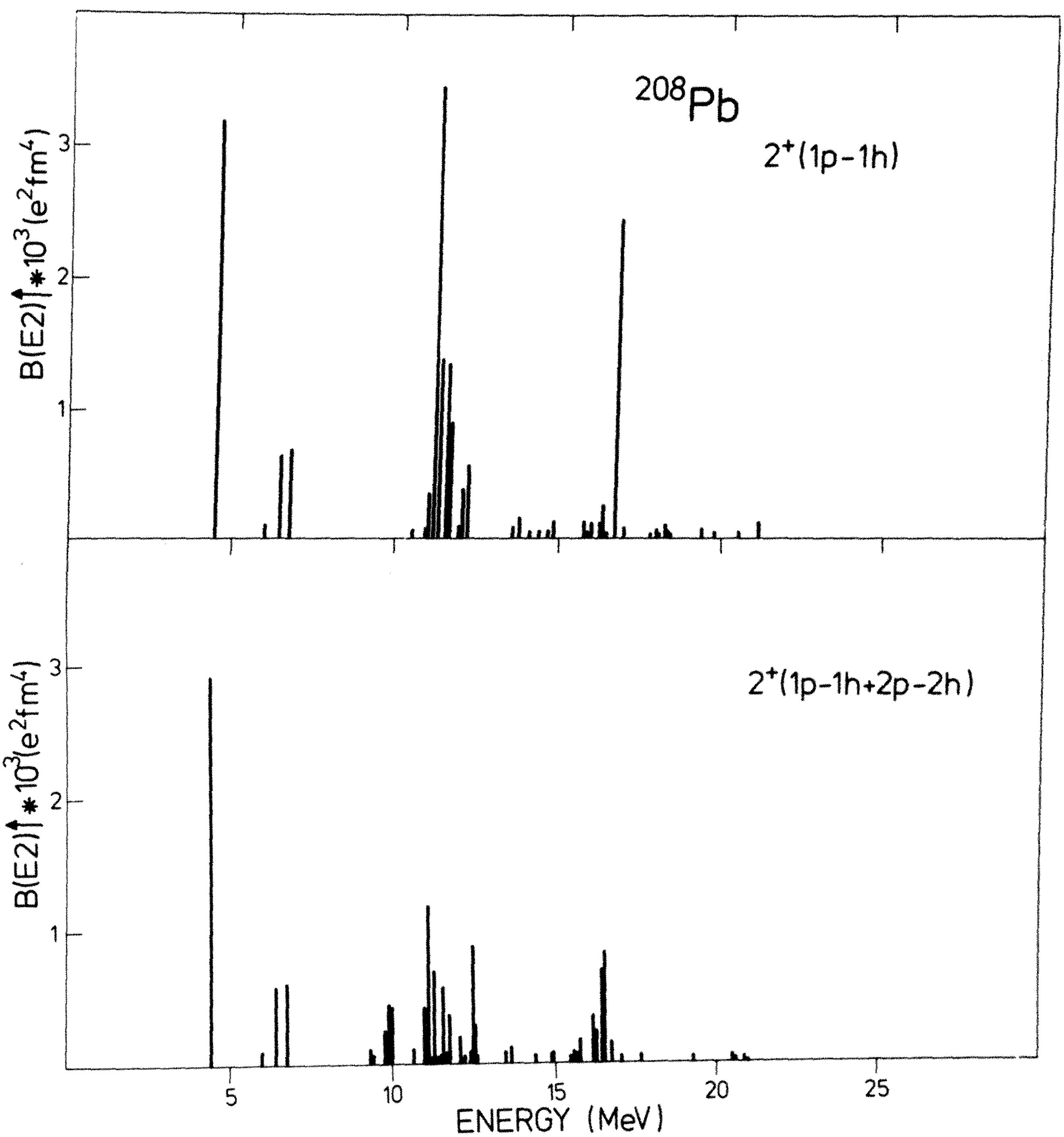

^{208}Pb
$2^+(1p-1h)$
$2^+(1p-1h+2p-2h)$
$B(E2)\uparrow * 10^3 (e^2 fm^4)$
$B(E2)\uparrow * 10^3 (e^2 fm^4)$
1
2
3
1
2
3
5
10
15
20
25
ENERGY (MeV)

Figure 25

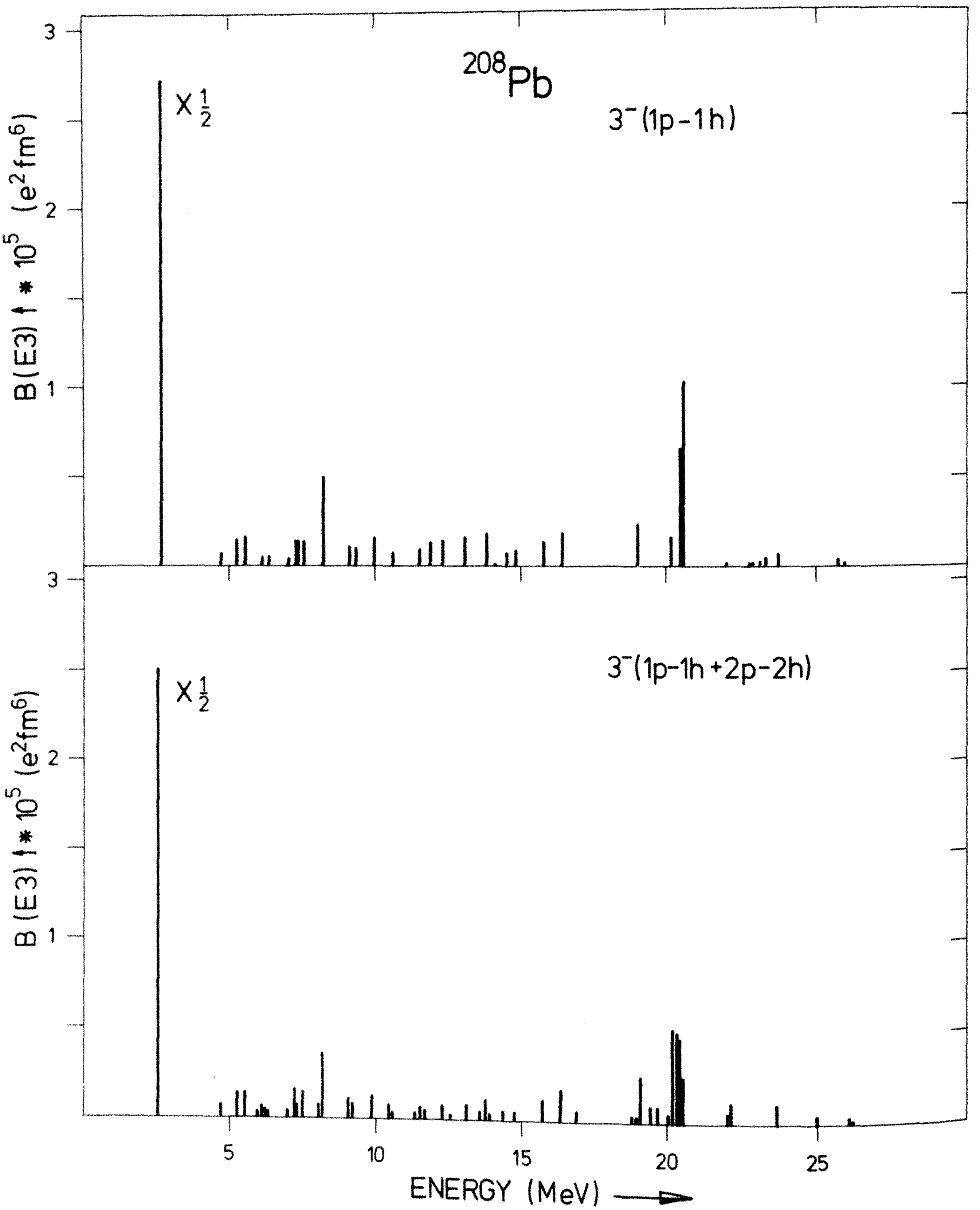

^{208}Pb
3^-(1p-1h)
3^-(1p-1h+2p-2h)
X $\frac{1}{2}$
X $\frac{1}{2}$
B(E3)↑ * 10^5 (e^2fm^6)
B(E3)↑ * 10^5 (e^2fm^6)
3
2
1
3
2
1
5
10
15
20
25
ENERGY (MeV)

Figure 26

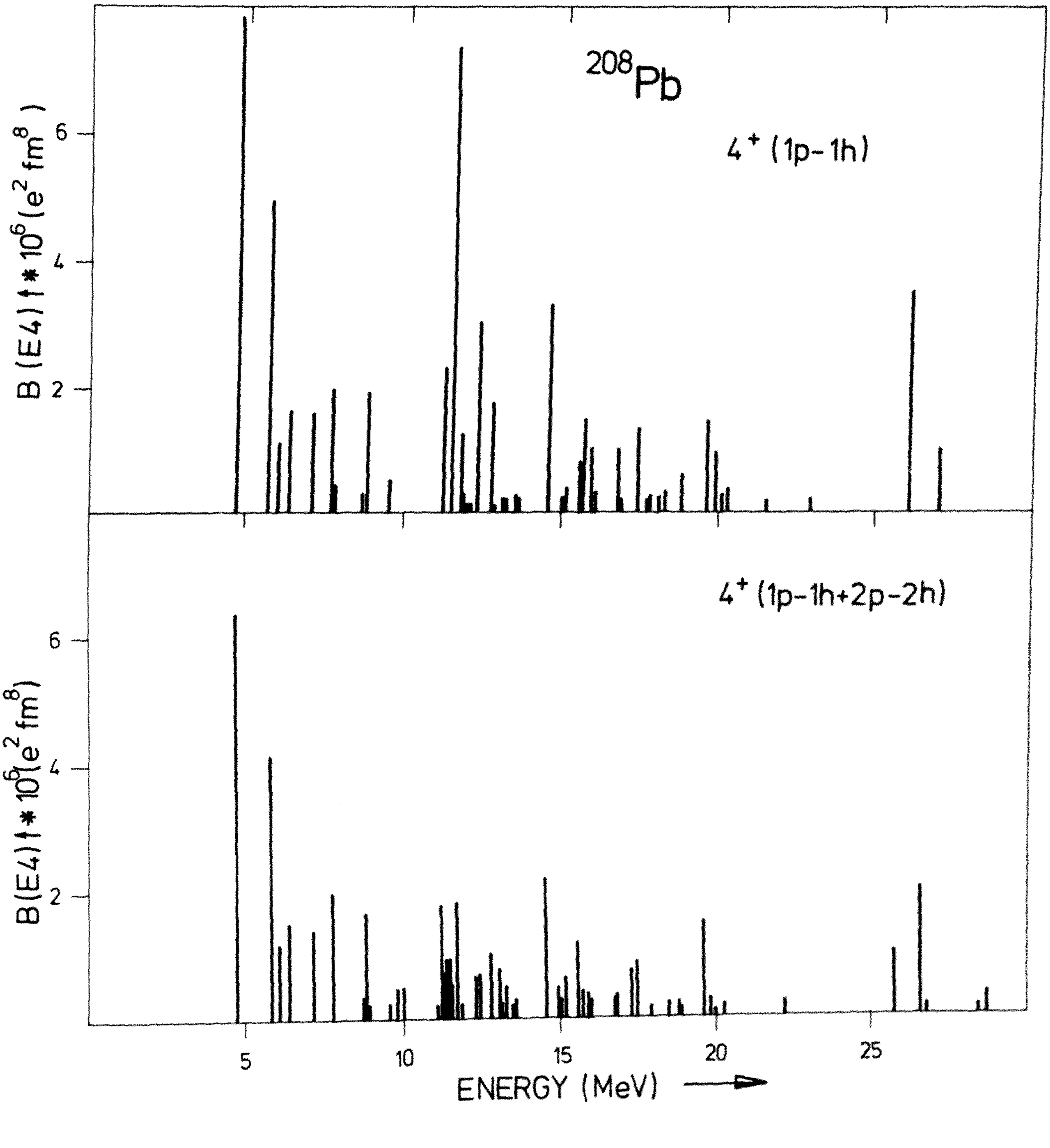

^{208}Pb
4^+ (1p-1h)
4^+ (1p-1h+2p-2h)
B (E4) ↑ * 10^6 (e^2 fm^8)
B (E4) ↑ * 10^6 (e^2 fm^8)
6
4
2
6
4
2
5
10
15
20
25
ENERGY (MeV)

Figure 27

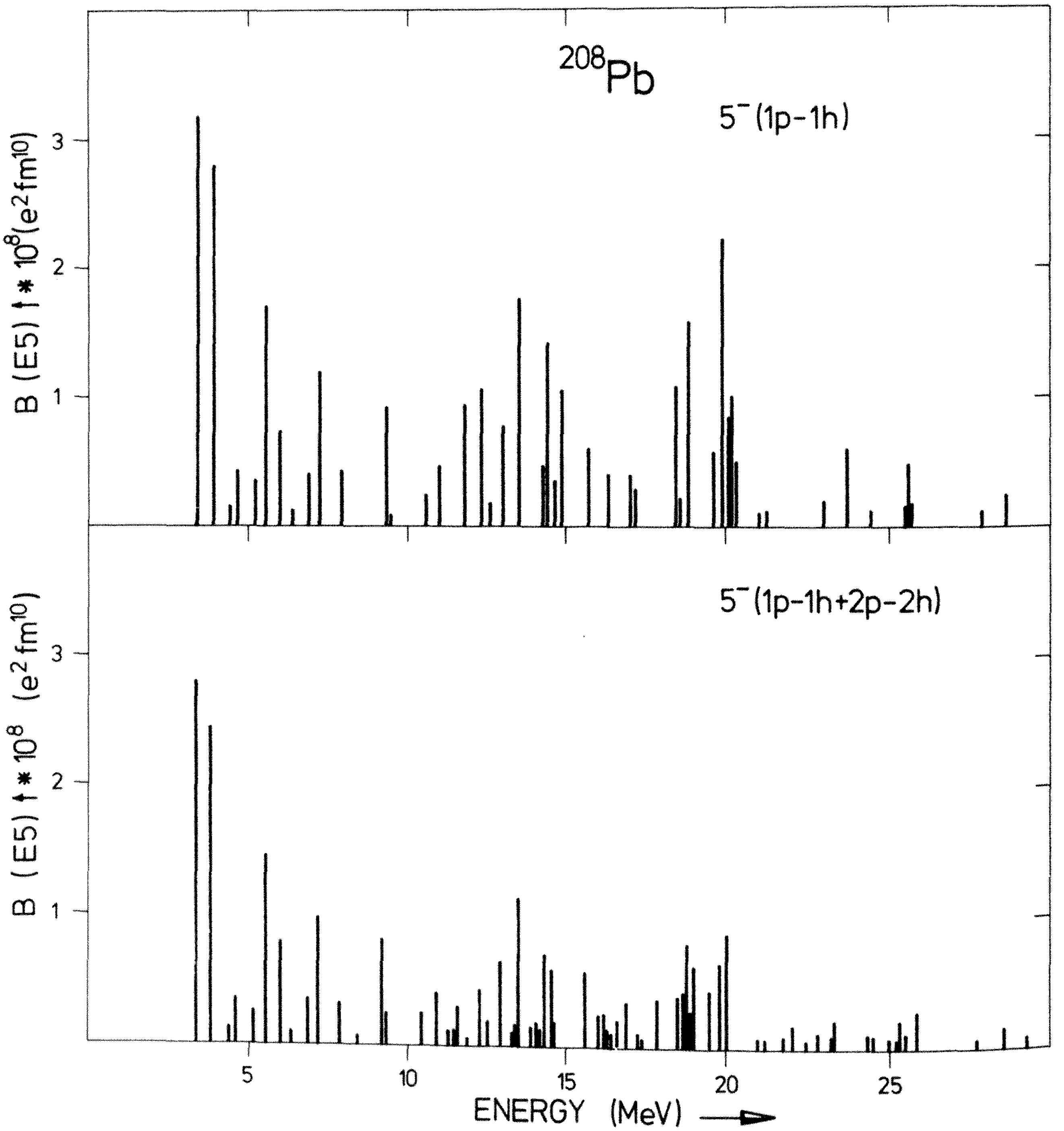
^{208}Pb
5^{-}(1p-1h)
B (E5) ↑ * 10^8($e^2 fm^{10}$)
3
2
1
5^{-}(1p-1h+2p-2h)
B (E5) ↑ * 10^8 ($e^2 fm^{10}$)
3
2
1
5
10
15
20
25
ENERGY (MeV)

Figure 28

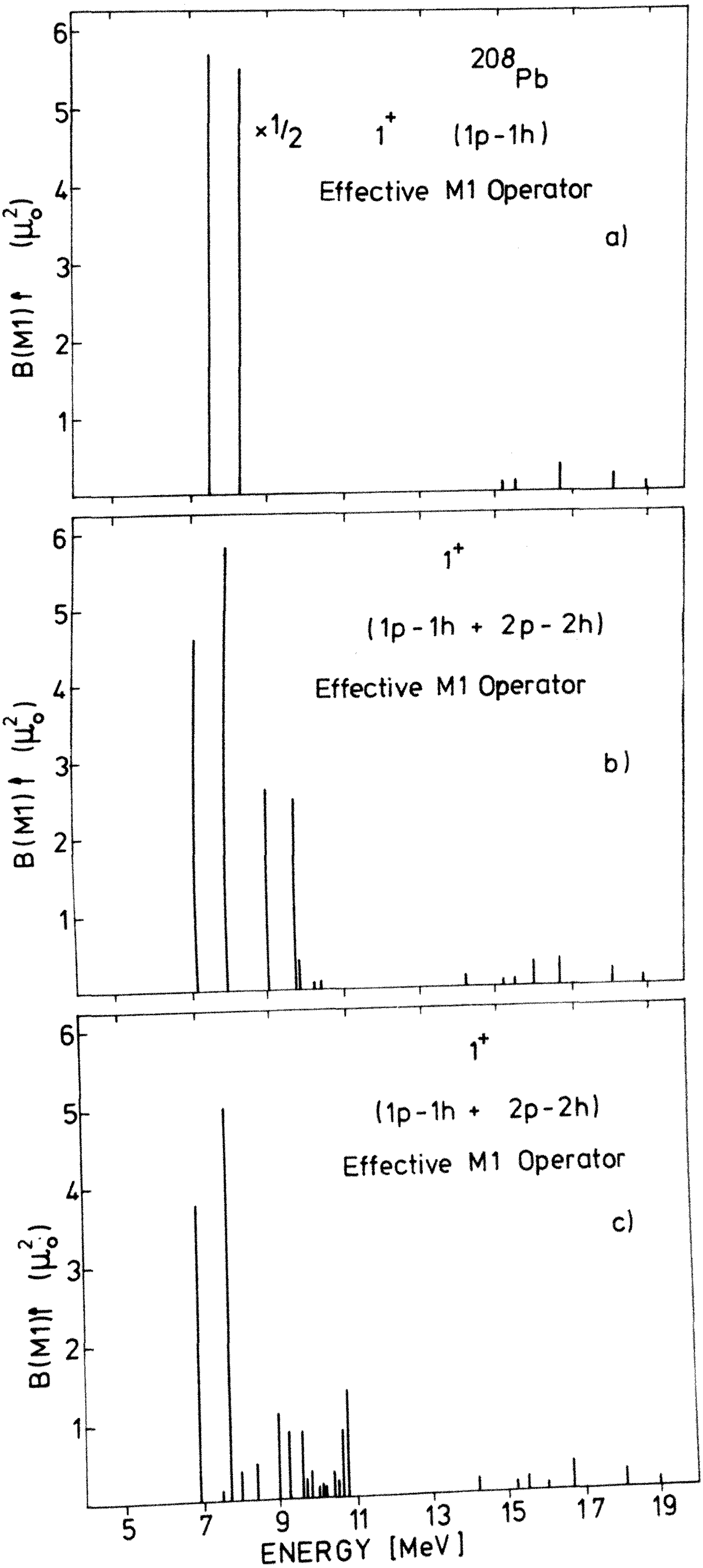

208Pb
×1/2
1+
(1p-1h)
Effective M1 Operator
a)
B(M1)↑ (μo2)
1+
(1p-1h + 2p-2h)
Effective M1 Operator
b)
B(M1)↑ (μo2)
1+
(1p-1h + 2p-2h)
Effective M1 Operator
c)
B(M1)↑ (μo2)
ENERGY [MeV]

Figure 29

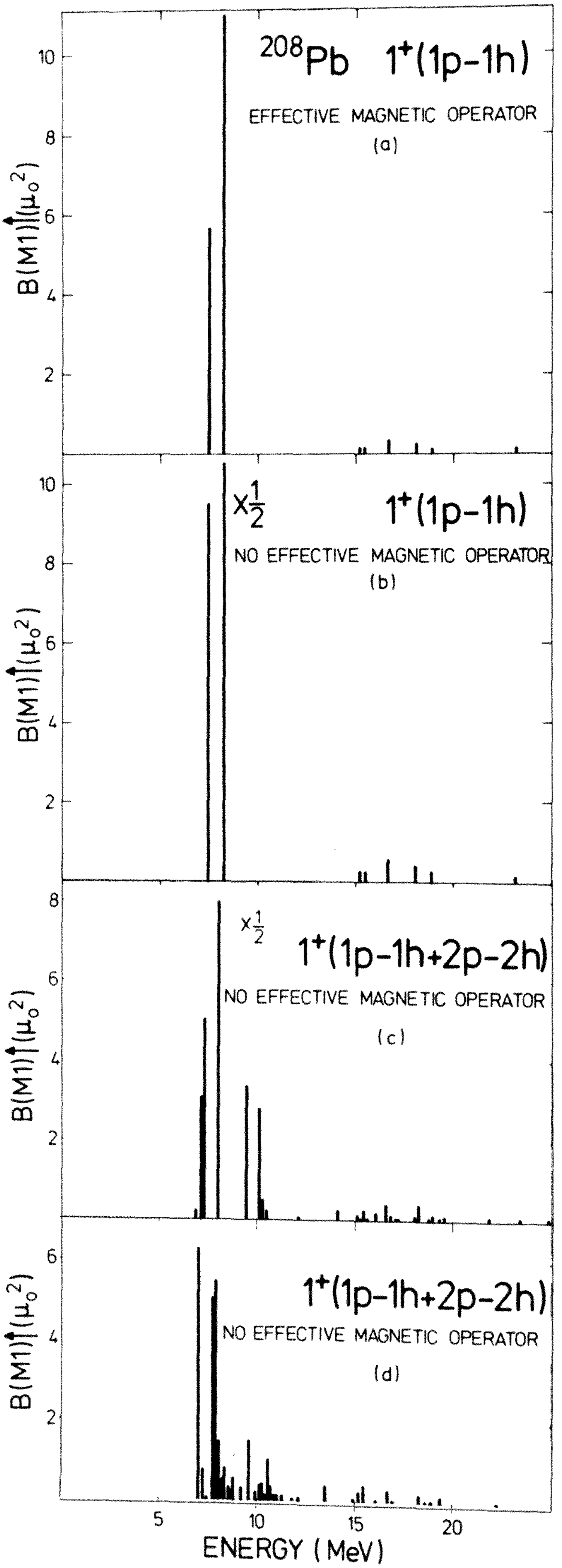

^{208}Pb 1$^+$(1p-1h)
EFFECTIVE MAGNETIC OPERATOR
(a)
X$\frac{1}{2}$
1$^+$(1p-1h)
NO EFFECTIVE MAGNETIC OPERATOR
(b)
x$\frac{1}{2}$
1$^+$(1p-1h+2p-2h)
NO EFFECTIVE MAGNETIC OPERATOR
(c)
1$^+$(1p-1h+2p-2h)
NO EFFECTIVE MAGNETIC OPERATOR
(d)
B(M1)↑(μ_o^2)
ENERGY (MeV)

Figure 30

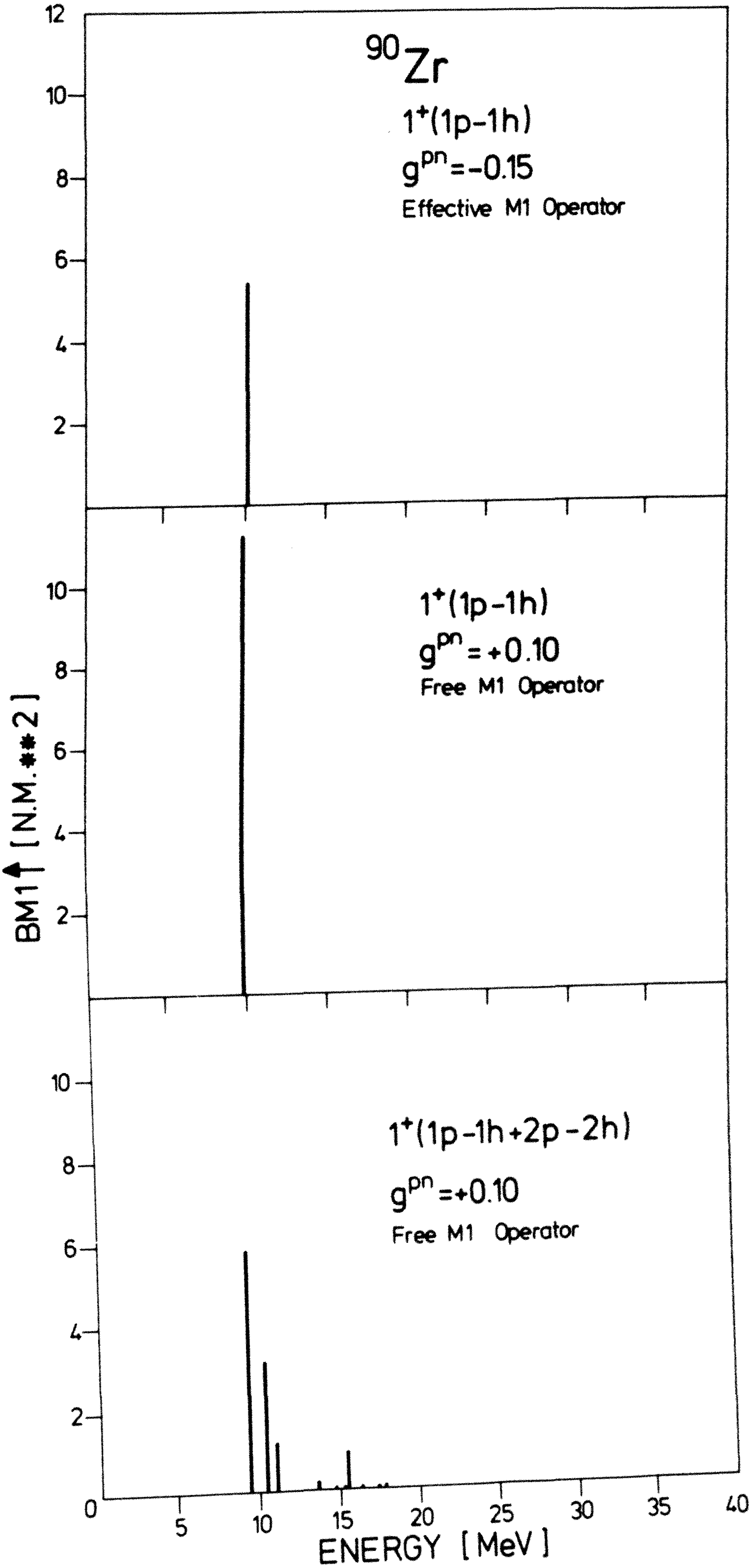

^{90}Zr
$1^+(1p-1h)$
$g^{pn}=-0.15$
Effective M1 Operator
$1^+(1p-1h)$
$g^{pn}=+0.10$
Free M1 Operator
$1^+(1p-1h+2p-2h)$
$g^{pn}=+0.10$
Free M1 Operator
BM1↑ [N.M.**2]
ENERGY [MeV]

Figure 32

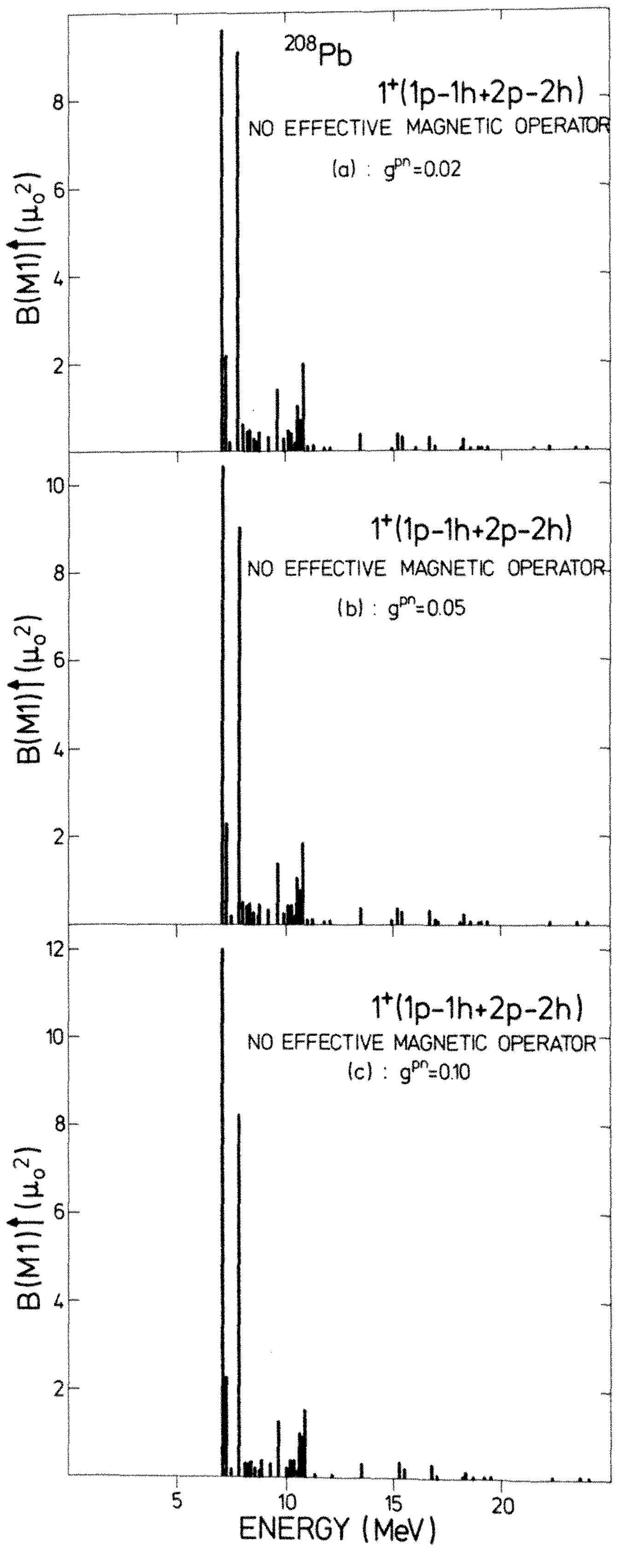

^{208}Pb
1^{+}(1p-1h+2p-2h)
NO EFFECTIVE MAGNETIC OPERATOR
(a) : g^{pn}=0.02
1^{+}(1p-1h+2p-2h)
NO EFFECTIVE MAGNETIC OPERATOR
(b) : g^{pn}=0.05
1^{+}(1p-1h+2p-2h)
NO EFFECTIVE MAGNETIC OPERATOR
(c) : g^{pn}=0.10
B(M1)↑ (μ_o^2)
ENERGY (MeV)

Figure 31

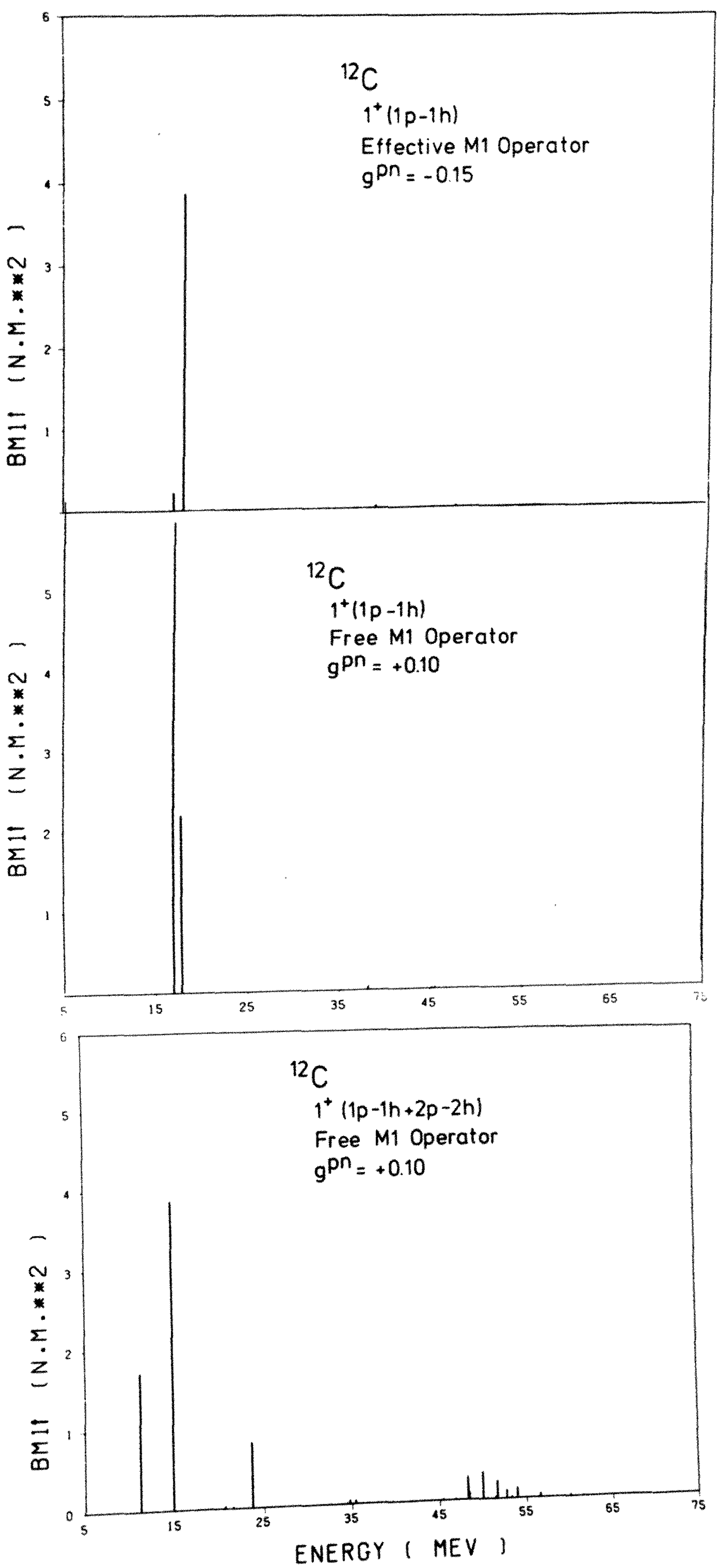

^{12}C
1$^+$(1p-1h)
Effective M1 Operator
g^{pn} = -0.15
^{12}C
1$^+$(1p-1h)
Free M1 Operator
g^{pn} = +0.10
^{12}C
1$^+$ (1p-1h+2p-2h)
Free M1 Operator
g^{pn} = +0.10
BM1↑ (N.M.**2)
ENERGY (MEV)

Figure 33

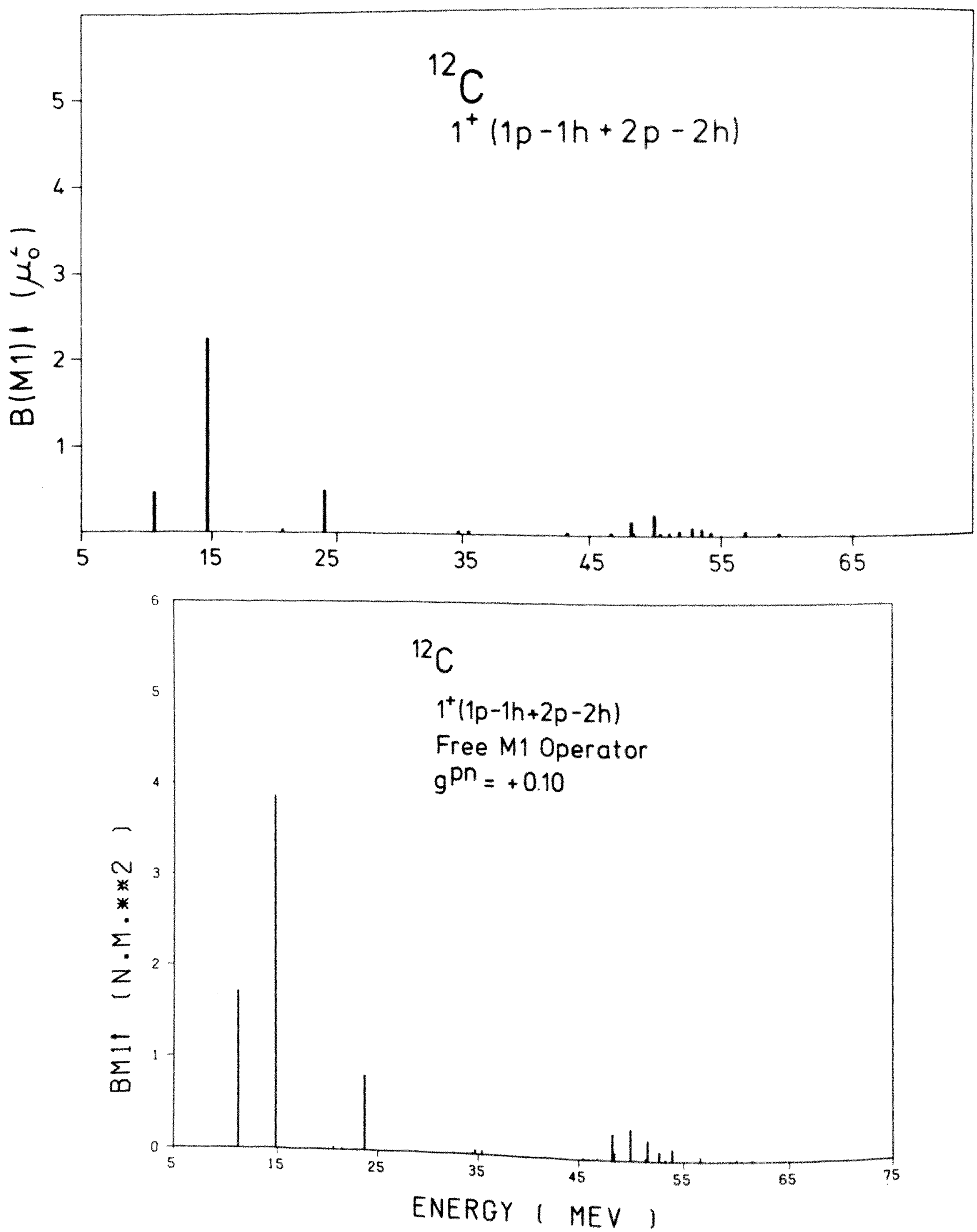

12C
1+ (1p-1h + 2p - 2h)
B(M1)↑ (μ0²)
5
4
3
2
1
5
15
25
35
45
55
65
12C
1+(1p-1h+2p-2h)
Free M1 Operator
gpn = +0.10
BM1↑ (N.M.**2)
6
5
4
3
2
1
0
5
15
25
35
45
55
65
75
ENERGY (MEV)

Figure 34

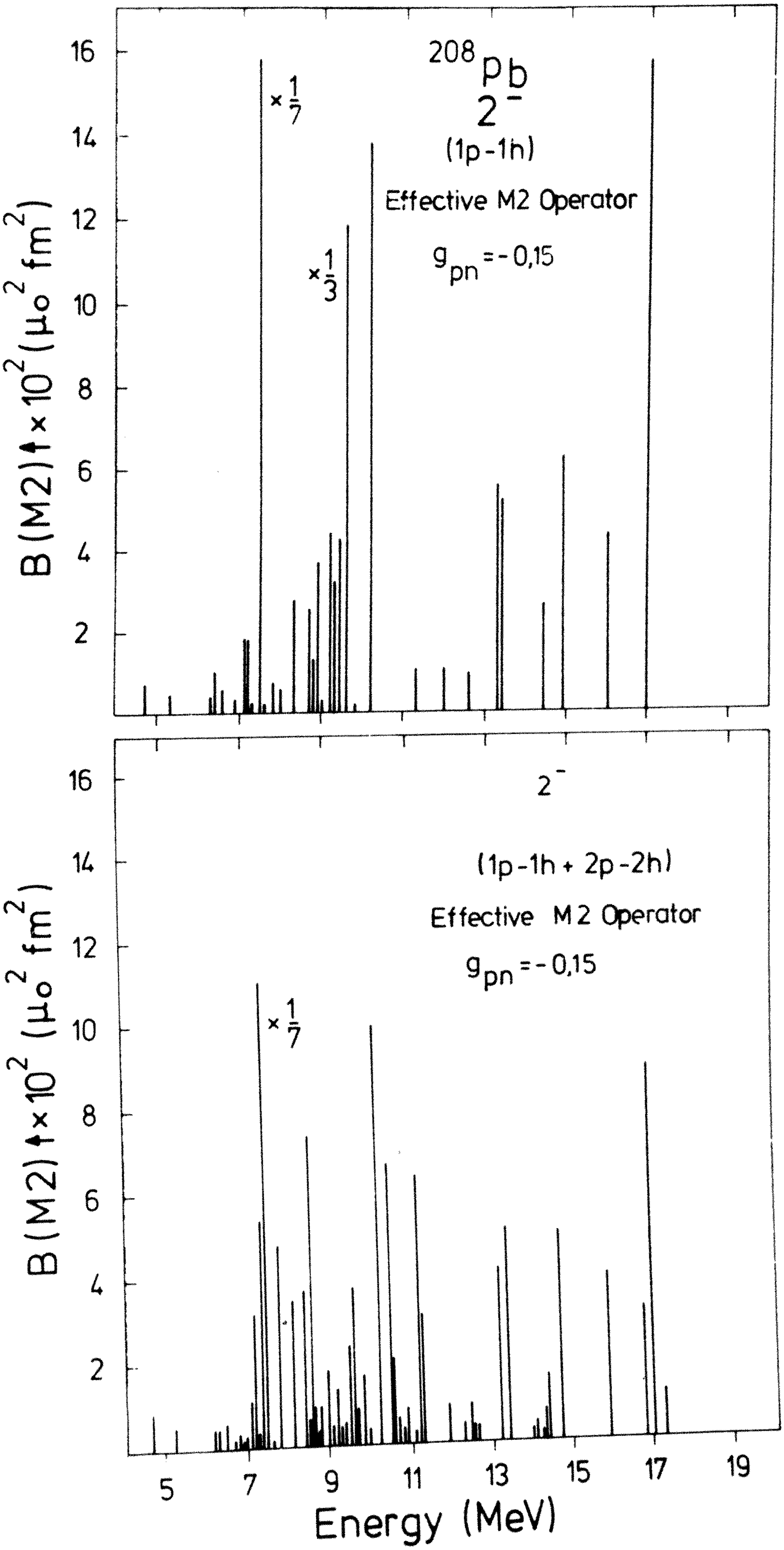

208 Pb
2^-
(1p-1h)
Effective M2 Operator
g_{pn} = - 0,15
× 1/7
× 1/3
B(M2)↑×10² (μo² fm²)
16
14
12
10
8
6
4
2
2^-
(1p-1h + 2p-2h)
Effective M2 Operator
g_{pn} = - 0,15
× 1/7
5
7
9
11
13
15
17
19
Energy (MeV)

Figure 35

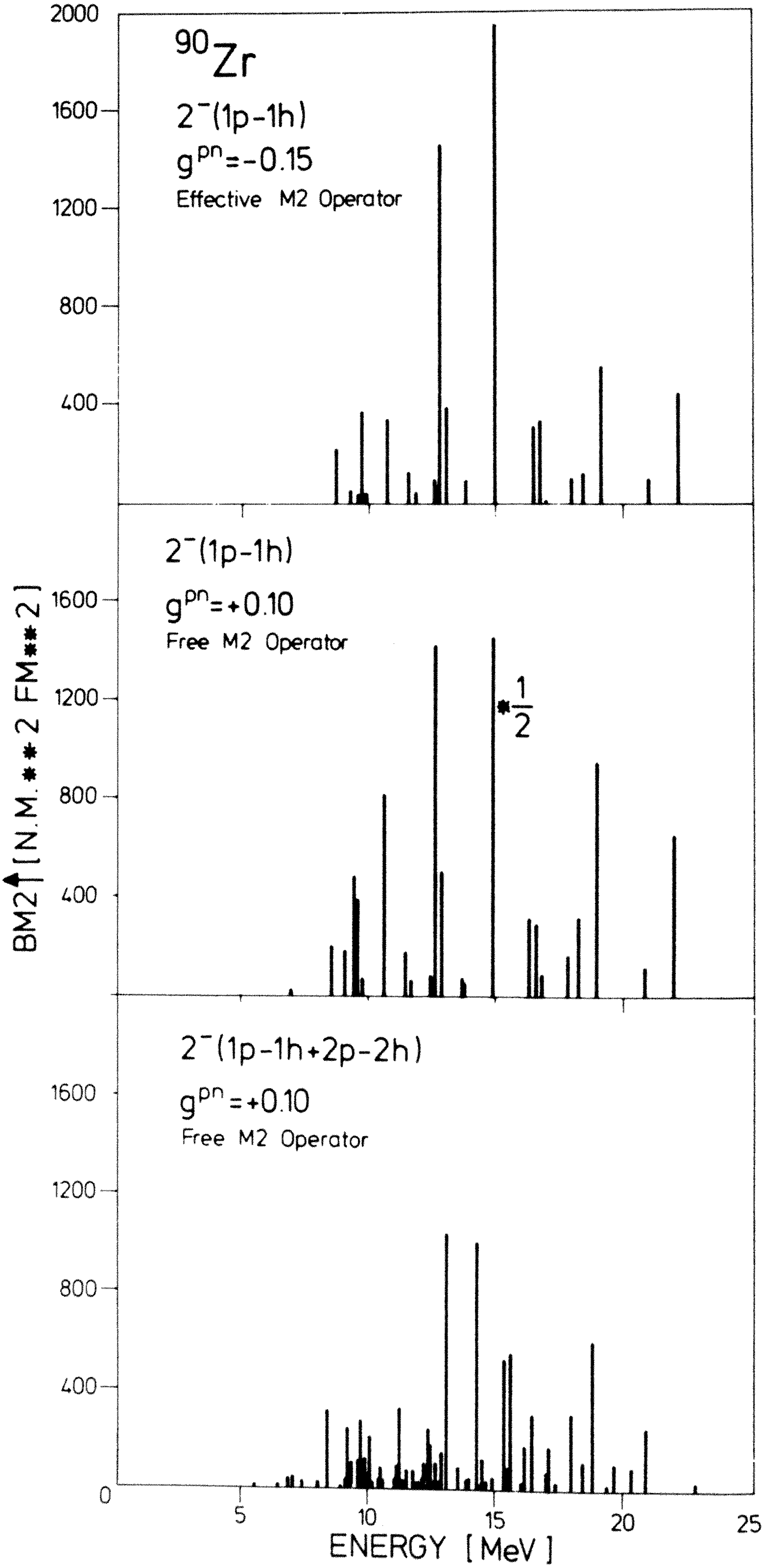

2000
1600
1200
800
400
^{90}Zr
2^-(1p-1h)
g^{pn}=-0.15
Effective M2 Operator
1600
1200
800
400
2^-(1p-1h)
g^{pn}=+0.10
Free M2 Operator
$*\frac{1}{2}$
BM2↑ [N.M.**2 FM**2]
1600
1200
800
400
0
2^-(1p-1h+2p-2h)
g^{pn}=+0.10
Free M2 Operator
5
10
15
20
25
ENERGY [MeV]

Figure 36

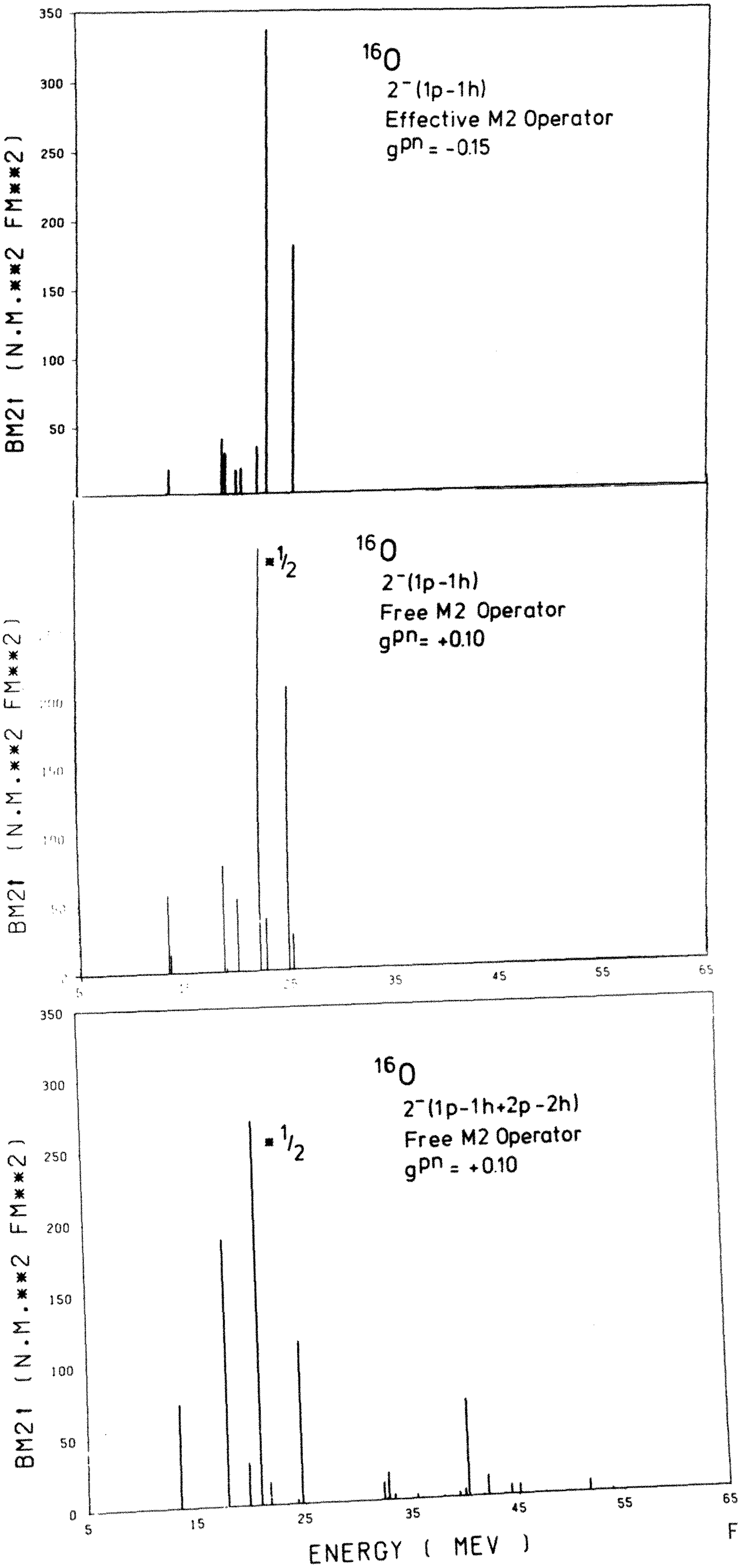

^{16}O
2^-(1p-1h)
Effective M2 Operator
g^{pn} = -0.15
^{16}O
2^-(1p-1h)
Free M2 Operator
g^{pn}= +0.10
* 1/2
^{16}O
2^-(1p-1h+2p-2h)
Free M2 Operator
g^{pn} = +0.10
* 1/2
BM2↑ (N.M.**2 FM**2)
ENERGY (MEV)

Figure 37

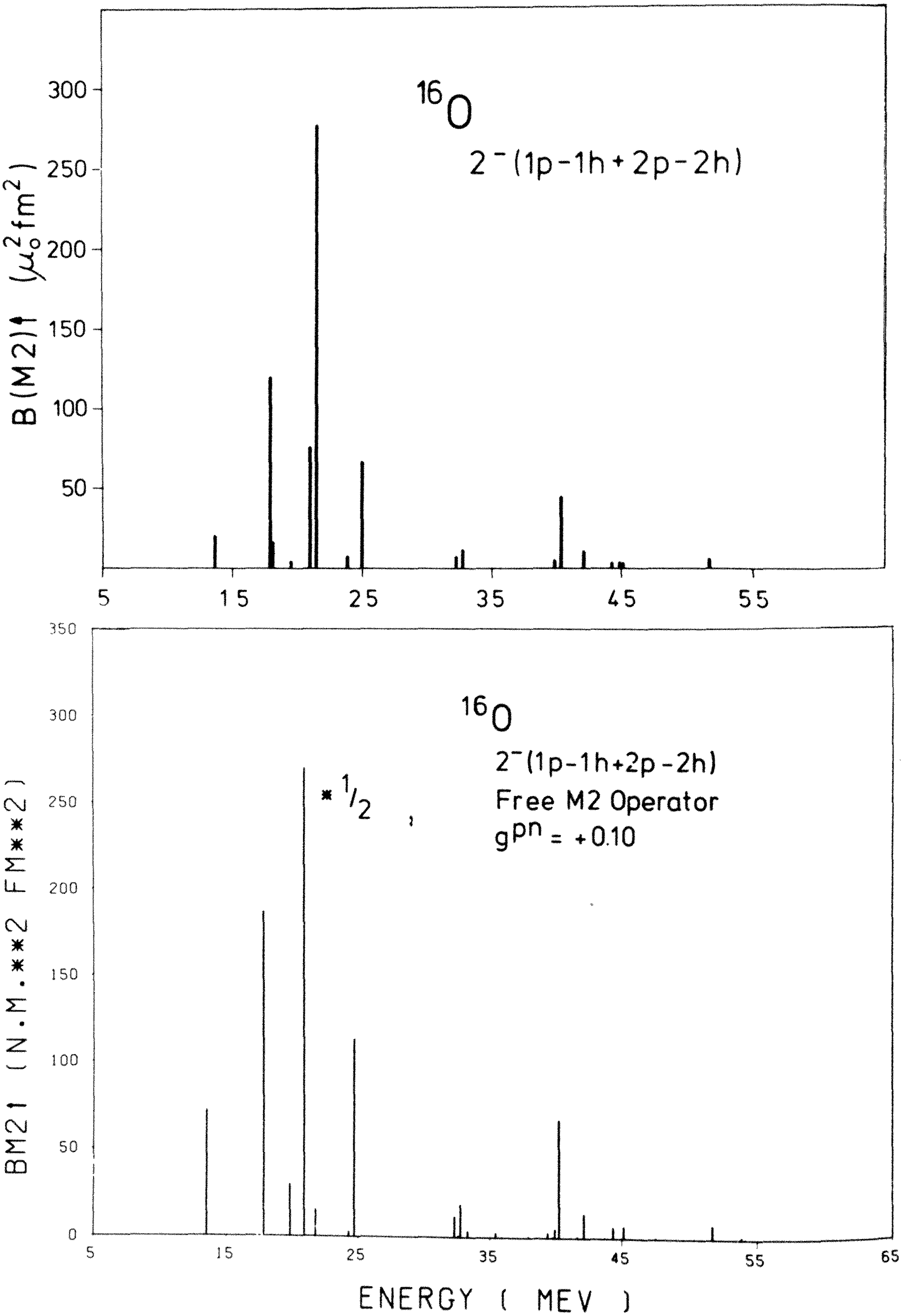

^{16}O
2^-(1p-1h+2p-2h)
B(M2)↑ ($\mu_0^2 fm^2$)
300
250
200
150
100
50
5
15
25
35
45
55
^{16}O
2^-(1p-1h+2p-2h)
Free M2 Operator
g^{pn} = +0.10
∗ 1/2
BM2↑ (N.M.∗∗2 FM∗∗2)
350
300
250
200
150
100
50
0
5
15
25
35
45
55
65
ENERGY (MEV)

Figure 38

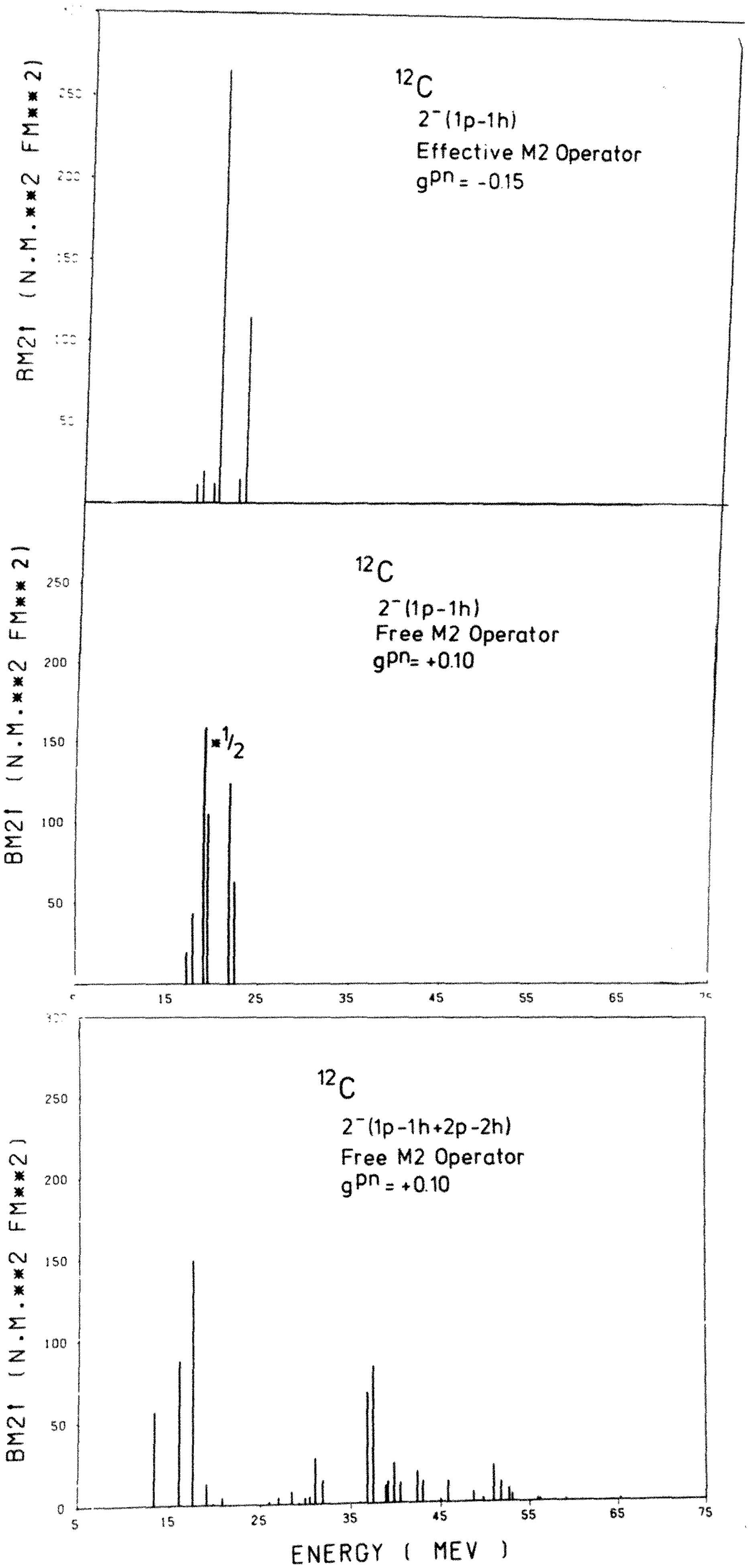

^{12}C
$2^-(1p-1h)$
Effective M2 Operator
$g^{pn} = -0.15$
^{12}C
$2^-(1p-1h)$
Free M2 Operator
$g^{pn} = +0.10$
*1/2
^{12}C
$2^-(1p-1h+2p-2h)$
Free M2 Operator
$g^{pn} = +0.10$
BM2↑ (N.M.**2 FM**2)
ENERGY (MEV)

Figure 39

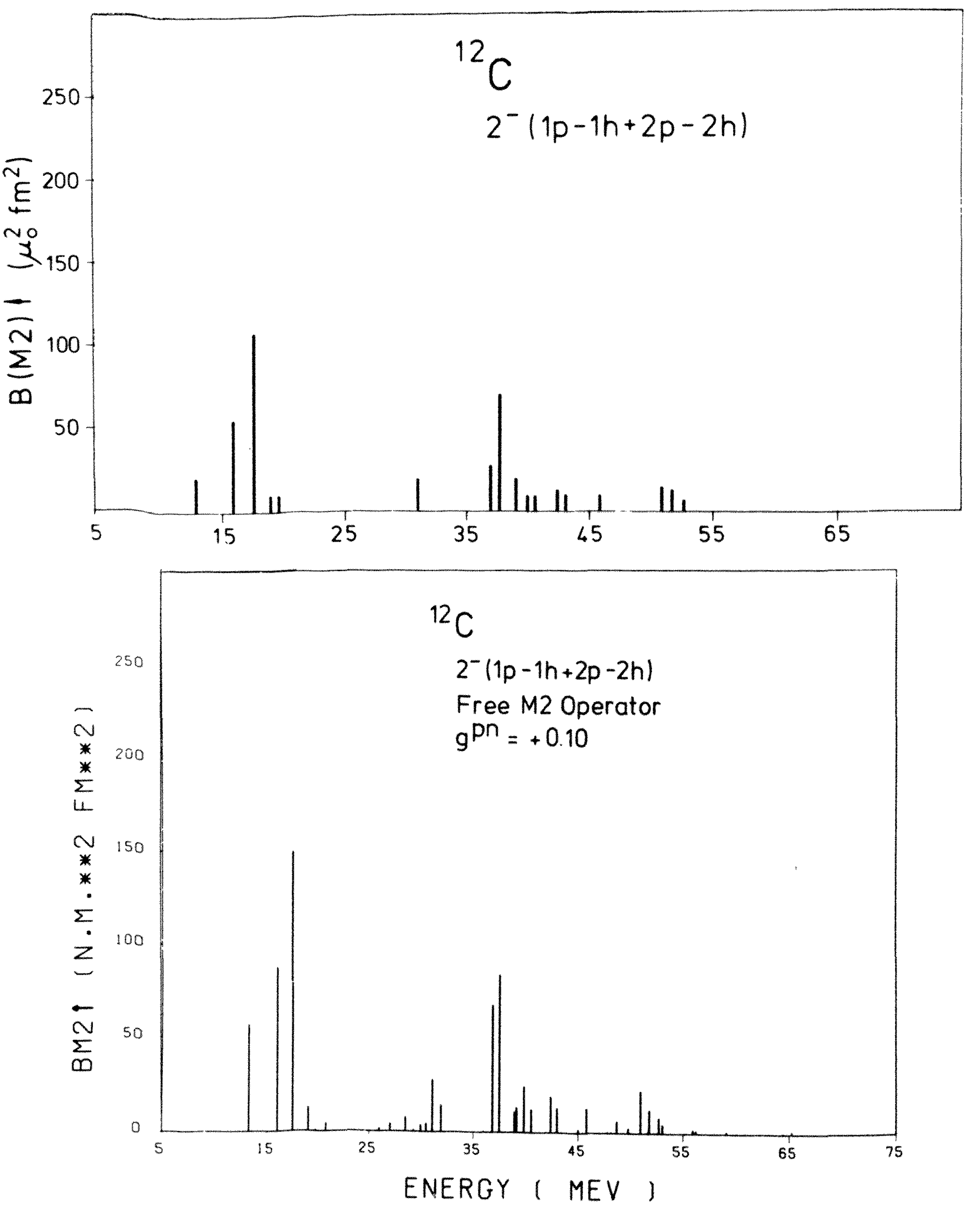

^{12}C
2^- (1p-1h+2p-2h)
B(M2)↓ (μ_o^2 fm^2)
250
200
150
100
50
5
15
25
35
45
55
65
^{12}C
2^-(1p-1h+2p-2h)
Free M2 Operator
g^{pn} = +0.10
BM2↑ (N.M.**2 FM**2)
250
200
150
100
50
0
5
15
25
35
45
55
65
75
ENERGY (MEV)

Figure 40

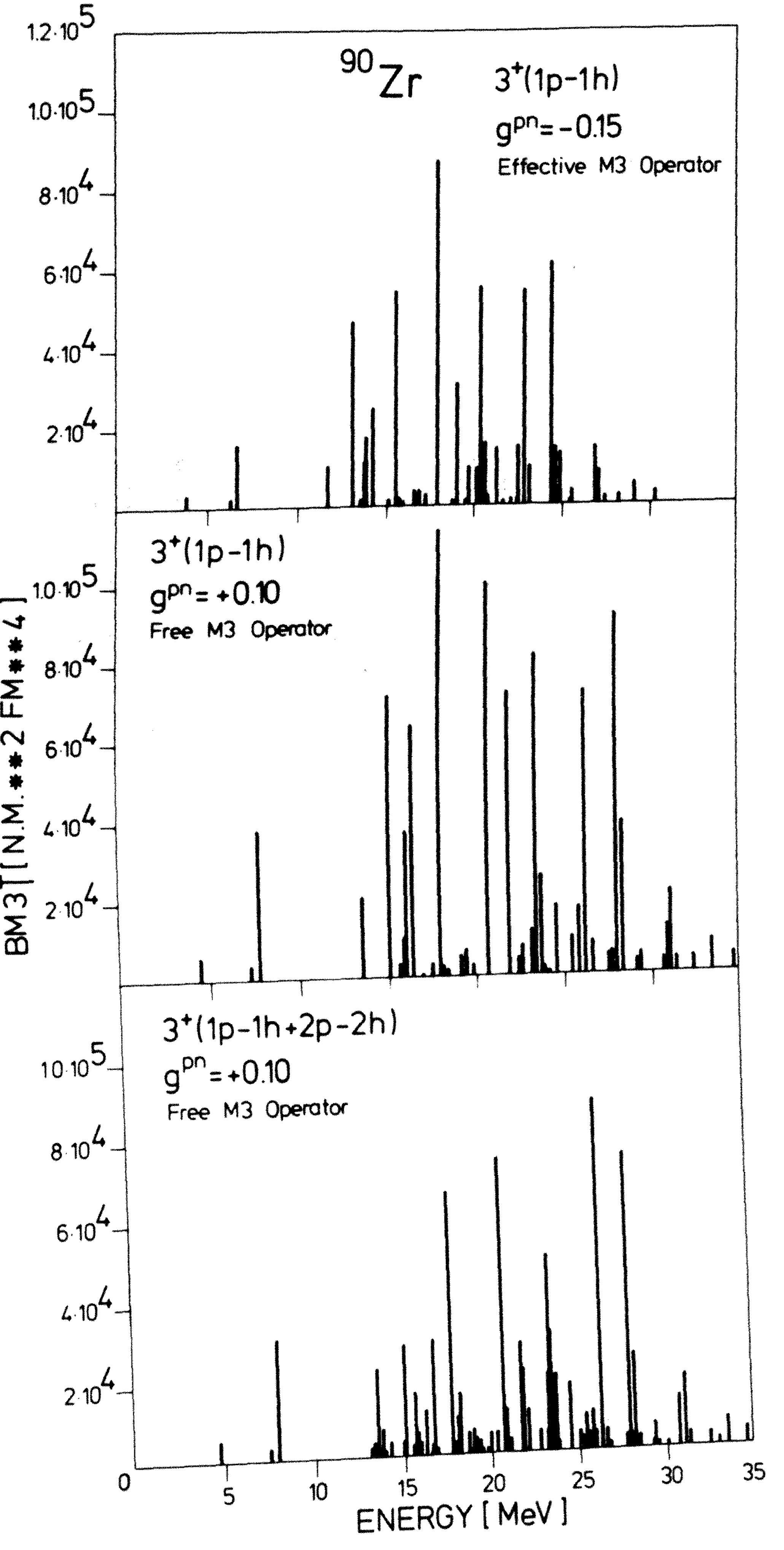

90Zr
3+(1p-1h)
gpn = -0.15
Effective M3 Operator
3+(1p-1h)
gpn = +0.10
Free M3 Operator
3+(1p-1h+2p-2h)
gpn = +0.10
Free M3 Operator
BM3↑ [N.M.**2 FM**4]
ENERGY [MeV]

Figure 41

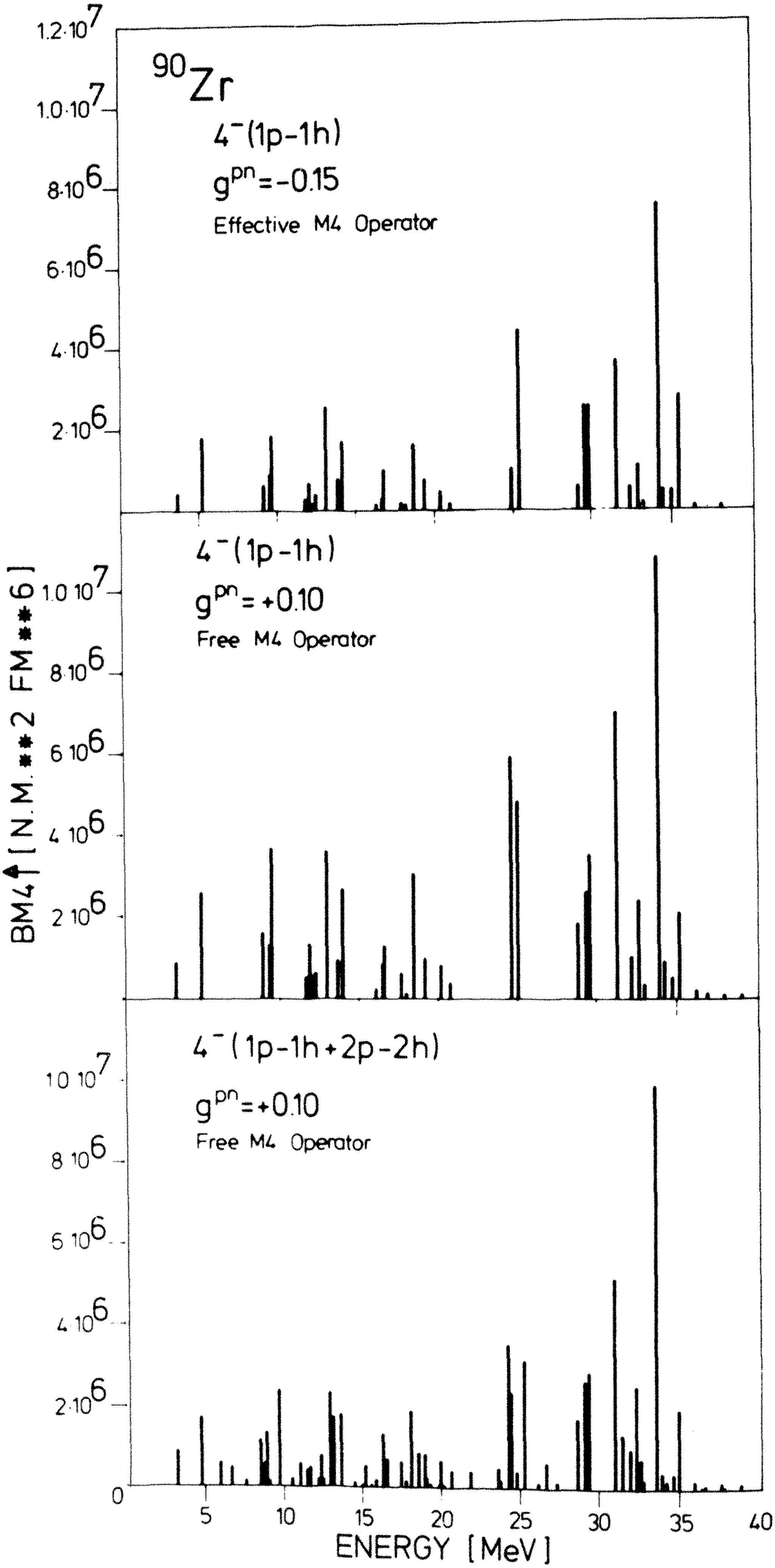

90Zr
4⁻(1p-1h)
g^pn=-0.15
Effective M4 Operator
4⁻(1p-1h)
g^pn=+0.10
Free M4 Operator
4⁻(1p-1h+2p-2h)
g^pn=+0.10
Free M4 Operator
BM4↑ [N.M.**2 FM**6]
ENERGY [MeV]

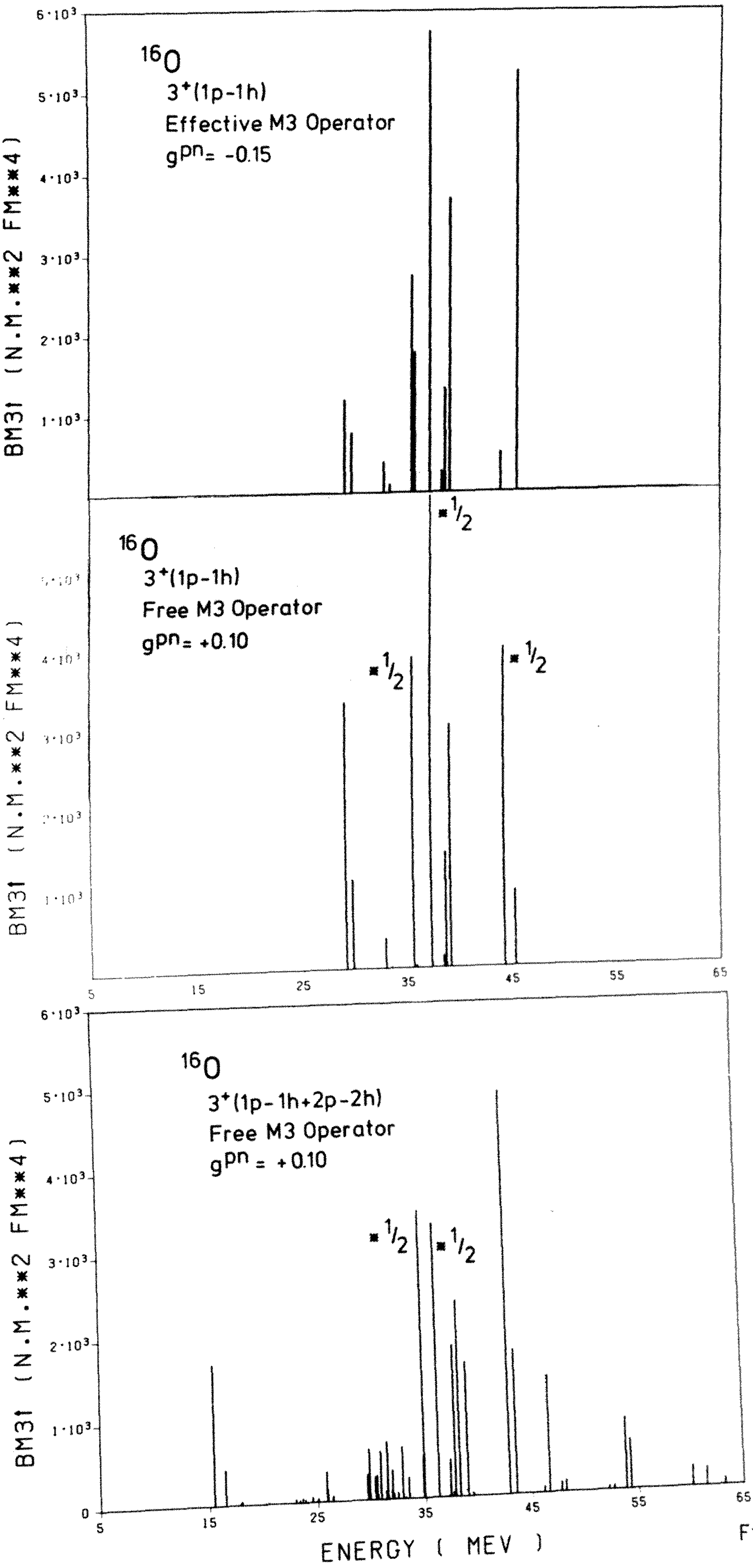
16O
3+(1p-1h)
Effective M3 Operator
gpn= -0.15
16O
3+(1p-1h)
Free M3 Operator
gpn= +0.10
*1/2
*1/2
*1/2
16O
3+(1p-1h+2p-2h)
Free M3 Operator
gpn = +0.10
*1/2
*1/2
BM3↑ (N.M.**2 FM**4)
ENERGY (MEV)

Figure 43

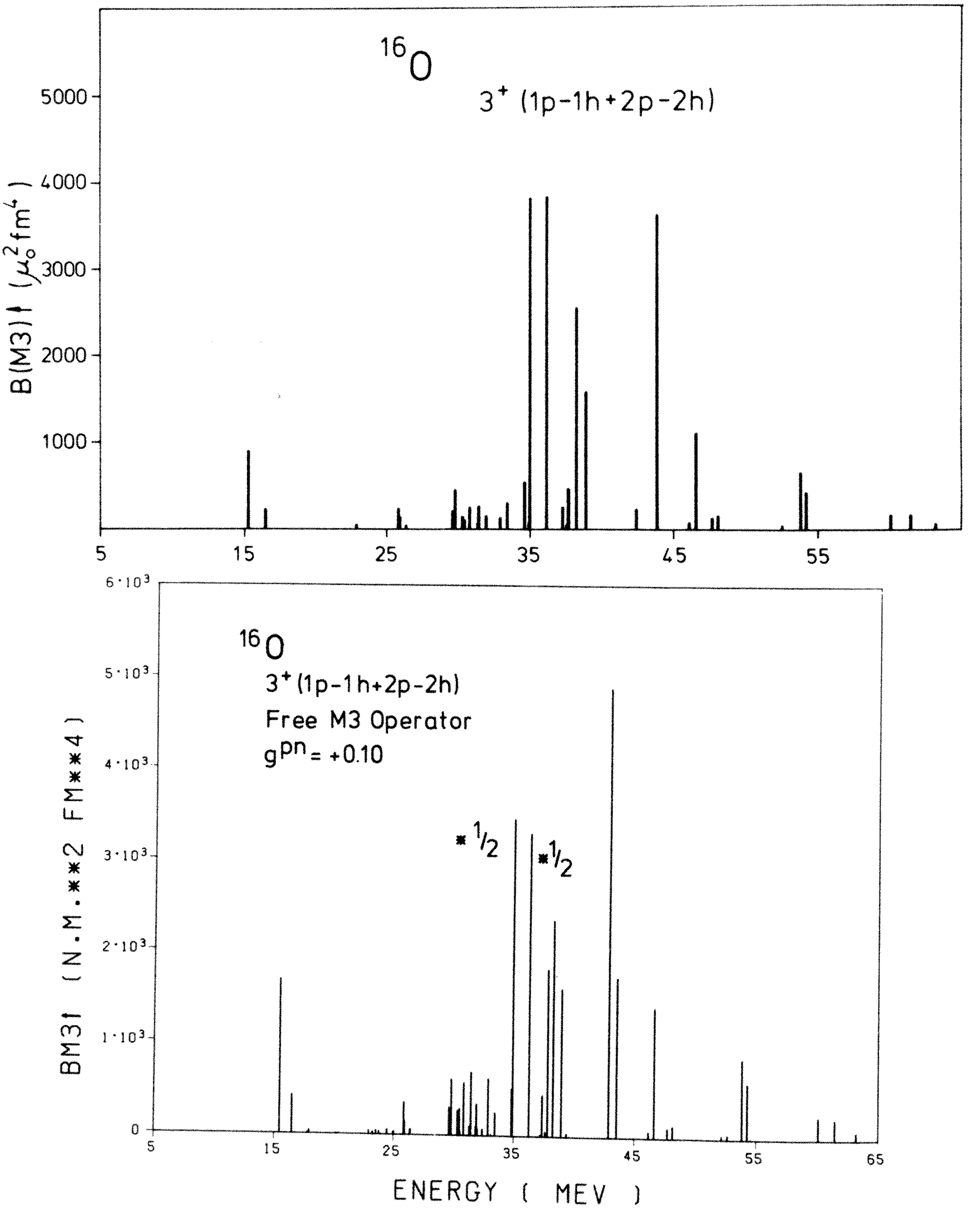

16O
3+ (1p-1h+2p-2h)
B(M3)↑ (μo2 fm4)
5000
4000
3000
2000
1000
5
15
25
35
45
55
16O
3+(1p-1h+2p-2h)
Free M3 Operator
gpn = +0.10
*1/2
*1/2
BM3↑ (N.M.**2 FM**4)
6·10³
5·10³
4·10³
3·10³
2·10³
1·10³
0
5
15
25
35
45
55
65
ENERGY (MEV)

Figure 44

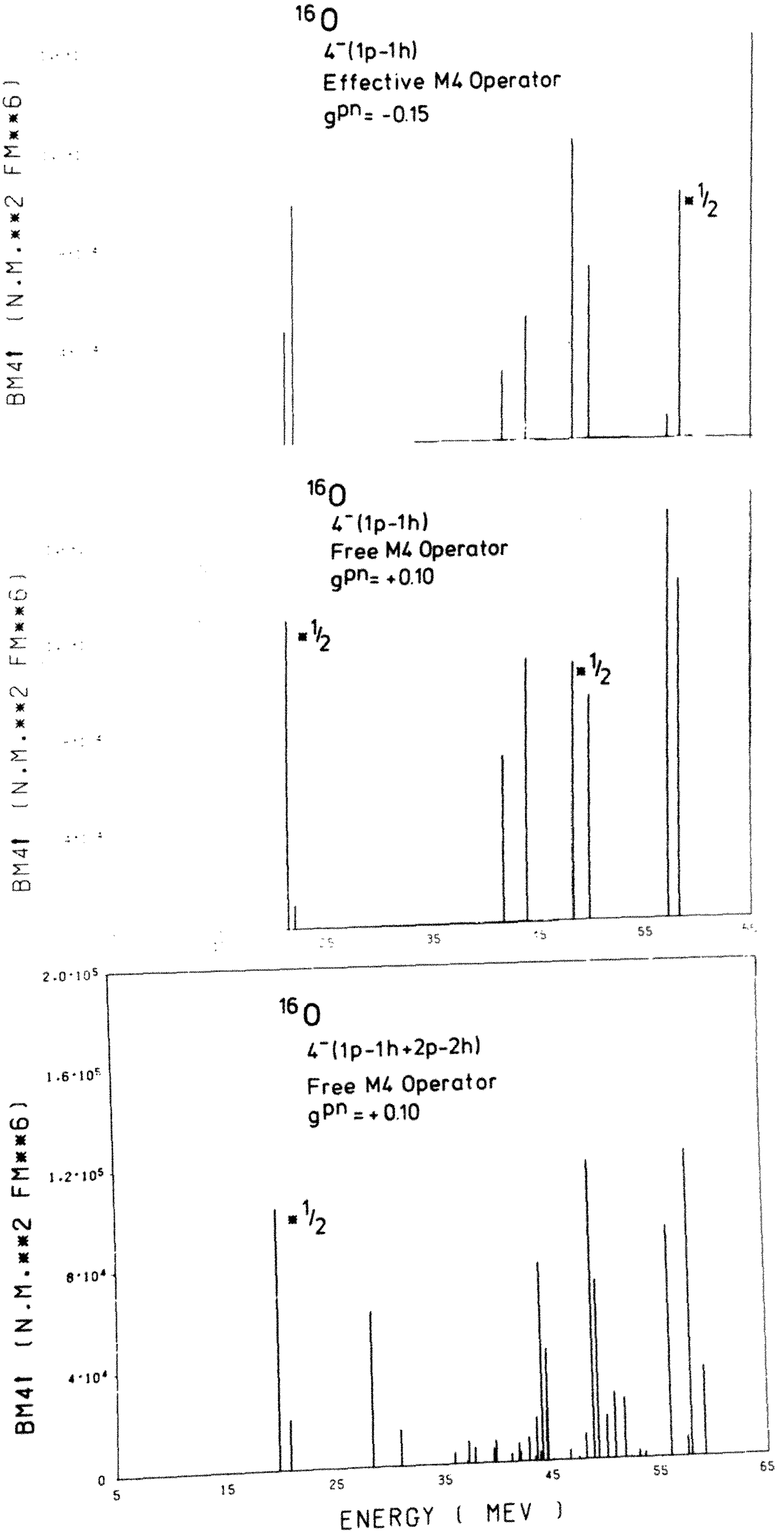

16O
4⁻(1p-1h)
Effective M4 Operator
gpn= -0.15
*1/2
BM4↑ (N.M.**2 FM**6)
16O
4⁻(1p-1h)
Free M4 Operator
gpn= +0.10
*1/2
*1/2
BM4↑ (N.M.**2 FM**6)
35
55
2.0·10⁵
1.6·10⁵
1.2·10⁵
8·10⁴
4·10⁴
0
16O
4⁻(1p-1h+2p-2h)
Free M4 Operator
gpn = +0.10
*1/2
BM4↑ (N.M.**2 FM**6)
5
15
25
35
45
55
65
ENERGY (MEV)

Figure 45

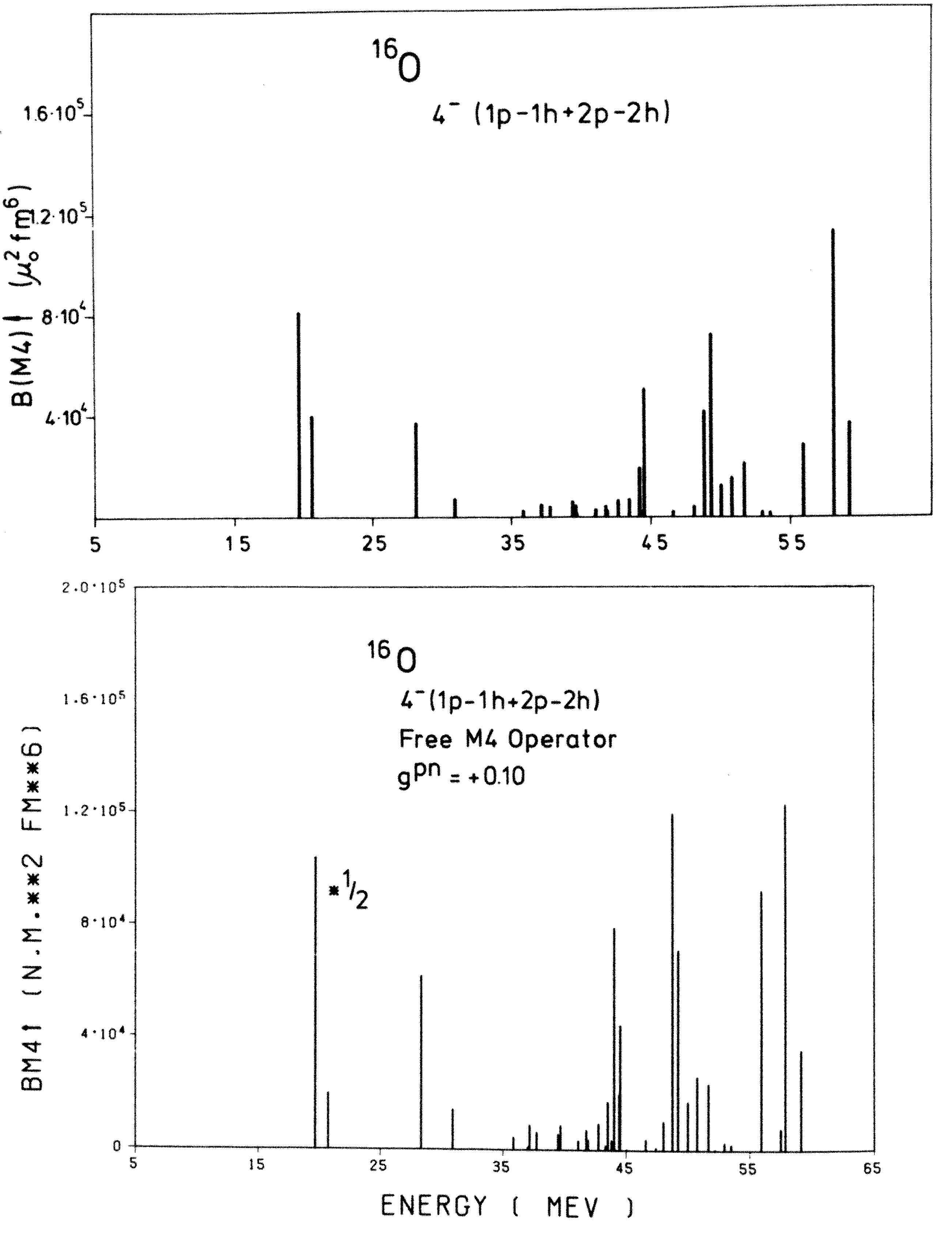

16O
4⁻ (1p-1h+2p-2h)
1.6·10⁵
1.2·10⁵
8·10⁴
4·10⁴
B(M4)↑ (μ₀² fm⁶)
5
15
25
35
45
55
2.0·10⁵
1.6·10⁵
1.2·10⁵
8·10⁴
4·10⁴
0
16O
4⁻(1p-1h+2p-2h)
Free M4 Operator
gpn = +0.10
*1/2
BM4↑ (N.M.**2 FM**6)
5
15
25
35
45
55
65
ENERGY (MEV)

Figure 46

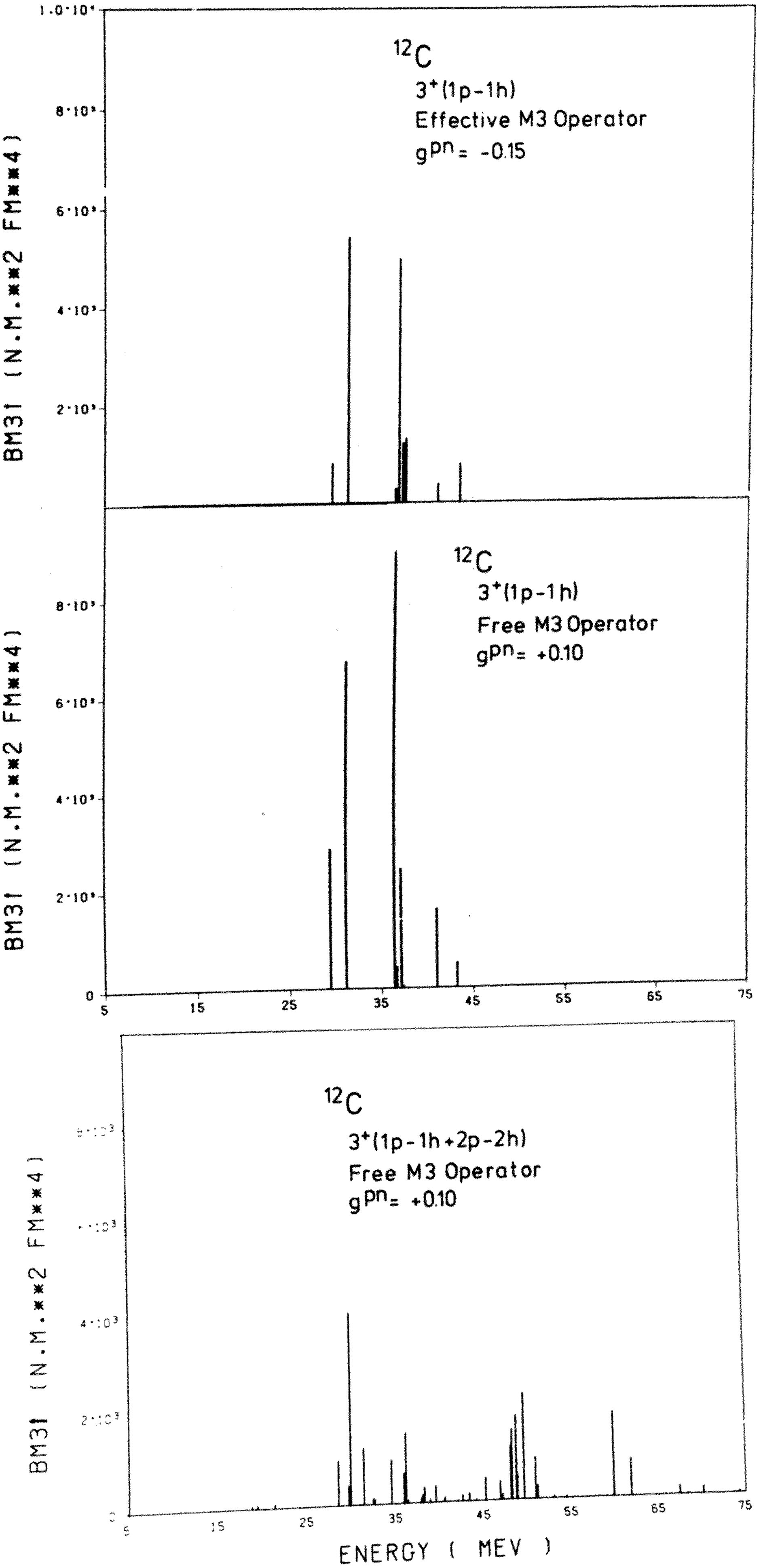

^{12}C
3^+(1p-1h)
Effective M3 Operator
g^{pn} = -0.15
^{12}C
3^+(1p-1h)
Free M3 Operator
g^{pn} = +0.10
^{12}C
3^+(1p-1h+2p-2h)
Free M3 Operator
g^{pn} = +0.10
BM3↑ (N.M.**2 FM**4)
ENERGY (MEV)

Figure 47

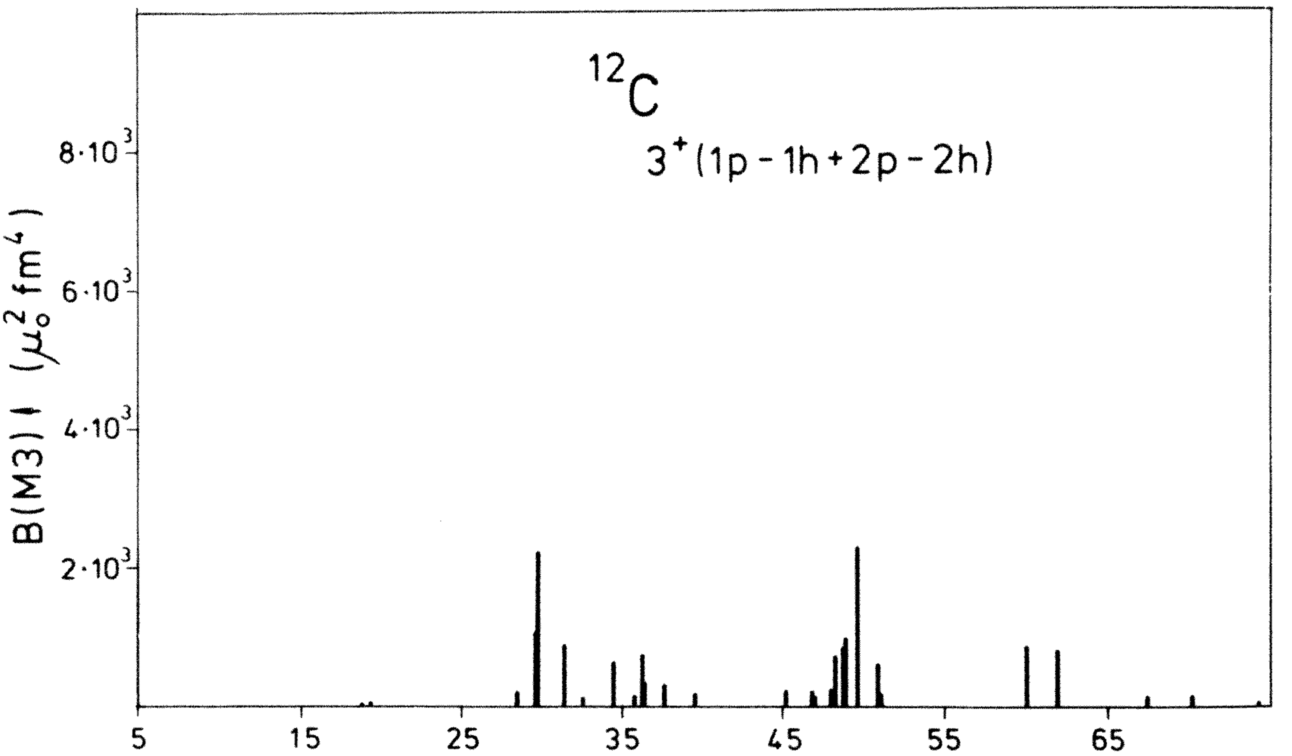

12C
3+(1p-1h+2p-2h)
B(M3)↑ (μo2 fm4)
8·103
6·103
4·103
2·103
5
15
25
35
45
55
65

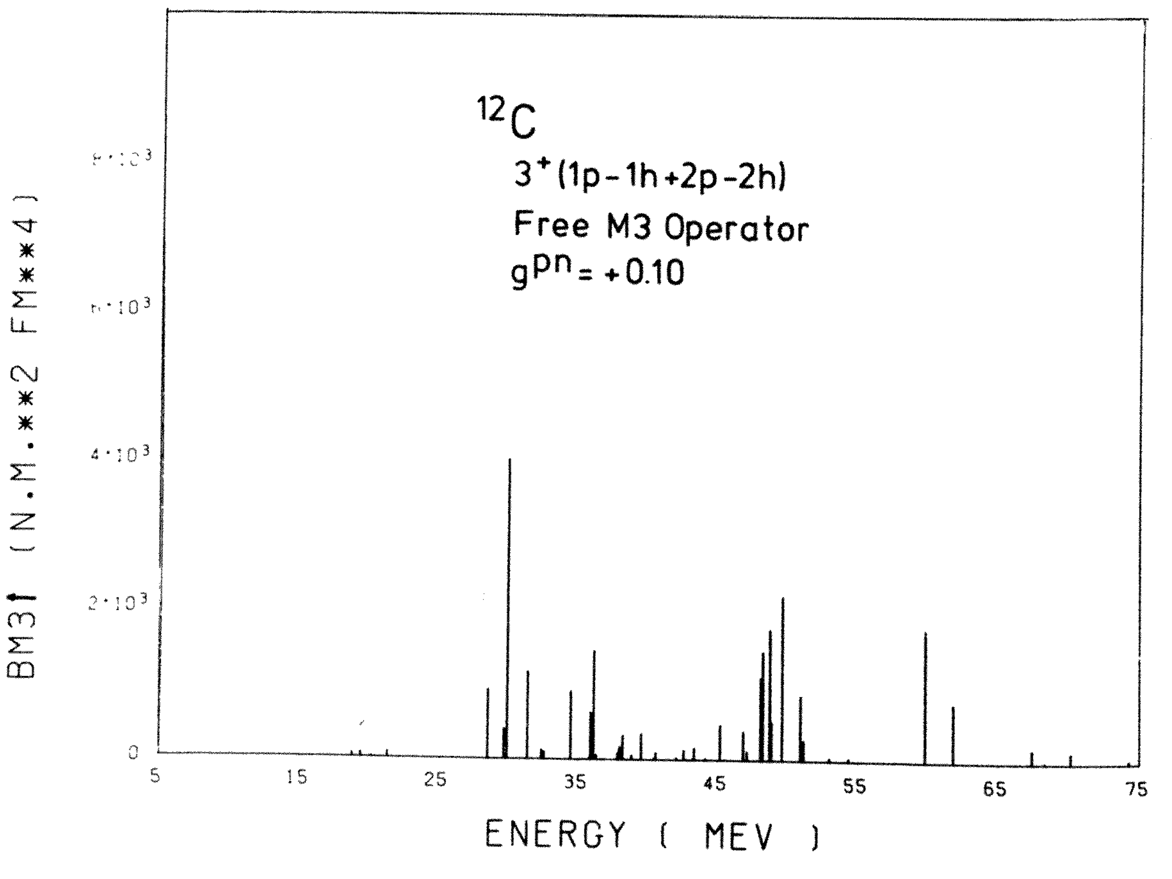

12C
3+(1p-1h+2p-2h)
Free M3 Operator
gpn= +0.10
BM3↑ (N.M.**2 FM**4)
4·103
2·103
0
5
15
25
35
45
55
65
75
ENERGY (MEV)

Figure 48

Fig. 49

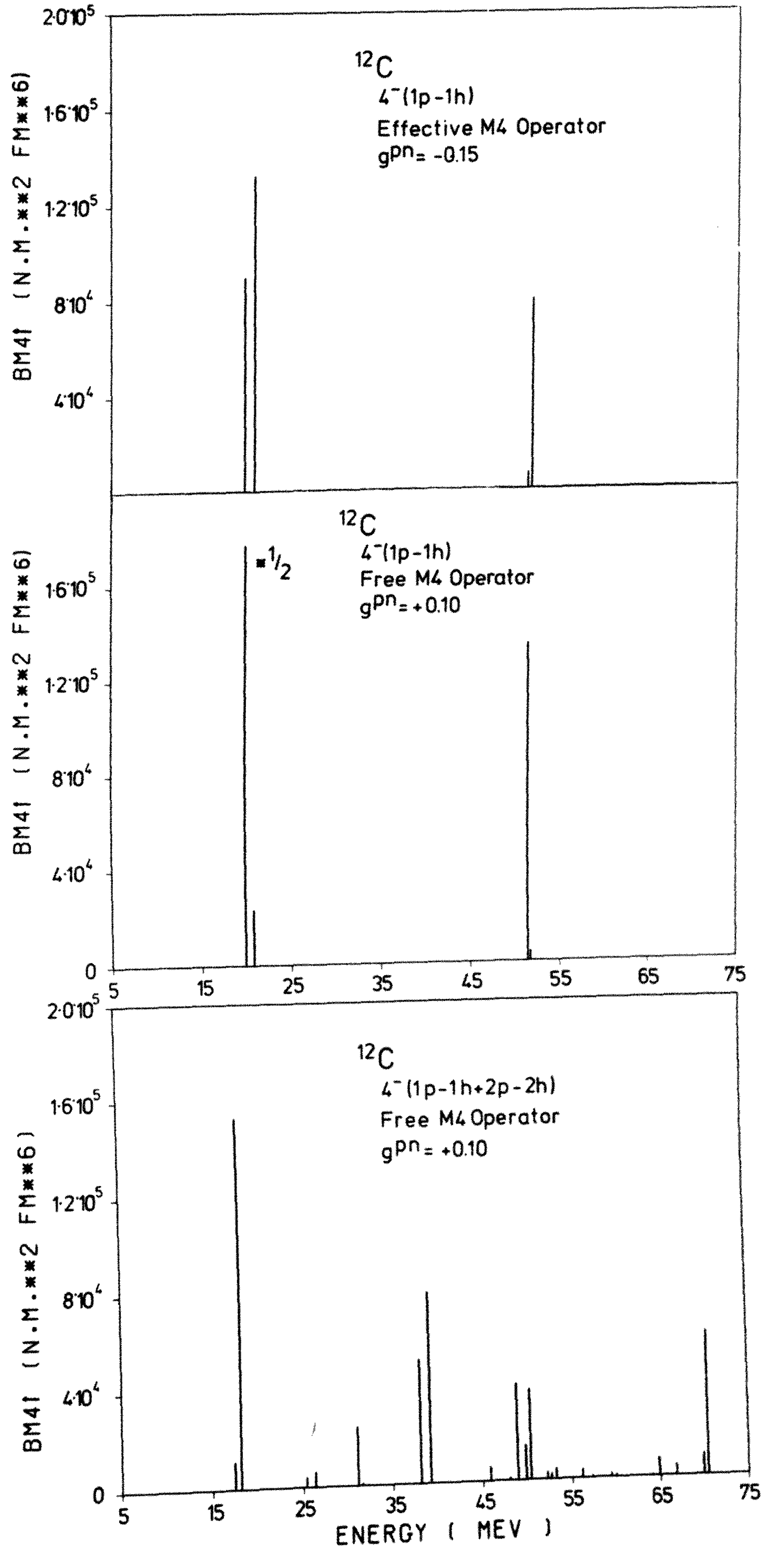

^{12}C
4^-(1p-1h)
Effective M4 Operator
g^{pn}= -0.15
^{12}C
4^-(1p-1h)
Free M4 Operator
g^{pn}= +0.10
*1/2
^{12}C
4^-(1p-1h+2p-2h)
Free M4 Operator
g^{pn}= +0.10
BM4↑ (N.M.**2 FM**6)
2·0·10^5
1·6·10^5
1·2·10^5
8·10^4
4·10^4
0
5
15
25
35
45
55
65
75
ENERGY (MEV)

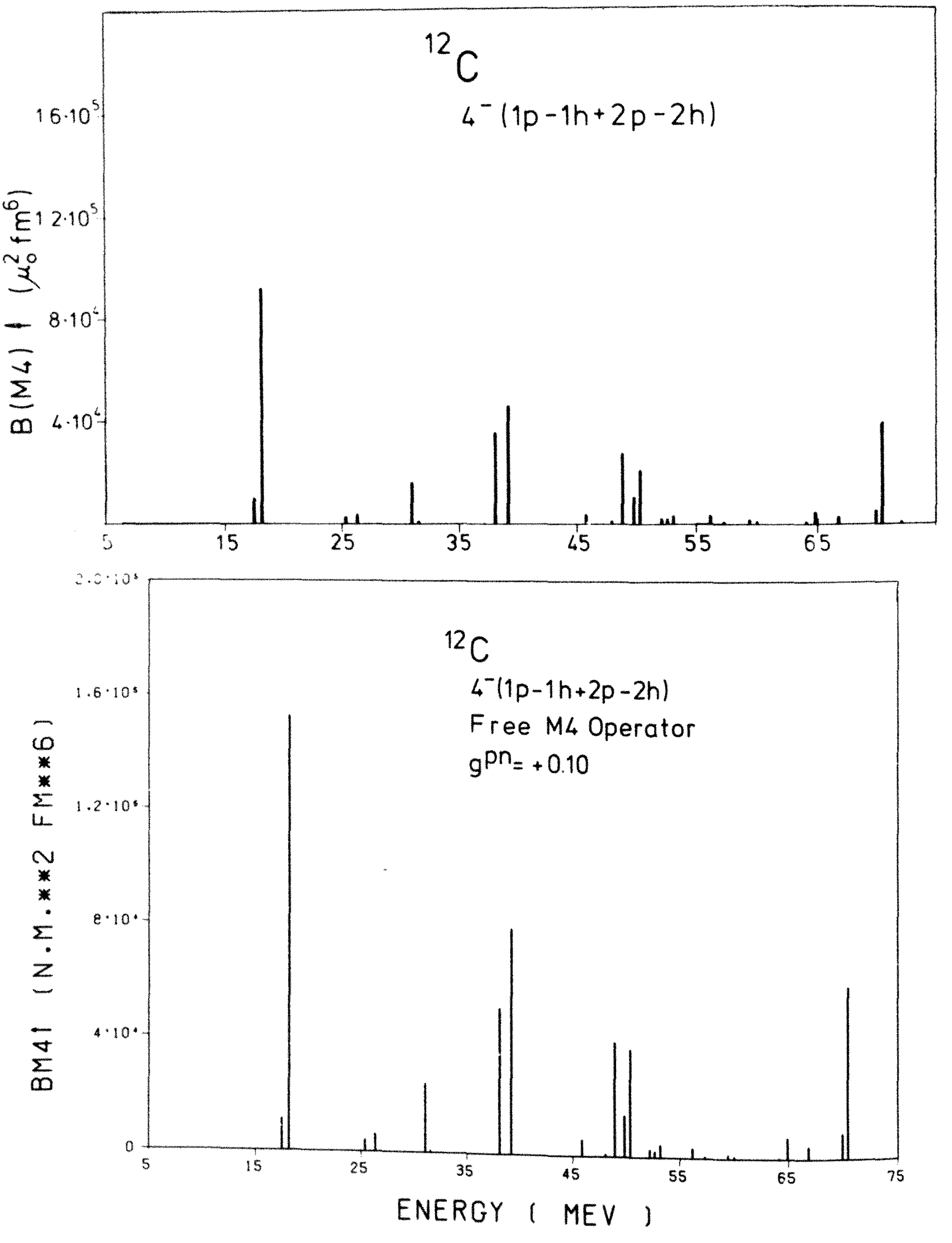

^{12}C
4^- (1p-1h+2p-2h)
B(M4) ↓ ($\mu_o^2 fm^6$)
16·10^5
12·10^5
8·10^4
4·10^4
5
15
25
35
45
55
65
^{12}C
4^-(1p-1h+2p-2h)
Free M4 Operator
g^{pn}= +0.10
BM41 (N.M.**2 FM**6)
1.6·10^5
1.2·10^5
8·10^4
4·10^4
0
5
15
25
35
45
55
65
75
ENERGY (MEV)

Figure 50